

1 **Progress in understanding of Indian Ocean circulation, variability, air-sea exchange and impacts on**
2 **biogeochemistry**

3 Helen E. Phillips^{1,2}, Amit Tandon³, Ryo Furue⁴, Raleigh Hood⁵, Caroline C. Ummenhofer^{6,7}, Jessica A. Benthuisen⁸,
4 Viviane Menezes⁶, Shijian Hu⁹, Ben Webber¹⁰, Alejandra Sanchez-Franks¹¹, Deepak Cherian¹², Emily Shroyer¹³, Ming
5 Feng^{14,15}, Hemantha Wijesekera¹⁶, Abhisek Chatterjee¹⁷, Lisan Yu⁶, Juliet Hermes¹⁸, Raghu Murtugudde¹⁹, Tomoki
6 Tozuka^{20,4}, Danielle Su²¹, Arvind Singh²², Luca Centurioni²³, Satya Prakash¹⁷, Jerry Wiggert²⁴

7

8 ¹Institute for Marine and Antarctic Studies, University of Tasmania, Hobart, 7005, Australia

9 ²Australian Antarctic Program Partnership, Institute for Marine and Antarctic Studies, University of Tasmania, Hobart,
10 7005, Australia

11 ³Department of Mechanical Engineering, College of Engineering, University of Massachusetts Dartmouth, 02747, USA

12 ⁴APL/JAMSTEC, Yokohama, Japan

13 ⁵University of Maryland Center for Environmental Science, Horn Point Laboratory, Cambridge, 21613, USA

14 ⁶Department of Physical Oceanography, Woods Hole Oceanographic Institution, Woods Hole, 02543, USA

15 ⁷ARC Centre of Excellence for Climate Extremes, University of New South Wales, Sydney, Australia

16 ⁸Australian Institute of Marine Science, Indian Ocean Marine Research Centre, Crawley, Australia

17 ⁹Institute of Oceanology, Chinese Academy of Sciences, Qingdao, China

18 ¹⁰School of Environmental Sciences, University of East Anglia, Norwich, NR4 7TJ, UK

19 ¹¹National Oceanography Centre, Southampton, UK

20 ¹²National Center for Atmospheric Research, Boulder, USA

21 ¹³College of Earth, Ocean and Atmospheric Sciences, Oregon State University, Corvallis, 97331, USA

22 ¹⁴CSIRO Oceans and Atmosphere, Indian Ocean Marine Research Centre, Crawley, Australia

23 ¹⁵Centre for Southern Hemisphere Oceans Research, Hobart, Australia

24 ¹⁶U.S. Naval Research Laboratory, Stennis Space Center, MS, 39529, USA

25 ¹⁷Indian National Centre for Ocean Information Services, Ministry of Earth Sciences, Hyderabad, India

26 ¹⁸South African Environmental Observation Network, Cape Town, South Africa

27 ¹⁹Department of Atmospheric and Oceanic Science, University of Maryland, College Park, 20742, USA

28 ²⁰Department of Earth and Planetary Science, Graduate School of Science, The University of Tokyo, Tokyo, Japan

29 ²¹Sorbonne Universités, UPMC Université Paris 06, CNRS, UMR 7159 LOCEAN-IPSL, Paris, France

30 ²²Physical Research Laboratory, Ahmedabad, India

31 ²³Scripps Institution of Oceanography, University of California San Diego, La Jolla, 92093, USA

32 ²⁴University of Southern Mississippi, Hattiesburg, 399406, USA

33

34

35 *Correspondence to:* Helen E. Phillips (h.e.phillips@utas.edu.au)

36 Dedicated to Dr Satya Prakash (1979-2021). This manuscript was written during the COVID-19 pandemic while many
37 juggled family and health issues under lockdown. Satya, our co-author and friend, passed away on 22nd July 2021. Satya
38 was the coordinator of the International Indian Ocean Expedition (IIOE-2) at the Indian National Centre for Ocean
39 Information Services (INCOIS). He played an integral part in Indian Ocean research. He is remembered for his enthusiasm,
40 commitment and smile. His passing is a massive loss to the Indian Ocean community, but there will be much that will still
41 be carried on in his memory thanks to his hard work and passion.

42

43 **Abstract.** Over the past decade, our understanding of the Indian Ocean has advanced through concerted efforts toward
44 measuring the ocean circulation and air-sea exchanges, detecting changes in water masses, and linking physical processes
45 to ecologically important variables. New circulation pathways and mechanisms have been discovered, which control
46 atmospheric and oceanic mean state and variability. This review brings together new understanding of the ocean-
47 atmosphere system in the Indian Ocean since the last comprehensive review, describing the Indian Ocean circulation
48 patterns, air-sea interactions and climate variability. Coordinated international focus on the Indian Ocean has motivated
49 the application of new technologies to deliver higher-resolution observations and models of Indian Ocean processes. As a
50 result we are discovering the importance of small-scale processes in setting the large-scale gradients and circulation,
51 interactions between physical and biogeochemical processes, interactions between boundary currents and the interior, and
52 between the surface and the deep ocean. A newly discovered regional climate mode in the southeast Indian Ocean, the
53 Ningaloo Niño, has instigated more regional air-sea coupling and marine heatwave research in the global oceans. In the
54 last decade, we have seen rapid warming of the Indian Ocean overlaid with extremes in the form of marine heatwaves.
55 These events have motivated studies that have delivered new insight into the variability in ocean heat content and
56 exchanges in the Indian Ocean, and have highlighted the critical role of the Indian Ocean as a clearing house for
57 anthropogenic heat. This synthesis paper reviews the advances in these areas in the last decade.

58 **Contents**

59 [1. Introduction](#)

60 [2 Large-scale setting](#)

61 [3 Air-sea interactions](#)

62 [3.1 Seasonal cycle and the monsoons](#)

63	<u>3.2 Intraseasonal air-sea interaction</u>
64	<u>3.2.1 Madden-Julian Oscillation - MJO</u>
65	<u>3.2.2 Monsoon Intraseasonal Oscillation - MISO</u>
66	<u>3.2.3 Intraseasonal drivers of heavy rainfall</u>
67	<u>3.3 Ocean internal variability impacts on air-sea interaction</u>
68	<u>4 Upper Ocean Circulation and Biogeochemical Variability</u>
69	<u>4.1 Overview</u>
70	<u>4.2 Southern Indian Ocean</u>
71	<u>4.2.1 South Equatorial Current</u>
72	<u>4.2.2 Western Boundary</u>
73	<u>4.2.3 Interior flows</u>
74	<u>4.2.4 Eastern Boundary</u>
75	<u>4.2.5 Biogeochemical Variability</u>
76	<u>4.3 Equatorial regime</u>
77	<u>4.3.1 Wyrtki Jets</u>
78	<u>4.3.2 5-30 Day Ocean Waves and Instabilities</u>
79	<u>4.3.3 Equatorial Upwelling and Downwelling</u>
80	<u>4.3.4 Equatorial Undercurrents</u>
81	<u>4.3.5 Cross-Equatorial Circulation</u>
82	<u>4.3.6 Biogeochemical Variability</u>
83	<u>4.4 Northern Indian Ocean</u>
84	<u>4.4.1 Bay of Bengal</u>
85	<u>4.4.1.1 Southwest/Northeast Monsoon Currents</u>
86	<u>4.4.1.2 East Indian Coastal Currents (EICC)</u>
87	<u>4.4.1.3 Undercurrents</u>
88	<u>4.4.1.4 Sri Lanka Dome</u>
89	<u>4.4.2 Arabian Sea</u>
90	<u>4.4.2.1 Somali current System</u>
91	<u>4.4.2.2 West India Coastal Current (WICC)</u>
92	<u>4.4.3 Biogeochemical Variability</u>
93	<u>5 Inter-ocean exchange</u>
94	<u>5.1 Indonesian Throughflow</u>
95	<u>5.1.1 General features</u>
96	<u>5.1.2 Variability, dynamics and influence</u>
97	<u>5.2 Agulhas Leakage</u>
98	<u>5.2.1 General features</u>
99	<u>5.2.2 Variability, dynamics and influence on climate</u>
100	<u>5.3 Supergyre connection to the South Pacific</u>
101	<u>5.4 Roles of salinity in inter-ocean exchange</u>

102	<u>6 Modes of Interannual Climate Variability in the Indian Ocean</u>
103	<u>6.1 ENSO teleconnection and the Indian Ocean Basin mode</u>
104	<u>6.2 The Indian Ocean Dipole</u>
105	<u>6.3 The subtropical Indian Ocean Dipole</u>
106	<u>6.4 Ningaloo Niño and marine heatwaves in the Indian Ocean</u>
107	<u>6.5 Monsoon variability and links to the Indian Ocean</u>
108	<u>7. Multiscale upper ocean processes in the Bay of Bengal</u>
109	<u>7.1 The Bay’s Forcing and Upper Ocean Structure</u>
110	<u>7.2 Lateral Processes</u>
111	<u>7.2.1 Stirring from the Margins</u>
112	<u>7.2.2 Inter-basin exchange</u>
113	<u>7.2.2.1 Andaman Sea Exchange</u>
114	<u>7.2.2.2 Arabian Sea Exchange</u>
115	<u>7.2.3 Equatorial Connections</u>
116	<u>7.3 Vertical Mixing</u>
117	<u>7.4 Where vertical and lateral processes meet: The Role of Submesoscale</u>
118	<u>7.5 Putting the Pieces Together</u>
119	<u>7.5.1 Coupled ocean-atmosphere phenomena</u>
120	<u>7.5.2 Implications for biogeochemistry in the Bay</u>
121	<u>8. Summary and open questions</u>
122	<u>Code Availability</u>
123	<u>Data Availability</u>
124	<u>Author Contributions</u>
125	<u>Competing interests</u>
126	<u>Acknowledgements</u>
127	<u>References</u>
128	
129	

130 **1. Introduction**

131 The physical processes taking place in the Indian Ocean and overlying atmosphere underpin the variability evident in
132 monsoons, extreme events, marine biogeochemical cycles, ecosystems, and ultimately human experience. The Indian
133 Ocean rim countries, accounting for one third of the Earth’s human population, depend on this ocean for food and
134 resources, and are dramatically impacted by its variability (Hermes et al., 2019). Increasing our understanding of

135 interactions between geologic, oceanic and atmospheric processes that control the complex physical dynamics of the
136 Indian Ocean region is a priority for many national, bilateral, and international programmes including the Indian Ocean
137 Observing System (IndOOS; Beal et al., 2020), the Climate and Ocean: Variability, Predictability and Change
138 (CLIVAR)/Intergovernmental Oceanographic Commission (IOC) - Indian Ocean Region Panel
139 (https://www.clivar.org/sites/default/files/documents/indian/135_IOP5.pdf), and the second International Indian Ocean
140 Expedition (IIOE-2), to name a few. While initiated through IIOE-2, this review draws on the collective results of all of
141 the programmes and individual efforts. We focus, in particular, on questions about the Indian Ocean circulation, climate
142 variability and change such as: 1) how have the atmospheric and oceanic circulation of the Indian Ocean changed in the
143 past and how will they change in the future; 2) how do these changes relate to geography and connectivity with the Pacific,
144 Atlantic and Southern oceans; and 3) what impact does the circulation, variability, and change have on biological
145 productivity and fisheries.

146 Recent focus on the Indian Ocean has motivated new international efforts in field campaigns and modelling studies, and
147 leveraged advances in global observations that contribute to the Indian Ocean Observing System (IndOOS; Beal et al.,
148 2020). The Argo profiling float array (Roemmich et al., 2012) reached full coverage in the Indian Ocean in 2006, the
149 RAMA moored buoy array (McPhaden et al., 2009) has now delivered multi-year time series of tropical oceanic and
150 atmospheric variability, with some sites dating back to 2000. Satellite systems continue to provide observations vital to
151 interpreting spatial and temporal variability in the in situ observations, and new technology is now enabling high resolution
152 observations of boundary current variability and small scale processes. Thus, since the reviews of Schott and McCreary
153 (2001) and Schott et al. (2009), the spatial coverage of observations and length of time series have increased substantially
154 such that the signals of many previously unresolved processes are now able to be observed.

155
156 These new higher-resolution observations and companion improvements in model simulations have highlighted the
157 importance of small scale processes in setting the large-scale gradients and circulation, interactions between physical and
158 biogeochemical processes, interactions between boundary currents and the interior, and between the surface and the deep
159 ocean. Overlaid on these interior Indian Ocean processes, ocean warming due to increasing greenhouse gas concentrations
160 has been shown to be pervasive and relentless (Wijffels et al., 2016), and extending to abyssal depths (Johnson et al.,
161 2008a; Desbruyeres et al., 2017).

162
163 The Indian Ocean plays a key role in the global climate system, enabling upwelling of the lower cell of the meridional
164 overturning circulation from abyssal to upper-deep and intermediate waters through diffusive mixing (Schmitz, 1995;
165 Lumpkin and Speer, 2007; McDonagh et al., 2008; Talley, 2013; Hernandez-Guerra and Talley, 2016) and exporting the
166 largest poleward heat flux of all Southern Hemisphere basins (Roxy et al., 2014). In recent decades, the upper 700 m of
167 the entire Indian Ocean has warmed rapidly (Desbruyères et al, 2017). In the southern Indian Ocean, the warming was

168 directly linked primarily to heat advection from a strengthened ITF and, secondly, to a decrease in mean air-sea flux
169 cooling (Li et al., 2017b; Zhang et al., 2018a). This coupling between the ocean and atmosphere in the Indian and Pacific
170 Oceans shifted the balance of global warming, accelerating ocean warming and causing a hiatus in the warming of Earth's
171 surface atmosphere (Section 6). Marine heatwaves have emerged as an increasing threat to marine ecosystems as ocean
172 temperatures warm (e.g. Oliver et al., 2018). Increasingly vulnerable populations need more reliable monsoon predictions,
173 a task complicated by variability across timescales from intraseasonal to interannual, decadal and beyond in a tightly
174 coupled ocean-atmosphere system (Hazra et al., 2017).

175
176 The starting point for this synthesis report are the reviews by Schott and McCreary (2001) and Schott et al. (2009),
177 describing the circulation patterns, air-sea interactions and climate variability on timescales from intraseasonal to
178 interannual, and relatively large spatial scales. We begin with a description of the large scale setting that has been well
179 established since Schott et al. (2009) (Section 2). We then consider the structure and propagation of variability in air-sea
180 interactions at seasonal and intra-seasonal scales, including the contribution of the mesoscale and the ocean's role in air-
181 sea interaction (Section 3). Section 4 discusses new advances in understanding of the upper ocean circulation, organised
182 by region (southern basin, equatorial and northern basin). This section includes an update of the near-surface circulation
183 maps of Talley et al. (2011), including recent work on boundary currents around Australia and Madagascar, and a
184 discussion of the biogeochemical variability observed in each region. The interocean connections with the Pacific, Atlantic
185 and Southern Oceans are discussed in Section 5. Section 6 describes the variability of the Indian Ocean circulation with
186 the recent advances in understanding the warming across the basin, climate modes such as the Indian Ocean Dipole,
187 connection with the El Niño-Southern Oscillation (ENSO), and Indian ocean marine heatwaves. Section 7 focuses on
188 multiscale processes in the Bay of Bengal as an "ocean laboratory", since there have been multiple international programs
189 in this Bay in the last decade. Recent advances from the large scales (>100 km) down to sub-mesoscales (100 m to 10 km)
190 and further down to mixing scales (mm) are discussed. We then link back from mixing to large scales via salinity budgets
191 and coupled phenomena such as the Madden-Julian Oscillation (MJO) to understand the complexity of these processes
192 across multiple scales. We end with a short summary and open questions that will need to be addressed over the next
193 decade.

194 **2 Large-scale setting**

195 The oceanic and atmospheric circulation of the Indian Ocean are unlike those in the Pacific and Atlantic oceans, largely
196 due to geography. The Asian landmass limits the northern extent of the Indian Ocean to around 25°N so that there is no
197 high-latitude cooling of the ocean, and consequently no dense water formation such as that seen in the North Atlantic and,
198 to some extent, the North Pacific. The intense seasonal variation in temperature over Asia drives the seasonal monsoons:
199 the southwest monsoon in boreal summer, and northeast monsoon in boreal winter. The timing of the onset of the monsoon,

200 and associated wet and dry periods in the Indian Ocean rim countries, varies considerably depending on a range of large-
201 scale climate modes and smaller-scale coupled ocean-atmosphere interactions. The seasonally-reversing winds drive
202 seasonally-reversing ocean currents in the northern Indian Ocean (Section 4.4), e.g. the southwest/northeast monsoon
203 current and the Somali Current. Equatorial currents in the Indian Ocean, eastward near the surface above westward
204 undercurrents (Section 4.3), provide rapid connection between the western and eastern basin and are also subject to
205 monsoon dynamics.

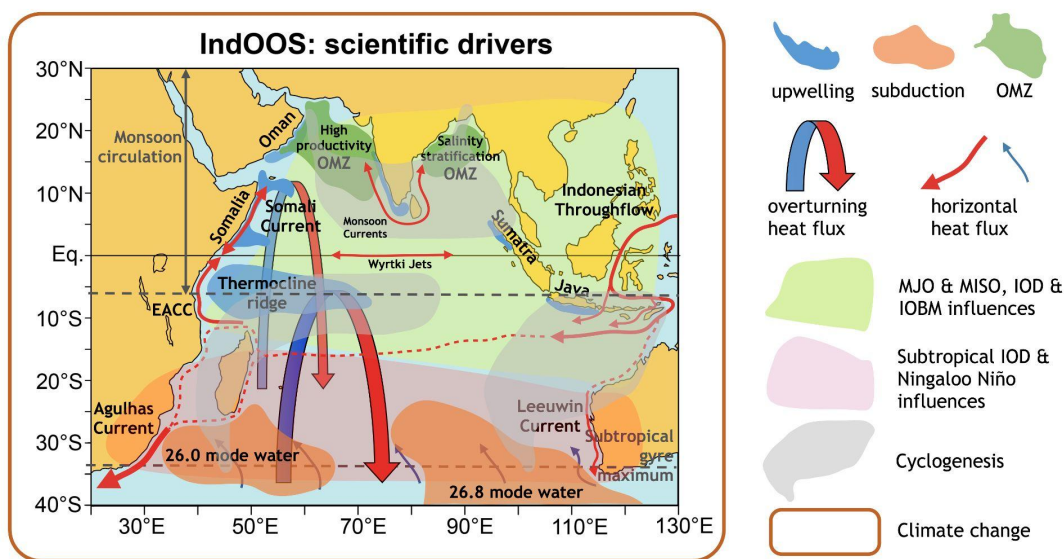
206 In the southern Indian Ocean (Section 4.2), the connection of the Indian and Pacific Oceans through the Indonesian Seas
207 also contributes to the unique circulation patterns. The very warm and fresh ITF water is funneled into the tropical southern
208 Indian Ocean and carried westward by the South Equatorial Current. The warm, fresh waters are much lighter than those
209 further south, creating a north-south density (pressure) gradient that drives near-surface broad, eastward geostrophic
210 currents between 16°S and 32°S and between Madagascar and Australia (Niiler et al., 2003). This pressure gradient also
211 generates the Leeuwin Current, a unique poleward-flowing eastern boundary current (Godfrey and Ridgway, 1985) that is
212 a downwelling region but is also, counter-intuitively, highly productive (Waite et al., 2007). These two features are not
213 found in the southeastern Atlantic and Pacific oceans. There, the eastern basin currents are characterised by a clear
214 subtropical gyre circulation with weak, equatorward flow and upwelling against the coast.

215 The tropical Indian Ocean (Section 4.3) is home to the largest fraction of sea surface temperature (SST) warmer than 28°C
216 (the tropical warm pool), and is therefore a key region for deep atmospheric convection: the upward part of the Walker
217 Circulation that drives cloud formation and precipitation over the tropical Indo-Pacific. Variation in SST is the primary
218 driver of variation in exchanges between the ocean and atmosphere and is thus a key focus in this paper. Sea surface
219 salinity effects on ocean-atmosphere exchanges have become better understood and are discussed throughout and in
220 particular in Section 7.

221 The tropical Indian Ocean sea surface temperature (SST) has warmed faster over the period since 1950 than either the
222 tropical Pacific or Atlantic (Han et al., 2014, Fox-Kemper et al., 2021), with implications for primary productivity (Roxy
223 et al., 2014, 2016). The Indian Ocean accounts for 50-70% of the total ocean heat uptake in the global upper (700 m) ocean
224 over the last decade, associated with anthropogenic warming (Lee et al., 2015). The deeper ocean (700-2000 m) is
225 warming across the globe with a robust signature of anthropogenic warming evident even in the short Argo record since
226 2005 (Wijffels et al. 2016, Rathore et al. 2020). Warming in the abyss is detectable and widespread, communicated from
227 the surface of the ocean along pathways from Antarctic Bottom Water formation regions (Purkey and Johnson, 2012).
228 Considerable variability in the Indian Ocean climate system exists on the backdrop of this strong, long-term warming
229 trend.

230 An extensive debate erupted in recent years about whether there was hiatus or a reduced rate of global warming
 231 (Lewandowsky et al. 2018). However, persistent cold anomalies in the eastern Pacific have been argued to have enhanced
 232 oceanic heat uptake, and the strengthened trade winds are consistent with this argument (Kosaka and Xie 2013, England
 233 et al. 2014). It has further been argued that the excess heat taken up by the tropical Pacific has been pumped into the Indian
 234 Ocean via the Indonesian throughflow (Lee et al. 2015). The tropical Indian Ocean is likely affected by the Southern
 235 Ocean trends at a rapid timescale of the order of a decade (Yang et al. 2020), and the Indian Ocean warming may accelerate
 236 the Atlantic meridional overturning circulation (Hu et al. 2019) and the Pacific response to anthropogenic forcing (Zhang
 237 et al. 2019). Based on these oceanic tunnels and atmospheric bridges into and out of the Indian Ocean, one could
 238 hypothesise that the Indian Ocean may be acting as the clearinghouse for oceanic warming under anthropogenic forcing.

239 Variability in the oceanic and atmospheric circulation of the Indian Ocean is the result of complex interactions that are
 240 both internal and external to the Indian Ocean. The recent review of the IndoOS plan (Beal et al., 2019, 2020) summarises
 241 the major scientific drivers, of which we still have limited understanding (Fig. 1). The over-arching signal is anthropogenic
 242 climate change, causing a background trend of ocean warming and increasing acidity due to uptake of heat and carbon
 243 dioxide and affecting the nature of large and small scale variability mechanisms.



244

245 **Figure 1: Schematic view of key phenomena in the Indian Ocean (from Beal et al. 2019).** The main scientific drivers
 246 of the Indian Ocean Observing System, including the Oxygen Minimum Zones (OMZs), upwelling and subduction
 247 zones, major heat flux components, the tropical modes of the Madden-Julian Oscillation (MJO), the Monsoon

248 **Intra-Seasonal Oscillation (MISO), the Indian Ocean Dipole (IOD) and Indian Ocean Basin Mode (IOBM), the**
249 **subtropical modes of Ningaloo Niño and subtropical IOD, cyclogenesis, and climate change.**

250 A net poleward flow of heat out of the Indian Ocean is accomplished by a combination of the horizontal circulation along
251 the boundaries, coupled with the Indian Ocean's part of the global meridional overturning circulation (MOC) and shallow
252 overturning cells. The ITF delivers heat from the Pacific into the Indian Ocean. The Agulhas Current moves heat rapidly
253 southward at surface and intermediate depths (Bryden and Beal, 2001), with 30% of Indian Ocean heat export thought to
254 be carried across 32°S by this gyre circulation (Talley, 2008). The shallow Leeuwin Current makes a smaller direct
255 contribution to the poleward flow of heat (Smith et al., 1991; Feng et al., 2003; Furue et al., 2017) but generates a rich
256 field of mesoscale eddies that carry heat and momentum into the Indian Ocean interior, contributing to heat export across
257 32°S (Domingues et al. 2006, Feng et al., 2007; Dilmahamod et al. 2018).

258 In the upper ocean, the shallow overturning consists of the cross-equatorial cell (Miyama et al. 2003; Schott et al. 2004)
259 and the subtropical cell (Schott et al. 2004). The ascending branches of these cells connect to different upwelling zones in
260 the southern and northern Indian Ocean and, therefore, play an important role in regulating the climatological mean,
261 seasonal, and interannual heat balance in the tropical Indian Ocean (Lee 2004; Lee and McPhaden 2008). At intermediate
262 depths (500-2000 m), mode waters of varying density enter the Indian Ocean from the Southern Ocean. Along their
263 northward path they mix with lighter waters above, progressively upwelling to the sea surface in a range of locations north
264 of 10°S to then return south in a widespread southward Ekman transport of near-surface waters (Schott et al., 2009). The
265 lower part of the mode water layer mixes with denser waters below and joins the southward flowing deep waters (2000-
266 4000 m). This southward flow also has a contribution from transformed abyssal waters: Antarctic Bottom Water moves
267 northward at abyssal depths, mixing with lighter waters above, progressively upwelling along its path from the Southern
268 Ocean to the Indian Ocean to return southward at shallower depths (Talley, 2013). Cross-equatorial flow is accomplished
269 both at abyssal levels and via the East Africa Coastal Current, seasonally reversing Somali Current (Schott et al., 2009)
270 and southward Ekman transport (Schott and McCreary, 2001).

271 The remaining elements of Fig. 1 refer to oxygen minimum zones (OMZ) in the Arabian Sea and Bay of Bengal and the
272 range of mechanisms that drive strong variations in sea surface temperature leading to shifts in atmospheric convection
273 and precipitation with major effects on rim countries. These mechanisms include: Madden-Julian oscillation (MJO) and
274 Monsoon Intraseasonal Oscillation (MISO), Indian Ocean Dipole (IOD), Indian Ocean Basin Mode, Subtropical IOD, and
275 Ningaloo Niño which are discussed further in Section 6. Cyclogenesis is not discussed in this synthesis. For discussion of
276 OMZ, the reader is referred to the review papers of McCreary et al. (2013) and Rixen et al. (2020).

277 Extreme precipitation in the Bay of Bengal and evaporation in the Red Sea and Arabian Sea lead to strong variability in
278 ocean salinity that in turn impacts ocean circulation and air-sea interaction. The surface salinity gradient in the northern

279 Indian Ocean decreases from the Arabian Sea in the west to the Bay of Bengal in the east. Strong evaporation over the
280 Arabian Sea results in highly saline surface waters (Antonov et al., 2010; Chatterjee et al., 2012), while surface waters in
281 the Bay of Bengal are comparatively fresh and highly stratified as a result of monsoon precipitation and outflow from river
282 systems such as the Ganges-Brahmaputra (Shetye et al., 1996; Vinayachandran et al., 2002). The surface forcing is
283 balanced by the seasonally reversing monsoon currents to maintain the climatological distribution of salinity.

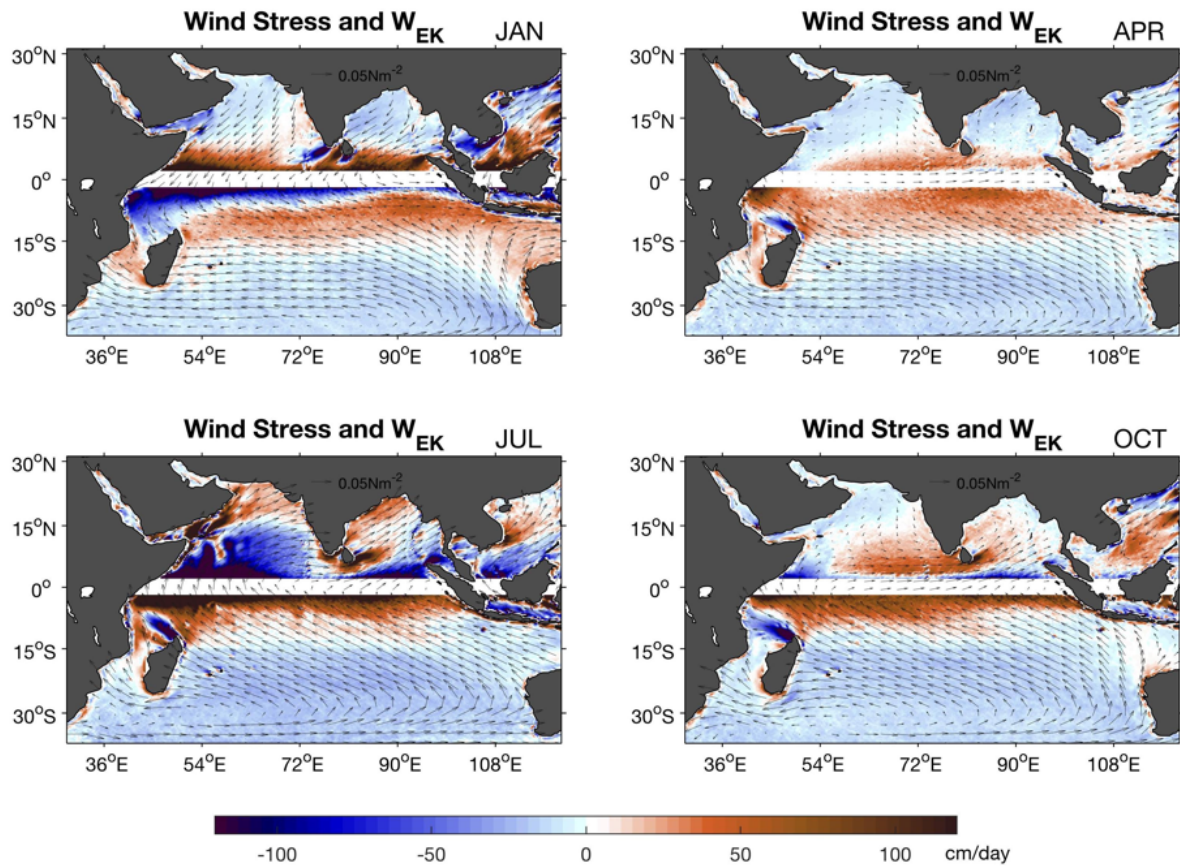
284 **3 Air-sea interactions**

285 The tropical Indian Ocean is highly variable across multiple scales, all of which involve atmosphere-ocean interaction:
286 from the locally intense heat and moisture fluxes that drives tropical cyclones to large-scale convection in the ascending
287 branch of the Hadley circulation, and basin scale ocean heat transport carried by overturning cells that contribute to decadal
288 variability and trends. At intermediate time scales, the intraseasonal oscillations involve strong air-sea coupling (e.g.,
289 Demott et al., 2015). The Indian Ocean Dipole (IOD) is an example of an inherently coupled mode of variability (Saji et
290 al., 1999, Webster et al. 1999, Murtugudde et al. 2000). The monsoonal rainfall around the Indian Ocean is largely fuelled
291 by warm SSTs and strong sea-to-air moisture fluxes. These phenomena emphasise the need to understand the mechanisms
292 of air-sea interaction within the Indian Ocean, with a particular focus on how these processes can be better represented in
293 models to aid predictions of variability in the Earth system.

294 **3.1 Seasonal cycle and the monsoons**

295 In the open ocean south of 10°S, the wind pattern throughout the year is southeasterly trade winds across the tropics and
296 subtropics and westerlies south of 35°S (Fig. 2). The evaporative cooling of the ocean surface by the trade winds leads to
297 high salinity throughout the subtropics. The curl of the wind stress drives year-round Ekman pumping (downwelling)
298 south of around 15°S (Fig. 2). Downwelling of these denser, high salinity surface waters supplies the downward limb of
299 the shallow Subtropical Cell, STC and Cross-Equatorial Cell, CEC (Schott et al. 2002; Miyama et al. 2003; Schott et al.,
300 2004; Lee 2004; Schott et al., 2009). The subsurface path of the shallow overturning is not well known, and the return to
301 the surface is in any of a number of upwelling zones including the Seychelles-Chagos Thermocline Ridge for the STC and
302 along Somalia, Oman and the west coast of India for the CEC. North of around 10°S, the winds over the Indian Ocean are
303 characterised by seasonal reversals due to the monsoons (Fig. 2), which in turn cause most of the near-surface currents in
304 these regions to seasonally reverse (Schott et al., 2009; Shankar et al., 2002, Section 4.4).

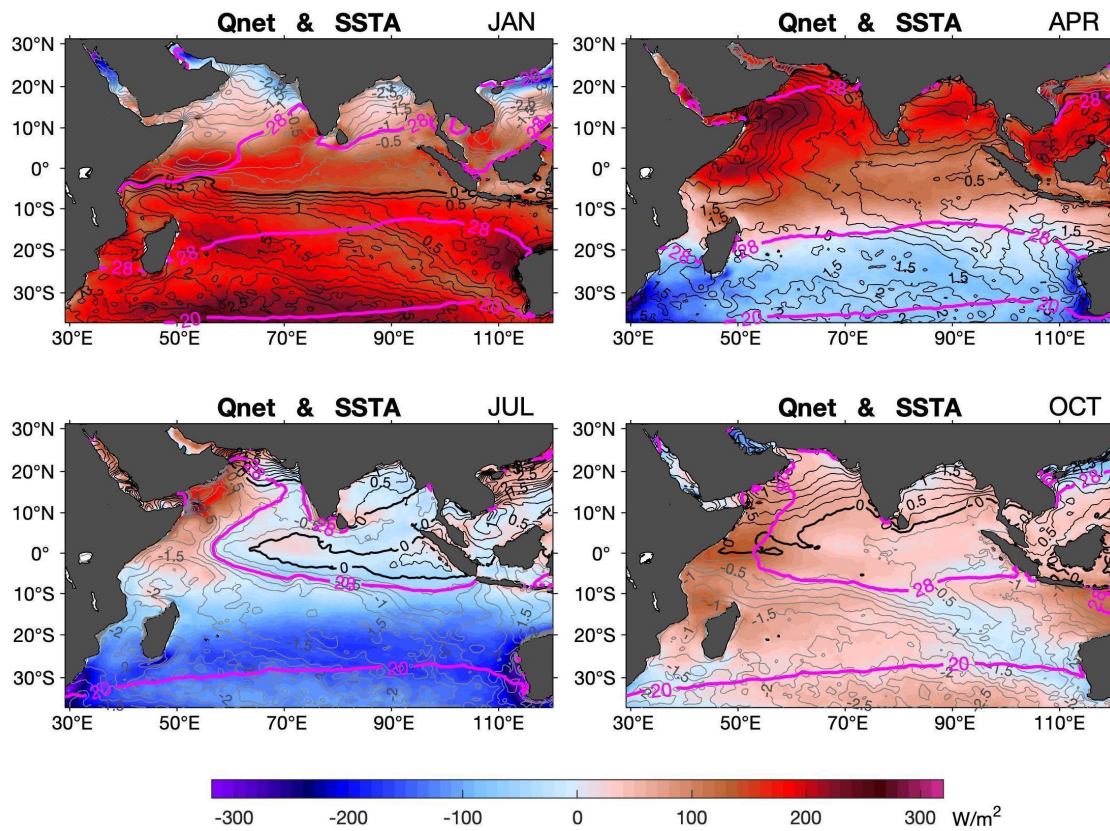
305



306

307 **Figure 2: Climatology (2001–2018) of monsoon wind stress (vectors) and Ekman pumping rate (colour shaded)**
 308 **with positive values denoting Ekman suction (upwelling) and negative values Ekman pumping (downwelling) for**
 309 **(a) January - NE monsoon, (b) April, (c) July - SW monsoon, and (d) October. The climatology was constructed by**
 310 **the Objectively Analyzed air-sea Flux High-Resolution (OAFlux-HR) analysis (adapted from Yu 2019).**

311 A strong positive correlation between seasonal net heat fluxes into the ocean and SST variability (Fig. 3) suggests that the
 312 seasonal cycle of SST is largely due to the seasonal cycle of winds and cloud cover (Yu et al., 2007). One prominent
 313 exception is the Seychelles-Chagos thermocline ridge (located between 5°S and 10°S and east of 50°E), where upwelling
 314 and horizontal advection exhibit substantial seasonal variations that in turn contribute to the seasonal cycle of SST (Hermes
 315 and Reason, 2008; Foltz et al., 2010). On the equator and to the north, seasonally reversing winds drive complex patterns
 316 of upwelling and downwelling that lead to complex SST variability.

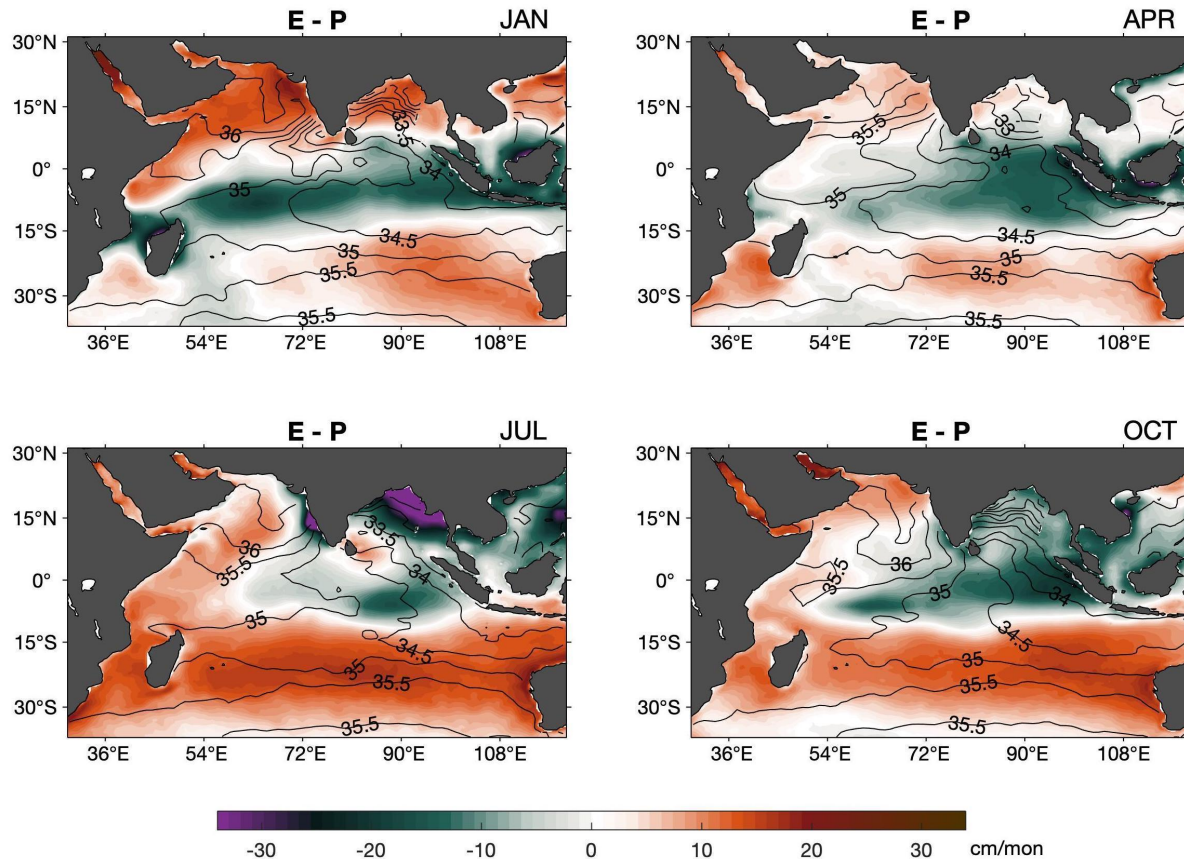


317

318 **Figure 3: Climatology (2001–2018) of ocean-surface net heat input (colour shaded; positive values denote ocean**
 319 **heat gain and negative values ocean heat loss), SST anomaly (black contours) and 20°C, 28°C SST contours (pink)**
 320 **for (a) January - NE monsoon, (b) April, (c) July - SW monsoon, and (d) October (adapted from Yu 2019). Net heat**
 321 **flux is the sum of solar radiation, longwave radiation, and turbulent latent and sensible heat fluxes. The turbulent**
 322 **heat flux climatology was constructed by the OAFflux-HR analysis and surface radiation climatology by the NASA**
 323 **CERES EBAF (Kato et al., 2013).**

324 In the Bay of Bengal and Arabian Sea, surface heat fluxes dominate the seasonal cycle of SST, with the exception of the
 325 upwelling zone along the western boundary of the Arabian Sea (Chowdary et al., 2015; Yu et al., 2007). However, salinity
 326 effects and subsurface processes (barrier layers, vertical entrainment, variations in the depth of penetration of solar
 327 radiation and zonal advection also influence SST variability (Thangaprakash et al., 2016). Rainfall variability driven by
 328 the monsoons creates near-surface salinity variability, most notably in the Bay of Bengal where there is a pronounced
 329 annual cycle of sea surface salinity (SSS; Fig. 4, Akhil et al., 2014). Freshwater input at the northern end of the Bay forms
 330 a shallow mixed layer stratified by low salinity and is advected southwards along the east coast of India, where it is
 331 eventually eroded by vertical mixing (Akhil et al., 2014). The variability in freshwater input contributes to the seasonal

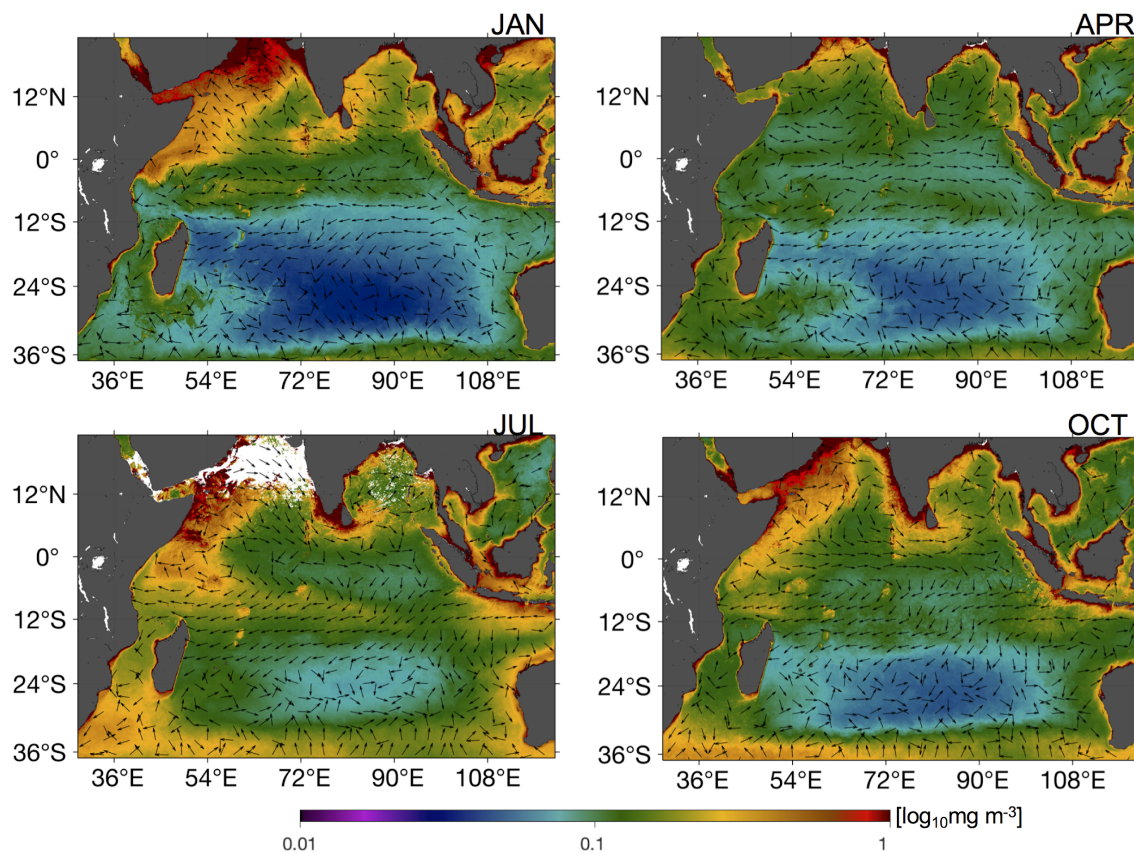
332 cycle of barrier layer thickness in the Bay of Bengal (Howden and Murtugudde, 2001; Thadathil et al., 2007), which in
333 turn modulates how strongly SST responds to surface forcing (Li et al., 2017). The seasonally reversing currents that
334 connect the salty Arabian Sea and fresh Bay of Bengal also strongly influence sea surface salinity patterns (Section 4.1.3).



335
336 **Figure 4: Climatology (2001–2018) of evaporation minus precipitation (colour shaded; positive values denote**
337 **freshwater leaving the ocean and negative values addition of fresh water to the ocean) and sea surface salinity**
338 **(black contours) for (a) January - NE monsoon, (b) April, (c) July - SW monsoon, and (d) October (adapted from**
339 **Yu 2019).**

340 The seasonal cycles in the atmosphere and ocean circulation strongly influence the biological productivity of the near-
341 surface Indian Ocean (Wiggert et al. 2006). Fig. 5 shows the seasonal cycle of satellite chlorophyll *a* and surface currents.
342 The dramatically low productivity in the subtropics, where wind stress curl drives large-scale downwelling (Fig. 2), and
343 highly productive coastal boundaries where wind-driven upwelling occurs, highlights the impact of the circulation and
344 atmosphere-ocean interaction on biological productivity. In turn, the chlorophyll *a* distribution has important implications
345 for air-sea interaction, since higher concentrations of phytoplankton lead to increased absorption of solar radiation (e.g.,

346 Morel and Antoine, 1994; Murtugudde et al. 2002; Giddings et al. 2021). Organisation of chlorophyll *a* at intraseasonal
347 timescales has also been reported (Section 3.2.1).



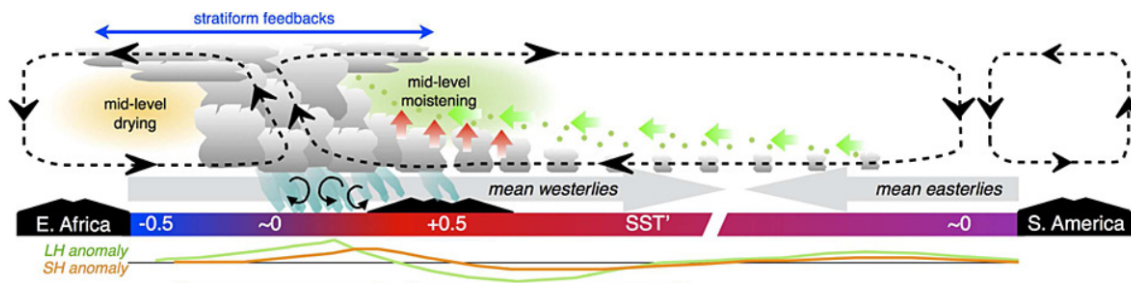
348
349 **Figure 5: Climatology (2002-2018) of chlorophyll-a concentrations (colormap) and current velocities (arrows) for**
350 **(a) January (b) April (c) July (d) October. Chlorophyll a climatology was obtained from the MODIS-Aqua product**
351 **and current velocities were obtained from the third-degree Ocean Surface Current Analysis Real-time (OSCAR)**
352 **product.**

353 3.2 Intraseasonal air-sea interaction

354 3.2.1 Madden-Julian Oscillation - MJO

355 The Madden-Julian Oscillation (MJO; Madden and Julian, 1972, 1971) is the dominant mode of variability in the Indian
356 Ocean at subseasonal time scales. The MJO (Fig. 6) is characterised by eastward-propagating features of enhanced and
357 reduced convection over distances of more than 10,000 km and with a periodicity of around 30–60 days (Zhang, 2005).

358 The MJO propagates slowly ($\sim 5 \text{ m s}^{-1}$) through the portion of the Indian and Pacific Oceans where the sea surface is
 359 warm, constantly interacting with the underlying ocean and influencing many weather and climate systems. Within the
 360 large-scale envelopes of enhanced convection, smaller-scale clusters of clouds propagate westward, and can produce local
 361 extremes in rainfall. Air-sea interaction is believed to sustain, and perhaps amplify, the patterns of enhanced and reduced
 362 convection as the MJO propagates eastward (Demott et al., 2015). Indo-Pacific warming trends are warping the life cycle
 363 of the MJO, which is spending less time over the Indian Ocean, more time over the Pacific and altering mean rainfall
 364 trends in parts of the globe (Roxy et al, 2019).



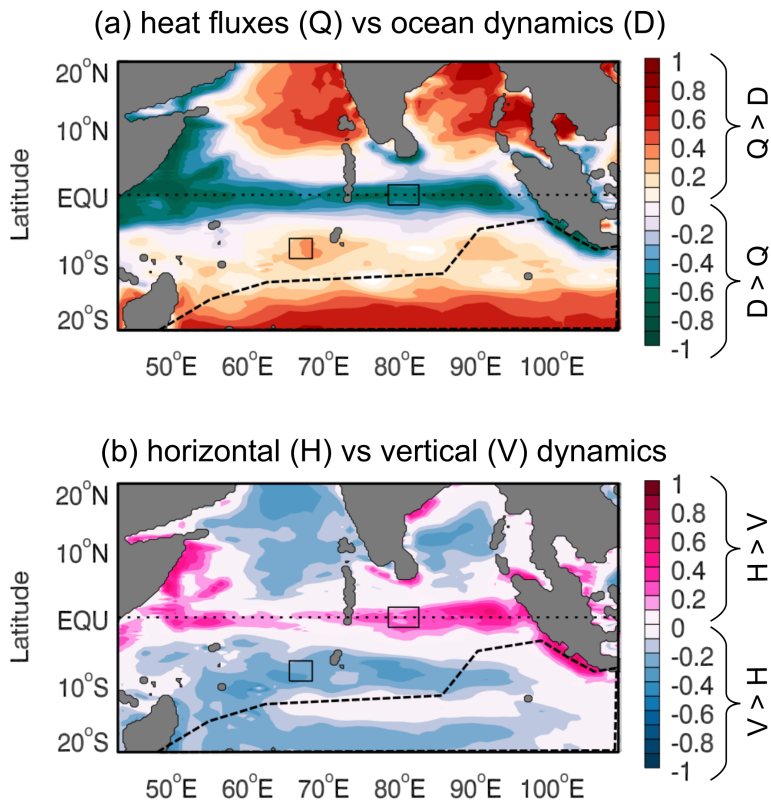
365
 366 **Figure 6: Schematic depiction of Indian and Pacific Ocean feedbacks to the MJO when convection (gray cloud**
 367 **elements) is maximized in the eastern Indian Ocean. Rainfall (aquamarine), circulation anomalies (black dashed**
 368 **cells), convective downdrafts (black rotor arrows), mean winds (faint gray arrows), and moistening by convective**
 369 **detrainment (small green dots) and horizontal and vertical advection (thick green and red arrows, respectively) are**
 370 **overlaid. Net moistening (drying) is shaded green (orange). Positive (red) and negative (blue) SST anomalies for a**
 371 **strong event are shaded, while latent (sensible) heat flux anomalies are shown with green (orange) curves. Central**
 372 **and East Pacific spatial scale is compressed relative to the Warm Pool. Adapted from DeMott et al. (2015).**

373 The MJO-related pattern of winds results in anomalous westerly (easterly) winds to the west (east) of the region of
 374 convergence, convection and enhanced rainfall (Fig. 6). These winds generate Kelvin and Rossby waves along the Equator.
 375 The Kelvin waves generated by the MJO have been hypothesised (Kessler et al, 1995; McPhaden 1999; Bergman et al.
 376 2001) to trigger ENSO events in the Pacific. In the Indian Ocean, there is a distinctive sequence of basin-scale ocean waves
 377 generated by the MJO. Eastward-propagating equatorial ocean Kelvin waves strike the coast of Sumatra, where they
 378 generate coastally-trapped Kelvin waves that propagate northward and southward away from the generation site. Kelvin
 379 waves also propagate into the Indonesian seas where they affect the ITF (Pujiana and McPhaden, 2020). Westward-
 380 propagating equatorial ocean Rossby waves are also formed, either due to direct intraseasonal wind forcing or through
 381 reflection of Kelvin waves at the eastern boundary (Oliver and Thompson, 2010; Webber et al., 2010; Nagura and
 382 McPhaden, 2012; Pujiana and McPhaden, 2020). These waves influence local upwelling and currents; they have been
 383 linked to variability in coastal currents around the Bay of Bengal (Vialard et al., 2009), to enhancement of the spring
 384 Wyrтки jets in the eastern equatorial Indian Ocean (Prerna et al., 2019), to changes in subsurface equatorial currents in the

385 central Indian Ocean (Iskandar and McPhaden, 2011) and to changes in upwelling and chlorophyll a concentration in the
386 off-equatorial central Indian Ocean (Webber et al., 2014). Such waves also propagate energy downwards into the deep
387 ocean (e.g., Pujiana and McPhaden, 2020), contributing to deep ocean variability at multiple time scales (e.g., Matthews
388 et al., 2007). Downwelling Rossby waves in the western Indian Ocean create positive SST anomalies through a
389 combination of reduced entrainment of cooler water from below and zonal advection (Rydbeck et al., 2017; Webber et al.,
390 2012b). These waves therefore act as a triggering mechanism for new MJO events (Rydbeck and Jensen, 2017; Webber
391 et al., 2010, 2012b, 2012a), and may also play a role in amplifying existing MJO events.

392 MJO-related winds also lead to variability in mixing within and at the bottom of the mixed layer. Westerly wind bursts
393 generate zonal currents that create strong vertical current shear (Moum et al., 2014). These currents and the associated
394 mixing persist after the passage of the atmospheric disturbance. Cooler waters from below the surface are mixed with
395 surface waters, leading to a reduction in available ocean heat content for the next MJO event and thus reducing its potential
396 amplitude (Moum et al., 2016). By examining the causes of SST variability in two separate MJO events, McPhaden and
397 Foltz (2013) showed that the presence or absence of barrier layers may play a crucial role in determining how strongly
398 mixing and vertical entrainment influence SST. They also found that zonal advection plays a relatively stronger role when
399 a barrier layer is present. Chi et al. (2014) confirmed the importance of barrier layers in influencing the turbulent heat flux,
400 but found that thin barrier layers can be eroded by strong current shear that occurs during active phases of the MJO. Wind
401 mixing and surface heat and freshwater fluxes both contribute in roughly equal proportions to intraseasonal variability in
402 mixed layer depth (Keerthi et al., 2016).

403 Various studies have investigated the relative importance of surface heat fluxes and subsurface ocean processes for the
404 evolution of SST at intraseasonal time scales. The Seychelles-Chagos Thermocline Ridge (SCTR), is a region of high
405 intraseasonal SST variability (Saji et al. 2006, Hermes and Reason, 2008). Several observational studies have concluded
406 that the SST variability here is predominantly generated by variability in surface heat fluxes (Jayakumar et al., 2011;
407 Vialard et al., 2008), while Drushka et al. (2012) suggest this finding applies across most of the tropical Indian Ocean.
408 Such studies, however, typically exhibit large uncertainty in the subsurface ocean terms. The shallow thermocline and
409 strong high frequency winds in the SCTR region enhance near-inertial waves and lead to strong mixing at the base of the
410 mixed layer as well as in the thermocline (e.g. Cuypers et al. 2013; Sabu et al. 2021). Modelling studies have shown that
411 ocean dynamics play an important role in generating SST variability (Halkides et al., 2015; Han et al., 2007). For example,
412 Fig. 7 from the study of Halkides et al. (2015) shows the relative contribution of modelled ocean dynamical processes and
413 thermodynamical processes (i.e., surface heat fluxes) in forcing intraseasonal SST variability. Fig. 7a shows that ocean
414 dynamical processes (green shading), including horizontal and vertical advection, are the dominant source of intraseasonal
415 SST variability on the equator and in upwelling regions off Indonesia, Sri Lanka and along the western boundary. The
416 ocean dynamical processes are in turn dominated by horizontal advection along the equator and tropical coastlines (Fig.
417 7b, pink shading), and vertical advection (blue shading) in the off-equatorial ocean interior.



418

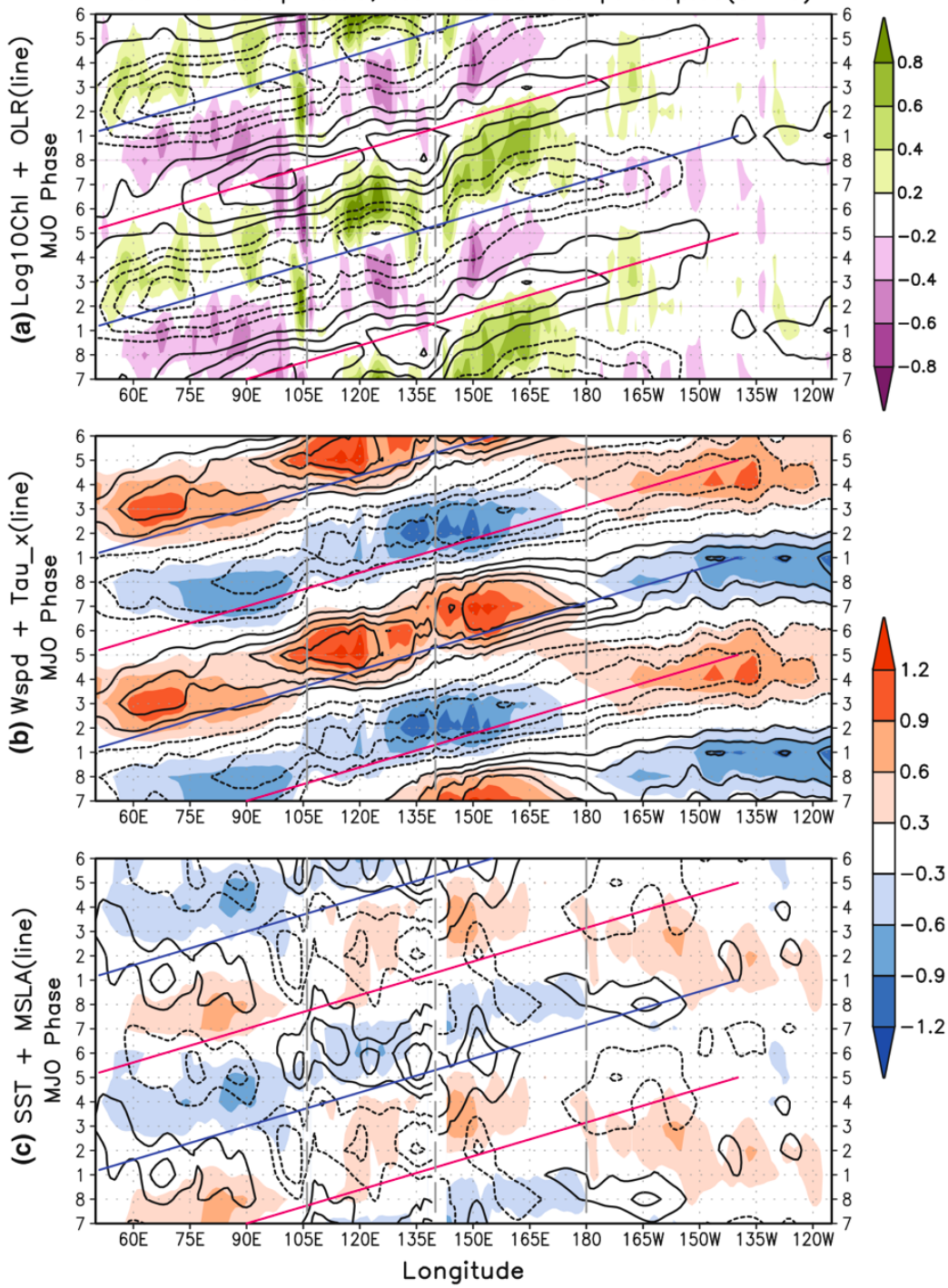
419 **Figure 7: Modelled balance of processes driving intraseasonal SST variability. (a) Relative role of heat fluxes (Q)**
 420 **and ocean dynamics (D) in driving SST variability, with red (green) colours implying Q (D) dominates forcing, (b)**
 421 **Relative role of horizontal (H) and vertical (V) processes in the dynamical forcing, with pink (blue) colours implying**
 422 **that H (V) processes dominate. All fields are derived from the ECCO-JPL ocean state estimate. The dotted line**
 423 **marks the Equator, dashed line in the southern hemisphere outlines a region in which the model does not fully**
 424 **resolve the ocean heat budget, and the boxes on the Equator and at 10°S mark regions for further analysis not**
 425 **described here. Modified from Halkides et al. (2015).**

426 Organisation of chlorophyll a at intraseasonal timescales has also been reported, with model studies indicating potential
 427 biophysical feedbacks due to the variability of penetrative radiation into the water column (Waliser et al. 2005, Jin et al.
 428 2013a; Giddings et al., 2021). In the Bay of Bengal, the proportion of incoming solar radiation absorbed within the mixed
 429 layer varies between 60% and 97% due to a combination of variability in chlorophyll a concentration and mixed layer
 430 depth (Lotliker et al., 2016) and an increase in chlorophyll of 0.3 mg/m³ can lead to SST increase of up to 0.35°C on
 431 intraseasonal time scales (Giddings et al., 2021). Representing the seasonal cycle of chlorophyll a concentration in the
 432 Arabian Sea in a coupled model led to substantial changes in the simulated SST and monsoon rainfall over India (Turner

433 et al., 2012), suggesting that incorporating this process into coupled models may be important to improve simulation of
434 monsoon rainfall and circulation around the Indian Ocean.

435 Figure 8 illustrates propagation of surface patterns in an MJO composite constructed by Jin et al. (2013a). In each panel
436 the peak in outgoing longwave radiation (OLR, a proxy for convection) is indicated by a red diagonal line. The MJO
437 generates substantial surface heat flux anomalies that create a pattern of surface heat fluxes and SST anomalies such that
438 warm (cool) SSTs lead enhanced (reduced) convection by a quarter of a phase (e.g., Shinoda et al., 1998). The MJO also
439 leads to low-frequency rectifications in the mean state of physical and ecosystem responses (Fig. 8, Waliser et al. 2003,
440 Jin et al., 2013a,b).

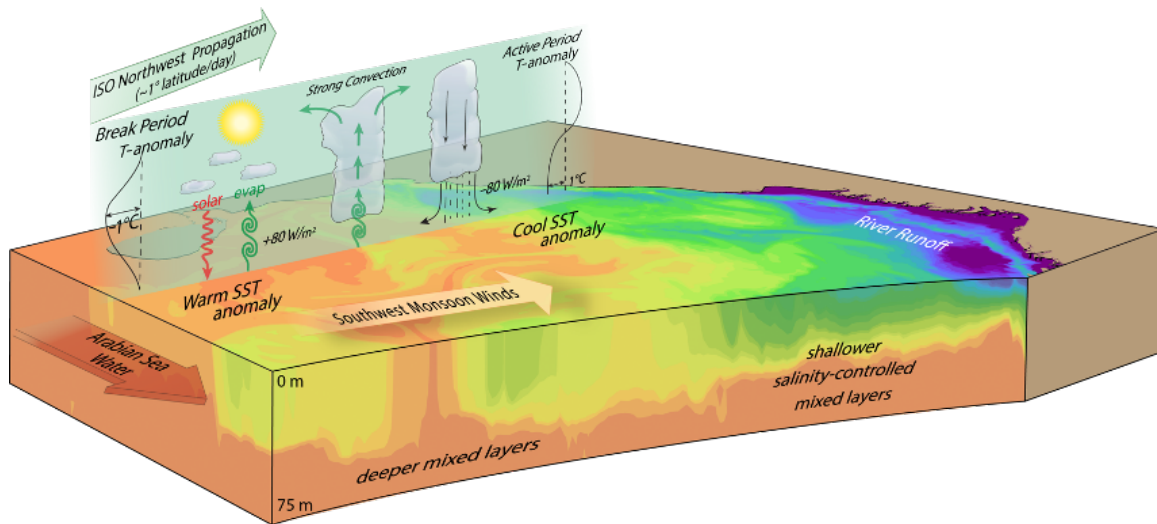
98~10 NovApr MJO, Normalized Comp. Tropics(3~7S)



442 **Figure 8: MJO composite evolution for the Boreal winter (Nov-Apr) averaged over latitudes 3°–7°S for the period**
443 **of November 1st, 1997 to October 31st, 2010, of a) $\text{Log}_{10}\text{Chl}$ from SeaWIFS satellite observations (shaded) and**
444 **satellite-derived outgoing longwave radiation (contour), b) wind speed (shaded) and zonal wind stress (contour),**
445 **both from the cross-calibrated multi-platform (CCMP) dataset, and c) NOAA-OI satellite SST anomalies (shaded)**
446 **and AVISO mean sea level anomaly (contour). All contour intervals match shading levels in (c), and solid (dash)**
447 **line indicates positive (negative) values. All variables are normalised, and the same MJO composite is repeated for**
448 **two cycles for convenience. There are between 127-227 events in the composite for each MJO phase. Red diagonal**
449 **lines indicate peak signals of positive OLR, and blue lines indicate negative OLR peak, so these are guides for the**
450 **MJO propagation. The relative location of each propagation line in all panels is the same. Left and center gray**
451 **vertical dashed line indicates the western and eastern boundary of the Maritime Continent, and the right gray line**
452 **is on the Dateline where chlorophyll a propagation stops. From Jin et al. (2013a).**

453 **3.2.2 Monsoon Intraseasonal Oscillation - MISO**

454 While the MJO dominates intraseasonal variability during October to April, during May to September (boreal summer,
455 southwest monsoon), the Monsoon Intraseasonal Oscillation (MISO; Goswami, 2012; Suhas et al., 2013) dominates. The
456 dominant timescale for MISOs is 30-60 days but MISOs can also occur on 10-20 day time scales (Goswami et al, 2016)
457 and there are studies that have identified a 3-7 day time scale for MISOs (e.g. Roman-Stork et al, 2020). MISOs can be
458 seen as low pressure systems laden with moisture which deliver rain from atmospheric instabilities (Fig. 9). The MISO is
459 also known as the Boreal Summer Intraseasonal Oscillation (BSISO; Lau and Waliser, 2012; Lee et al., 2013). The MISO
460 oscillations are dynamically linked to the equatorial MJO (e.g., Sperber and Annamalai, 2008), but exhibit northeastward
461 and northwestward propagating features, with the main centre of action being the Bay of Bengal. These northward-
462 propagating bands of enhanced and reduced rainfall exhibit a similar relationship with SST to the MJO: warm SST leading
463 increased rainfall (cool SST leading reduced rainfall) that then determine the wet/dry (or active/break) cycles of the South
464 Asian monsoon (Vecchi and Harrison, 2002; Roxy et al., 2013; Suhas et al., 2013; Zhang et al., 2018). These SST
465 anomalies are primarily forced by variations in surface heat fluxes in the Bay of Bengal (Girishkumar et al., 2017; Vialard
466 et al., 2012), while variations in wind-induced mixing, Ekman pumping and entrainment drive SST variability in the
467 Arabian Sea (Duncan and Han, 2012; Vialard et al., 2012).



468

469 **Figure 9: A schematic of the Monsoon Intraseasonal Oscillation (MISO) in the Bay of Bengal, showing the coupled**
 470 **ocean-atmosphere 30–60 day mode northwestward propagation and associated processes in the atmosphere and**
 471 **the ocean. (From Mahadevan et al., 2016a).**

472 Simulations of the MISO are still generally poor in state-of-the-art coupled models (e.g., Goswami et al., 2013; Jayakumar
 473 et al., 2017; Sabeerali et al., 2013; Sharmila et al., 2013) and re-analysis products (e.g. Sanchez-Franks et al., 2018).
 474 Evidence exists from observations of low-level convergence and OLR, as well as from forced atmospheric and coupled
 475 ocean-atmosphere model experiments, that both MJOs and MISOs are phenomena that require coupling between the ocean
 476 and atmosphere to exist. This is even though the scales of SST anomalies tend to be an order of magnitude smaller than
 477 the scales of the propagating atmospheric systems (Waliser et al., 1999; Zhou and Murtugudde, 2009). Including air-sea
 478 coupling in simulations of the MISO has been identified as key to improving simulation of this oscillation in some models
 479 (e.g., Jayakumar et al., 2017; Li et al., 2018; Roxy et al., 2013; Sharmila et al., 2013), and has been shown to improve
 480 aspects of simulation in others (e.g., Bellon et al., 2008; Peatman and Klingaman, 2018).

481 While new theories continue to be proposed for MJOs (e.g., Wang et al., 2016), MISOs have not received similar attention
 482 likely due to their more local nature compared to the global impacts of MJOs (e.g. their impact on ENSO). The mechanism
 483 that causes the northward propagation of the MISO is still a topic of research. The most recent theory for MISOs proposed
 484 by Zhou et al. (2017a, b) invokes an explicit coupling between the ocean and the atmosphere in a so-called Central Indian
 485 Ocean mode. Zonal winds at intraseasonal timescales over the Indian Ocean are argued to be coupled to SSTs to produce
 486 a barotropic instability in the meridional gradient of the zonal winds. The horizontal atmospheric eddy fluxes generated
 487 by the barotropic instability are invoked to explain the northward propagation and the advection of momentum and
 488 moisture as a coupled phenomenon. Key questions remain about the oceanic and air-sea interaction processes that

489 reorganise the SSTs in the Central Indian Ocean mode as well as the respective roles of the vertical and horizontal shears
490 in driving northward propagation of MISOs.

491 Observations and models indicate that MISOs may be slowing down because of the warming in the Indian Ocean
492 (Sabeerali et al., 2013), which needs to be understood better for providing reliable monsoon predictions and projections in
493 this climate vulnerable region. This is underscored by the observational evidence that climate variability and change are
494 increasing the frequency of dry spells and the intensity of wet spells in the Indian summer monsoon, which are directly
495 related to MISO (Singh et al., 2014).

496 **3.2.3 Intraseasonal drivers of heavy rainfall**

497 As the MJO season begins to wind down in April, northward propagating MISOs begin to become dominant in the northern
498 Indian Ocean, north of around 5°N. While the southwesterlies produce some of the strongest coastal upwelling off Somalia
499 and cool the Arabian Sea, the Bay of Bengal remains warm and largely above the convective threshold (28°C) owing to
500 the freshwater input from rainfall as well as rivers discharging into the Bay (Roxy and Tanimoto, 2007). The freshwater
501 input creates a shallow density stratification (barrier layer) within the temperature mixed layer and thereby weakens the
502 upwelling of cold water from the thermocline. MISOs deliver rain from atmospheric instabilities, but what controls the
503 rainfall at intraseasonal timescales during the summer can be expected to be region specific with moisture supply
504 determining the rainfall variability over land (Pathak et al., 2017).

505 Over the ocean, the largely evaporative Arabian Sea is relatively cool but the southwesterlies begin to slow down as they
506 approach the Western Ghats mountain range on the west coast of India, leading to maximum rainfall there during the
507 boreal summer monsoon season (Xi et al., 2015). Rather counterintuitively, the warm SST in the Bay of Bengal remains
508 above the convective threshold (Gadgil et al., 1984; Roxy, 2013) and yet, the ocean is not in direct control of the
509 intraseasonal rainfall events. Once the SSTs are warm enough to support atmospheric convection, it is baroclinic
510 instabilities, and not static instabilities induced by warm SSTs, that drive the majority of rainfall over the Bay of Bengal
511 (Xi et al., 2015).

512 **3.3 Ocean internal variability impacts on air-sea interaction**

513 Mesoscale eddies are ubiquitous in the ocean. In the tropical Indian Ocean, however, linear dynamics dominate and the
514 impacts of eddies are (or seem) small. While the Indian Ocean has the largest SST variability occurring at seasonal
515 timescales, strong mesoscale variability is also observed along the Somali coast where the western boundary current
516 crosses the Equator. The slope of the East African coastline and the equatorial crossing of the low-latitude jet produce
517 multiple eddies (Nof and Olson, 1993), which are shown to generate strong air-sea coupling at mesoscales (Schott and
518 McCreary, 2001; Schott et al., 2009; Vecchi et al., 2004; Seo et al., 2008). Some intraseasonal oscillations in the ocean

519 were reported in the southwestern tropical Indian Ocean (Kindle and Thompson, 1989) but generally, the impact of ocean
520 internal variability on SSTs in the tropical Indian Ocean has not been widely studied. At the eastern boundary of the
521 subtropical Indian Ocean, instability of the poleward Leeuwin Current generates a rich field of mesoscale eddies that carry
522 heat into the Indian Ocean interior, contributing to air-sea exchange of heat and the oceanic interior poleward heat transport
523 (Domingues et al. 2006, Feng et al., 2007; Dilmahamod et al. 2018). In the subtropical southeast Indian Ocean, mesoscale
524 eddies, and possibly annual and semiannual Rossby waves propagating from the eastern boundary, were found to influence
525 the seasonal variation of the surface layer heat balance through horizontal advection (Cyriac et al. 2019).

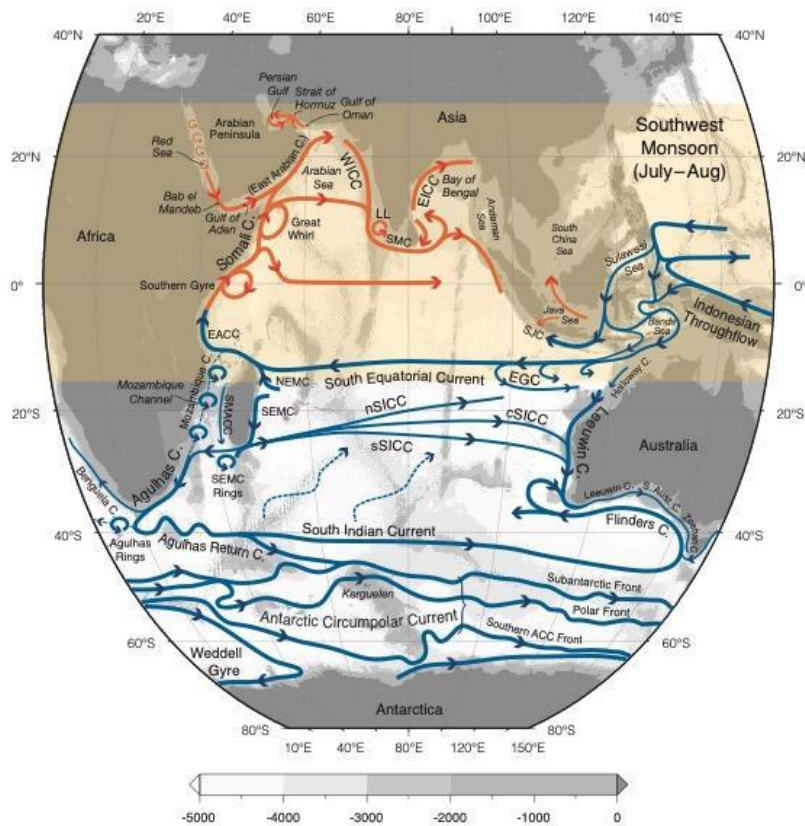
526 Low-frequency internal variability is also possible. Jochum and Murtugudde (2004) performed forced ocean model
527 experiments with climatological forcing alone to demonstrate that significant low-frequency variability at interannual
528 timescales is generated in the Indian Ocean by mesoscale eddies and other types of nonlinearity. The role of internal
529 variability in regional coupled climate variability as well as ecosystem and biogeochemistry remain interesting problems
530 for this already warm ocean, in which even small SST anomalies can be important for generating large-scale ocean
531 atmosphere interactions (Palmer and Mansfield, 1994).

532 **4 Upper Ocean Circulation and Biogeochemical Variability**

533 **4.1 Overview**

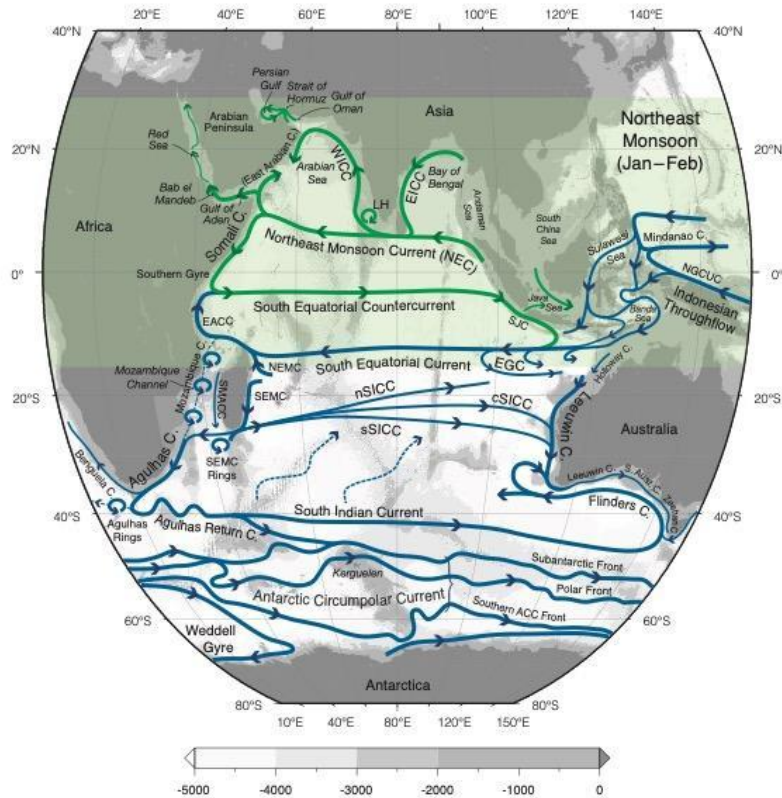
534 The near surface circulation in the Indian Ocean consists of the monsoon-dominated, seasonally reversing currents north
535 of around 10°S, and the steady currents to the south, as illustrated in Fig. 10a for the southwest monsoon (July-August)
536 and Fig. 10b for the northeast monsoon (January-February). This figure has been updated from Talley et al. (2011) to
537 recognise recent advances in understanding of circulation patterns. In the northern Indian Ocean, additions are a revision
538 of the Red Sea circulation (Menezes et al., 2019). In the southern Indian Ocean, moving in an anti-clockwise direction
539 from the Maritime Continent, additions are: 1) seasonally reversing flows in the Java Sea; 2) the Holloway Current along
540 Australia's Northwest Shelf (Holloway and Nye, 1985; Holloway, 1995; Brahmanpour et al., 2016); 3) revised position
541 of the salinity-driven Eastern Gyral Current that flows eastward from around 90°E along approximately 15°S, recirculating
542 Indonesian Throughflow Water from the South Equatorial Current and supplying the poleward-flowing Leeuwin Current
543 (Meyers et al., 1995; Domingues et al., 2007; Menezes et al., 2013, 2014); 4) the near-surface South Indian Countercurrent
544 with 3 distinct branches, northern, central and southern, flowing from the southern tip of Madagascar to Australia where
545 they merge with the poleward-flowing Leeuwin Current (Menezes et al., 2014 and references therein); and 5) the splitting
546 of the Flinders Current near 110°E, with one branch recirculating back toward Australia, and the other a westward
547 continuation of the Flinders Current, previously not shown (Duran et al., 2020).

548



549

550 **Figure 10a: Schematic near-surface circulation during the Southwest Monsoon (July-August). Blue: year-round**
 551 **mean flows with no seasonal reversals. Orange: monsoonally reversing circulation (after Schott & McCreary,**
 552 **2001). The ACC fronts are taken directly from Orsi, Whitworth, and Nowlin (1995). Acronyms: EACC, East**
 553 **African Coastal Current; NEMC, Northeast Madagascar Current; SEMC, Southeast Madagascar Current;**
 554 **SMACC, Southwest Madagascar Coastal Current; WICC, West Indian Coastal Current; EICC, East Indian**
 555 **Coastal Current; LH and LL, Lakshwadeep high and low; SJC, South Java Current; EGC, Eastern Gyral Current;**
 556 **SICC, South Indian Countercurrent (south, central and southern branches); NEC, Northeast Monsoon Current.**
 557 **Updated from Talley et al. (2011), originally based on Schott and McCreary (2001). The light gray shading shows**
 558 **seafloor bathymetry.**



559

560 **Figure 10b: Schematic near-surface circulation during the Northeast Monsoon (January-February). Details as for**
 561 **Fig. 10a.**

562 The intermediate and deep circulation and overturning cells will not be examined in this synthesis. The reader is referred
 563 to Talley et al. (2011) and references therein, and in addition, Nagura and McPhaden (2018) who used Argo and CTD data
 564 to map out the circulation and water masses in density classes associated with the shallow overturning circulation, with
 565 emphasis on the southern hemisphere. There has been some progress on understanding circulation at intermediate and
 566 deeper depths in the equatorial band, which is summarised in Huang et al (2018).

567

568 4.2 Southern Indian Ocean

569 4.2.1 South Equatorial Current

570 The South Equatorial Current (SEC), the northern limb of the southern Indian Ocean subtropical gyre, carries Indonesian
 571 Throughflow (ITF) waters into the interior Indian Ocean, flowing westward between 10–20°S (Fig. 10a and 10b). Upon

572 reaching the northern tip of eastern Madagascar, it bifurcates and supplies the Northeast Madagascar Current (NEMC;
573 Schott and McCreary, 2001; Song et al., 2004; Valsala and Ikeda, 2007) and the Southeast Madagascar Current (SEMC)
574 and contributes to the development of Mozambique Channel eddies. The mean flow through the Mozambique Channel is
575 weak (Song et al., 2004), although there is an indication from ocean model results that the eddy-dominated flow contributes
576 on the order of 20 Sv southward (Durgadoo et al., 2013). The Mozambique Channel eddies, eddies from the SEMC and
577 recirculation combine to feed into the Agulhas Current (Schott and McCreary, 2001).

578
579 Between 50 and 80°E the SEC is coincident with the southern half of the Seychelles-Chagos Thermocline Ridge (SCTR,
580 Vialard et al., 2009). The SCTR is characterized by a relatively shallow thermocline and thin mixed layer (~30m) across
581 the southern tropical Indian Ocean in the latitude band 5-15°S. Between 50 and 80°E the SCTR/SEC is a region of
582 significant upwelling (Hermes and Reason, 2008; Vialard et al., 2009; Resplandy et al., 2009; Dilmahamod, 2014), which
583 affects biogeochemistry, and even fisheries (Resplandy et al., 2009; Robinson et al., 2010; Dilmahamod, 2014).

584
585 In the eastern IO, the intraseasonal variation of the SEC is mostly attributed to the baroclinic instability of the mean current
586 (Feng and Wijffels, 2002), which is important for the meridional heat transport in the region and contributes to the demise
587 of Indian Ocean Dipole events (Ogata and Masumoto, 2011; Yang et al. 2015). Barotropic instability of the SEC has also
588 been proposed to be a key mechanism for generating intraseasonal variability (Yu and Potemra, 2006). These intraseasonal
589 signals propagate westward as Rossby Waves, influencing the SEC variability in the western Indian Ocean (Zhou and
590 Murtugudde, 2008).

591
592 Interannual variability in the ITF due to ENSO, IOD and other influences is communicated into the interior Indian Ocean
593 along the SEC and via Kelvin and Rossby waves (Godfrey, 1989, 1996; Meyers et al., 1995; Meyers, 1996; Wijffels and
594 Meyers, 2004). Pressure anomalies associated with ENSO and IOD are communicated through the Indonesian seas as
595 Kelvin and Rossby waves. These anomalies propagate westward into the Indian Ocean as Rossby waves. At the same time
596 the pressure anomalies drive variations in ITF and SEC transport and induce temperature/salinity variability via advection.
597 Geostrophic transport variability in the long-time repeat XBT line IX1 shows that the SEC is stronger during La Niña and
598 positive Indian Ocean Dipole events (Meyers, 1996; Liu et al., 2015). Similarly, the Pacific Decadal Oscillation alters the
599 SEC and ITF transports and associated water properties (Section 6.1). During the climate change hiatus period of 2000-
600 2011, the enhanced heat transport of the SEC/ITF was a key mechanism for the fast warming trend in the southern
601 subtropical Indian Ocean (Section 6.1).

602

603 4.2.2 Western Boundary

604 The Agulhas Current (Fig. 10) has long been known as one of the strongest western boundary currents in the global oceans,
605 with an average transport of 75 Sverdrups and current speeds in excess of 2 m s^{-1} (Beal et al., 2015; Beal et al., 2011).
606 The Agulhas Current plays a vital role in the global thermohaline circulation, advecting warm, salty, subtropical water
607 southwards, following the continental shelf of South Africa and meandering less than 150 km offshore (Gründlingh, 1983;
608 Lutjeharms 2006). The strength and warmth of the Agulhas Current influences atmospheric storm tracks and storm
609 development. The large moisture source of the warm Agulhas Current region contributes significantly to the frequency
610 and strength of African precipitation, which significantly impacts rain-fed subsistence farming (Hermes et al. 2019 and
611 references therein).

612
613 South of the tip of Africa, the Agulhas Current retroflects eastwards into the South Indian Ocean (Fig. 10). This
614 retroflection area is highly variable, occluding rings that propagate into the South Atlantic Ocean. The Agulhas variability
615 is linked upstream to modes of variability including ENSO (Elipot and Beal, 2018, Trott et al., 2021) and downstream
616 with the Atlantic meridional overturning circulation, providing an essential link between the Pacific, Indian and Atlantic
617 Oceans (Beal et al., 2011). Estimates of the rate of mass and heat exchange carried by Agulhas leakage south of Africa
618 (and the number of rings shed per year) vary and are difficult to verify reliably (Weijer et al., 2014). Daher et al (2020)
619 recently used a combination of drifters and Argo floats to derive an estimate of Agulhas leakage of 20 Sv. van Sebille et
620 al. (2011) and le Bars et al. (2014) suggested upstream variability of the Agulhas Current has an effect on inter-ocean
621 exchange between the South Indian and South Atlantic oceans, primarily by influencing the frequency of ring shedding at
622 the Agulhas retroflection. However, a few recent papers suggest instead that its variability is driven by the Southern
623 Hemisphere Westerlies (Durgadoo et al, 2013; Loveday et al., 2014; Elipot and Beal, 2015).

624
625 The Agulhas Current has a seasonal cycle and is strongest in summer (Krug and Tournadre, 2012; Beal and Elipot, 2016)
626 and tied to a baroclinic adjustment of near-field winds (Hutchinson et al, 2018). Seasonal changes in the Agulhas
627 retroflection region (Lutjeharms and van Ballegooyen, 1988; Quartly and Srokosz, 1993) and in the southwest Indian
628 Ocean (Ffield et al., 1997) have been suggested from hydrographic and satellite data (Krug et al., 2012), but with weak
629 statistical significance due to a lack of sufficiently long time series.

630
631 Although long term observations in this region are limited there are numerous recent studies that have further elucidated
632 our understanding of the Agulhas Current. Beal and Elipot (2016) used 3 years of in situ data to show that, contrary to
633 expectations, the Agulhas Current has not intensified since the early 1990s. Instead, it has broadened as a result of more
634 eddy activity, driven by intensifying winds. Variability in the path and strength of the Agulhas Current has mostly been
635 attributed to solitary Agulhas meanders within the Current system (also known as Natal pulses) which drive upwelling

636 and cross-shelf transports, affecting marine productivity, fisheries and recruitment over the Agulhas Bank (Beal and
637 Bryden, 1999; Roberts et al., 2010, Elipot and Beal, 2015). Recent work has highlighted the importance of submesoscale
638 eddies in the Agulhas Current frontal region driving an inshore edge flow reversal which can have important consequences
639 on fisheries (Krug et al., 2017).

640

641 The advance in models has also helped improve our understanding of the Agulhas Current, which is generally not well
642 represented in global ocean models. Hutchinson et al. (2018) used idealized models to expose a link between the
643 seasonality of the Agulhas Current and propagation of first baroclinic mode Rossby waves communicating the wind stress
644 signal across the western portion of the Southern Indian Ocean, with the signal from winds further east having little effect.

645 **4.2.3 Interior flows**

646 In the central-eastern South Indian Ocean between 20°S and 30°S, the surface geostrophic flow is generally eastward,
647 opposite to the prediction of both the Ekman and Sverdrup theories (Sharma 1976; Sharma et al., 1978; Godfrey and
648 Ridgway, 1985; Schott et al., 2009). This flow is driven by the large-scale, poleward drop in the dynamic height (steric
649 height) near the sea surface (Godfrey and Ridgway, 1985; Schott et al., 2009) related to the meridional transition from the
650 very fresh and warm SEC waters to the increasingly cooler, saltier and denser waters to the south. The flow generally
651 extends from the sea surface to ~200–300 m (Domingues et al., 2007; Palastanga et al., 2007; Divakaran and Brassington,
652 2011; Menezes et al., 2014). The mechanisms that determine the vertical extent of the interior eastward flow remains
653 unclear, although this depth coincides with the depth of the shelf break at the eastern boundary and the bottom of the
654 Leeuwin Current along that boundary. This correspondence may be achieved by the westward propagation of baroclinic
655 Rossby waves (Weaver and Middleton, 1989; Furue et al., 2013). Below the near-surface eastward flows, the flow is
656 weakly westward (Domingues et al., 2007; Schott et al., 2009; Furue et al., 2017).

657

658 Embedded in this general eastward flow are narrower eastward jets (Maximenko et al., 2009; Divakaran and Brassington,
659 2011; Menezes et al., 2014), collectively known as the South Indian (Ocean) Countercurrent (SICC; Palastanga et al. 2007;
660 Siedler et al. 2006; Menezes et al., 2014). They start out as a single jet emanating from the southern tip of Madagascar
661 around 25°S, possibly fed by a partial retroflexion of the SEMC (Palastanga et al., 2007; Siedler et al., 2006, 2009) and
662 divide into separate jets around the Central Indian Ridge (65°E–68°E) (Menezes et al., 2014). Eastward flows exist in
663 similar latitude bands in the North and South Pacific and North and South Atlantic (Yoshida and Kidokoro, 1967; Merle
664 et al., 1969; Takeuchi, 1984; Kubokawa, 1999; Qiu and Chen, 2004; Kobashi and Kubokawa, 2012). However, the jets in
665 these basins are weaker and shallower than the SICC and do not extend all the way to the eastern boundary (Menezes,
666 2015).

667

668 Three main jets (Fig. 10a) are evident in geostrophic velocity calculated from both altimetric sea surface height and
669 hydrography and are captured in OGCMs (Maximenko et al., 2009; Divakaran and Brassington, 2011; Menezes et al.,
670 2014). The stronger southern jet (3–4 Sv) crosses the basin around 26°S and has an associated thermal front at depths
671 around 100–200 m (Sharma 1976; Siedler et al., 2006; Menezes et al., 2014; Palastanga et al., 2007). This front suggests
672 that the southern SICC has physics similar to the Subtropical Countercurrents (STCCs) of the Pacific Ocean (Kubokawa,
673 1999; Kobashi and Kubokawa, 2012, Menezes et al., 2014). The location and strength of the SICC vary between studies,
674 from well-defined jets (Siedler et al. 2006, Palastanga et al. 2007, Divakaran and Brassington 2011, Menezes et al. 2014)
675 to a mean velocity structure (Jia et al., 2011a), or even absence of the SICC (Srokosz et al. 2015). Depending on the region
676 and time in which its characteristics were determined, the SICC varies from a weak mean current of 2–3 cm/s (Jia et al.,
677 2011a) to a strong jet of 50 cm/s eastward flow (Siedler et al., 2006).

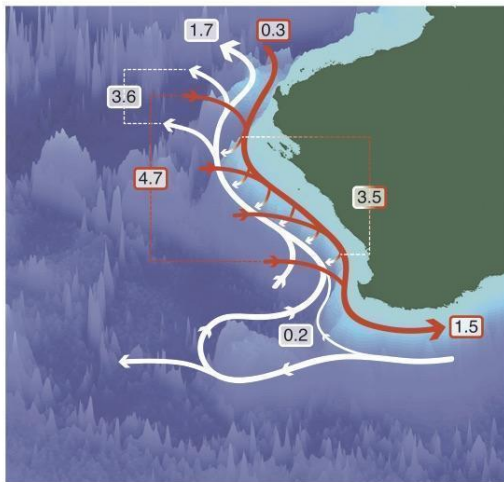
678
679 The eastward flowing Eastern Gyral Current (EGC) is part of an anticyclonic recirculation centred at the Indonesian-
680 Australian basin (5°S–20°S and 100°E–125°E) (Domingues et al., 2007; Menezes et al., 2013, and references therein).
681 Part of the northern SICC merges with the EGC around 15°S, 100°E (Fig. 10a). The EGC supplies ITF-origin water to
682 the Leeuwin Current (LC) and is an essential component of the LC dynamics (Domingues et al., 2007; Benthuisen et al.,
683 2014; Lambert et al., 2016; Furue et al., 2013, 2017; Yit Sen Bull and van Sebille, 2016). The geostrophic flow of the
684 EGC is controlled by the meridional salinity gradient, making its dynamics distinct from the temperature dominated SICC
685 (Menezes et al., 2013). This salinity front is formed by the encounter of the fresh Indonesian Throughflow Water carried
686 westward by the SEC and the salty subtropical underwater formed at the Southern Indian Ocean subtropical salinity
687 maximum. The seasonal cycles of the EGC and the SICC are also distinct: the EGC is stronger in austral winter (3–5 Sv)
688 and weaker (<0.5 Sv) in summer with the cycle in phase with the Leeuwin Current (Feng et al., 2003; Menezes et al.,
689 2013; Furue et al., 2017). The SICC is overall stronger in spring-summer and weaker in winter (Palastanga et al., 2007;
690 Jia et al., 2011a; Menezes et al., 2014) and experiences strong interannual variability, which peaks at biennial timescales
691 and is decadal modulated (Menezes et al., 2016).

692
693 The multiple jets of the SICC are embedded in a zone of high eddy kinetic energy, with eddies generated by instabilities
694 of the Leeuwin Current and of the SICC itself (Palastanga et al., 2007; Divakaran and Brassington, 2011; Huhn et al.,
695 2012; Jia et al., 2011a, 2011b; Menezes et al., 2014, 2016; Siedler et al., 2006). By co-locating Argo floats and satellite
696 data, Dilmahamod et al. (2018) described the passage of surface and subsurface South Indian Ocean eddies (SIDDIES).
697 These westward-propagating, long-lived features (>3 months) originate in areas of high evaporation in the eastern Indian
698 Ocean and prevail over a preferential latitude band, forming a permanent structure linking the eastern to the western Indian
699 Ocean (the “SIDDIES Corridor”). This corridor of eddy passage allows the advection of water masses and biogeochemical
700 properties across the basin (Dilmahamod et al., 2018).

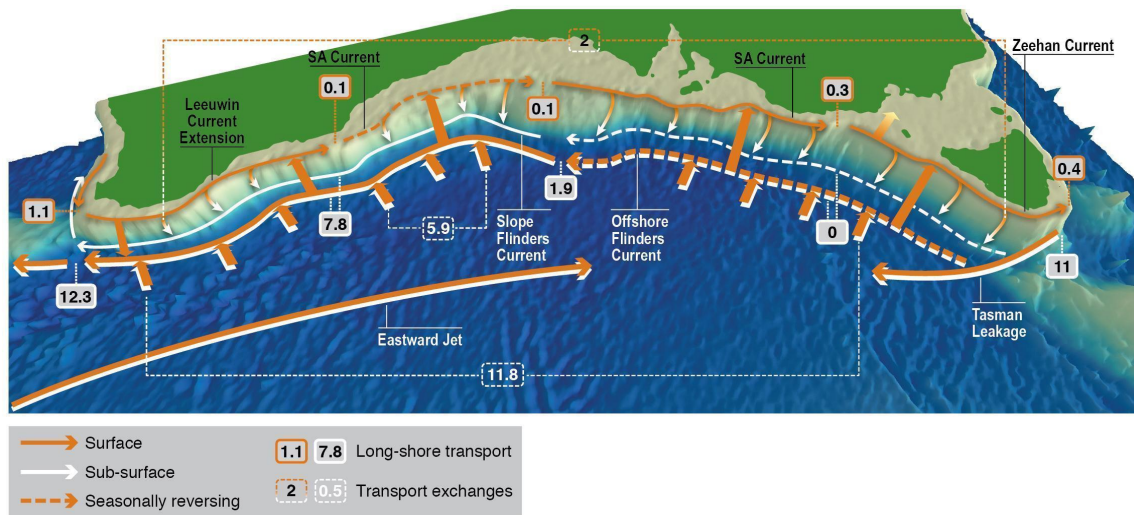
701

702 4.2.4 Eastern Boundary

703 Unlike any other eastern boundary current, the Leeuwin Current (LC; Figs. 10 and 11a) flows poleward, along the shelf
704 break of the west coast of Australia (Smith et al., 1991). Figure 11a presents the long-term average volume transport of
705 the LC System from an observational climatology with similar structure found in a $1/10^\circ$ ocean general circulation model
706 (Furue et al., 2017). The primary source waters for the LC are the interior eastward flows (Section 4.2.3) that turn
707 southeastward as they approach the coast and merge with the LC (Fig. 11a; Domingues et al., 2007; D’Adamo et al., 2009;
708 Menezes et al., 2013, 2014; Furue et al., 2017, 2019). On average, the LC carries 0.3 Sv southward at 22°S , gains 4.7 Sv
709 from the Indian Ocean interior, loses 3.5 Sv through downwelling to the layer beneath, and carries 1.5 Sv at its southern
710 limit. The LC is approximately 200–300 m deep, extends from 22°S (North West Cape) to 34°S (Cape Leeuwin) and exists
711 throughout the year despite significant seasonality (Feng et al., 2003; Ridgway and Godfrey, 2015; Furue et al., 2017).
712 The Holloway Current, which flows southwestward on the North West Shelf (D’Adamo et al., 2009; Bahmanpour et al.,
713 2016), is another weaker source to the LC from the north. Inshore of the LC, there exist seasonal equatorward flows that
714 recirculate waters of distinct watermass properties influenced by air-sea interaction over the continental shelf (Woo et al.,
715 2006).



716



717
 718 **Figure 11: a) Schematic summary of Australia's Leeuwin Current System three-dimensional transports (Sv). The**
 719 **red arrows and red-outline numbers represent the upper-layer (0–200 m) meridional transport of the poleward**
 720 **Leeuwin Current and meridionally-integrated zonal transport of the shallow eastward flows. The white arrows**
 721 **represent the lower-layer (200–900 m) flows of the Leeuwin Undercurrent. Taken from Furue et al. (2017). ©**
 722 **American Meteorological Society. Used with permission. b) Schematic summary of the Southern Australia Current**
 723 **System three-dimensional transports (Sv). Long-shore transport for the Shelf Break Currents and Flinders**
 724 **Current in grey box with orange and white outlines, respectively. Integrated vertical and onshore flow transport**
 725 **in dashed outline box. Reprinted from Duran et al. (2020), with permission from Elsevier, Progress in**
 726 **Oceanography. Both schematics are based on a geostrophic calculation in the CARS 1/8-degree climatology.**

727
 728 The mean state of the LC is driven by the meridional pressure gradient in the upper ocean (e.g., Godfrey and Ridgway,
 729 1985; Godfrey and Weaver, 1989, 1991), evident as a large poleward decrease in SSH balanced by an eastward surface
 730 geostrophic current (Section 4.2.3.1). The eastward flow approaches the eastern boundary, inducing downwelling and a
 731 surface poleward current (Fig. 11; Godfrey and Ridgway, 1985; McCreary et al., 1986; Thompson, 1987; Weaver and
 732 Middleton, 1989, 1990; Furue et al., 2013; Benthuyssen et al., 2014), in opposition to the prevailing southerly winds. As a
 733 poleward boundary current, the LC waters are relatively fresh and warm from tropical origins (Rochford, 1969; Andrews,
 734 1977; Legeckis and Cresswell 1981; Domingues et al., 2007; Woo and Pattiaratchi, 2008). Saltier Indian Central Water,
 735 the surface water of the Subtropical South Indian Ocean, joins the LC as it flows poleward (Section 4.2.3) increasing the
 736 mean density of the LC. Surface cooling along the poleward path also contributes to the increase in density (Woo and
 737 Pattiaratchi, 2008; Furue, 2019).

738 The LC flows around the southwestern corner of Australia and continues to flow eastward along the shelf break of the
739 south coast of Australia to reach the southern tip of Tasmania near 42°S, 140°E (Fig. 11b, Oliver et al., 2016; Oke et al.,
740 2018; Duran et al., 2020). This 5500-km long boundary current was first documented as a continuous flow by Ridgway
741 and Condie (2004). When the longshore current is weak, however, it tends to be somewhat fragmentary (Oke et al., 2018;
742 Duran et al., 2020) and sometimes even reverses in places (Duran et al., 2020). For this reason, and additionally because
743 of the scarcity of observational sampling, the current is not traditionally regarded as a single current. Along southern
744 Australia, the boundary currents can be described following Ridgway and Condie's (2004) naming convention. The
745 current's western sector is called the Leeuwin Current Extension, the central part, to the south of the Great Australian
746 Bight, is called the South Australian Current, and the easternmost part along Tasmania is called the Zeehan Current. They
747 are collectively known as the Shelf-Break Currents (SBCs) of the Southern Australia Current System (Duran et al., 2020).
748 It is not clear whether the SBCs along the south coast of Australia are, dynamically, an extension of the LC. The SBCs
749 are at least consistent with the local northward Ekman drift (Ridgway and Condie, 2004; Duran et al., 2020) and hence
750 would exist without the LC.

751
752 On seasonal timescales, the LC transport generally tends to be strongest in austral autumn and weakest in austral summer
753 (McCreary et al., 1986; Smith et al., 1991; Feng et al., 2003; Furue et al., 2017). There are two theories to explain this
754 seasonality. In one, the local winds, which generally induce an offshore Ekman drift and therefore tend to weaken the LC,
755 reach their annual maximum or minimum when the LC transport reaches its minimum or maximum, respectively
756 (McCreary et al., 1986; Furue et al., 2013). In the other, a seasonal pressure anomaly originates in the Gulf of Carpentaria
757 and propagates counterclockwise along the shelf break, driving the seasonality of the LC and of the SBCs to the south of
758 Australia (Ridgway and Godfrey, 2015). Like the LC, the SBCs tend to be strongest in austral autumn and weakest in
759 austral summer (Ridgway and Condie, 2004; Oke et al., 2018; Duran et al., 2020). In particular, the eastern part of the
760 South Australian Current is seen to reverse in summer (Duran et al., 2020). This variability is consistent with the
761 counterclockwise propagation of pressure anomaly shown by Ridgway and Godfrey (2015) and also with the seasonality
762 of the wind stress along the south coast of Australia, with onshore (offshore) Ekman drift tending to drive eastward
763 (westward) shelf-break flow (Duran et al. 2020).

764
765 On interannual time scales, the LC is modulated by the El Niño Southern Oscillation owing to the steric height anomalies
766 in the western equatorial Pacific Ocean propagating through the Indonesian Seas and along Western Australia (Feng et al.,
767 2003). During El Niño and La Niña periods, the LC transport weakens and strengthens, respectively, and is correlated with
768 Fremantle sea level (Feng et al., 2003). During the strong 2010–2011 La Niña event, the LC reached record strength speeds
769 (Feng et al., 2013) and the consequences of the unprecedented marine heat wave that resulted are described in Section 6.4.
770 On multidecadal timescales, the major boundary currents around Australia, including the LC, are reported to have
771 strengthened during 1979–2014 in an eddy-resolving OGCM, consistent also with observations (Feng et al., 2016; see

772 Section 6.1 for associated changes). At intraseasonal timescales, winds or heat anomalies on the North West Shelf region
773 due to MJO events lead to intraseasonal variability of the Holloway Current on the North West Shelf and then of the LC
774 (Marshall and Hendon, 2014; Marin and Feng, 2019).

775
776 The LC is accompanied by mesoscale eddies that cause the LC to meander energetically (Pearce and Griffiths, 1991; Feng
777 et al., 2005; Waite et al., 2007; Meuleners et al., 2008). Those eddies are, at least partially, generated by barotropic,
778 baroclinic, or mixed instability of the LC itself (Pearce and Griffiths, 1991; Feng et al., 2005; Meuleners et al., 2008). The
779 eddy kinetic energy is greatest when the LC transport is strongest, in May–June (Fang and Morrow, 2003; Feng et al.,
780 2005). Some of these eddies cause a large meander of the LC: a large anti-cyclonic eddy often forms at 28°–29°S and at
781 31°–32°S (Feng et al., 2003; Feng et al., 2007) steering the LC offshore to return to the continental shelf further south.
782 This state typically starts during May–June and ends in July–August (Feng et al., 2007). Similarly, it is suggested that the
783 eastern part of the SBCs becomes unstable in boreal autumn and winter, generating eddies, which subsequently propagate
784 westward south of Australia (Oke et al., 2018). Turbulent mixing has been found to be enhanced in anticyclonic eddies
785 near the surface, and in cyclonic eddies at deeper levels (500–1000 m) due to the interaction of the eddies and near-inertial
786 waves, which has implications for watermass modifications and the meridional overturning circulation (Cyriac et al. 2021).

787
788 Just below the Leeuwin Current is the equatorward Leeuwin Undercurrent (LUC; Thompson, 1984; Church et al., 1989;
789 Smith et al., 1991; Fig. 11a). The LUC hugs the continental slope and extends from 200 m to 900 m (Furue et al., 2017).
790 The LUC begins at Cape Leeuwin (34°S, 114°E) and is fed by a northward bend of a small fraction of the Flinders Current
791 (FC; Fig. 10, 11; Furue et al., 2017). The remaining part of the FC continues westward but another small fraction of it
792 appears to retroflect eastward and join and augment the LUC (Duran, 2015; Furue et al., 2017). Near 22°S, most of the
793 LUC volume leaves the continental slope and flows offshore (Duran, 2015), apparently following the southern flank of
794 the Exmouth Plateau although its bottom at 900 m is much shallower than the topographic feature (Fig. 11a).

795
796 To the south of Australia, an undercurrent has been recently identified below the Zeehan Current in a numerical simulation
797 (Oke et al., 2018) and in a geostrophic calculation based on a gridded T–S climatology (Duran et al., 2020). Traditionally
798 this flow was identified as a branch of the FC (Cirano and Middleton, 2004; Rosell-Fieschi et al., 2013; Feng et al., 2016)
799 because the former flows in the same direction as the latter, but the FC as the northern boundary current of the subtropical
800 gyre cannot exist on an eastern boundary (Anderson and Gill, 1975; Philander and Yoon, 1982; McCreary et al., 1992)
801 and it lacks the vertical structure of an undercurrent (Duran et al., 2020). This northwestward- or westward-flowing
802 undercurrent appears to exist all the way from the west coast of Tasmania to Cape Leeuwin (the southwestern tip of
803 Australia) but its separation from the FC is less clear to the south of the Great Australian Bight and further west, where
804 the FC accelerates and tends to overwhelm the undercurrent (Duran et al., 2020). Below, we call this current “slope FC”
805 following Duran et al. (2020).

806
807 The mechanisms responsible for the LUC and undercurrent off southern Australia remain an open question, although
808 models have been developed to investigate potential processes. The linear, continuously stratified models of McCreary et
809 al. (1986) and Kundu and McCreary (1986) produce a surface poleward and a subsurface equatorward current, resembling
810 the LC and LUC, along the eastern boundary. This class of model, however, requires large vertical diffusivity to produce
811 a realistic LC and LUC (McCreary, 2013, personal communication). Along a continental slope, alongshore and cross-shelf
812 buoyancy advection cause a shelf break front, forming a surface intensified poleward current, like the LC, and an
813 equatorward undercurrent by thermal wind shear (Benthuyssen et al., 2014). Analytical shelf models have been extended
814 to include cross-shelf buoyancy gradients to derive a poleward undercurrent like the LUC (Schloesser, 2014). These
815 process-based analytical theories have not been tested in an eddy-resolving model.

816
817 The LUC and the slope FC are connected to the LC and the SBCs, respectively, by downwelling (Fig. 11; Furue et al.,
818 2017; Duran et al., 2020), suggesting a common, but as yet unexplained, dynamics. Note, however, that for the LC–LUC
819 pair, the mean downwelling appears to occur along isopycnal surfaces, and hence the LC water mass is not found in the
820 LUC (Furue, 2019). For the SBCs and the slope FC, the nature of the downwelling is not known. The seasonality of these
821 undercurrents are not well known. No systematic seasonal variability of the LUC was evident in a hydrographic
822 climatology and ocean general circulation model (Furue et al., 2017).

823

824 **4.2.5 Biogeochemical Variability**

825 The ITF impacts both ocean currents and basin-scale biogeochemistry (Talley and Sprintall, 2005; George et al., 2013;
826 van Sebille et al., 2014). Talley and Sprintall (2005) mapped silicate on the 31.96 potential density surface, revealing a
827 striking silicate maximum associated with the SEC that extends westward to at least 60°E, highlighting the broad reach of
828 ITF nutrient influence into the Indian Ocean. Ayers et al. (2014) estimated the depth- and time-resolved nitrate, phosphate,
829 and silicate fluxes at the three main exit passages of the ITF that feed into the SEC: Lombok Strait, Ombai Strait, and
830 Timor Passage. They found that the nutrient flux is significant relative to basin wide new production, and that the majority
831 of ITF nutrient supply to the Indian Ocean via the SEC is to thermocline waters, where it is likely to support primary
832 production and significantly impact biogeochemical cycling.

833

834 Satellite chlorophyll and primary production estimates suggest that values in the SEC are considerably higher than those
835 found in the southern hemisphere subtropical gyre to the south, with Chla from ~0.10 to 1.0 mg/m³ and primary production
836 from ~400 to 1000 mgC m⁻² d⁻¹ (Fig. 5; Figs. 5 and 6 in Hood et al., 2017) The highest concentrations and rates in the
837 SEC are observed in the Eastern Indian Ocean in July and August during austral winter, associated with the ITF nutrient
838 sources and upwelling off Java. The lowest chlorophyll concentrations and rates are observed in January (austral summer).

839

840 Model results and satellite observations show that the SEC/SCTR region exhibits an annual cycle in surface chla
841 concentration and primary production, with the highest values in austral winter (June-August; $> 0.20 \text{ mg/m}^3$ and >600
842 $\text{mgC m}^{-2} \text{ d}^{-1}$, respectively) due to the strong southeasterly winds that increase wind stirring and induce upwelling
843 (Resplandy et al., 2009; Dilmahamod, 2014; Fig. 5; Figs. 5 and 6 in Hood et al., 2017). Vertical sections of the SEC/SCTR
844 region also reveal a deep chla maximum (George et al., 2013). Along 65°E this maximum shoals from $> 100 \text{ m}$ at 16°S to
845 $\sim 50 \text{ m}$ at 10°S due to upwelling. The increases in surface Chl-a concentrations in austral winter are associated with
846 decreases in the subsurface chla maximum (Resplandy et al., 2009; Dilmahamod, 2014). Surface freshening associated
847 with the core of the SEC also influences the chla distribution in the SCTR region by modulating the static stability and
848 mixed layer depth (George et al. (2013).

849

850 The SEC provides relatively oligotrophic (low nutrient, low chlorophyll and low primary production) tropical source
851 waters that feed into the EACC, NEMC, SEMC and the Mozambique channel. Chlorophyll *a* concentrations and
852 production rates in Mozambique Channel surface waters are generally low ($< 0.4 \text{ mg/m}^3$ and $< 700 \text{ gC m}^{-2} \text{ d}^{-1}$, Fig. 5),
853 and not significantly different in cyclonic and anticyclonic eddies (Lamont et al., 2014; Barlow et al., 2014; Figs. 5, 6 and
854 20 in Hood et al., 2017). Deep chlorophyll maxima are observed between 25 and 125 m depth depending on the proximity
855 to the shelf and the influence of mesoscale eddies (Barlow et al., 2014; Lamont et al., 2014). Eddies in the Mozambique
856 Channel also have a strong influence on the lateral transport of nutrients and chlorophyll from the coasts of Madagascar
857 and Africa. Indeed, enhanced phytoplankton production within both cyclonic and anticyclonic eddies in the Mozambique
858 Channel often occurs in response to lateral nutrient inputs into the euphotic zone by horizontal advection from the coasts
859 of Madagascar and Africa rather than through eddy induced upwelling and downwelling (José et al., 2014; Lamont et al.,
860 2014; Roberts et al., 2014). In contrast, in the Southeast Madagascar Current, topographically-induced coastal upwelling
861 brings cold, nutrient-rich water up to the surface, which supports high rates of primary production (Lutjeharms and Machu,
862 2000; Ho et al., 2004; Quartly and Srokosz, 2004). This upwelling and its impacts are observed in both the austral summer
863 and winter (Ho et al., 2004).

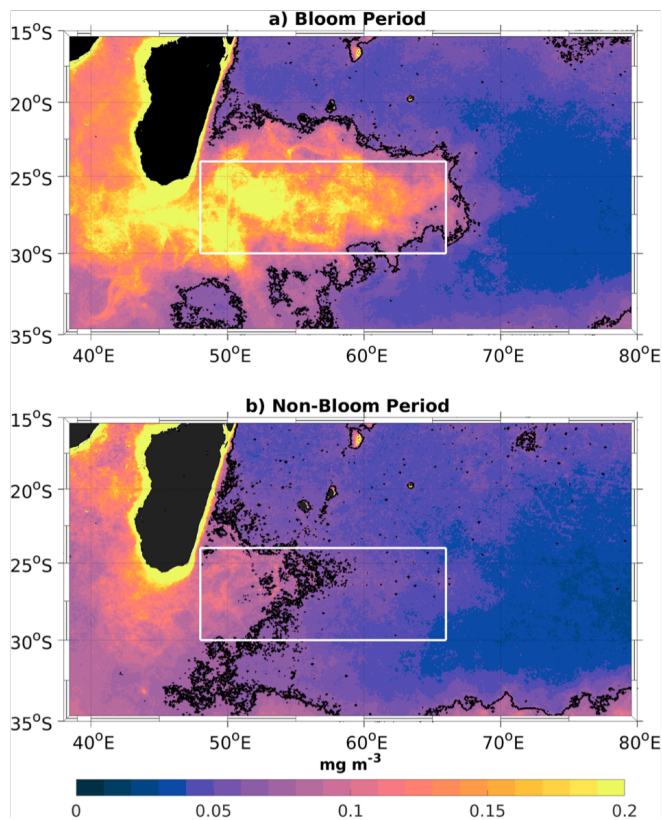
864

865 The Agulhas Current itself is warm and oligotrophic with sources derived from low nutrient and low chlorophyll surface
866 waters from the Mozambique Channel, Southeast Madagascar Current and the southwestern tropical Indian Ocean (Fig.
867 5; Lutjeharms, 2006). Chlorophyll *a* concentrations and production rates in Agulhas Current surface waters are particularly
868 low during austral summer ($< 0.2 \text{ mg/m}^3$ and $< 500 \text{ mgC m}^{-2} \text{ d}^{-1}$) with higher concentrations and rates in the austral winter
869 (Machu and Garcon, 2001; Figs. 5, 6 and 20 in Hood et al., 2017). The Agulhas Current can drive upwelling and elevate
870 primary production in the coastal zone through meandering and topographic interactions, but it can also dramatically
871 suppress primary production when it impinges onto the shelf (Schumann et al., 2005).

872

873 In general, chlorophyll concentrations and primary production are elevated in the coastal zone of southeast Africa along
874 the inshore side of the Agulhas Current (Fig. 5; Machu and Garcon, 2001; Goschen et al., 2012; Figs. 5, 6 and 20 in Hood
875 et al., 2017). This enhancement is most pronounced in austral summer and further southward downstream, and it is
876 associated with upwelling-favourable (easterly) winds and the aforementioned topographically-induced upwelling.

877 The near-surface eastward flows are generally associated with very low (oligotrophic) nutrient and chlorophyll-*a* (Chl-*a*)
878 concentrations ($< 0.1 \text{ mg/m}^3$) and also very low primary production ($< 500 \text{ mgC m}^{-2} \text{ d}^{-1}$; Fig. 5 Figs. 5 and 6 in Hood et
879 al., 2017). A well-defined deep Chl-*a* maximum is observed between 50 and 150 m during the austral fall along 55°E
880 between 20 and 30°S (Coles et al., unpublished data). An exception to this, however, is the South-East Madagascar bloom
881 (SMB). The SMB occurs in near-surface waters off the southeastern coast of Madagascar in the late austral summer/fall
882 (Jan-April). It was first described as a dendroid bloom by Longhurst (2001), owing to its branching shape that projects
883 eastward (Fig. 12). The bloom can extend over a 2,500 km² area with Chl-*a* concentrations reaching 2-3 mg/m³ (Longhurst,
884 2001), making it a ‘hot spot’ for primary production in an otherwise oligotrophic region. Fig. 12 illustrates the bloom’s
885 large spatial variability, with high Chl-*a* filaments apparently co-occurring and being transported with mesoscale and
886 submesoscale eddies and jets.



887

888 **Figure 12: (a) Spatial maps of mean Chl-*a* concentration (mg/m³) during months of maximum austral summer**
 889 **bloom. (b) Same as (a) but during January of minimum Chl-*a* concentration in austral summer. The black contour**
 890 **denotes the 0.07 mg/m³ threshold used to distinguish between bloom and non-bloom years. From Dilmahamod et**
 891 **al. (2019).**

892 Why the SMB flourishes in late austral summer is unclear. Longhurst (2001) attributed SMB development to mixed layer
 893 deepening and entrainment of nutrients by the vigorous mesoscale eddy field. These nutrients could stimulate
 894 phytoplankton growth in the photic zone, with the eddies shaping the eastward propagation of the enhanced surface Chl-
 895 *a* concentrations. However, Uz (2007), Srokosz and Quartly (2013), and Dilmahamod et al. (2019) subsequently showed
 896 that the bloom occurs within a warm (> 26.5°C), shallow mixed layer (~30 m) overlying a strong pycnocline. Furthermore,
 897 they suggested that diazotrophs known to inhabit the region (Poulton et al., 2009) might introduce new nitrogen (N) from
 898 N₂ fixation that could support the enhanced Chl-*a* concentration as observed elsewhere (Mulholland et al., 2014; Hood et
 899 al. 2004; Coles et al., 2004). Subsequent studies also highlight the role of mesoscale eddies (Fig. 12), that could advect,

900 disperse and co-mingle nutrients and/or phytoplankton biomass (Dilmahamod et al. 2019; Huhn et al., 2012; Raj et al.,
901 2010; Srokosz and Quartly, 2013; Srokosz et al., 2004, 2015; Uz, 2007).

902 A different explanation of the SMB and its eastward projection was proposed by Srokosz et al. (2004). In their proposed
903 mechanism, the bloom initiates off Madagascar due to coastal processes that bring limiting nutrients to the photic zone
904 and phytoplankton are transported horizontally by mesoscale eddies, resulting in an eastward propagation of the bloom.
905 Dilmahamod et al. (2020) extend this further using a model to suggest that, from a nutrient flux analysis, horizontal
906 advection of low-salinity nutrient-rich Madagascan coastal waters can indeed trigger a phytoplankton bloom.
907 Alternatively, the apparent eastward propagation of the SMB has recently been attributed to advection by the SICC (Fig.
908 10; Dilmahamod et al., 2019; Huhn et al., 2012; Wilson and Qiu, 2008). Indeed, Huhn et al. (2012) further suggested that
909 the bloom is shaped by a meridional barrier of jet-like Lagrangian coherent structures associated with the SICC.

910 At the eastern boundary, the tropical source waters and downwelling tendency of the Leeuwin Current combine to create
911 a warm, oligotrophic current with low productivity. Chl-*a* concentrations are usually < 30 mgChl_a m⁻² and rates of primary
912 production rates generally do not exceed 500 mgC m⁻² d⁻¹ (Koslow et al., 2008; Lourey et al., 2006; Lourey et al., 2013).
913 Productivity in the Leeuwin Current is lowest during austral summer, when the water column is stratified. During summer,
914 subsurface chlorophyll maxima are found between 50 and 120 m depth (Hanson et al., 2007) as observed in open ocean
915 subtropical oligotrophic waters (e.g., Venrick, 1991). However, rates of primary production in near shore upwelling
916 regions (e.g., off of the North West Cape during summer) can sometimes attain very high levels (3000–8000 mgC m⁻²
917 day⁻¹) as observed in other eastern boundary upwelling zones (Furnas, 2007).

918 In all seasons, meanders in the Leeuwin Current give rise to warm core, anticyclonic eddies that carry moderately high
919 chlorophyll coastal water offshore. The elevated chlorophyll concentrations in these eddies is due to the presence of
920 coastal diatom communities. These diatoms are transported offshore into cooler oligotrophic waters that are dominated
921 by much smaller open ocean phytoplankton species (Waite et al., 2007a; Paterson et al., 2008; Waite et al., 2016). These
922 eddies, which can extend to more than 2000 m depth, are unusual because they are downwelling (anticyclonic) circulations
923 that should inhibit the input of new nutrients from depth. Nonetheless, these eddies, and the elevated chlorophyll
924 concentrations that are associated with them, persist for months (Feng et al., 2007; Moore et al., 2007; du Fois et al., 2014).
925 It has been hypothesized that the diatom communities in these eddies are supported by internal nutrient recycling and/or
926 lateral supply (Waite et al., 2007a; Paterson et al., 2013; Thompson et al., 2007, 2011).

927 Generation of these warm (and cold) core eddies by the Leeuwin Current is prolific between 20° and 35° S (Gaube et al.,
928 2013). Most of these eddies move directly westward and some may be very long-lived (Feng et al., 2005; Feng et al.,
929 2007; Moore et al., 2007; Gaube et al., 2013; du Fois et al., 2014). The persistence and potential biogeochemical/ecological
930 impacts of these eddies in the open ocean have not been investigated fully.

932 4.3 Equatorial regime

933 4.3.1 Wyrтки Jets

934 Owing to the seasonally reversing monsoon winds, the equatorial Indian Ocean (EIO) exhibits unique characteristics and
935 is in contrast with the equatorial Atlantic and Pacific Oceans. Unlike the other basins, the annual winds along the EIO are
936 very weak and mostly meridionally oriented except during the two intermonsoon seasons between boreal winter (April-
937 May) and summer (Oct-Nov) when strong westerly wind bursts prevail along the EIO (see Schott and McCreary, 2001
938 and references therein). The semi-annual cycle in the zonal wind is well known observationally and was shown to be due
939 to the meridional advection of easterly momentum by the cross-equatorial monsoon winds (Ogata and Xie, 2011). The
940 westerly winds force strong eastward jets in the top 100 m along the equator that are known as spring and fall Wyrтки Jets,
941 respectively (Wyrтки, 1973). These surface jets are usually confined within the top 100 m of the water column (Han et al.,
942 1999; Iskander et al., 2011) and deepen (shoal) the thermocline and elevate (lower) the sea level in the east (west) (Rao et
943 al., 1989; Schott and McCreary, 2001; Nagura and McPhaden, 2010a). These jets play a major role in zonal redistribution
944 of mass, heat, salt and other water properties at the Equator and in off-equatorial basins (Reppin et al., 1999; Murtugudde
945 and Busalacchi, 1999; Han et al., 1999; McPhaden et al., 2015; Chatterjee et al., 2017). Long term ADCP observations
946 from the RAMA equatorial mooring suggest that the fall jet in the central EIO is usually stronger with a maximum transport
947 of ~ 19.7 Sv compared to the spring jet which shows maximum transport of ~ 14.9 Sv with comparable standard deviations
948 (McPhaden et al., 2015).

949 These eastward surface zonal currents tend to propagate westward during spring and eastward during fall (Nagura and
950 McPhaden, 2016). The westward phase propagation speed during spring is estimated to be on average between 0.7-1.5 m
951 s^{-1} (Qiu et al., 2009; Nagura and McPhaden, 2010a) and driven primarily by the westward propagating surface zonal winds
952 associated with atmospheric deep convection that moves from the Maritime Continent to the northern Bay of Bengal
953 during spring (Nagura and McPhaden, 2010b; Nagura and McPhaden, 2016). Equatorial Rossby waves may also contribute
954 to this westward propagation (Nagura and McPhaden, 2010a). In contrast, during fall, as the deep convection moves
955 southeastward, the surface equatorial zonal winds, and thus surface currents, propagate eastward.

956 The spring and fall Wyrтки Jets also show considerable intraseasonal and interannual variability. While the intraseasonal
957 variability of the Wyrтки Jets has been shown to be influenced by their own instability (Sengupta et al., 2001, 2007; Han
958 et al., 2004) and local winds (Masumoto et al., 2005, Sengupta et al., 2007, Iskander et al., 2009; Prerna et al., 2019), the
959 interannual variability of the Wyrтки Jets is mainly caused by the anomalous wind forcing along the EIO associated with
960 ENSO (Murtugudde et al., 2000; Gnanaseelan et al., 2012; Joseph et al., 2012) and IOD (Nagura and McPhaden, 2010b;
961 Nyadjro and McPhaden (2014); Prerna et al., 2019): IOD weakens (strengthens) the equatorial zonal winds during its

962 positive (negative) phase. While IOD modulates the zonal winds along the entire equator, the influence of ENSO is
963 primarily limited to the eastern part of the EIO (Gnanaseelan et al., 2012). Moreover, it has been shown that these climate
964 modes affect the boreal fall jet more significantly than the boreal spring jet. Recent modelling studies suggest that MJO
965 convection can lead to a stronger spring Wyrki jet particularly in the eastern EIO. The interannual variability of MJO can,
966 therefore, contribute to the observed interannual variability of this equatorial jet as well (Deshpande et al., 2017; Prerna et
967 al., 2019).

968 **4.3.2 5-30 Day Ocean Waves and Instabilities**

969 Meridional velocity along the equator shows prominent high frequency variability at all depths, in the periodic band of
970 10-20 days with a peak at ~15 days (referred to as biweekly variability) and in the 20-30 days band with a peak at ~25
971 days (Masumoto et al., 2005; David et al., 2011; Chatterjee et al., 2013; Smyth et al., 2014). This variability is attributed
972 to Yanai waves, first discovered in the atmosphere (also referred to as mixed Rossby-Gravity waves; Yanai and Maruyama
973 1966; Arzeno et al., 2020; Pujiana and McPhaden, 2021). Unlike Kelvin and Rossby waves, Yanai wave phases can
974 propagate westward or eastward depending upon their frequency, but their group velocity is always eastward (Miyama et
975 al., 2006). These waves lead to convergent meridional heat flux into the equatorial regime (Shinoda, 2009; Smyth et al.,
976 2014). While these waves were first observed in the ocean in the late 1990s, the establishment of the equatorial RAMA
977 moorings (McPhaden et al., 2009) over the last two decades has provided more insight into these processes. Bi-weekly
978 (10-20 day) is shown to be forced by the direct meridional wind stress (Sengupta et al., 2004) and to some extent by the
979 meridional gradient of the zonal wind stress (Miyama et al., 2006). The 20–30-day band can be excited by off-equatorial
980 barotropic/baroclinic instabilities in addition to direct wind forcing. A detailed review of the biweekly variability is
981 provided in Schott et al. (2009) and hence, we focus on the 20-30 day variability in this review.

982 While the 20-30-day oscillation in meridional velocity is reported near the surface in the central EIO (David et al., 2011),
983 in the eastern EIO these variabilities are seen only in subsurface layers (100-200 m depth) of the water column (Masumoto
984 et al., 2005). This indicates a possible downward energy propagation of a vertical beam that carries energy to deeper
985 depths. In the central EIO, these 20-30-day Yanai waves are excited by horizontal shear between the westward-flowing
986 South Equatorial Current and the eastward-flowing Southwest Monsoon Current during IOD events (Fig. 10a; David et
987 al., 2011). In the western EIO, these waves are primarily driven by cross equatorial meridional winds (Chatterjee et al.,
988 2013). During early boreal summer (June/July), when the Somali current begins to cross the Equator along the western
989 boundary of the basin, it bends offshore to conserve potential vorticity (Schott and McCreary, 2001) and forms a gyral
990 circulation known as the Southern Gyre (Fig. 10a). Subsequently, these swift currents turn barotropically unstable and
991 generate eddy flow that is advected southward to the Equator near the western boundary i.e. at ~50-55°E. They generate
992 a westward propagating cross-equatorial flow with a wavelength set by the eddy field which is similar to the wavelength
993 of 20-30 day Yanai waves and thus excite these frequencies efficiently (Chatterjee et al., 2013).

994 The ocean response to convectively coupled Kelvin waves (CCKW) in the atmosphere was investigated using ocean glider
995 measurements from the CINDY/DYNAMO field experiment (Webber et al., 2014; Matthews et al., 2014). CCKW are
996 atmospheric weather systems that propagate eastward along the Equator and are an important constituent of the MJO
997 convection (Baronowski et al., 2016). CCKW enhance surface wind speed and latent heat flux during their passage
998 suppressing the diurnal cycle of SST and leading to sustained decrease in bulk SST of around 0.1°C, one third of the SST
999 anomaly due to a single, average MJO event, suggesting the oceanographic impact could have a strong feedback on the
1000 MJO cycle (Baronowski et al., 2016). Using RAMA moored measurements of upper ocean and surface atmosphere
1001 variability, Pujiana and McPhaden (2018) demonstrated that CCKW force oceanic Kelvin waves, affect surface heat fluxes
1002 and generate upper ocean turbulence.

1003 **4.3.3 Equatorial Upwelling and Downwelling**

1004 In the Pacific and Atlantic Oceans, permanent easterlies drive permanent equatorial upwelling due to Ekman
1005 divergence, but in the Indian Ocean where the mean winds are weak and westerly, permanent upwelling does not
1006 exist (Schott and McCreary, 2001). Mean westerly winds along the Equator are downwelling favorable, driving
1007 surface convergence and thermocline divergence, which has been observed and described with Argo and RAMA data
1008 (Wang and McPhaden, 2017). Instead of upwelling along the equator, coastal upwelling along the coasts of Sumatra
1009 and Java is prominent. During June-October, south-easterly trade winds blow close to the Equator and drive the
1010 offshore Ekman transport away from the Sumatra-Java coast (Quadfasel and Cresswell, 1992; Sprintall et al., 1999;
1011 Susanto et al., 2001). The associated wind-driven upwelling intensifies as the monsoon progresses, reaching its peak
1012 by August and finally weakening by October as the monsoon winds wane. Recent studies suggest that when the
1013 easterly winds prevail during summer, upwelling favourable Kelvin waves also contribute to intensifying the
1014 equatorial upwelling (Iskander et al., 2009; Chen et al., 2016). During boreal winter-early spring (December-March),
1015 an intermittent/weaker subsurface thermocline shoaling is evident (Chen et al., 2016). Subsequently, the prevalence
1016 of westerly winds, which drive downwelling Kelvin waves, depress the thermocline in the east (Susanto et al., 2001;
1017 Prerna et al., 2019). Apart from this seasonal cycle, interannual climatic variability associated with ENSO and IOD
1018 events (Saji et al., 1999; Vinayachandran et al., 1999, Nyadjiro and McPhaden, 2014) also influences the upwelling
1019 intensity in this region (Section 6.2).

1020

1021 **4.3.4 Equatorial Undercurrents**

1022 In the Pacific and Atlantic, easterly winds produce an eastward mean undercurrent in the thermocline but in the
1023 Indian Ocean westerly winds do not produce a mean westward undercurrent. The reason is that nonlinear momentum
1024 advection drives mean eastward currents in the thermocline that flow up the zonal pressure gradient (Nagura and
1025 McPhaden, 2014). The Indian Ocean Equatorial Undercurrent (EUC) is, therefore, a much weaker and seasonally

1026 varying transient feature driven by seasonally reversing monsoon winds (Reppin et al., 1999; Schott and McCreary,
1027 2001). The equatorial RAMA moorings have recorded an eastward EUC with a core within the thermocline during
1028 boreal winter and spring (Chen et al., 2015, 2019) and occasionally in summer and fall at a depth of 90-170 m
1029 (Iskandar and McPhaden, 2011). During winter, the eastward EUC is forced by the upwelling Kelvin and Rossby
1030 waves that are in turn forced by easterly winds along the equator in that season. During summer, the westward EUC
1031 is primarily forced by the eastward pressure gradient generated by the downwelling reflected Rossby waves off the
1032 eastern boundary of the basin. On intraseasonal timescales of 30-70-days, the EUC variability is dominated by that of
1033 Kelvin and Rossby waves of lower order baroclinic modes (Iskander and McPhaden, 2011). The undercurrents also
1034 undergo significant interannual variations related to the IOD. These variations are important in the mass and heat
1035 balance on IOD time scales, with significant impacts on upwelling and SST (Zhang et al., 2014; Nyadjro and
1036 McPhaden, 2014)

1037

1038 **4.3.5 Cross-Equatorial Circulation**

1039 The cross-equatorial circulation in the upper ocean is achieved by the Cross-Equatorial Cell (CEC), driven by
1040 southern hemisphere southeasterly winds and the seasonally-reversing monsoon winds in the northern hemisphere
1041 (Miyama et al. 2003; Schott et al. 2002, 2004, 2009). Thermocline waters subducted in the subtropical southeast
1042 Indian Ocean move equatorward and enter the northern hemisphere via the western boundary to upwell off Somalia
1043 and Oman. The return across the Equator, the surface branch of the CEC, is via the near-surface meridional flow in
1044 the interior Indian Ocean that is southward in the mean at nearly all longitudes (Miyama et al., 2003; Lee, 2004). This
1045 cell is unique to the Indian Ocean and is consistent with Sverdrup dynamics, being driven by the predominantly
1046 negative wind stress curl (Godfrey et al., 2001; Miyama et al., 2003; Wang and McPhaden, 2017). It carries most of
1047 the cross-equatorial transport of mass and heat (Schott and McCreary, 2001) and helps to moderate the seasonal
1048 climate of the region. The seasonal cross-equatorial mass flux is oppositely directed along the western boundary and
1049 in the interior (Beal et al., 2013). Flow in the interior is directed from the summer to the winter hemisphere (Horii
1050 et al., 2013; Wang and McPhaden, 2017) consistent with monsoon wind forced Ekman and Sverdrup dynamics as
1051 proposed in the model study of Miyama et al. (2003).

1052

1053 In OGCMs, the southward flow of the CEC was found to occur just below the surface, beneath a northward surface
1054 current (Wacogne and Pacanowski, 1996; Miyama et al. 2003). This “equatorial roll”, also unique to the Indian
1055 Ocean, is only of order 100 m depth and so has little impact on the cross-equatorial heat transport of the CEC. Horii
1056 et al. (2013) and Wang and McPhaden (2017) presented the first observational evidence for the equatorial roll.

1057

1058 The spatial structure and time evolution of the cross-equatorial circulation is difficult to depict due to its dependence

1059 on the fluctuating monsoon winds. Consequently, the flow patterns obtained from an Eulerian average as in Fig. 10
1060 cannot capture the monsoon-dependent streamlines that a flow will follow at a given moment. Lagrangian methods
1061 based on ocean drifter velocities (Laurindo et al. 2017) and real and simulated surface drifter trajectories identify
1062 pathlines that connect the monsoonal Indian Ocean, revealing three cross-equatorial gyre pathways that connect the
1063 Somali Current with the interior flow north and south of the Equator (Fig. 7 in l'Hegaret et al., 2018).

1064 **4.3.6 Biogeochemical Variability**

1065 Much of the current understanding of biogeochemical variability in the equatorial zone of the Indian Ocean is based on
1066 satellite ocean color observations and models, augmented by some additional, relatively sparse, in situ measurements.
1067 Seasonal climatologies of near-surface chlorophyll concentrations and primary production show a significant seasonality
1068 in equatorial waters that is clearly associated with monsoon forcing (Fig. 5, Wiggert et al., 2006; Strutton et al., 2015;
1069 Figs. 5 and 6 in Hood et al., 2017). In general, Chl-*a* concentrations and primary production increase northward from the
1070 equator with the lowest concentrations ($< 0.1 \text{ mg m}^{-3}$) and rates ($< 800 \text{ mg C m}^{-2} \text{ d}^{-1}$) occurring during the boreal spring
1071 intermonsoon period. During the southwest monsoon, Chl-*a* concentrations and rates of primary production increase in
1072 western equatorial waters in response to monsoon-forced mixing and upwelling. However, concentrations and rates in the
1073 central and eastern equatorial waters stay relatively low ($< 0.5 \text{ mg m}^{-3}$, $< 800 \text{ mgC m}^{-2} \text{ d}^{-1}$, respectively). Island wake
1074 effects can be seen advecting high chlorophyll water ($> 0.5 \text{ mg m}^{-3}$) along the equator from the Chagos-Laccadive ridge
1075 at 73°E eastward during the autumn intermonsoon period and westward during spring (see Fig. 1 in Strutton et al., 2015).

1076 Well-developed deep Chl-*a* maxima have been observed in the equatorial Indian Ocean along 65°E centered at about 50
1077 m depth in November-December (George et al., 2013) and along 80°E centered at about 75 m in August-September
1078 (Sorokin et al., 1985). It is unknown whether or not this subsurface Chl-*a* maximum exists along the equator throughout
1079 the year, but it is probably present whenever the water column is stratified. Models predict the presence of a subsurface
1080 (60 m) Chl-*a* maximum in eastern Indian Ocean equatorial waters along 87°E (Wiggert et al., 2006) that is present
1081 throughout the year except during the southwest monsoon when high chlorophyll surface water is advected into the region.

1082 Physical processes at time scales from intraseasonal to interannual (i.e., Wyrтки Jets, MJO and IOD) have been shown to
1083 influence biogeochemistry. For example, IOD events can significantly increase chlorophyll concentrations and primary
1084 production in eastern Indian Ocean equatorial waters (Wiggert *et al.*, 2009). In addition, relaxation of an IOD can deplete
1085 upper ocean nutrients, decreasing biological productivity (Kumar *et al.*, 2012). Biogeochemical responses to the IOD also
1086 have significant higher trophic level impacts (Marsac and Le Blanc, 1999).

1087 Satellite observations and biophysical model simulations show how chlorophyll concentrations and primary production
1088 near the Seychelles-Chagos thermocline ridge, can be increased by MJO-induced wind mixing and nutrient entrainment
1089 (Resplandy et al., 2009). They also concluded that IOD-driven interannual variability of thermocline depth influences the

1090 biogeochemical response to MJO: the deepened nutricline following IOD events inhibits nutrient input into the mixed
1091 layer and thus decreases the biogeochemical response to MJO.

1092 In model simulations, Wyrтки jets depress the thermocline and nitracline along the equator on the eastern side of the basin
1093 and, as a result, lower equatorial primary production when they arrive in the spring and autumn (Wiggert et al. 2006). This
1094 pattern was observed in a 25 day time series study on the equator at 80.5°E in late 2006 that showed a deepening of the
1095 surface layer, nutracline and subsurface Chl-*a* maximum during the autumn Wyrтки jet period (Kumar et al., 2012).

1096 Finally, Strutton et al. (2015) examined time-series measurements of near-surface chlorophyll concentration from a
1097 mooring deployed in 2010 at 80.5 E in the equatorial Indian Ocean. These data revealed at least six spikes in chlorophyll
1098 from October through December, separated by approximately 2-week intervals and coinciding with the development of
1099 the fall Wyrтки jets. The chlorophyll pulses were associated with increases in eastward surface winds and eastward currents
1100 in the mixed layer and inconsistent with upwelling dynamics because eastward winds that cause intensification of the
1101 Wyrтки jet should drive downwelling. Strutton et al. (2015) concluded that the chlorophyll spikes could be explained by
1102 two alternative mechanisms: (1) turbulent entrainment of nutrients and/or chlorophyll from across the base of the mixed
1103 layer by wind stirring or Wyrтки jet-induced shear instability or (2) enhanced southward advection of high chlorophyll
1104 concentrations into the equatorial zone associated with wind-forced biweekly Yanai waves.

1105 **4.4 Northern Indian Ocean**

1106 The two main basins of the northern Indian Ocean, the Bay of Bengal (BoB) and the Arabian Sea (AS), are characterized
1107 at the surface by remarkably contrasting sea surface salinity with differences of the order of 3 psu (e.g. Chatterjee et al.
1108 2012, Gordon et al. 2016, Hormann et al. 2019) decreasing from west to east (Fig. 4). The fresh surface layer of the BoB
1109 is maintained by large freshwater input deriving from direct rainfall over the ocean and river runoff, especially during the
1110 South Asian monsoon. The salt balance of the BoB is maintained by the subsurface supply of salt water via the Southwest
1111 Monsoon Current (Fig. 10, Vinayachandran et al., 2013). The saltier SSS of the AS is the consequence of an evaporative
1112 regime (e.g., Rao & Sivakumar, 2003; Sengupta et al., 2006). A reversing monsoonal near-surface circulation (Fig. 10 a,b)
1113 plays a central role in the exchanges of freshwater and heat between the BoB and the AS (McCreary et al. 1993, Hormann
1114 et al. 2019).

1115 Recent multi-year deployments of satellite tracked surface drifters drogued at 15 m depth (Wijesekera et. al, 2016,
1116 Centurioni et al. 2018) have helped to better constrain the amplitude and structure of the circulation and the exchange
1117 processes between the two basins, and to refine the findings reported by other authors (e.g. Schott and McCreary, 2001).
1118 Additionally, implementation of a moored buoy network along the slope and shelf of the Indian coast has helped

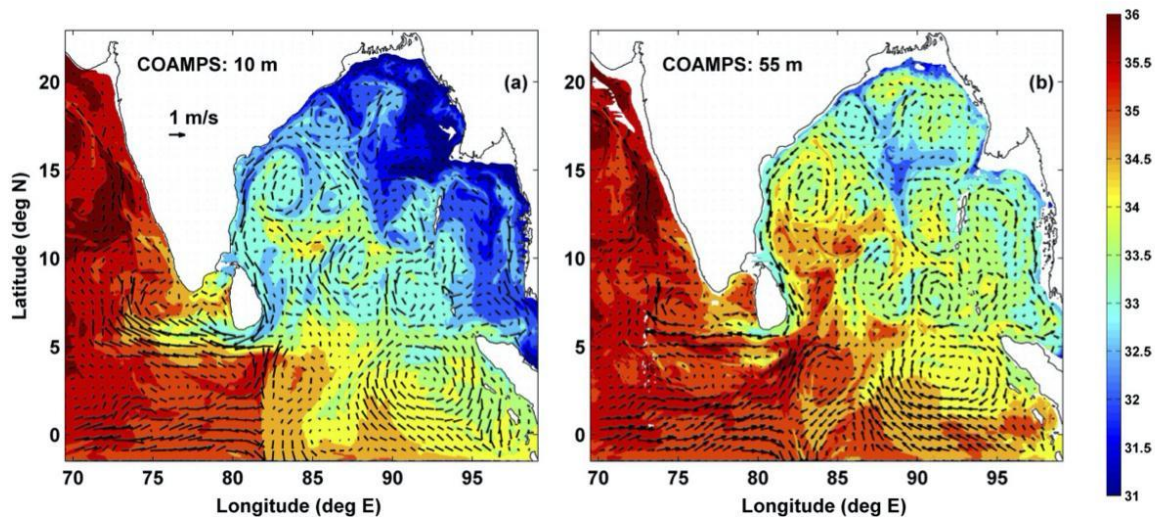
1119 significantly in enhancing our understanding of the east India Coastal Current (EICC) and west India Coastal Current
1120 (WICC) (Fig. 10, Mukherjee et al., 2014; Amol et al., 2014; Mukhopadhyay et al., 2020; Chaudhuri et al. 2020).

1121 4.4.1 Bay of Bengal

1122 In a climatological sense, the main features of the near-surface circulation of the western BoB (Figs. 10a and 10b) are the
1123 reversing EICC, the Southwest/Northeast Monsoon Current (SMC/NMC) and the seasonally variable Sri Lanka Dome.
1124 The eastern side of the BoB, extending into the Andaman Sea, is characterised by a sluggish circulation.

1125 4.4.1.1 Southwest/Northeast Monsoon Currents

1126 During the boreal summer SW monsoon, the Southwest Monsoon Current (SMC, Fig. 10a) flows eastward around the
1127 Indian subcontinent supplying salty water from the Arabian Sea to the fresher Bay of Bengal (e.g., Jensen, 2001; Jensen
1128 et al., 2016; Vinayachandran et al., 2013; Wijesekera et al., 2015, 2016). During the winter monsoon, the Northeast
1129 Monsoon Current (NMC, Fig. 10b) reverses the flow carrying fresher water into the Arabian Sea. Figure 13 provides a
1130 snapshot from an operational forecast system, the Coupled Ocean-Atmosphere Mesoscale Prediction System (COAMPS),
1131 of the NMC flow and route for freshwater to enter the Arabian Sea (Wijesekera et al., 2015).



1132
1133 **Figure 13: COAMPS velocity vectors (arrows) and salinity (psu, color shading) at (a) 10 m and (b) 55 m on 18**
1134 **December 2013. Modified from Wijesekera et al. (2015).**

1135 A more recent study has found that the origins of the Arabian Sea high salinity water are specifically from the western
1136 Arabian Sea and western Equatorial Indian Ocean, and they reach the Bay of Bengal via a combination of the Indian Ocean

1137 EUC and the SMC (Sanchez-Franks et al., 2019; Section 8.2). Changes in the supply of salty water to the Bay of Bengal
1138 varies interannually due to the strength in the equatorial currents, forced by the local wind field and ENSO (Sanchez-
1139 Franks et al., 2019), and is expected to influence the salinity budget of the Bay of Bengal (Vinayachandran et al., 2013)
1140 and thus modulate SST variability (Fig. 10a, Jensen, 2001; Jensen et al., 2016; Li et al., 2017; Vinayachandran et al., 2013,
1141 2018; Webber et al., 2018).

1142 **4.4.1.2 East Indian Coastal Currents (EICC)**

1143 The EICC forms the western boundary current of the Bay of Bengal and plays an important role in the basin-scale heat
1144 and salt budget of the Indian Ocean, and hence in determining the local climate (Shenoi et al, 2002), biological processes
1145 (Madhupratap et al, 2003; Vinayachandran et al, 2005; Naqvi et al, 2006; Dileepkumar, 2006; McCreary et al, 2009) and
1146 marine fisheries (Vivekananda and Krishnakumar, 2010) of this region. It reverses its direction seasonally north of 10°N
1147 in response to a combination of local alongshore winds, remote alongshore winds in the eastern BoB, remote forcing from
1148 the equatorial Indian Ocean and the interior Ekman pumping of the basin (Shankar et al., 1996; McCreary et al., 1996;
1149 Vinayachandran et al., 1996; Mukherjee et al., 2018). The EICC is generally equatorward south of 10°N throughout the
1150 year. While local winds dominate the EICC forcing during summer and winter, remote forcing dominates during the inter-
1151 monsoon periods (Shankar et al., 1996; McCreary et al., 1996; Suresh et al., 2013).

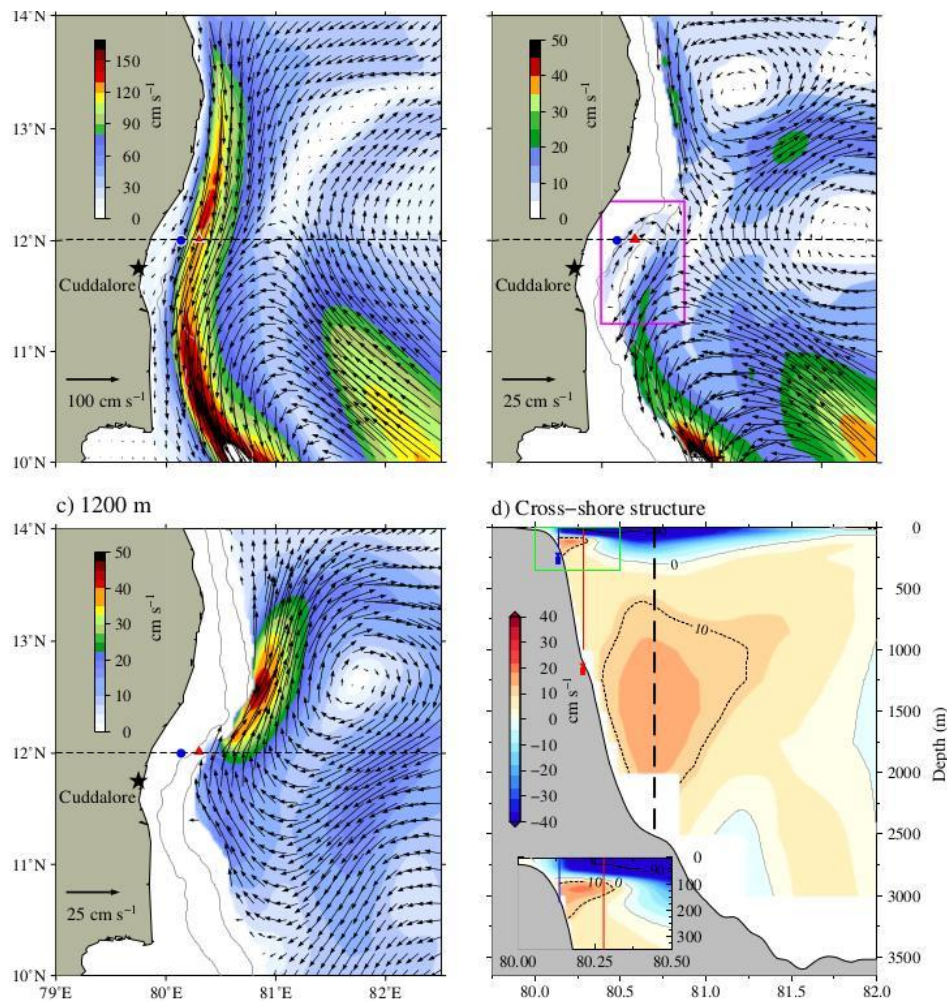
1152 Climatological ship-drift and hydrographic data suggest the EICC flows poleward during February-September (Shetye et
1153 al., 1993) and turns equatorward during November-January (Shetye et al., 1996; Fig. 10). While the annual cycle is driven
1154 by local alongshore winds and interior Ekman pumping, the semiannual cycle is the result of asymmetry in the monsoon
1155 and equatorial forcing (Mukherjee et al., 2018). During boreal spring (March-May), the EICC is strongest with a magnitude
1156 exceeding 1m/s with unidirectional currents to about 150 m, forming the western boundary current of a cyclonic basin-
1157 wide gyre of the BoB. The local alongshore winds are weakest and the stronger EICC is primarily forced by the interior
1158 anticyclonic Ekman pumping over the basin (McCreary et al., 1996; Shankar et al., 1996; Vinayachandran et al., 1996;
1159 Mukherjee et al., 2018). During boreal summer, the EICC is weaker and is restricted to within the top 70 m of the water
1160 column. The poleward flow is generally limited to the central part of the coast between 10-18°N and often switches to
1161 short pulses of poleward currents along the coast (Mukherjee et al., 2018; Francis et al., 2020). The poleward flow is
1162 driven by local winds, but the response of the interior cyclonic Ekman pumping and equatorial winds driving an opposite
1163 flow along the coast causes a weaker poleward EICC in summer than in spring (McCreary et al., 1996; Vinayachandran
1164 et al., 1996; Shankar et al., 2002). The basin-scale gyre also disappears in summer and the EICC then consists of several
1165 eddies along the coast. The EICC turns equatorward during November-January (Shetye et al., 1996).

1166 Near-surface alongshore currents also display significant 120 day and intraseasonal variability. The magnitude of the 120
1167 day variability is generally weaker than the semiannual period, particularly in the southern part of the coast. As for the

1168 annual period, upward phase propagation along the coast is also evident for the semiannual and 120 day period, except at
1169 Cuddalore where downward phase propagation is common during summer and winter months (Mukherjee et al., 2014;
1170 Mukhopadhyay et al., 2020). Further, unlike annual and semiannual periods, the 120 day and intraseasonal variability
1171 decorrelate along the coast indicating that these high frequencies are dominated by local responses rather than remote
1172 forcing (Mukherjee et al., 2018; Mukhopadhyay et al., 2020).

1173 **4.4.1.3 Undercurrents**

1174 ADCP observations suggest that during summer and winter, when the near-surface current is shallow, the EICC often
1175 exhibits undercurrents along the continental slope. As the EICC is deeper in the north, the undercurrent is observed at a
1176 depth of 100-150 m and can extend up to 700 m. However, in the south undercurrents are seen at relatively shallow depths
1177 of about 70-75 m (Francis et al., 2020). While these undercurrents are observed throughout the coast, they are much more
1178 prominent and more frequent at Cuddalore, the southernmost station of the coast (Fig. 14, Mukherjee et al., 2014;
1179 Mukhopadhyay et al., 2020).



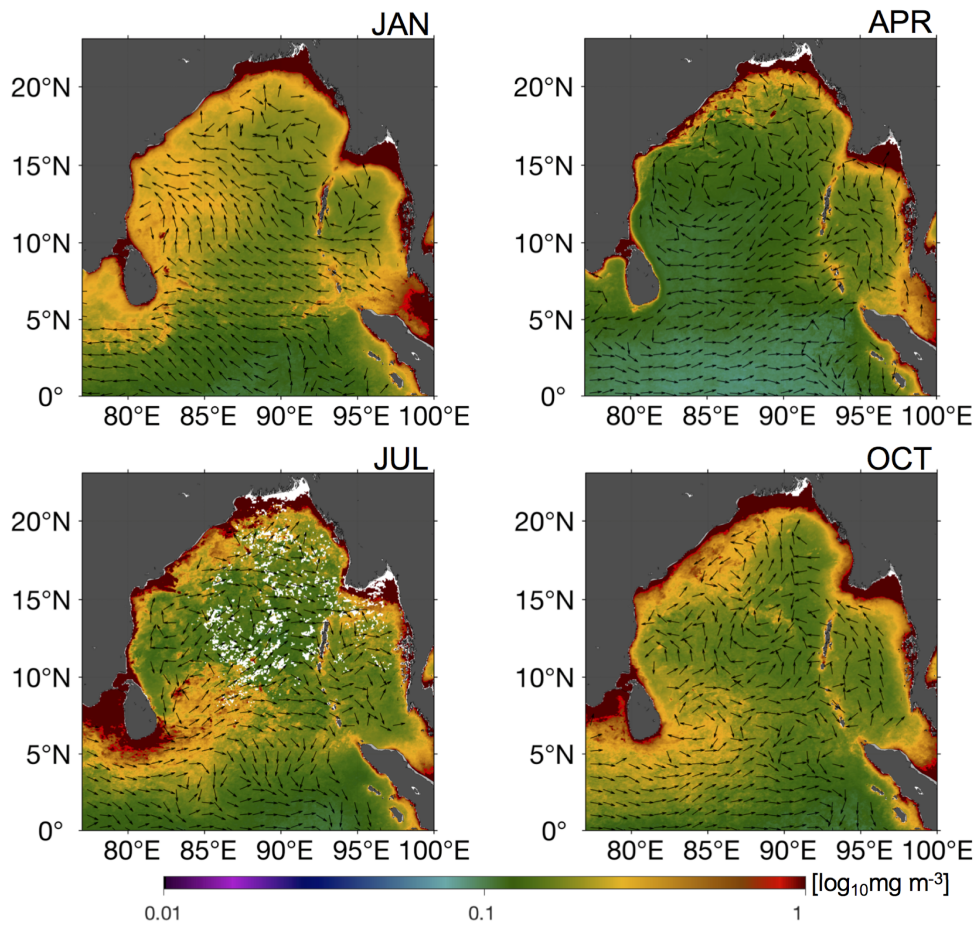
1180
 1181 **Figure 14: Circulation pattern in the southwestern Bay of Bengal at (a) surface (b) 200 m and (c) 1200 m on 15**
 1182 **November 2014. Vectors show the current direction, and overlaid is the current magnitude (cm s^{-1}). Note that the**
 1183 **scales of current vectors and color bars are different at each subplot. Blue circle (red triangle) represents the**
 1184 **location of ADCP deployed on the shelf (slope) off Cuddalore. Dashed black line represents the 12°N latitude.**
 1185 **Continuous gray lines represent the 100 m and 1000 m bathymetric contours. Rectangular box (magenta) indicates**
 1186 **the subsurface eddy near the shelf break. (d) Cross-shore structure of alongshore currents across 12°N . Dashed**
 1187 **black vertical line shows the core of the undercurrent, and red (blue) vertical lines show the location of ADCP**
 1188 **mooring on the slope (shelf). Inset plot is the zoomed view of shelf break region indicated by green box (Reproduced**
 1189 **from Francis et al., 2020).**

1190 The prominent upward phase propagation of the annual signal in the subsurface layers, particularly in the southern stations,
 1191 suggests downward propagation of energy and is thereby attributed as one of the main causes of the undercurrents

1192 (Mukherjee et al., 2014). A recent modelling study suggests that the wintertime undercurrent off Cuddalore consists of
1193 two separate subsurface anticyclonic eddy circulations: a shallow small scale circulation at a depth range of 100-200 m
1194 and a broader and deep flow below 500 m depth off the continental slope (Francis et al., 2020). The shallow subsurface
1195 anticyclonic eddy was found to spin off from the zonal shear of the mean near-surface EICC along the shelf break (Fig.
1196 14). These eddies exhibit high frequency fluctuations and have 20-30 km length scales. Since the zonal share of the EICC
1197 is primarily linked to the strength of the EICC itself, the variability and strength of this undercurrent is also linked with
1198 the EICC.

1199 **4.4.1.4 Sri Lanka Dome**

1200 The Sri Lanka Dome (Vinayachandran et al. 1999; Schott and McCreary, 2001; Wijesekera et. al, 2016, Cullen and
1201 Shroyer, 2019) is mainly visible as a closed anticyclonic (clockwise) eddy in the near-surface geostrophic current velocity
1202 field starting in May and lasting through October (Fig. 15c). It is a recurring upwelling dome that forms east of Sri Lanka
1203 between 5-10°N, 83–87°E. The SLD is embedded within the Southwest Monsoon Current (SMC) system (Gadgil, 2003)
1204 and enhances the SMC exchange from the Arabian Sea to the Bay of Bengal (Anutaliya et al., 2017). Upwelling associated
1205 with the SLD influences the vertical exchange of water properties, enhances biological productivity, and cools sea surface
1206 temperature (SST) which affects local atmospheric convection (Vinayachandran et al., 2004; de Vos et al., 2014).



1207

1208 **Figure 15: Climatology (2002-2018) of chlorophyll-a concentrations (colormap) and current velocities (arrows) in**
 1209 **the Bay of Bengal for (a) January (b) April (c) July (d) October. Chlorophyll climatology was obtained from the**
 1210 **MODIS-Aqua product and current velocities were obtained from the third-degree Ocean Surface Current Analysis**
 1211 **Real-time (OSCAR) product.**

1212

1213

1214 4.4.2 Arabian Sea

1215 Like the Bay of Bengal (BoB), the Arabian Sea (AS) near surface circulation is also driven primarily by the seasonally
 1216 reversing monsoon winds. The AS is connected to the BoB through the passage between the southern tip of India and the
 1217 equatorial wave guide, and to the southern hemisphere by the cross equatorial flow via the Somali current system. The
 1218 Somali current (Fig. 10) forms one of the western boundary currents of the AS. Another major boundary current system

1219 is along the west coast of India, the WICC (Fig. 10), which transports heat and salt from the northern Arabian Sea to the
1220 BoB, and vice-versa. Recent observations (Chatterjee et al., 2012) and modelling studies (Shankar et al., 2016; Vijith et
1221 al., 2016) indicate that the northern extent of the WICC reaches up to 20°N during the winter monsoon, carrying fresher
1222 BoB water to the northern latitudes and modulating the wintertime convection there. In the last couple of decades, the
1223 strengthening of WICC and NMC has decreased the SSS in the eastern Arabian Sea (Varna et al., 2021).

1224 **4.4.2.1 Somali current System**

1225 The Somali Current is a seasonally reversing western boundary current and is often composed of discontinuous non-linear
1226 eddy driven flows. During summer it flows poleward and the upwelling here is nearly as large as for the eastern boundary
1227 upwelling regimes of the Pacific and Atlantic Oceans (See Schott and McCreary, 2001 for a detailed review).
1228 Unfortunately, owing to piracy, direct in-situ observations are very rare in this region and mostly date back to the early
1229 1960s and 1970s. Hence, the scientific community has mostly relied on numerical model simulations to enhance
1230 understanding of this region over the last few decades.

1231 Recent modelling studies suggest that during the summer monsoon, unlike other western boundary currents, the Somali
1232 Current system can be divided into three dynamically distinctive regions (Wang et al., 2018; Chatterjee et al., 2019):
1233 northern (north of 8°N), central (3-8°N) and the southern (south of 3°N) part. The northern and southern parts are driven
1234 by the large anticyclonic gyres called the Great Whirl (GW) and the southern Gyre (SG), respectively (Fig. 10a). Local
1235 southwesterly alongshore winds known as the Findlater Jet (Findlater, 1969) drives Ekman transport all along the Somali
1236 coast (Schott and McCreary, 2001) with varied magnitude which is strongest in the southern part, and significantly
1237 weakens northward (Chatterjee et al., 2019). The wind stress forcing leads to Ekman Pumping in the central Arabian Sea,
1238 setting up a bowl-shaped mixed layer and warming at the 100 m level. Ekman downwelling velocities are strongest in the
1239 northern part and likely contribute to the formation of the Great Whirl front which upwells cold subsurface water in this
1240 part of the coast. The central part, in contrast, is mainly driven by the local winds and remotely forced Rossby waves. In
1241 fact, the annual Rossby waves radiated out of the southwestern coast of Sri Lanka seem to play a major role in the reversal
1242 of currents to poleward flow in the northern part of the Somali coast as early as mid April. This reversal likely initiates
1243 the generation of the Great Whirl (Beal and Donohue, 2013; Vic et al., 2014), a month before the strong northeastward
1244 Findlater Jet commences along the Somali coast. As the monsoon progresses, these downwelling favourable Rossby waves
1245 oppose the coastal Ekman upwelling and thereby start to weaken the upwelling all along the coast. Moreover, as the
1246 alongshore winds peak, this favours enhanced mixing at the bottom of the mixed layer, which deepens the thermocline
1247 further. This process is more conspicuous in the central part of the coast, where the depth of the 22°C isotherm deepens
1248 by about 30-40 m from June to August (Chatterjee et al., 2019). By this time, the upwelling becomes limited to the northern
1249 part of the coast along the Great Whirl front of the Somali region.

1250 Climatological characteristics of the Somali Undercurrent (SUC) have been revealed by a new multi-decadal time series
1251 of temperature, salinity and geostrophic velocity constructed from repeat XBT transects and Argo observations (Zang et
1252 al. 2021). They find that the SUC flows southeastward during the monsoon transition periods in boreal spring (April-June)
1253 and fall (September-November), against the northeastward flow of the Somali Current. The depth of the SUC core is
1254 shallower during the spring transition (~500 dbar in April) and has a maximum depth of ~1200 dbar in September. Core
1255 speeds are 2.5-4 cm s⁻¹ in spring; in fall the core speed strengthens from 0.2 to 10.6 cm s⁻¹ from September to November
1256 and then disappears in December. Volume transport of the Somali Current and SUC (0-2000 dbar) has a maximum of 29.6
1257 Sv northeastward in the summer monsoon and minimum of 13 Sv southwestward during the fall transition when the SUC
1258 is strong.

1259 4.4.2.2 West India Coastal Current (WICC)

1260 The WICC reverses its direction annually: flowing equatorward (upwelling favourable) during the summer monsoon (May
1261 to September; Fig. 10a) and poleward (downwelling favourable) during the winter monsoon (November to February; Fig.
1262 10b). The equatorward flow during the summer characterises the WICC as a classical eastern boundary current (Shetye
1263 and Shenoi, 1988). Interestingly, as the monthly mean alongshore winds off the west coast of India are always equatorward
1264 throughout the year, the surface currents flow against the winds during the winter, driven by coastally-trapped Kelvin
1265 waves forced remotely in the BoB and along the east coast of India (McCreary et al., 1993; Shankar and Shetye, 1997;
1266 Shankar et al., 2002; Suresh et al., 2016). Recent observations based on satellite data and alongshore ADCP moorings
1267 reveal strong interannual variability of this seasonal cycle. Vialard et al. (2009b), based on a short ADCP record during
1268 2006-2008, reported an absence of seasonal cycle off Goa and they attributed this absence to the radiation of Rossby waves
1269 south of the critical latitude. As the longer record of ADCP data became available, a clear seasonal cycle in the WICC
1270 became evident with weaker amplitudes in the south, stronger poleward (Amol et al., 2014).

1271 The WICC also shows significant intraseasonal variability at times, particularly during boreal winter, exhibiting much
1272 stronger energy in the intraseasonal band than in the seasonal band (Vialard et al., 2009b; Amol et al., 2014). Unlike the
1273 seasonal cycle, intraseasonal variability is stronger in the south and weakens poleward. Vialard et al. (2009b) attributed
1274 this intraseasonal variability to the atmospheric MJO forcing. Recently, a modelling study suggested that interception of
1275 the intraseasonal equatorial Rossby waves by the southern tip of India and Sri Lanka excites coastal Kelvin waves which
1276 contribute significantly (~60–70%) to the intraseasonal variability along the west coast (Suresh et al., 2013). A satellite
1277 sea level study by Dhage and Sturb (2016) confirmed the model-based findings of Suresh et al. (2013) and revealed that
1278 large-scale winds from the south of India and Sri Lanka also contribute to the coastal signals along the west coast of India.

1279 Another striking feature observed in these ADCP data is the clear signature of upward phase propagation in all timescales
1280 during both monsoon seasons. This upward phase propagation is more conspicuous for the seasonal period than for the

1281 intraseasonal. As a result, the phase of the surface currents often tends to be opposite that in the subsurface layers (Amol
1282 et al., 2014). Moreover, it is found that the strength of this undercurrent intensifies northward along the west coast with
1283 strongest undercurrent off Mumbai and the weakest off Kanyakumari (southernmost point of Indian mainland), indicating
1284 a possible downward propagation of energy along the ray path as suggested earlier by Nethery and Shankar (2007). Since
1285 the ray angle (θ) depends on the frequency (σ) and stratification (N_b) according to $\theta = \sigma / N_b$ (McCreary, 1984; Nethery and
1286 Shankar, 2007) the angle the beam makes from the horizontal is deeper for the intraseasonal band than for the seasonal.
1287 As a result, intraseasonal beams propagate energy deeper into the water column. Therefore, while the WICC shows some
1288 coherence along the coast in the seasonal time scale, it completely decorrelates horizontally for the intraseasonal period.

1289

1290 **4.4.3 Biogeochemical Variability**

1291 In the Bay of Bengal, the large freshwater input gives rise to enhanced stratification that inhibits upwelling and wind-
1292 mixing and therefore nutrient supply to surface waters (Kumar et al., 2002; Vinayachandran et al., 2002; Madhupratap et
1293 al., 2003; Vinayachandran, 2009). Nonetheless, increased productivity is observed along the coast primarily in association
1294 with riverine nutrient inputs (Vinayachandran, 2009). These nutrients stimulate diatom blooms (Sasamal et al., 2005)
1295 leading to significant increases in Chl-*a* concentration ($\sim 30\text{--}100 \text{ mgChla m}^{-2}$) and production ($\sim 0.55\text{--}1 \text{ gC m}^{-2} \text{ d}^{-1}$) near
1296 the coast (Gomes et al., 2000; Fig. 15). This high Chl-*a* river water flows either along the coast or offshore, up to several
1297 hundred kilometers, depending on the coastal current pattern (Vinayachandran, 2009). Along the Indian coast, the flow
1298 of Chl-*a*-rich water is determined by the EICC, which flows northward during the spring intermonsoon period and
1299 Southwest Monsoon and southward during the autumn intermonsoon and Northeast Monsoon (Fig. 15). When the EICC
1300 meanders seaward from the Indian coast, it leads to offshore increases in high chlorophyll water. During the spring
1301 intermonsoon and Southwest Monsoon the northward-flowing EICC is upwelling favorable, which may contribute to
1302 increases in Chl-*a* concentration and primary production along the coast (Hood et al., 2017)

1303

1304 Elevated productivity is observed further offshore in the southwestern Bay of Bengal during the Northeast Monsoon
1305 (Vinayachandran and Mathew, 2003; Vinayachandran, 2009). Modeling studies suggest that this is caused by wind-driven
1306 entrainment, not only of subsurface nutrients, but also of phytoplankton from the subsurface chl_a maximum that is present
1307 during the autumn intermonsoon period (Vinayachandran et al., 2005). In contrast, productivity near the coast is
1308 suppressed during the Northeast Monsoon when the EICC flows southward (Fig. 14). Presumably, this is due to a
1309 combination of the downwelling-favorable currents and winds. However, primary production over the shelf in the northern
1310 part of the Bay increases during the Northeast Monsoon (Gomes et al., 2000; Fig. 15), possibly due to river nutrient inputs
1311 (Vinayachandran, 2009) and / or wind-stress and buoyancy-driven nutrient entrainment as is observed in the northern
1312 Arabian Sea during the Northeast Monsoon (Wiggert et al., 2000; 2005; Hood et al., 2017).

1313
1314 Subsurface Chl-*a* maxima are observed in the Bay of Bengal during all seasons whenever and wherever wind forcing
1315 and/or currents are insufficiently strong to upwell or entrain them into the surface layer (Sarma and Aswanikumar, 1991;
1316 Murty et al., 2000; Sarjini and Sarma, 2001; Kumar et al., 2007). During the intermonsoon periods the Bay of Bengal
1317 transitions to more oligotrophic conditions with relatively low surface chlorophyll concentrations ($< 0.6 \text{ mg/m}^3$; Fig. 15)
1318 and production rates ($< 700 \text{ mgC m}^{-2} \text{ d}^{-1}$; see Fig. 6 in Hood et al., 2017). *Trichodesmium erythraeum* blooms have been
1319 observed during the intermonsoon periods along with high abundances of *Synechococcus* and heterotrophic dinoflagellates
1320 (Sarjini and Sarma, 2001; Jyothibabu et al., 2008). In offshore waters subsurface chlorophyll maxima are generally located
1321 between 40 and 70m in autumn and 60 and 90m in spring (Kumar et al., 2007). These deep Chl-*a* maxima tend to shoal
1322 near the coast (Sarma and Aswanikumar, 1991; Murty et al., 2000) and their depth and chlorophyll concentrations are
1323 strongly influenced by eddies (Kumar et al., 2007).

1324
1325 Strong upwelling also occurs along the southern coast of Sri Lanka during the Southwest Monsoon (Vinayachandran,
1326 2004; 2009; de Vos et al., 2014). Satellite SST and chlorophyll images reveal dramatic eastward advection of cool ($< 28^\circ$
1327 C) chlorophyll rich upwelled water by the SMC (Vinayachandran, 2004; 2009; de Vos et al., 2014). Chlorophyll-rich
1328 waters from the southwestern coast of India are also advected by the SMC towards Sri Lanka during the Southwest
1329 Monsoon (Vinayachandran, 2004; 2009; Strutton et al., 2015). Surface chlorophyll concentrations and rates of primary
1330 production along the southern coast of Sri Lanka during the Southwest Monsoon can exceed 10 mgChla m^{-3} (de Vos et
1331 al., 2014) and $1000 \text{ mgC m}^{-2} \text{ d}^{-1}$ (Fig. 6 in Hood et al., 2017), respectively, compared to much lower concentrations and
1332 rates during the Northeast Monsoon when the NMC flows westward (de Vos et al., 2014; Hood et al., 2017).
1333 Vinayachandran (2004; 2009) attribute the productivity response during the Southwest Monsoon to nutrient enrichment
1334 from coastal upwelling driven by monsoon winds. Presumably, these high chlorophyll concentrations and production rates
1335 are associated with diatom blooms. This elevated productivity extends to the east of Sri Lanka during the peak of the
1336 Southwest Monsoon (Vinayachandran et al., 1999; Vinayachandran, 2004; 2009). This eastward extension into the
1337 southern Bay of Bengal occurs along the path of the SMC (Vinayachandran et al., 1999) and is associated with upward
1338 Ekman pumping east of Sri Lanka. This Ekman pumping also leads to the formation of the aforementioned Sri Lanka
1339 Dome (Vinayachandran and Yamagata, 1998).

1340
1341 The western side of the northern Indian Ocean transitions during the southwest monsoon to a eutrophic coastal upwelling
1342 system in response to the upwelling favorable winds and currents (Wiggert et al., 2005; Hood et al., 2017 and references
1343 cited therein; Fig. 5 ; Figs. 5 and 6 in Hood et al., 2017; Lakshmi et al., 2020). These changes can be seen in ocean color
1344 data as substantial increases in chl a concentrations along the coasts of Somalia, Yemen and Oman (e.g., Brock and
1345 McClain, 1992; Banse and English, 2000; Kumar et al., 2000; Lierheimer and Banse, 2002; Wiggert et al., 2005; George
1346 et al., 2013; Hood et al., 2017). Chlorophyll-*a* concentrations in the western Arabian Sea can exceed 40 mgChla m^{-2} during

1347 the southwest monsoon with production rates $> 2.5 \text{ gC m}^{-2}\text{d}^{-1}$ (Marra et al. 1998; Fig. 6 in Hood et al., 2017). However,
1348 the environmental conditions vary significantly between the eutrophic coastal zones to the west and the oligotrophic open
1349 ocean waters offshore that are influenced by wind-curl induced downwelling to the southwest of the Findlater Jet (Lee et
1350 al., 2000; Lakshmi et al., 2020). The surface nitrate and Chl-*a* concentrations decline dramatically from > 10 to < 0.02
1351 μM and from > 1.0 to $< 0.2 \text{ mgChla m}^{-3}$, respectively, from the west coast to open ocean in the Arabian Sea (Brown et al.,
1352 1999; Wiggert et al., 2005; Hood et al., 2017). In general, the phytoplankton community structure transitions to larger
1353 cells (diatoms) during the southwest monsoon in the western Arabian Sea (Brown et al., 1999; Tarran et al., 1999;
1354 Shalapyonok et al., 2001; Lakshmi et al., 2020). However, small primary producers remain important, even in areas
1355 strongly influenced by coastal upwelling (Brown et al., 1999; Lakshmi et al., 2020). In contrast, during the oligotrophic
1356 spring and fall intermonsoon periods, surface waters in the western Arabian Sea are dominated by picoplankton (Garrison
1357 et al., 2000). Subsurface Chl-*a* maxima are observed between 40 and 140 meters in the central southeastern Arabian Sea
1358 during all seasons (Gundersen et al., 1998; Goericke et al., 2000; Ravichandran et al., 2012), at times occurring in layers
1359 below the oxyclines of the oxygen minimum zone (Goericke et al., 2000). These features are strongly influenced by
1360 mesoscale features (Gundersen et al., 1998).

1361
1362 During the southwest monsoon off Oman and Somalia, the presence of the topographically-locked eddies generate strong
1363 offshore flows that advect high nutrient, high Chl-*a* concentrations and coastal phytoplankton communities hundreds of
1364 kilometers offshore (Keen et al., 1997; Latasa and Bidigare, 1998; Manghnani et al., 1998; Gundersen et al., 1998;
1365 Hitchcock et al., 2000; Lee et al., 2000; Kim et al., 2001). These advective effects can be seen, for example, in association
1366 with the Great Whirl off the coast of northern Somalia (Hitchcock et al., 2000) and in the filaments that develop off the
1367 Arabian Peninsula during the southwest monsoon (Wiggert et al. 2005; Hood et al., 2017). In contrast, during the northeast
1368 monsoon, the circulation and winds transition to downwelling favourable. During the northeast monsoon, cold dry
1369 northeasterly winds from southern China and the Tibetan Plateau flow across the northern Arabian Sea. The sheer from
1370 these winds, combined with surface cooling and buoyancy-driven convection, drive mixing and entrainment of nutrients
1371 that, in turn, promote modest increases in chlorophyll and primary production over the northern Arabian Sea (Wiggert et
1372 al., 2000; Wiggert et al., 2005; Fig. 5; Figs. 5 and 6 in Hood et al., 2017). These increases in Chl-*a* have been associated
1373 with increased diatom abundance (Banse and McClain, 1986; Sawant and Madhupratap, 1996). In the last decade,
1374 however, there appears to have been a shift in the composition of winter phytoplankton blooms in the northern and central
1375 Arabian Sea from diatom dominance to blooms of a large, green mixotrophic dinoflagellate, *Noctiluca scintillans* (Gomes
1376 et al., 2014; Goes et al., 2020).

1377
1378 During the southwest monsoon, the upwelling-favorable WICC induces upwelling along the west coast of India, which
1379 increases Chl-*a* concentrations by more than 70% compared to the central Arabian Sea (Kumar et al., 2000; Naqvi et al.,
1380 2000; Luis and Kawamura, 2004; Hood et al., 2017). The increased Chl-*a* concentrations near the coast are associated

1381 with increases in diatom abundance (Sawant and Madhupratap, 1996). However, these increases in Chl-*a* and their offshore
1382 extent are modest compared to the western Arabian Sea (Fig. 5; Fig. 5 in Hood et al., 2017). In contrast, during the
1383 northeast monsoon the WICC is downwelling-favorable and tends to suppress primary production off the southwestern
1384 coast of India. The depletion of nutrients in this region during the northeast monsoon coincides with blooms of
1385 *Trichodesmium* and dinoflagellate species (Parab et al., 2006; Matondkar et al., 2007) resulting in the extremely high rates
1386 of nitrogen fixation (Gandhi et al., 2011, Kumar et al., 2017). However, as discussed above, further north and offshore,
1387 nutrient entrainment enhances phytoplankton biomass and primary production during the northeast monsoon (Wiggert et
1388 al., 2000; McCreary et al., 2001; Luis and Kawamura, 2004; Gomes et al., 2014; Goes et al., 2020; Fig. 5). Near-surface
1389 Chl-*a* and primary production off the west coast of India (estimated from satellite ocean color measurements) increases
1390 from ~9 to 24 mgChl_a m⁻² and from ~1 to 2.25 g C m⁻² d⁻¹, respectively, from winter to the summer monsoon (Luis and
1391 Kawamura, 2004; Fig. 5; Figs. 5 and 6 in Hood et al., 2017). The elevated productivity during the southwest monsoon is
1392 modulated by the coastal Kelvin waves that originate from the Bay of Bengal and propagate along the West Indian Shelf,
1393 modifying circulation patterns and upwelling (Luis and Kawamura, 2004).

1394 **5 Inter-ocean exchange**

1395 **5.1 Indonesian Throughflow**

1396 **5.1.1 General features**

1397 The Indonesian Throughflow (ITF) transfers low-salinity tropical waters from the Pacific to the Indian Ocean via the
1398 Indonesian seas (Fig. 10). The ITF is the only tropical oceanic pathway that links ocean basins and plays an important role
1399 in the global ocean circulation and climate system (Sprintall et al., 2014; 2019). The simultaneous measurements in the
1400 exit channels of the ITF from the International Nusantara Stratification and Transport (INSTANT) program during 2004-
1401 2006 (Gordon et al., 2008; Sprintall et al., 2009) suggested that the ITF has a mean transport of 15 Sv into the Indian
1402 Ocean. The ITF pathway is composed of many narrow channels within the Indonesian seas, among which about 80% of
1403 the total ITF is through the Makassar Strait (Fig. 10, Gordon et al., 2008, 2010). The remaining passages include the
1404 Maluku Sea, Lifamatola Passage, Karimata Strait and Sibutu Passage (Fang et al., 2010; Gordon et al., 2012; Susanto et
1405 al., 2013).

1406 **5.1.2 Variability, dynamics and influence**

1407 The interannual variability of the ITF is mainly dictated by the ENSO-related wind forcing through the Pacific waveguide
1408 with stronger transport during La Niña years (Meyers, 1996; England and Huang, 2005; Hu and Sprintall, 2016), but the
1409 IOD occasionally offsets the Pacific ENSO influences through the Indian Ocean wind variability and Indian Ocean

1410 waveguide (Sprintall and Révelard, 2014; Liu et al. 2015; Feng et al., 2018). For the strong negative IOD event in 2016,
1411 the Indian Ocean influence overwhelmed that of the Pacific leading to record low ITF volume transports because of the
1412 reduction in the interbasin pressure gradient (Pujiana et al., 2019). Strong wind forcing over the equatorial Indian Ocean
1413 triggers equatorial Kelvin waves and influences the ITF variability on intraseasonal, semi-annual and interannual time
1414 scales (Drushka et al., 2010; Pujiana et al., 2013; Shinoda et al., 2012). Kelvin waves through the Indian Ocean waveguide
1415 are suggested to influence the interannual variability in the tropical Pacific Ocean (Yuan et al., 2013; Pujiana and
1416 McPhaden, 2020).

1417 The ENSO cycle also influences the outflowing ITF transport through the salinity effect in the downstream buoyant pool,
1418 contributing about 36% of the total ITF interannual transport variation (Hu and Sprintall, 2016; Section 6.1). Fresh
1419 anomalies in the buoyant pool during La Nina years can be as large as 0.2 in practical salinity averaged over the upper 180
1420 m of the water column (Phillips et al. 2005). Such salinity anomalies can strengthen the volume transport of the LC through
1421 an increase in the zonal density gradient driving stronger southward flow (Feng et al., 2015a). The Inter-decadal Pacific
1422 Oscillation/Pacific Decadal Oscillation (IPO/PDO), through modulations of decadal wind stress in the tropical Pacific, has
1423 also directly influenced the strength of the ITF (Feng et al., 2011; Hu et al., 2015; Mayer et al., 2018). This has, in turn
1424 influenced heat and freshwater transports, causing upper ocean heat content to increase in the southern Indian Ocean (Feng
1425 et al., 2010; Schwarzkopf and Böning, 2011; Nidheesh et al., 2013; Sprintall, 2014; Lee et al., 2015; Nieves et al., 2015;
1426 Du et al., 2015; Ummenhofer et al., 2017) and produced interhemispheric contrasts in sea surface temperature (Dong and
1427 McPhaden, 2016). During the negative IPO phase, such as during the hiatus in warming of the globally averaged surface
1428 atmosphere (1998-2012), enhanced trade winds in the Pacific strengthened the ITF volume and heat transport into the
1429 Indian Ocean, driving a rapid warming trend in the Southern Indian Ocean (England et al., 2014; Nieves et al., 2015; Lee
1430 et al., 2015; Liu et al., 2015, Zhang et al., 2018). Contributions from air-sea exchanges (Jin et al. 2018a,b) have also been
1431 suggested to be important, as has a reduction in the oceanic heat exported from the Indian Ocean at its southern boundary
1432 (Lisa Beal, personal communication).

1433 Using a combination of theory, ocean reanalyses, OGCM simulations, and coupled climate model simulations, Jin et al.
1434 (2018a,b) found eastern and western Indian Ocean heat content to be affected by remote Pacific forcing through two
1435 distinct mechanisms: oceanic influences transmitted through the ITF and the atmospheric bridge. The intensified
1436 freshwater input within the Maritime Continent during the past decade was found to strengthen the ITF and its heat and
1437 freshwater transports into the Indian Ocean, causing significant warming and freshening trends and accelerated sea-level
1438 rise in the eastern Indian Ocean (Hu and Sprintall, 2017a, 2017b; Zhang et al., 2018; Jyoti et al., 2019). The decadal
1439 enhancement of the ITF transport has increased upper ocean heat content anomalies in the southeast Indian Ocean and
1440 increased the likelihood of marine heatwaves off the west coast of Australia (Feng et al., 2015b; Section 6.4).

1441 **5.2 Agulhas Leakage**

1442 **5.2.1 General features**

1443 At the tip of Africa, the southward-flowing Agulhas Current retroflects with most of the flow heading eastwards along the
1444 northern edge of the ACC, recirculating back into the Indian Ocean (Fig. 10, Section 4.2.2). Around 20-30% of the
1445 Agulhas Current enters the Atlantic Ocean as Agulhas leakage in the form of Agulhas rings and cyclones (van Sebille,
1446 2010a). Agulhas leakage estimates are sensitive to the definition used to calculate the leakage, ranging roughly between
1447 10 and 20 Sv (van Sebille et al., 2010b; Beron-Vera et al., 2013; Cheng et al., 2016; Holton et al., 2017). Bars et al. (2014)
1448 proposed an algorithm to measure Agulhas leakage anomalies using absolute dynamic topography data from satellites.

1449 The division of flow between Agulhas Leakage and Agulhas retroflexion can be influenced by the upstream Agulhas
1450 Current. In a Lagrangian particle tracking experiment, van Sebille et al. (2009) found that a weaker Agulhas Current,
1451 detaching farther downstream and generating anti-cyclonic vorticity, potentially leads to more Agulhas leakage and larger
1452 Indian-Atlantic inter-ocean exchange. However, eddy-resolving model results suggest that as model resolution increases,
1453 the sensitivity of the leakage to Agulhas Current transport anomalies is reduced (Loveday et al., 2014). In addition, the
1454 ITF potentially influences the Agulhas leakage (Le Bars et al., 2013) as model outputs suggest that the Indian Ocean
1455 contributes 12.6 Sv to the Agulhas leakage, half of which is from the ITF (Durgadoo et al., 2017).

1456 **5.2.2 Variability, dynamics and influence on climate**

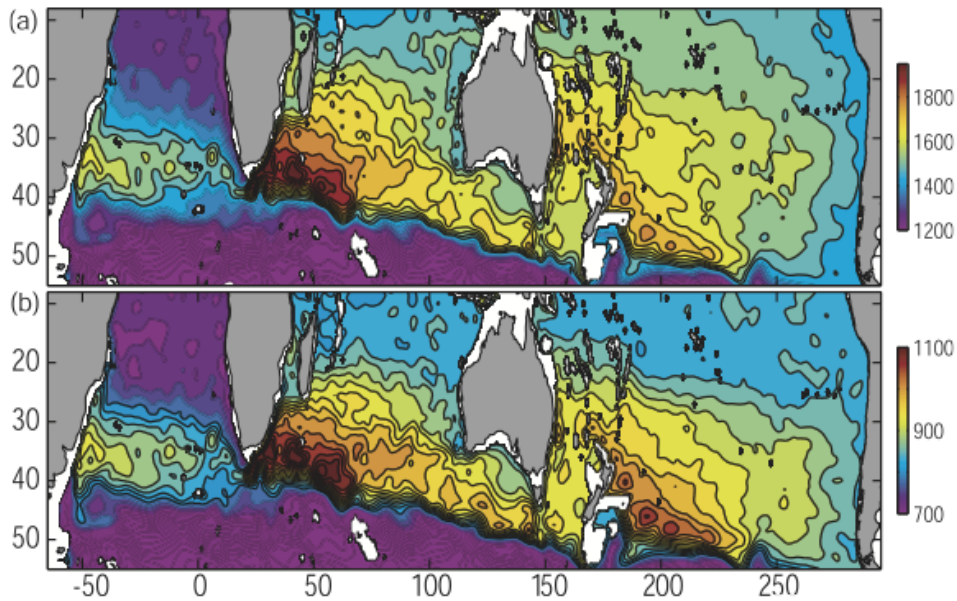
1457 The magnitude of the Agulhas leakage is controlled by wind forcing including the trade winds and the Southern
1458 Hemisphere Westerlies (e.g., Durgadoo et al., 2013). The poleward shift in the Southern Hemisphere westerlies associated
1459 with anthropogenic forcing induced a clear increase in the Agulhas leakage during 1995-2004 as shown in numerical
1460 simulations (Biastoch et al., 2009; Biastoch and Böning, 2013). Increased wind stress curl in the South Indian Ocean
1461 associated with the southward shift of westerlies led to significant warming in the Agulhas Current system since the 1980's
1462 (Rouault et al., 2009); however further work showed that this is due to an increase in eddies leading to a broadening of the
1463 current as opposed to intensification (Beal and Elipot, 2016). Given the non-linear nature of Agulhas leakage, the difficulty
1464 of observing it and ocean model biases in the region, quantifying Agulhas leakage is very challenging (Holton et al., 2017).
1465 At seasonal time scales, the Agulhas leakage variability is controlled by eddies, however recent studies have shown that
1466 eddies might not contribute as significantly to leakage as was thought and the non-eddy leakage transport is likely to be
1467 constrained by large-scale forcing at longer time scales (e.g., Cheng et al., 2018). A recent study shows that the subsurface
1468 signal from the ENSO cycle influences the Agulhas leakage through Rossby waves with a time lag of 2 years (Paris et al.,
1469 2018).

1470 The Agulhas leakage carries warm and saline water from the Indo-Pacific Ocean into the Atlantic Ocean. The Agulhas
1471 leakage has been suggested to influence the Atlantic Meridional Overturning Circulation strength (AMOC; Beal et al.
1472 2011; Weijer and van Sebille, 2014; Biastoch et al. 2015) and modify the AMOC convective stability (e.g., Haarsma et
1473 al., 2011; Caley et al., 2012; Castellanos et al., 2017). It is suggested that the increases in the Agulhas leakage due to
1474 anthropogenic warming during the past decades would act to strengthen the Atlantic overturning circulation (e.g., Beal et
1475 al., 2011).

1476 The Agulhas leakage is an important source of decadal variability in the AMOC through Rossby waves (Biastoch et al.,
1477 2008; 2015). Source waters from the Agulhas Current take more than four years and mostly one to four decades to arrive
1478 in the North Atlantic Ocean (van Sebille et al., 2011; R hls et al., 2013). The increased Agulhas leakage during 1995-2004
1479 has contributed to the salinification of the South Atlantic thermocline waters (Biastoch et al., 2009). Hindcast experiments
1480 suggest that the Agulhas leakage increased by about 45% during the 1960s-2000s, leading to the observed warming trend
1481 in the upper tropical Atlantic Ocean (L bbecke et al., 2015).

1482 **5.3 Supergyre connection to the South Pacific**

1483 The extreme strong westerly wind stress in the Southern Hemisphere gives rise to a wide and energetic subtropical
1484 supergyre (Figure 16), the Southern Hemisphere supergyre, that connects three ocean basins (e.g., Ridgway and Dunn,
1485 2007; Speich et al., 2007; Lambert et al., 2016; Maes et al., 2018; Cessi, 2019). Although the near-surface circulation is
1486 eastward across the southern Indian Ocean, there are subsurface westward flows beneath (Section 4.2.3; Schott and
1487 McCreary 2001; Domingues et al. 2007; Furue et al. 2017), and the depth-integrated circulation reveals the westward
1488 return flow of the equatorward side of the Indian Ocean's anti-clockwise subtropical gyre. In Figure 16, the southern side
1489 of the Indian Ocean subtropical gyre extends eastward south of Australia to connect with the western Pacific subtropical
1490 gyre. The return flow is accomplished via a pathway that includes the East Australian Current, the South Pacific's western
1491 boundary flow; the Tasman Leakage, a westward flow south of Tasmania that carries Pacific Ocean water back to the
1492 Indian Ocean (distinct from the Flinders Current that hugs the continental slope, Duran et al 2020; Section 4.2.4); and
1493 northward flow in the eastern Indian Ocean to close the circulation. The ITF and Leeuwin Current are also part of the
1494 supergyre, connecting the Indian and Pacific Oceans through the Indonesian seas (e.g. Ridgway and Dunn, 2007).



1495
 1496 **Figure 16: The interbasin supergyre system for the Pacific and Indian Oceans as shown by the depth-integrated**
 1497 **steric height (a) $P_{0/2000}$, and (b) $P_{400/2000}$, derived from the CARS climatological temperature and salinity fields. The**
 1498 **contour interval in (a) is 50 m^2 and in (b) is 25 m^2 . Taken from Ridgway and Dunn 2007.**

1499 The supergyre is the subtropical gyre of the southern hemisphere. As such, its flow is primarily determined by the westward
 1500 integration of wind stress curl from the eastern boundaries as determined by Sverdrup dynamics. The latitudinal position
 1501 of the Subtropical Front at the southern edge of the supergyre is found to be controlled by strong bottom pressure torque
 1502 due to the interaction between the ACC and the ocean floor topography (De Boer et al., 2013). According to one analysis
 1503 in SODA (Simple Ocean Data Reanalysis), the water masses in the supergyre became cooler and fresher and shifted
 1504 southward by about 2.5° due to changes in the basin-scale wind forcing during 1958–2007 (Duan et al., 2013). A recent
 1505 study using altimeter observations shows a clear strengthening of the Southern Hemisphere supergyre in all three oceans
 1506 since 1993 as indicated in the large trends of sea surface height and their contrast. Argo observations and ECCO
 1507 assimilations suggest that the strengthening extends to deeper than 2000 m (Qu et al., 2019). The spin-up of the Southern
 1508 Hemisphere supergyre is attributed to the poleward shift and strengthening of westerly winds that are linked to an
 1509 increasingly positive southern annular mode (Qu et al., 2019).

1510 **5.4 Roles of salinity in inter-ocean exchange**

1511 Ocean salinity is one of the basic variables that determines the oceanic stratification, sea level change and climate change
 1512 (e.g., Llovel and Lee, 2015; Kido and Tozuka, 2017; Sprintall et al., 2019). However, the role of salinity in ocean
 1513 circulation has been largely underestimated until the recent decade when *in situ* observations of subsurface and surface

1514 salinity from Argo and satellite salinity missions became available. These new observations have revolutionized our
1515 understanding of the influence of salinity on ocean circulation and dynamics (Vinogradova et al. 2019, and references
1516 therein).

1517
1518 Four major processes control the salinity in the Indian Ocean: net air-sea fluxes (evaporation minus precipitation),
1519 freshwater inflow from large rivers in the Bay of Bengal, inflow of relatively fresh waters from the Pacific Ocean via the
1520 Indonesian Throughflow, and inflow of saltier waters from the Red Sea and the Persian and Arabian Gulfs. These different
1521 drivers combine to give the Indian Ocean salinity its unique flavour: a strong east-west gradient in the North Indian Ocean
1522 (salty in the Arabian Sea and fresh in the Bay of Bengal) and strong north-south gradients in the South Indian Ocean (fresh
1523 in the tropics, and salty in the subtropics) (Fig. 4).

1524
1525 Salinity is a crucial variable to understand Indian Ocean dynamics. For instance, salinity has strong ties with the Indian
1526 Ocean Dipole (e.g., Du and Zhang, 2015; Durand et al., 2013; Grunseich et al., 2011; Kido and Tozuka, 2017; Nyadjro
1527 and Subrahmanyam, 2014; Zhang et al. 2016; Section 6.2), the EGC (Menezes et al., 2013; Section 4.2.3), LC transport,
1528 Ningaloo Niño and marine heatwaves off western Australia (e.g., Feng et al., 2015a), and the El Niño/La Niña climate
1529 mode (e.g., Hu and Sprintall, 2016; Zhang et al., 2016). Salinity plays an essential role in the dynamics of the seasonal
1530 Wyrki Jets in the equatorial zone (e.g., Masson et al., 2003), extra-equatorial Rossby waves (Heffner et al., 2008; Menezes
1531 et al., 2014b; Vargas-Hernandez et al., 2015; Banks et al., 2016), Madden-Julian and Intraseasonal Oscillations (e.g.,
1532 Grunseinch et al., 2013; Guan et al., 2014; Subrahmanyam et al., 2018), barrier-layer dynamics (e.g., Drushka et al., 2014;
1533 Felton et al., 2014), and the North Indian Ocean (e.g., D'Addezio et al., 2015, Fournier et al., 2017; Mahadevan et al.,
1534 2016; Nyadjro et al., 2011, 2012, 2013; Wilson and Riser, 2016; Spiro Jaeger and Mahadevan, 2018).

1535
1536 Salinity variability within the Indonesian Seas has been shown to control the transport of the ITF. Andersson and
1537 Stigebrandt (2005) proposed that a downstream buoyancy pool in the outflowing ITF region acts to regulate the ITF
1538 transport. Gordon et al. (2003, 2012) pointed out that low salinity surface water from the South China Sea is drawn into
1539 the Java Sea. Combined with the monsoonal precipitation over the Maritime Continent and seasonal monsoon winds, this
1540 freshwater plug contributes to the seasonal fluctuation of the Makassar Strait Throughflow transport and inhibits the inflow
1541 of tropical Pacific surface water from the Mindanao Current (e.g., Gordon et al., 2012; Lee et al., 2019). Recently, Hu and
1542 Sprintall (2016) found that about 36% of the interannual ITF transport is attributable to the salinity effect associated
1543 with freshwater input anomalies due to the ENSO cycle. Jyoti et al. (2019) further examined this salinity effect and found
1544 that the unprecedented sea-level rise in the southern Indian Ocean since the beginning of the 21st Century is attributed to
1545 the accelerated heat and freshwater intrusion by the ITF. A significant strengthening of the ITF transport in the 2000s has
1546 given rise to a subsequent warming and freshening of the eastern Indian Ocean (e.g., Hu and Sprintall, 2017a, 2017b,

1547 Section 6.1). The southeast Indian Ocean is one of the few places in the global ocean where the halosteric component of
1548 sea level rise is as large as the thermosteric component (Llovel and Lee, 2015).
1549

1550 **6 Modes of Interannual Climate Variability in the Indian Ocean**

1551 **6.1 ENSO teleconnection and the Indian Ocean Basin mode**

1552 ENSO influences the Indian Ocean circulation through the Pacific-to-Indian Ocean oceanic waveguide and atmospheric
1553 teleconnections. Through the atmospheric bridge, El Niño conditions in the Pacific induce an anticyclonic wind anomaly
1554 pattern in the southeast Indian Ocean (Xie et al., 2002), whereas La Niña induces a cyclonic wind anomaly pattern (Feng
1555 et al., 2013). The ENSO teleconnection also drives SST variability over the western Indian Ocean during ENSO
1556 development. The tropical Indian Ocean experiences prolonged warming (cooling) that peaks in the following boreal
1557 spring and persists into boreal summer, after the decay of El Niño (La Niña) events, the so-called Indian Ocean Basin
1558 (IOB) mode (Yang et al., 2007). The westward propagating Rossby waves induced by ENSO may also help sustain the
1559 warming (cooling) of the tropical Indian Ocean (Xie et al., 2002), fueled by regional air-sea coupling (Du et al., 2009).
1560 The IOB warming has a capacitor effect for El Niño to influence boreal summer climate, such as for the Indian monsoon
1561 (Zhou et al., 2019), and remote impacts in the northwest Pacific (Xie et al., 2009, 2016), including China and Japan (Hu
1562 et al., 2019). Details of the Indo-Western North Pacific capacitor effect are summarized in Xie et al. (2016) and Kosaka et
1563 al. (2021). The relationship between ENSO and IOB varies on decadal time scales (e.g., Xie et al., 2010; Chowdary et al.,
1564 2012) and under global warming scenarios. The IOB warming tends to persist longer after El Niño events according to
1565 CMIP5 model simulations (Zheng et al., 2013).

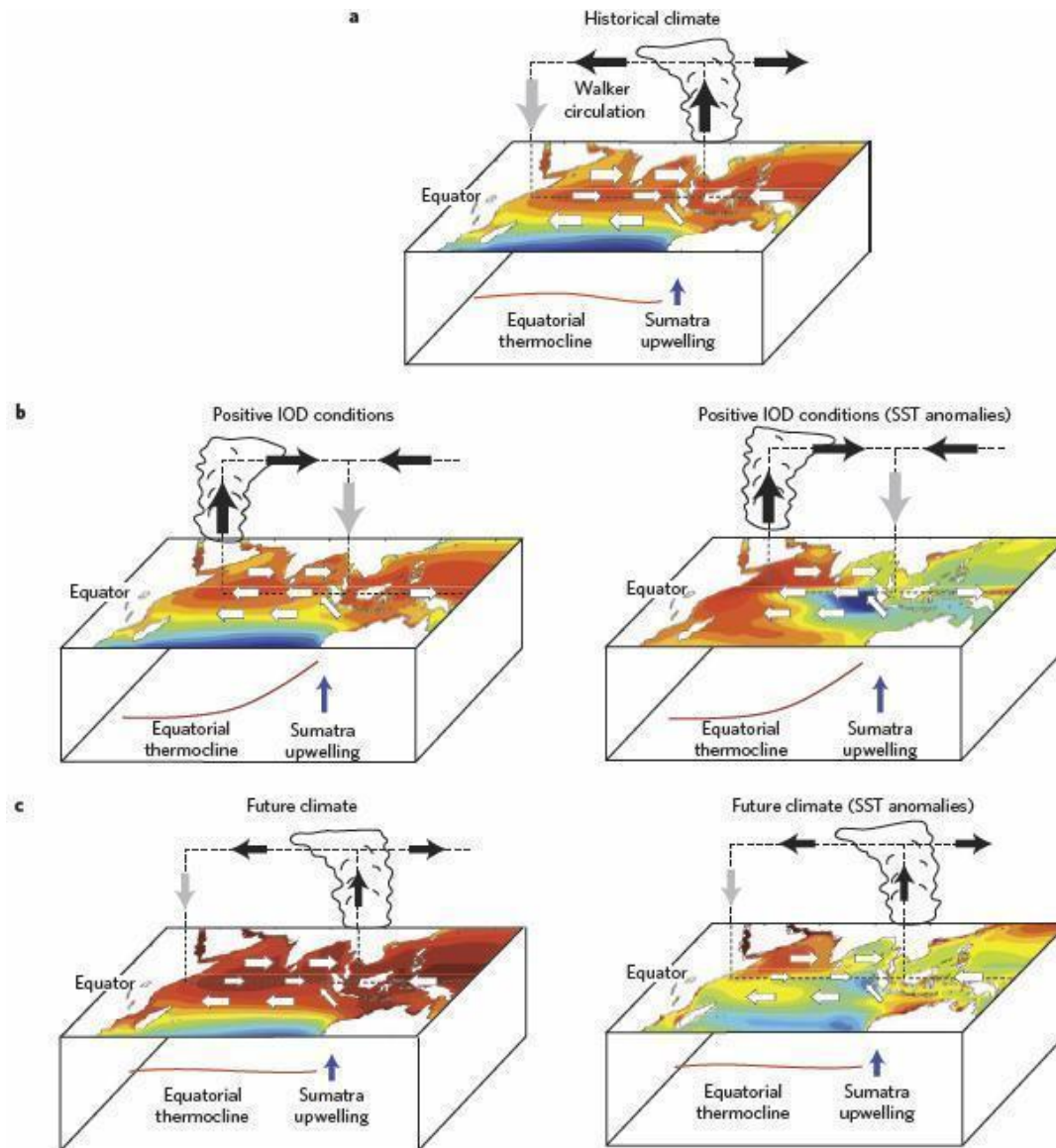
1566 The ITF variability lags ENSO by 8-9-months, found in ocean model results (England and Huang, 2005) and derived from
1567 the geostrophic transport across an Australia-Indonesia XBT section (Liu et al., 2015). The variability of the ITF transport
1568 drives sea level and upper ocean heat content anomalies in the southeast Indian Ocean. Through the waveguide, ENSO
1569 has a direct influence on the strength of the Leeuwin Current (Section 4.2.4), with a stronger poleward volume and heat
1570 transport during a La Niña event (Feng et al., 2008). A stronger Leeuwin Current during La Niña events leads to greater
1571 baroclinic instability of the current and enhanced generation of eddies that leads to interannual variability of the eddy
1572 kinetic energy in the southeast Indian Ocean (Feng et al., 2005; Zheng et al., 2018). The increase of the ITF transport and
1573 enhancement of rainfall in the Indonesian Seas during strong La Niña events can drive up to 0.2-0.3 psu freshening
1574 anomalies in the upper southeast Indian Ocean (Phillips et al., 2005; Feng et al., 2015a; Hu and Sprintall, 2017a; Section
1575 5.1.2), which may have a compound effect in accelerating the Leeuwin Current (Feng et al., 2015a). Both ENSO and the

1576 IOD (see Section 6.2) influence the ITF and thus the exchange of heat from the Pacific into the Indian Ocean, but in
1577 concurrent IOD and ENSO events it appears that the influence from the IOD dominates (Sprintall and Revelard, 2014).

1578 Due to the opposing effects of the winds and dissipation, ENSO induced sea level and upper ocean heat content anomalies
1579 in the southeast Indian Ocean do not propagate far into the western Indian Ocean; instead, wind anomalies generate sea
1580 level and heat content anomalies of opposite signs in the western Indian Ocean through Rossby wave propagations
1581 (Masumoto and Meyers, 1998; Xie et al., 2002; Zhuang et al., 2013; Ma et al., 2019; Volkov et al., 2020; Nagura and
1582 McPhaden, 2021). Thus, the joint forcing of the oceanic waveguide and atmospheric teleconnection results in variations
1583 of meridional overturning circulation and heat transport in the Indian Ocean on a multi-year time scale, in phase with the
1584 ITF variability (Ma et al., 2019).

1585 **6.2 The Indian Ocean Dipole**

1586 There is increasing evidence that positive IOD events are more frequent and intense during the 20th century (e.g., Abram
1587 et al., 2008; Cai et al., 2013; Abram et al., 2020a,b; and references therein). A rare occurrence of three consecutive positive
1588 IOD events took place in 2006–2008 (Cai et al., 2009b). The skewness towards more positive and fewer negative IOD
1589 events (Cai et al., 2009a) is due potentially to an anthropogenically-driven shoaling thermocline in the eastern Indian
1590 Ocean (Cai et al., 2008). The three consecutive positive IOD events rarely occurred in Coupled Model Intercomparison
1591 phase 5 (CMIP5) models and the more recent frequent occurrence was consistent with regional Indo-Pacific Walker
1592 circulation trends (Cai et al., 2009c,d). An anthropogenic contribution was proposed since positive IOD events became
1593 more frequent over the period 1950–1999 in the CMIP5 models. Projected mean-state changes in the Indian Ocean with
1594 stronger easterly winds and a shoaling thermocline in the southeast Indian Ocean during austral spring favour positive
1595 IOD development, with a reduction in skewness between positive and negative IOD events likely (Cai et al., 2013; Figure
1596 17), and a three-fold increase in frequency of extreme positive IOD events by 2100 compared to the previous century (Cai
1597 et al., 2014a). However, model biases in Indian Ocean mean-state and IOD variability challenge these projected changes:
1598 models with excessive IOD amplitude bias tend to project a strong IOD-like warming pattern and increase in extreme
1599 pIOD occurrences, consistent with an enhanced Bjerknes feedback, and hence the projected IOD changes could represent
1600 spurious artefacts of model biases (Li et al., 2016). Yet, paleoclimate evidence supports trends observed in recent decades:
1601 based on a millennial IOD reconstruction from corals, extreme positive IOD events, as were observed in 1997 and 2019,
1602 were historically rare (Abram et al., 2020b). In the reconstruction, only ten extreme positive IOD events occurred and yet
1603 four events occurred in the last 60 years (Abram et al., 2020b). The increase in event frequency and intensity highlights
1604 the need to improve preparedness in regions affected by IOD events to minimize future climate risks posed by them.



1605

1606 **Figure 17: Historical austral spring mean climate and positive IOD conditions for the twentieth century, and future**
 1607 **austral spring mean climate. a, Historical mean climate, indicating SSTs, surface winds, the associated atmospheric**
 1608 **Walker circulation, the mean position of convection and the thermocline. In the western Indian Ocean, the**
 1609 **descending branch is broad and not well-defined, as indicated by a grey arrow. b, Typical conditions during a**
 1610 **positive IOD event. c, Projected future mean climate based on a CMIP5 multi-model ensemble average. Diagrams**
 1611 **with total SST fields are shown on the left; diagrams with SST anomalies referenced to the 1961–1999 mean for b,**

1612 **and referenced to the basin mean for c, are shown on the right. Reprinted from Cai et al. (2013) with permission**
1613 **from Springer Nature.**

1614 While model simulations and paleo proxy records suggest changes in the frequency and magnitude of IOD events in a
1615 warming climate, there is less observational evidence from other sources. Given the short observational record in the
1616 Indian Ocean, the role of decadal to multi-decadal variability across the broader Indo-Pacific region has recently emerged
1617 as a compounding factor: the number and frequency of IOD events have been observed to vary on decadal timescales.
1618 Decadal variations in SST featuring an IOD-like out-of-phase pattern between the western and eastern tropical Indian
1619 Ocean have been linked to the PDO (Krishnamurthy and Krishnamurthy, 2016) or IPO (Dong et al., 2016). A combination
1620 of processes transmits the signal from the Pacific to the Indian Ocean through both the atmospheric and oceanic bridges,
1621 leading to variations in the subsurface temperature structure in the Indian Ocean (Zhou et al., 2017; Jin et al., 2018a).
1622 Decadal modulations of the background state of the eastern Indian Ocean thermocline depth can thus pre-condition the
1623 Indian Ocean to more or less IOD events (Annamalai et al., 2005). Consequently, positive IOD events were unusually
1624 common in the 1960s and 1990s with a relatively shallow eastern Indian Ocean thermocline, while the deeper thermocline
1625 in the 1970s and 1980s was associated with frequent negative IOD and rare positive IOD events (Ummenhofer et al.,
1626 2017). The Indian Ocean stands out as a region with high skill in decadal predictions (Guemas et al., 2013) and improved
1627 understanding of decadal modulation of IOD events can aid in decadal prediction efforts for the Indian Ocean region.

1628 The relationship between ENSO and the IOD has been subject to ongoing debate. Recent research has shown that around
1629 two-thirds of IOD variability arises as a remote response to ENSO (Stuecker et al., 2017; Yang et al., 2015), with the
1630 remaining variability being independent of ENSO. Stuecker et al. (2017) argue that the ENSO-driven IOD can be seen as
1631 a combination of remotely driven wind and heat flux anomalies modulated by seasonally-varying Bjerknes feedback in
1632 the Indian Ocean. Further, they suggest that the ENSO-independent IOD events arise out of white noise atmospheric
1633 forcing coupled to these feedbacks (Stuecker et al., 2017). Variability internal to the Indian Ocean basin and unrelated to
1634 ENSO, arising from ocean-atmosphere feedback processes, does however modulate the evolution of IOD events and can
1635 lead to early termination of IOD events; as a result, including internal variability improves the predictability of the IOD
1636 (Yang et al., 2015). IOD variability internal to the Indian Ocean resembles recharge oscillator dynamics for ENSO, but
1637 equatorial heat content is less effective as a precursor for the IOD than for ENSO because of the strong impact of remote
1638 forcing from the Pacific on the IOD. Internal Indian Ocean dynamics however may contribute to the biennial nature of
1639 the IOD through the cycling of Kelvin/Rossby wave energy across the basin (McPhaden and Nagura, 2014). The
1640 relationship between ENSO and the IOD is not only one-way: IOD events have also been shown to influence the
1641 development of ENSO in the following year (Izumo et al., 2010; Wang et al., 2019; Cai et al., 2019; and references therein).

1642 Different types of IOD events have been described, each with distinct evolution and regional impacts (Du et al., 2013;
1643 Endo and Tozuka, 2016). Du et al. (2013) distinguished three types of IOD events according to the timing of their peak

1644 amplitude and overall duration: ‘unseasonable’ events that develop and mature mostly within June-August (JJA), ‘normal’
1645 events that develop and mature mostly within September-November (SON), and ‘prolonged’ events that develop in JJA
1646 and mature in SON, with the latter two described as the canonical IOD events (Du et al., 2013). The unseasonable IOD
1647 events have only been observed since the mid-1970s and have been suggested to be a response to the rapidly warming
1648 Indian Ocean SST and a weakened Walker circulation during austral winter (Du et al., 2013). The seasonal evolution and
1649 type of ENSO also seems to play a role in determining the IOD evolution and type, with atmospheric influences transmitted
1650 through variations in the Walker Circulation and oceanic ones through anomalous oceanic Rossby waves affecting timing
1651 and evolution of IOD events, especially during their developing phase (Guo et al., 2015; Zhang et al. 2015; Fan et al.,
1652 2017). However, Sun et al. (2015) suggested more IOD events independent of ENSO since the 1980s, along with higher
1653 correlations between the IOD and Indian summer monsoon activity, likely due to mean-state change in the tropical Indian
1654 Ocean due to weaker equatorial westerlies. The relationship between ENSO and the IOD has weakened in recent decades,
1655 linked to changes in the ENSO-induced rainfall anomalies over the Maritime Continent (Han et al., 2017).

1656 Recent advances in understanding variability and change in IOD characteristics have implications for the relationships
1657 between SST and regional rainfall patterns in Indian Ocean rim countries. For example, different types of IOD events
1658 exhibit distinct regional impacts, with only the canonical events associated with enhanced rainfall over East Africa due to
1659 the low-level moisture convergence over the region (Endo and Tozuka, 2016). The effect of Indian Ocean SST on East
1660 African rainfall is most pronounced during the short rains (September-November), though Williams and Funk (2011)
1661 argued that warming Indian Ocean SST in recent decades was also associated with reduced long rains for the March-June
1662 season in Ethiopia and Kenya. Changes in the tropical atmospheric circulation across the Indo-Pacific on multi-decadal
1663 timescales (Vecchi and Soden, 2007; L’Heureux et al., 2013) have further implications for the relationship between Indian
1664 Ocean SST and regional rainfall: When the Pacific Walker cell weakened and the Indian Ocean one strengthened post-
1665 1961, the East African short rains became more variable and wetter (Nicholson, 2015). Similarly, Manatsa and Behera
1666 (2013) described an epochal strengthening in the relationship between the IOD and East African rainfall post-1961, with
1667 73% of short rain variability in East Africa explained by the IOD, up from 50% in previous decades. After 1997, this
1668 increased further to 82%, explaining spatially coherent events across the region and frequent rainfall extremes (Manatsa
1669 and Behera, 2013). Recent observed and projected changes in frequency and intensity of IOD events highlight the
1670 increasing need for preparedness in vulnerable regions affected by these events. One such event is the recent 2019 positive
1671 IOD, the largest IOD on record since the 1960s (Du et al. 2020), which was linked to unusual hydroclimate around the
1672 Indian Ocean rim and further afield. It was linked to extreme rainfall and floods in East Africa (e.g., Wainwright et al.,
1673 2021), anomalously wet Indian monsoon season (Ratna et al., 2021), abnormally warm conditions in many parts of East
1674 Asia (Doi et al., 2020), unusually wet subsequent summer monsoon season in Japan and China due to downwelling Rossby
1675 waves that had affected Western Pacific SST (Takaya et al. 2020; Zhou et al., 2021), and was seen as a contributing factor
1676 to the severe bushfire season experienced in Australia in 2019/2020 (e.g., Wang and Cai, 2020). The 2019 IOD was unique

1677 in that it developed independently from any El Niño events and resulted from westward propagating Rossby waves in the
1678 southwest tropical Indian Ocean (Du et al., 2020) and/or an interhemispheric pressure gradient over the Maritime continent
1679 (Lu and Ren, 2020).

1680 **6.2.1 Biogeochemical Variability**

1681 IOD events are associated with distinct changes in primary productivity, as measured by chlorophyll. During positive IOD
1682 events, increased chlorophyll indicative of phytoplankton blooms is apparent in the normally oligotrophic eastern Indian
1683 Ocean in fall (Wiggert et al., 2009; Currie et al., 2013). Positive chlorophyll anomalies occur in the southeastern Bay of
1684 Bengal in boreal winter, while negative anomalies are observed over much of the Arabian Sea and southern tip of India.
1685 In a case study of the 2006 positive IOD event, Iskandar et al. (2010) using an eddy-resolving biophysical model found
1686 the offshore chlorophyll signal in the southeastern Indian Ocean to be associated with regions of high eddy kinetic energy
1687 implying that cyclonic eddies injected nutrient-rich water into the upper layer enabling the bloom. Currie et al. (2013)
1688 emphasize the importance of assessing the relative contributions of IOD events and remote impacts from ENSO on primary
1689 productivity in the Indian Ocean through their respective influence on upper-ocean properties for improved understanding
1690 and ultimately predictions of productivity, ecosystems, and fisheries within the basin. Little attention has been paid so far
1691 to resultant effects of these blooms on biogeochemical cycling (Wiggert et al., 2009).

1692 **6.3 The subtropical Indian Ocean Dipole**

1693 The subtropical Indian Ocean Dipole (SIOD) is a climate mode in the southern Indian Ocean, which tends to arise and
1694 peak in the austral summer (Behera and Yamagata, 2001). During the SIOD's positive phase, the climate mode has positive
1695 SST anomalies in the southwestern Indian Ocean and negative SST anomalies in the northeastern region (Behera and
1696 Yamagata, 2001; Suzuki et al., 2004; Hermes and Reason, 2005). During the positive phase, enhanced precipitation occurs
1697 over southern Africa (Behera and Yamagata 2001; Reason 2001, 2002). Recent studies have shown that the SIOD affects
1698 the Indian summer monsoon rainfall (Terray et al., 2003), rainfall over southwestern Australia (England et al., 2006) and
1699 tropical cyclone trajectories in the southern Indian Ocean (Ash and Matyas, 2012).

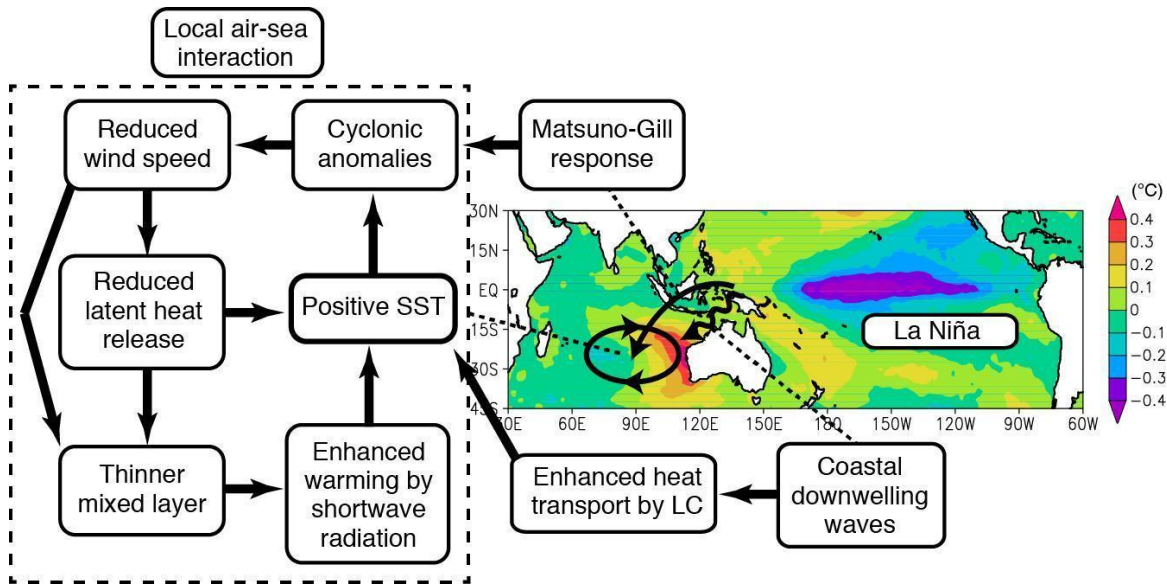
1700 Initially, SST anomalies associated with the SIOD were considered to be generated directly by latent heat flux anomalies
1701 (Behera and Yamagata, 2001). However, recent studies (Morioka et al. 2010, 2012) based on a mixed layer heat budget
1702 analysis revealed the importance of mixed layer depth anomalies generated by latent heat flux anomalies. Wind anomalies
1703 associated with the anomalous Mascarene High suppress latent heat loss and shoal the mixed layer in the southwestern
1704 part, while latent heat release is enhanced and the mixed layer deepens anomalously in the northeastern part (Morioka et
1705 al. 2010, 2012). With these changes in the upper ocean heat capacity, warming of the surface mixed layer by the

1706 climatological shortwave radiation is enhanced in the southwestern part and becomes less effective in the northeastern
1707 part. As a result, the dipole SST anomalies appear in the southern Indian Ocean.

1708 Because the above mechanism operates more effectively as the thickness of the mixed layer becomes thinner, the return
1709 period of the SIOD is becoming shorter associated with the shoaling trend of the mixed layer (Yamagami and Tozuka,
1710 2015). Whether this mechanism is associated with decadal-to-interdecadal variations and/or global warming awaits further
1711 study. Many coupled models are relatively successful in simulating the SIOD with some biases in the location and structure
1712 of the SST anomaly (Kataoka et al., 2012). However, no study has examined if the SIOD is modulated by climate modes
1713 of variability with decadal-to-interdecadal timescales or changes with global ocean warming.

1714 **6.4 Ningaloo Niño and marine heatwaves in the Indian Ocean**

1715 The Ningaloo Niño (Niña) phenomenon is an interannual climate mode associated with anomalously warm (cold) water
1716 in the eastern Indian Ocean (Feng et al., 2013; see Figure 18). This mode is seasonally phase-locked, with a peak during
1717 austral summer (Kataoka et al., 2014). The mode exerts significant impacts on rainfall over Australia (Kataoka et al., 2014)
1718 and affects marine ecosystems and fisheries (e.g. Pearce et al. 2011). The phenomenon can alter biological productivity,
1719 with negative chlorophyll anomalies during Ningaloo Niño (Narayanasetti et al., 2016). Ningaloo Niños can develop in
1720 response to remote ENSO forcing from the western Pacific transmitted as a coastally trapped wave (Kataoka et al., 2014).
1721 During the La Niña events, high sea level anomalies propagate poleward along the west coast of Australia, intensifying
1722 the Leeuwin Current and causing poleward advection of heat and anomalously warm waters (e.g. Benthuisen et al., 2014;
1723 Section 4.2.4). Poleward transport of tropical, low salinity waters can further enhance the total geostrophic transport of
1724 the Leeuwin Current (Feng et al., 2015a).



1725

1726 **Figure 18: Schematic diagram illustrating generation mechanisms (i.e. local air-sea interaction, atmospheric**
 1727 **teleconnection, and oceanic wave propagation) of the Ningaloo Niño. SST anomalies are regressed against the**
 1728 **Ningaloo Niño Index to illustrate typical SST anomalies associated with the phenomenon.**

1729 Atmospheric teleconnection can further enhance the development of Ningaloo Niño. A reduction in southerly winds over
 1730 the shelf, which would strengthen the Leeuwin Current, can arise through a Gill-type response with low sea level pressure
 1731 anomalies in the southeast Indian Ocean owing to the Niño3.4 SST anomalies (Feng et al., 2013; Tozuka et al., 2014).
 1732 Ningaloo Niños can arise from local air-sea interactions off western Australia, through the wind-evaporation-SST feedback
 1733 during its initial stage (Marshall et al., 2015) and coastal SST-wind-Leeuwin Current (Bjerknes) feedback (Kataoka et al.
 1734 2014). In the coastal feedback mechanism, positive SST anomalies lead to northerly alongshore wind anomalies and
 1735 coastal downwelling anomalies, causing enhancement of the positive SST anomalies (Kataoka et al., 2014). During the
 1736 Ningaloo Niño's development phase, estimates of air-sea heat flux contributions have been found to be dependent on
 1737 products and their resolution and bulk flux algorithms (Feng and Shinoda, 2019). Since the late 1990s, Ningaloo Niño
 1738 events have occurred more frequently (Feng et al., 2015b). This decadal increase is corroborated by coral proxy records
 1739 of Leeuwin Current strength, with the most extreme SST anomalies associated with Ningaloo Niños occurring since 1980
 1740 (Zinke et al., 2014).

1741 More generally, marine heatwaves refer to prolonged, extremely warm water events. Over the past decade, most studies
 1742 on marine heatwaves in the Indian Ocean have focused on the eastern sector of the Indian Ocean. Major events in the
 1743 Indian Ocean have been associated with phases of ENSO. Along the west coast of Australia, marine heatwaves have
 1744 occurred predominantly at subtropical reefs during La Niña events due to increased heat transport (Zhang et al., 2017).

1745 The term “marine heatwave” was first coined owing to a +5°C warm water event in 2011 off Western Australia during a
1746 strong La Niña (Pearce et al., 2011). The 2011 event was associated with the strongest recorded Leeuwin Current transport
1747 anomaly, bringing warm tropical waters south, and was partly due to air-sea heat fluxes (Feng et al., 2013; Benthuisen et
1748 al., 2014).

1749 Across Australia’s northwestern shelf, marine heatwaves have been found to occur at tropical coral reefs from El Niño
1750 due to solar radiation and a weakened monsoon (Zhang et al., 2017). During the strong El Niño of 2015-2016, the southeast
1751 tropical Indian Ocean experienced the warmest and longest marine heatwave on record, with weakened monsoon activity
1752 and anomalously high air-sea heat flux into the ocean (Benthuisen et al., 2018). The anomalously warm water conditions
1753 persisted into winter, during one of the strongest negative IOD events (Benthuisen et al., 2018). The 2016 marine heatwave
1754 was associated with coral bleaching spanning Australia’s inshore Kimberley region to remote coral reef atolls (Gilmour et
1755 al., 2019). More broadly across the Indian Ocean during 2016, marine heatwaves have been studied in terms of their
1756 ecological impacts, such as coral bleaching in the western Indian Ocean (e.g. Gudka et al., 2018), the Maldives (e.g.
1757 Ibrahim et al., 2017) and consequences for fishes in the Chagos Archipelago (Taylor et al., 2019).

1758 Trends in marine heatwave metrics indicate widespread regions across the Indian Ocean where events have increased in
1759 frequency, based on SST from 1982-2016, especially in the central and southwestern sectors (Oliver et al., 2018). Over
1760 the same time period, the duration and intensity of marine heatwaves have increased in the Indian Ocean and globally
1761 (Oliver et al. 2018, Marin et al. 2021). Primary climate modes of variability correlated with an increased occurrence of
1762 marine heatwaves include the following: (1) the positive phase of the Dipole Mode Index for the northwestern sector, the
1763 tropical sector, and south to the Seychelles Islands, (2) the positive phase of the Niño3.4 index for the south-central sector,
1764 and (3) the negative phase of the El Niño Modoki index, which measures the strength of the Central Pacific ENSO, for the
1765 eastern Indian Ocean (Holbrook et al., 2019). While the marine heatwaves in the eastern Indian Ocean have been well
1766 documented, there have been fewer studies into the physical mechanisms causing marine heatwaves across the basin and
1767 other regions and less confidence, for example in the Bay of Bengal, in the local processes causing reported events on a
1768 range of time scales (Holbrook et al. 2019). There are indications that increased extremes in El Niño (Cai et al., 2014b)
1769 and La Niña events (Cai et al., 2015) due to mean ocean warming trends increase the likelihood of marine heatwave
1770 occurrence in the southeast Indian Ocean (Zhang et al., 2017).

1771 **6.5 Monsoon variability and links to the Indian Ocean**

1772 Several monsoon systems surround the Indian Ocean, notably the South Asian monsoon, the East Asian monsoon and
1773 the Australian monsoon. These monsoon systems are remotely influenced by global coupled modes of variability such as
1774 ENSO, which is often associated with dry conditions in the South Asian monsoon (e.g., Rasmusson and Carpenter,
1775 1983; Ropelewski and Halpert, 1987) and Australian monsoon (e.g., Risbey et al., 2009; Jourdain et al., 2013), although

1776 the relationship with the Indian monsoon has recently weakened (e.g., Kumar et al., 1999). In the Indian Ocean, the IOD
1777 has a strong influence on the Asian monsoon systems, but is weak during the Australian monsoon period. The IOD tends
1778 to oppose the ENSO teleconnection to the South Asian monsoon by enhancing monsoon rainfall (e.g., Ashok et al.,
1779 2004; Chowdary et al., 2015; Krishnaswamy et al., 2015; Pokhrel et al., 2012). However, the exact combination of SST
1780 patterns between the Indian Ocean and the Pacific is crucial for determining the rainfall response in the Asian monsoons
1781 (e.g., Lau and Wu, 2001; Ratna et al., 2020; Yuan and Yang, 2012), and the relative strengths of the teleconnections
1782 have varied over time (Krishnaswamy et al., 2015). Furthermore, there is evidence that the Indian Ocean forcing of the
1783 South Asian monsoon may be primarily driven by ENSO, with pure IOD events only weakly influencing monsoon
1784 rainfall (Cretat et al., 2017).

1785
1786 The monsoon systems around the Indian Ocean tend to vary in phase and are also linked to the western North Pacific
1787 Monsoon (e.g., Gu et al., 2010). There is a biennial oscillation in the strength of the monsoon systems, with a strong
1788 Asian monsoon preceding a negative IOD and coinciding with cold eastern Pacific SSTs, followed by a strong
1789 Australian monsoon and subsequently by a reversal in the SST patterns (Loschnigg et al., 2003; Meehl & Arblaster,
1790 2011). Thus, each monsoon system interacts with the ocean dynamics and thermodynamics and with the other monsoon
1791 systems through a complex set of teleconnections.

1792
1793 At a regional scale, upwelling in the Arabian Sea reduces rainfall along the western Ghats of India during the monsoon
1794 due to a reduction in evaporation and water vapour transport (Izumo et al., 2008). Moisture fluxes across the Arabian
1795 Sea are crucial to accurate simulation of the Indian Monsoon, yet many models fail to accurately capture these (Levine
1796 and Turner, 2012). In the Bay of Bengal, the shallow surface mixed layer, supported by the vertical salinity gradient,
1797 leads to rapid variations in SST (e.g., Sengupta and Ravichandran, 2001; Vecchi and Harrison, 2002) that interact with
1798 intraseasonal oscillations (Gao et al., 2019) in the atmosphere and thus with the active/break cycles on the monsoon
1799 (e.g., Lucas et al., 2014). This strong and rapid variability in upper ocean conditions in the Bay of Bengal, and the
1800 potential feedbacks on the monsoon, motivated multiple observational research programmes with field campaigns in the
1801 Bay of Bengal, as discussed in the next section.

1802 **7. Multiscale upper ocean processes in the Bay of Bengal**

1803 Reflective of its name, the Bay of Bengal is in many ways analogous to a large-scale estuary with seasonally reversing
1804 winds and boundary currents that facilitate the transport, stirring, and mixing of water masses. To the north, the Ganga-
1805 Brahmaputra-Meghna watershed delivers on average 1300 km³ in annual runoff of freshwater with a seasonal peak in
1806 discharge from July to September (Sengupta et al., 2006). During the southwest monsoon (boreal summer), the Summer
1807 Monsoon Current (Fig. 10) flows eastward advecting high salinity waters from the Arabian Sea into the southern Bay of

1808 Bengal, balancing the Bay's net outflow of freshwater. Instabilities and eddies result in mesoscale stirring of these different
1809 water types and create a strongly filamented and complex near-surface thermohaline structure. Lateral and vertical
1810 gradients in stratification are further modified by submesoscale processes, instabilities, and mixing. The resultant shallow
1811 stratification allows for rapid coupling with the atmosphere. Collectively, these conditions present a natural laboratory to
1812 study multi-scale mixing processes and their link to air-sea interaction. This section discusses new understanding of
1813 physical processes in the Bay from the large-scale to sub-mesoscale and finally at the smallest mixing scales.

1814 Recent focus on the Bay of Bengal's upper ocean structure has been prompted by the need to understand atmosphere and
1815 ocean coupling with the aim of ultimately informing monsoon forecasting efforts at the intraseasonal timescale and shorter.
1816 Several bi-lateral international collaborations (Lucas et al., 2014; Wijesekera et al., 2016; Mahadevan et al., 2016;
1817 Vinaychandran et al., 2018; Gordon et al., 2019, 2020) have collectively supported multiple field campaigns, beginning
1818 in 2013 and concluding in 2019, using a combination of shipboard, moored, and autonomous platforms. These atmospheric
1819 and oceanic measurements have provided new insights into the BoB's structure and the processes that regulate that
1820 structure, particularly at fine lateral scales (<5 km).

1821 Results from these combined efforts span from large-scales, e.g., the quantification of coastal transport along the Sri
1822 Lankan coast (Lee et al., 2016) and the mesoscale stirring of freshwater (Sree Lekha et al., 2018), to intermediate scales,
1823 e.g., high-resolution (order 100 m) frontal surveys that hint at the roles of submesoscale (Ramachandran et al., 2018) and
1824 non-hydrostatic processes in setting stratification (Sarkar et al., 2016), to small-scales with direct measurements of
1825 microstructure yielding new insights into the BoB's mixing regimes (Jinadasa et al., 2016; Thakur et al., 2019; Cherian et
1826 al. 2020).

1827 **7.1 The Bay's Forcing and Upper Ocean Structure**

1828 At the largest scales, the Bay is forced by air-sea fluxes of buoyancy and momentum, which are strongly modulated by
1829 the monsoon and vice versa. Precipitation and multiple river systems, including the Ganga-Brahmaputra-Meghna system,
1830 contribute to freshwater input that creates a barrier layer in the surface Bay of Bengal, which is strongest in the northern
1831 Bay weakening toward the south. The Bay's stratification, in particular its barrier layer, is unique in how it impacts the
1832 evolution of seasonal SST, in turn setting the lower boundary condition for the development of the monsoon (Li et al.,
1833 2017). For this reason, recent emphasis has been placed on understanding processes that determine the Bay's upper ocean
1834 salinity and temperature structure.

1835 The monsoon cycle of surface forcing plays a first-order role in controlling the Bay's upper ocean temperature structure.
1836 Direct flux measurements are a critical component in our ability to accurately capture/represent and predict the magnitude
1837 and variability of monsoon air-sea coupling. Recent studies have shown that of the air-sea heat flux terms, shortwave

1838 radiation and latent heat flux are the largest drivers of variability to the total heat tendency. These variables are also those
1839 which reanalysis products struggle most to accurately represent, showing biases up to 75 W/m^2 (Sanchez-Franks et al.,
1840 2018). High-quality air-sea surface flux measurements over the BoB historically have been limited to the few sites
1841 maintained by the RAMA array (McPhaden et al., 2009). However, regional measurement efforts have expanded and
1842 baseline surface measurements are now collected and sustained through India's National Institute of Ocean Technology's
1843 met-ocean buoy program (Venkatesan et al., 2018), as well as the recent transition of an 18°N air-sea flux buoy from
1844 Woods Hole Oceanographic Institution to Indian National Centre for Ocean Information Services (Weller et al., 2016).

1845 Precipitation and riverine discharge along the Bay's margins respectively contribute roughly 60% and 40% of the 0.14 Sv
1846 net freshwater delivered to the Bay (Sengupta et al. 2006; Wilson and Riser, 2016). Precipitation peaks in early summer
1847 (June) with a value near 0.4 m month^{-1} , while discharge peaks slightly later in summer (August) with a value near 0.3 m
1848 month^{-1} . Evaporative loss (included in the net 0.14 Sv) is relatively steady throughout the year at 0.1 m month^{-1} (Wilson
1849 and Riser, 2016). Estimates of river discharge from gauged sources are known to have uncertainties (underestimates)
1850 related to unmonitored tributaries and streams. For large deltas, altimeter-based elevations offer a means of extrapolating
1851 gauge data over space and time. Papa et al. (2010, 2012) applied such an approach to the Ganga-Brahmaputra River
1852 system for the period 1998-2011. This time series allows for assessment of interannual variability over time ranges not
1853 spanned by gauged efforts. Papa et al. (2012) note a $12,500 \text{ m}^3/\text{s}$ standard deviation in interannual variability in the Ganga-
1854 Brahmaputra discharge. Importantly, such data sets are also easily accessible by the general public, facilitating progress
1855 and understanding by the scientific community.

1856 The Bay's upper ocean temperature and salinity structure is an integrated representation of the above summarized
1857 sources/sinks of heat and freshwater, combined with the physical processes that redistribute these quantities. The
1858 thermohaline structure of the Bay is remarkable in several regards—for shallow mixed layer depths ($< 5 \text{ m}$, Sengupta and
1859 Ravichandran, 1998), for inversions of temperature (Shroyer et al., 2016, 2019; Thadathil et al. 2016), for large-scale
1860 coherent layering that spans 100 kms (Shroyer et al., 2019), an active mesoscale field and the strong influence of river
1861 discharge over the interior basin. The Bay's salinity stratification is a critical, if not dominant, contributor to the upper
1862 ocean density stratification. It supports the formation of barrier layers that are frequently observed to be warmer than the
1863 mixed layer thereby providing a substantial subsurface heat reservoir with the potential to modify air-sea interaction
1864 (Girishkumar et al., 2011; Shroyer et al., 2016). For example, in conditions supportive of formation of a diurnal warm
1865 layer (low winds, strong insolation), subsurface turbulent fluxes can act to modulate the diurnal SST cycle by transporting
1866 (typically) warm barrier layer waters into the mixed layer at night while still cooling the base of the diurnal warm layer
1867 (DWL) during the day (Shroyer et al., 2016). A similar phenomenon, albeit on a much different scale, results with passage
1868 of cyclones, which often show a salty wake even in the absence of a cool wake which is common for cyclones elsewhere
1869 (for e.g. Chaudhuri et al. 2019, Qiu et al. 2019). Below, we review recent progress on understanding of processes that
1870 determine the Bay's upper ocean thermohaline structure.

1871 **7.2 Lateral Processes**

1872 **7.2.1 Stirring from the Margins**

1873 The Bay of Bengal has an active mesoscale eddy field that stirs diverse source waters into the interior of the Bay of Bengal.
1874 The origins of these source waters are the Arabian Sea waters to the west, the Ganga-Brahmaputra-Meghna at the northern
1875 tip, Andaman Sea waters to the east, and Equatorial waters to the south. This stirring effectively contributes to a quasi-
1876 stationary balance of the fresher waters from the north and the high salinity waters from the west and south over time.
1877 Lateral advection is a fundamental contributor to the formation of the barrier layer (George et al., 2019) and the freshwater
1878 budget of the Bay (e.g. Sree Lekha et al., 2018). In the northern Bay, the dispersal of water from the periphery into the
1879 interior depends critically on mesoscale stirring and the time varying Ekman transport, as indicated from mooring (Sree
1880 Lekha et al., 2018) and ship-based surveys (Shroyer et al., 2019), and constrained by modelling results (Sree Lekha et al.,
1881 2018). Here, the advection of freshwater by the mesoscale stirring also plays an important role in determining SST over
1882 the northern BoB (Buckley et al. 2020), as these waters are typically associated with relatively shallow mixed layers. In
1883 the southern Bay, measurements have suggested the competing influences of mixing and advection of salty Arabian Sea
1884 water in the erosion and reformation of the barrier layer during the southwest monsoon (George et al., 2019;
1885 Vinayachandran et al., 2018). In particular, George et al. (2019) show that maintenance of the barrier layer and the
1886 associated maximum depth of mixing was critically dependent on horizontal advection through its impact on stratification.
1887 Surface freshwater input also has an impact on barrier layer evolution; several freshening events were captured at various
1888 stages of their seasonal evolution in the southern Bay of Bengal in recent observations (Vinayachandran et al., 2018).
1889 These events play a significant role in the formation of a thick barrier layer, showing that during the southwest monsoon
1890 the shoaling of the mixed layer in the southern BoB has a similar magnitude and behaviour to that in the northern BoB
1891 (Vinaychandran et al., 2018).

1892 **7.2.2 Inter-basin exchange**

1893 Inter-basin exchange is critical to the Bay's salinity budget; since the Bay receives net freshwater input, this freshwater
1894 must be balanced by salty water imported from either the Arabian Sea or the western equatorial Indian Ocean (Jensen et
1895 al., 2001; Sanchez-Franks et al., 2019), and turbulent transport of salt into the fresh water layer is necessary to maintain
1896 the BoB's long-term salinity balance. Observations show that intrusion of high salinity water from the Arabian Sea enters
1897 the BoB between 80°-90°E during the southwest monsoon, (e.g. Murty et al, 1992; Vinayachandran et al., 2013) and has
1898 been found in several models (e.g. Vinayachandran et al., 1999; Han and McCreary, 2001 and Jensen, 2001). More recent
1899 observational and modeling studies show that both lateral and vertical transfer of heat and salt occur at multiple space-
1900 time scales. Seasonal currents play an important role in transporting heat and salt in and out of the BoB, but the role of
1901 mesoscale eddies on lateral transports is not well known.

1902 Using unique year-long mixing measurements detailed in Section 7.3, Cherian et al. (2020) tentatively estimated a
1903 turbulent salt flux of $1.5e-6$ psu ms^{-1} out of Arabian Sea water averaged between $85^{\circ}E$ and $88.5^{\circ}E$ at $8^{\circ}N$ through the
1904 34.75 psu isohaline between August and January. Over those 6 months, this flux would increase the salinity of a $75m$ layer
1905 of water by 0.3 psu, though much of this would be cancelled out by surface fluxes. The magnitude and timing of this salt
1906 flux roughly match that necessary to restore the Bay's near-surface salinity after the large freshwater input in August as
1907 estimated by a few modelling studies (Akhil et al., 2014; Benshila et al., 2014; Wilson and Riser, 2016). This is the first
1908 direct measurement of turbulence that supports the hypothesis of intrusion of high salinity water from the Arabian Sea
1909 during the southwest monsoon (Vinayachandran et al., 2013).

1910 **7.2.2.1 Andaman Sea Exchange**

1911 The Irrawady river drains into the Andaman Sea, a marginal sea at the eastern edge of the Bay. Export from the Andaman
1912 is then another source of freshwater for the Bay, particularly at intermediate densities ($22-25$ $kg\ m^{-3}$). A striking example
1913 of the interaction between strong surface forcing and an anticyclonic eddy can be found in the fortuitous crossing of an
1914 intrathermocline eddy (ITE) in 2013 as reported by Gordon *et al.* (2017). The water mass characteristics clearly identify
1915 ITE waters from the Andaman Sea; and, analysis of ancillary Argo data suggest a similar water type often penetrates
1916 westward into the Bay extending from the three passages connecting the two basins. While at the time of transit the
1917 observed ITE had a very weak surface expression, a week prior to encountering the ITE a clear sea surface high (>10 cm)
1918 is evident in AVISO SSHA. Tropical cyclone Lehar passed near the location of this sea surface high in the interim, and
1919 the working conjecture is that the winds associated with Lehar were sufficient to modify a typical mode-1 anticyclone into
1920 the observed ITE.

1921 **7.2.2.2 Arabian Sea Exchange**

1922 Near-surface exchange from the Arabian Sea into the Bay of Bengal is influenced by the Sri Lanka Dome (SLD), an
1923 upwelling thermal dome that recurs seasonally within the SMC in the wind shadow of Sri Lanka (Vinayachandran and
1924 Yamagata 1998, de Vos et al. 2014, Burns et al. 2017). The SLD has long been recognized as a prominent circulation
1925 feature in the southwestern bay during the summer monsoon; and it has been noted as a region of enhanced productivity
1926 (Vinayachandran et al., 2004, de Vos et al. 2014), cool SST (Burns et al. 2017), and consequently depressed convection
1927 (Figure 15). The SLD displays pronounced interannual variability (Cullen and Shroyer 2019). In some years the SLD has
1928 a strong surface manifestation (amplitude of the low ~ 30 cm) that persists well beyond the southwest monsoon; in other
1929 years the SLD has a weak expression that is intermittent and short-lived ($\sim 1-2$ months). The SLD is not fixed in location
1930 despite its strong association with the wind stress curl. Its position varies from year-to-year as well as over the course of
1931 one season. Variations in its location and strength may influence the properties of waters entrained and upwelled within
1932 the SLD.

1933 At intermediate depths (<~200 m), the signature of the neighboring Arabian Sea is notable across much of the basin
1934 (Gordon et al., 2016). During summer, Arabian Sea High Salinity Water (ASHSW; density near 22-24 kg m⁻³) is
1935 carried/advectioned into the Bay of Bengal as a ‘high salinity core’ via the Southwest Monsoon Current (SMC, Webber et
1936 al., 2018; Sanchez-Franks et al., 2019) and then spread north along the bay’s central spine (Hormann et al., 2019). During
1937 this journey, salt is mixed upward into the near-surface fresh layer (Cherian et al 2020; Section 7.3). A nearly two-year
1938 long moored current record in the southern BoB captured seasonally varying large eddies generated by the SMC and
1939 Northeast Monsoon Current. These eddies included a cyclonic eddy, the SLD, and an anticyclonic eddy south of the SLD
1940 (Wijesekera et al. 2016c). These observations revealed that the average transport over a nearly two year period into the
1941 BoB was about 2 Sv (1 Sv = 10⁶ m³ s⁻¹) but likely exceeded 15 Sv during summer of 2014, which is consistent with the
1942 transport associated with the SMC (e.g., Schott et al. 2009; Webber et al. 2018). The observations further indicate that the
1943 water exchange away from coastal boundaries, in the interior of the BoB, may be largely influenced by the location and
1944 strength of the two eddies that modify the path of the SMC. The strength and location of the SMC itself is dependent on
1945 a combination of local and remote forcing (Webber et al., 2018).

1946 As discussed above several hypotheses have been suggested for cyclonic eddy (SLD) and anticyclonic eddy formation in
1947 the southern BoB. It has been suggested that the cyclonic wind stress-curl over southwestern BoB generates the SLD
1948 (McCreary et al., 1996; Vinayachandran and Yamagata 1998; Schott et al., 2001; Cullen and Shroyer 2019). Based on
1949 numerical simulations, de Vos et al., (2014) argued that the separation of SMC from the (southern) boundary of Sri Lanka
1950 may lead to SLD, where a cyclonic vorticity is generated by lateral frictional effects. A mechanism for the anticyclonic
1951 eddy formation has been proposed by Vinayachandran and Yamagata (1998), where the interaction of the SMC with
1952 Rossby waves arriving from the eastern boundary leads to the anticyclonic eddy. Pirro et al (2020a) proposed a new
1953 hypothesis wherein the anticyclonic eddy is generated by a topographically trapped Rossby wave response of the SMC to
1954 perturbations by the Sri Lankan coast. They reported that observations of the size, location and origins of the SLD were
1955 broadly consistent with their hypothesis, based on a laboratory experiment designed to mimic natural flow in the BoB by
1956 creating an eastward jet (SMC) on a simulated β plane.

1957 High-resolution sampling of the interior BoB has provided a more detailed look at the lateral extent of typical ‘patches’ of
1958 Arabian Sea water, which tend to remain well-defined over scales of 10-50 km, suggesting the importance of eddy activity
1959 in exchange (Shroyer et al., 2019). While many studies have traced origins of ASHSW from the eastern Arabian Sea,
1960 entering the Bay of Bengal directly via the southwest monsoon current (e.g., Jensen et al, 2016); a recent study suggests
1961 an equatorial pathway may also be relevant (Sanchez-Franks et al., 2019; Section 7.2.3). Highly salty and highly
1962 oxygenated waters from the Persian Gulf and the Red Sea have also been noted in the southern regions of the Bay of
1963 Bengal (Jain et al., 2017). These waters are injected into the Bay of Bengal via current systems (equatorial and the
1964 southwest monsoon current) with important repercussions for the oxygen concentrations of the Bay of Bengal oxygen
1965 minimum zone (Sheehan et al., 2020).

1966 Velocity and hydrographic profiles from a shipboard survey in December 2013 combined with drifter observations,
1967 satellite altimetry, global ocean nowcast/forecast products, and coupled model simulations were used to examine the
1968 circulation in the southern Bay of Bengal during the Northeast monsoon (Wijesekera et al. 2015). The observations
1969 captured the southward flowing East India Coastal Current (EICC, e.g., Shetye et al. 1994) off southeast India and east of
1970 Sri Lanka. The EICC was approximately 100 km wide, with speeds exceeding 1 m s^{-1} in the upper 75 m. East of the EICC,
1971 a subsurface-intensified 300-km-wide, northward current was observed, with maximum speeds as high as 1 m s^{-1} between
1972 50 m and 75 m. The EICC transported low-salinity water out of the bay and the subsurface northward flow carried high-
1973 salinity water into the bay during typical northeast monsoon conditions (Wijesekera et al. 2015; Jensen et al. 2016).

1974 **7.2.3 Equatorial Connections**

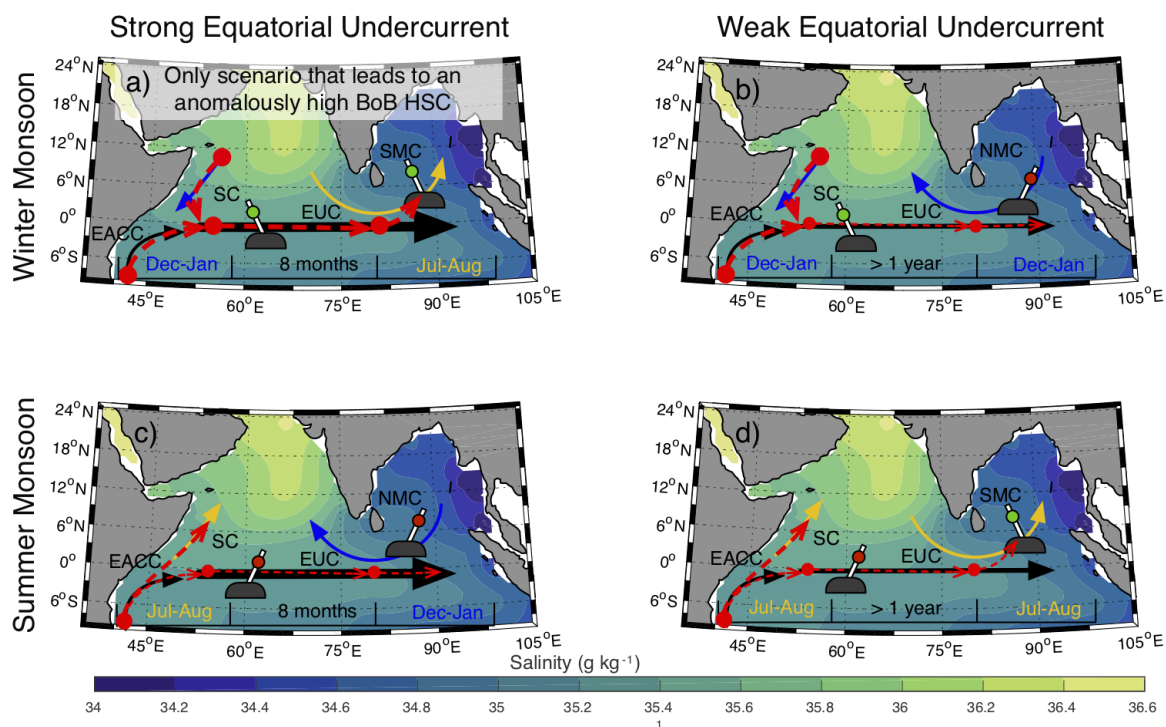
1975 The Equatorial undercurrent (EUC) in the Indian ocean is seasonally variable. The summer–fall EUC tends to occur in the
1976 western basin in most years but exhibits evident interannual variability in the eastern basin (Chen et al. 2015), with
1977 different processes dominating its generation in the western and eastern basins. In the eastern basin reflected Rossby waves
1978 from the eastern boundary play a crucial role in the EUC, whereas directly forced Kelvin and Rossby waves control the
1979 EUC in the western basin.

1980 Equatorial Kelvin waves, commonly interpreted as Wyrтки (1973) jets, propagate eastward along the equator during
1981 April/May and September/October. Upon reflection from the IO eastern boundaries, energy of Wyrтки jets is reflected
1982 back in part as long Rossby waves that disperse slowly during the following two months and reach the central-eastern BoB
1983 during July-August (Han et al., 1999, 2001; Han, 2005; Nagura and McPhaden, 2010a). The remaining energy is
1984 partitioned into two coastally-trapped Kelvin waves traveling poleward (Moore, 1968), which excite long Rossby waves
1985 propagating westward. Therefore it is suggested that planetary waves driven by remote forcing from the interior IO
1986 contribute significantly to the formation, strength and intensity of the BoB circulation (Vinayachandran et al. 1998; Nagura
1987 and McPhaden, 2010b; Chen, 2015). A subset of these planetary waves are the mainstay of intraseasonal oscillations
1988 (ISOs), a sub-seasonal phenomenon of period less than 120 days. The genesis of oceanic ISOs has been attributed to
1989 multiple mechanisms: external forcing (e.g., atmospheric ISOs and Ekman pumping, e.g. Duncan and Han 2012) and
1990 internal processes (upper ocean processes and instabilities e.g. Zhang et al. 2018).

1991 Observations in the IO have captured a range of variabilities in the 30 – 120 days frequency band (e.g., Girishkumar et al.,
1992 2013), and past research has identified roughly three distinct ISO bands in the context of the thermocline: 30-60 days, 60-
1993 90 days, and 120 days (Han et al., 2001; Girishkumar et al., 2013). Pirro et al. (2020b) discussed interaction between 30-
1994 60 day ISOs and the SMC in the southern BoB using long-term moored observations. They estimated that the background
1995 mean flow acceleration resulting from the meridional divergence of wave momentum flux in the thermocline was about
1996 10^{-8} m s^{-2} . As a result, within a wave period, ISOs can enhance the eastward flow in the thermocline by about 25%. The

1997 negative shear production computed for the same period is consistent with this finding suggesting that the mean flow
 1998 gained kinetic energy at the expense of the ISO band. The meridional heat-flux divergence was $-10^{-7} \text{ }^\circ\text{C s}^{-1}$ and has a
 1999 tendency for cooling the thermocline by about 0.5°C when ISOs are active (Pirro et al., 2020b). Observations have also
 2000 captured energetic and consequential 5-20 day convectively coupled Kelvin waves in the atmosphere (Baranowski et al,
 2001 2016) that generate oceanic Kelvin waves, affect surface heat fluxes and generate upper ocean turbulence (Pujiana and
 2002 McPhaden, 2018).

2003 High salinity waters from the western Arabian Sea and the western Equatorial Indian Ocean can route to the Bay of Bengal
 2004 via the Somali Current and the Indian Ocean EUC (Sanchez-Franks et al., 2019). Changes in strength of the Bay of Bengal
 2005 high salinity core are linked to the convergence of the East Africa Coastal Current and the wintertime southward-flowing
 2006 Somali Current, with anomalously strong equatorial Undercurrent (Fig. 19). Because of the seasonal reversal of currents,
 2007 two junctions form naturally, one in the western equatorial Indian Ocean (Somali Current) and another south of India
 2008 (monsoon currents), which effectively act as ‘railroad switches’ rerouting water masses to different basins in the Indian
 2009 Ocean depending on the season (Fig. 19, Sanchez-Franks et al., 2019).



2010

2011 **Figure 19: Seasonal circulation pathways in the northern Indian Ocean, or Railroad Switch schematic, on**
 2012 **subsurface (90 m) salinity climatology (psu; shaded) from the Argo optimally interpolated product for the four**
 2013 **Equatorial Undercurrent scenarios: (a, b) winter monsoon and strong (weak) Equatorial Undercurrent and (c, d)**

2014 **summer monsoon and strong (weak) Equatorial Undercurrent. Red dashed arrows indicate high-salinity advection.**
2015 **BoB = Bay of Bengal; HSC = high-salinity core; SMC = Southwest Monsoon Current; SC = Somali Current; EUC**
2016 **= Equatorial Undercurrent; EACC = East African Coastal Current. From Sanchez-Franks et al. (2019).**

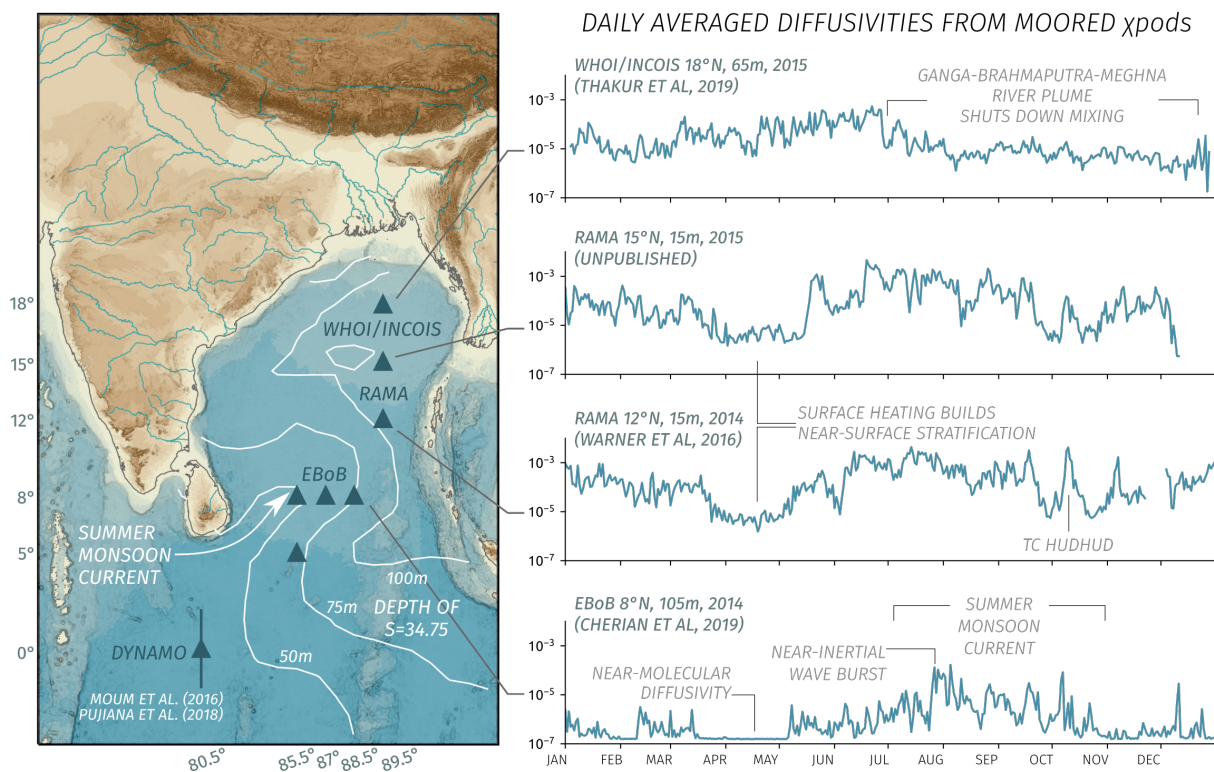
2017 **7.3 Vertical Mixing**

2018 Strong stratification in the Bay of Bengal plays a critical role in setting the upper ocean turbulence, notably leading to
2019 relatively weak mixing compared to other regions (e.g. Gregg et al., 2006). However, large-scale inferences suggest that
2020 mixing must play a key role in at least two regards. First, the net surface flux during the southwest monsoon on average is
2021 warming but yet the SST cools (Shenoi et al, 2002). Second, the large-scale salt balance must be closed through upward
2022 mixing of high-salinity water carried into the Bay via the Summer Monsoon Current (Vinayachandran et al., 2013).

2023 Recent year-long direct measurements of mixing in the Bay have helped link the seasonal cycle in mixing to the seasonal
2024 cycle of winds, currents and freshwater. These year-long measurements were recorded by mixing meters called χ pods.
2025 χ pods consist of two temperature microstructure sensors and a suite of ancillary sensors necessary to infer the rate of
2026 dissipation of temperature variance at 1Hz frequency for up to a year (Moum & Nash, 2009). χ pods have been deployed
2027 on moorings in three different regions of the Bay (Figure 20): the air-sea buoy at 18°N, top 65m (Thakur et al., 2019),
2028 RAMA moorings along 90°E (mixing measurements at 15m, 30m and 45m; Warner et al. 2016), and the EBoB array in
2029 the south-central Bay (mixing measurements spanning between 30m and 100m at sites in the region 85°E-88°E, 5°N-8°N,
2030 Cherian et al., 2020). Across the basin, turbulence within and near the base of the mixed layer shows strong seasonality
2031 that parallels the monsoon cycle in winds (Thakur et al., 2019, Warner et al., 2016). In the thermocline of the south-central
2032 Bay (EBoB array), mixing is correlated with packets of downward propagating near-inertial waves implicating wind
2033 forcing. As depicted in Figure 20, both near-surface and thermocline mixing are relatively high during the NE and SW
2034 monsoons (Dec-Feb, May-Sep) and relatively low during the transition (Mar, Apr). Cyclones during the post-monsoon
2035 months of October and November can drive a hundredfold increase in near-surface mixing both locally and throughout
2036 the Bay (Warner et al. 2016). Turbulence profiles collected by a fast thermistor on a CTD rosette during a basin-wide
2037 survey before and after the passage of cyclone Madi (6-12 Dec, 2013) show a basin-wide increase in diffusivity linked to
2038 near-inertial waves forced by the cyclone (Wijesekera et al., 2016b).

2039 Indirect estimates of turbulent diffusivity and turbulent heat fluxes at the base of the mixed layer can be found as the
2040 residual of a mixed layer heat budget whose terms are estimated using a combination of mooring and satellite
2041 measurements. Girishkumar et al. (2020) use this approach to indirectly estimate seasonal median turbulent diffusivities
2042 using decade-long RAMA mooring records at 90°E. They find a robust seasonal cycle of mixing at 8°N, 12°N, and 15°N;
2043 and strong latitudinal variability in turbulence, with larger diffusivities inferred at 8°N relative to 12°N and 15°N in all

2044 seasons. When comparisons are possible, the indirect estimates compare well against the more direct but time-limited
 2045 estimates of Warner et al (2016) at 90°E, 12°N.



2046

2047 **Figure 20: Annual cycle of daily averaged temperature diffusivities derived from χ pod measurements. The data**
 2048 **are from two different years, 2014 and 2015, depending on location. Note the similar wind-forced seasonal cycle at**
 2049 **12°N, 15m and 15°N, 15m and the dramatically different seasonal cycle at 8°N, 105m (reflecting near-inertial wave**
 2050 **activity) and at 18°N, 65m reflecting freshwater influence.**

2051 The influence of freshwater is a critical caveat to the above generalizations: the arrival in August of the Ganga-
 2052 Brahmaputra-Meghna freshwater plume at 18°N has been observed to suppress turbulence (diffusivity $K_T < 10^{-5} \text{ m}^2 \text{ s}^{-1}$)
 2053 for multiple months (Aug-Nov) at depths of approximately 50-65 m (Figure 20). This buoyant lens limited the vertical
 2054 extent of the influence of Tropical Cyclone Komen as compared to a previous (weaker) storm (Chaudhuri et al 2019,
 2055 Thakur et al 2019). Similar observations of extremely weak turbulence below strong, salinity-stratified surface layers have
 2056 been reported throughout the Bay using data from a variety of platforms: ship-based microstructure (Jinadasa et al, 2016)
 2057 profiling floats with a temperature microstructure sensor (Shroyer et al, 2016) and glider-based microstructure
 2058 measurements (St. Laurent and Merrifield, 2017). Lucas et al (2016) find that near-inertial shear was elevated at the base
 2059 of the mixed layer but not elevated at the base of the barrier layer — direct evidence that salinity stratification can insulate

2060 deeper depths from the effects of near-surface forcing (downward propagating near-inertial waves in this case). Li et al.
2061 (2017) use a combination of observations and modelling results to demonstrate that barrier layers in the Bay of Bengal
2062 influence the amplitude of intraseasonal oscillations in SST and precipitation. However, a recent coarse resolution coupled
2063 modelling study suggests that freshwater has little influence on SST or rainfall, since the SST tendency caused by a
2064 reduction in mixing is offset by changes in surface heat fluxes (Krishnamohan et al., 2019)

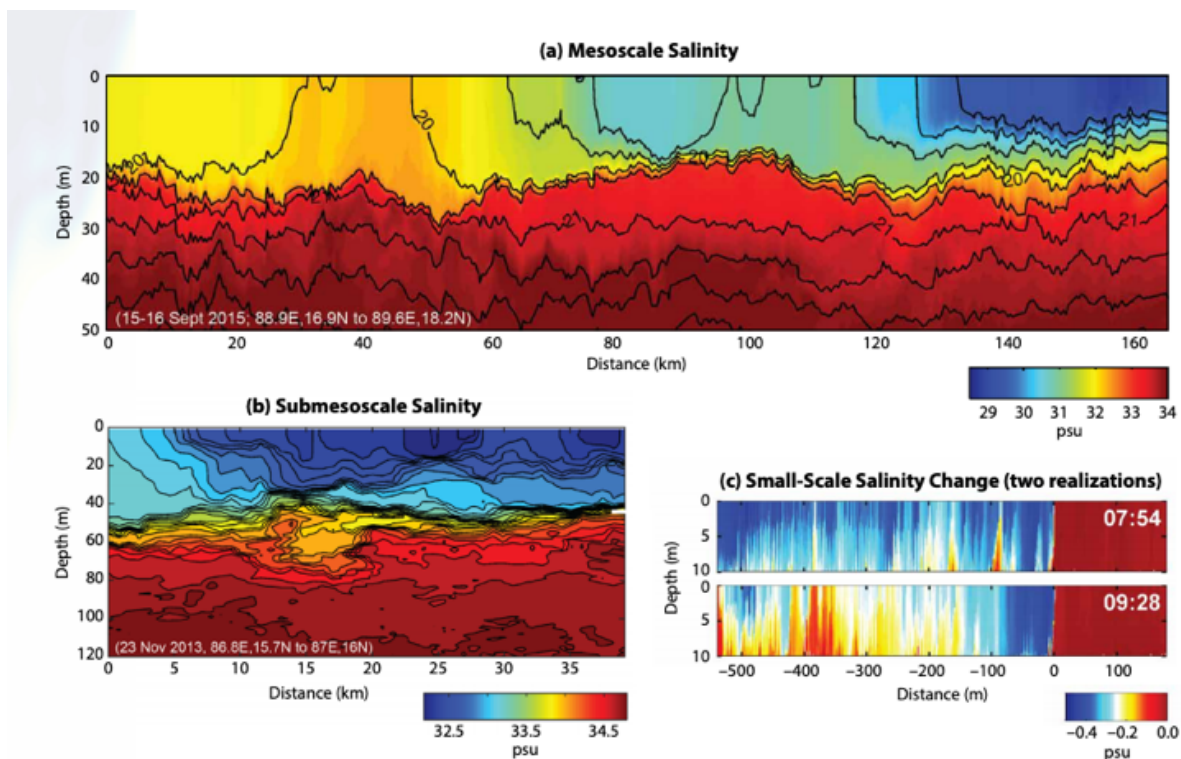
2065 Surface freshwater advection can create subsurface reservoirs of heat and salt that can be accessed when the winds are
2066 strong enough, such as during cyclones that regularly form in the Bay during October and November. In one dramatic
2067 example Qiu et al (2019) report up to 5 psu increases in SSS and only a smaller 0.5°C decrease in SST following the
2068 passage of Cyclone Phailin (2013). In this case, mooring records indicate that mixing was limited to the isothermal layer
2069 (Chaudhuri et al. 2019). Subsurface warm layers (i.e. temperature inversions stabilized by strong salinity stratification)
2070 are also observed, representing a reservoir of heat that can be accessed if a storm excites enough turbulence, as appears to
2071 have happened during the passage of Cyclone Hudhud (Warner et al, 2016). The influence of stratification in limiting the
2072 extent of vertical mixing and creating subsurface warm layers mean that cyclone-induced cooling is generally either weak
2073 or negligible in the Bay, unlike in other ocean basins (Sengupta et al, 2008). Subsurface warm layers influence SST on
2074 longer timescales too: Girishkumar et al (2013) find that the wintertime SST at 8°N, 90°E is quite sensitive to the thickness
2075 of the barrier layer, and to the presence of temperature inversions (subsurface warm layers) in the barrier layer on
2076 intraseasonal and interannual timescales.

2077 Long periods of near-molecular diffusivities (weeks to a month) were also inferred at multiple χ pods along 8°N between
2078 50 m and 100 m during transition months of March and April. Here freshwater insulation does not appear to be the major
2079 factor. Instead the period of weak turbulence may be linked to low levels of near-inertial energy (a consequence of weak
2080 wind forcing in March and April) and the absence of strong mean oceanic flows during these transition months (Cherian
2081 et al 2020). Relatively weak diffusivities are also present in the LADCP fine structure estimate of depth-integrated
2082 (thermocline to bottom) turbulent kinetic energy dissipation ε (Kunze et al, 2006) and the Argo fine structure-based 250-
2083 500 m diffusivity estimates of Whalen et al. (2012). The extended presence of such weak turbulence suggests that the
2084 Bay's internal wave field is weaker than might be expected from the Garrett-Munk internal wave spectrum at least during
2085 some months of the year. Another (related) question is the issue of representation of such weak background mixing in
2086 climate models and whether that matters to known biases in such models.

2087 Published efforts so far have been directed towards understanding the modulation of turbulence by larger-scale variations
2088 in the wind, currents and freshwater. Questions remain as to the impact of small-scale mixing on the large-scale long-term
2089 T-S structure in the Bay as well as the influence of subsurface mixing and the ensuing modification of SST on coupled
2090 ocean-atmosphere phenomena such as the MJO and the MISO (Section 3.2)

2091 **7.4 Where vertical and lateral processes meet: The Role of Submesoscale**

2092 Freshwater inflow from the Ganga-Brahmaputra-Meghna (GBM) and the Irrawady river in the Bay of Bengal is stirred by
2093 the mesoscale eddies into sharp frontal gradients (in salinity and in density) at $O(1-10\text{km})$ scales with shallow vertical
2094 extent. These fronts are acted upon by winds seasonally, setting up complex sub-mesoscale structures with salinity
2095 differences $O(1\text{ psu})$ over 1-10 km, developing bore-like features with $O(0.5\text{ psu})$ difference over a few meters horizontally
2096 (Nash et al 2016; Figure 21). Wavenumber spectra of temperature at $O(1-10\text{km})$ scale show a -2 slope in many regions
2097 of the Bay (Mackinnon et al 2016), a signature of frontogenesis in the Bay at these scales. The BoB is thus replete with
2098 fronts which evidently slump at sub-mesoscales due to both symmetric and baroclinic instabilities (Ramachandran et al.
2099 2018), and show higher stratification near fronts (Sree Lekha 2019).



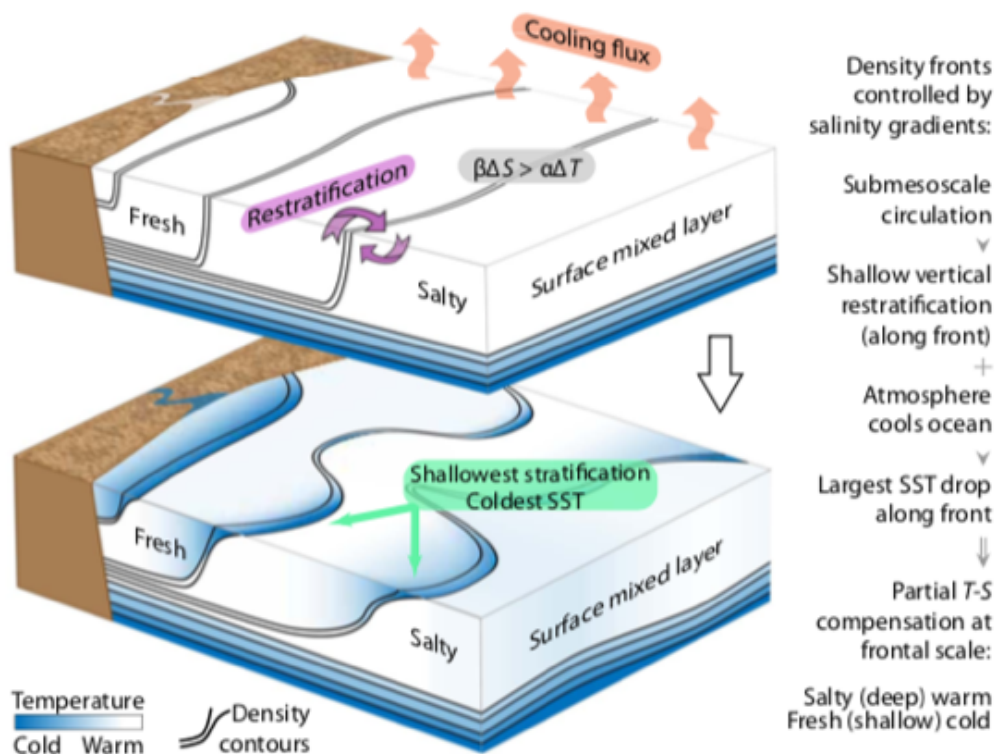
2100

2101 **Figure 21: Observed salinity gradients at mesoscale, sub-mesoscales and small horizontal scales from in the Bay of**
2102 **Bengal (Nash et al. 2016).**

2103 The fronts and filaments at $O(1-10\text{km})$, which are dominated by salinity gradients and weakly compensated, have strong
2104 implications for setting up the density stratification in the top 50-100m in the BoB (Section 4.4.1). The stratification in
2105 this depth range often has multi-layered structure with stratification varying at $O(1-10\text{km})$ scales (Lucas et al 2016),
2106 showing evidence that the stratification in the Bay cannot be explained simply in terms of vertical processes, and horizontal

2107 submesoscale processes are intimately coupled with the vertical processes at these scales. Ramachandran et al. (2018)
 2108 show that a mesoscale strained region with strong fronts ($O(1\text{kg/m}^3)$ over 40km) and weak down front wind shows multiple
 2109 dynamical signatures of sub-mesoscale instabilities. Ageostrophic secondary circulations arising near the fronts and the
 2110 accompanied sheared advection plays an important role in setting the stratification (Pham and Sarkar 2019). Both
 2111 observations and process modeling show $O(1-10\text{km})$ patches of low potential vorticity consisting of subducted warm water
 2112 patches due to a combination of baroclinic and forced symmetric instabilities, creating barrier layers whose thickness
 2113 varies laterally at sub-mesoscales (Ramachandran and Tandon, 2020 JGR-in review).

2114 During winter, the temperature gradients in the horizontal compensate for the salinity gradients to reduce the density
 2115 gradient, and the sub-mesoscale processes in BoB lead to a unique situation. Jaeger & Mahadevan (2018) show that surface
 2116 cooling fluxes combined with submesoscale instabilities of the haline fronts during wintertime leads to shallower mixed
 2117 layers on the less saline (cooler) side. Therefore, cold SSTs in wintertime in the Bay mark surface trapped waters (Fig.
 2118 22), whereas in other regions of the world ocean, cold filaments mark upwelling of nutrient-rich waters. Further, since the
 2119 shallow fresher mixed layers lead to larger drops in temperature, this develops the correlation between SST and SSS at
 2120 $O(1-10\text{km})$ scales.



2121

2122 **Figure 22: Interaction of submesoscale salinity gradients with atmospheric cooling leads to shallow cold regions**
2123 **(From Spiro Jaeger and Mahadevan, Science Advances 2018)**

2124 **7.5 Putting the Pieces Together**

2125 **7.5.1 Coupled ocean-atmosphere phenomena**

2126 Due to the presence of a barrier layer over much of the Bay of Bengal, entrainment and upwelling of waters from the
2127 thermocline are inhibited, and the evolution of SST is largely driven by net air-sea heat flux variability (Duncan and Han,
2128 2009). However, the dependency of SST on surface fluxes is controlled by subsurface processes such as formation of
2129 barrier layers, entrainment warming and cooling of the mixed layer, penetrative solar radiation and zonal advection
2130 (Thangaprakash et al., 2016). Advection is important in influencing the SST as lateral variations in the mixed layer depth
2131 alone can result in variations in air-sea fluxes of roughly 20 Wm^{-2} over distances of kilometers (Adams et al., 2019). This
2132 magnitude is similar to uncertainty in air-sea flux products (Weller et al. 2016) thus implying that variations in sub-
2133 mesoscales are important for heat balance in the northern BoB. The coupling of the ocean-atmosphere over BoB at large
2134 scales implicates the air-sea interaction and the mixed layer heat budget in the BoB (Rahaman et al. 2019), although at
2135 oceanic mesoscale and finer scales in the horizontal and at sub-seasonal timescales this coupling is a topic of active
2136 research.

2137 **7.5.2 Implications for biogeochemistry in the Bay**

2138 Eddies in the central BoB arise not by the baroclinic instability of boundary currents but rather due to planetary wave
2139 dynamics off the equator that triggers coastal Kelvin waves around the Bay. The Kelvin waves then trigger south-westward
2140 propagating Rossby waves, which result in large mesoscale structures in the Bay (Cheng et al. 2018). The Andaman and
2141 Nicobar Islands are also shown to be very important for the generation of these eddies; without these islands the number
2142 of eddies would have reduced to almost half in the western bay of Bengal (Mukherjee et al., 2019). These eddies provide
2143 much of the horizontal stretching and stirring of the tracers, including those relevant to the ecosystems

2144 Eddies have tremendous potential to influence ocean biogeochemistry by providing “new” nutrients to the ocean’s
2145 euphotic layer (Stramma et al., 2013). However, we do not fully understand the spatial distribution of nutrients within the
2146 eddy surface area – e.g., there is a debate whether nutrients upwell at the core and downwell at the edge of the eddy, or
2147 vice versa. Further, such discrepancy also continues in the type of eddies – i.e., whether upwelling occurs in cyclonic and
2148 downwelling occurs in anticyclonic eddies and vice versa (Mahadevan, 2014; Mahadevan et al., 2012; Martin and
2149 Richards, 2001). But there is a consensus that eddies do impact biogeochemistry (McGillicuddy et al., 2007).

2150 There have been only a handful of studies on the role of eddies in biological productivity in this region (Kumar et al.,
2151 2007; Singh et al., 2015). Kumar et al. (2007) observed an increase in surface nutrients in the Bay through eddies during
2152 both fall-2002 and spring-2003 followed by higher biomass. Despite being highly eutrophic, biological activity did not
2153 increase following cyclonic eddies during the summer-2003 in the northern Bay (Muraleedharan et al., 2007). But primary
2154 production switched from 'regenerated' to 'new' production during summer-2003. In a ¹⁵N based new production estimate
2155 to assess the role of cyclonic eddies in enhancing primary production, Singh et al. (2015) carried out measurements of
2156 primary production at four stations in the Bay of Bengal (around a cyclonic eddy close to 17.8°N, 87.5°E) during winter
2157 2007. The measurements sampled one cyclonic eddy during the campaign. The highest surface productivity (2.71 μM C
2158 d⁻¹) and chlorophyll a (0.18 μg L⁻¹) were observed within the eddy due to intrusion of nutrients from subsurface waters.
2159 Given new nitrogen input via vertical mixing, river discharge or aerosol deposition, the additional primary production due
2160 to this new nutrient input and its contribution to the total production increased from 40% to 70%. Eddies could be a reason
2161 for the otherwise unexplained high new production rates in the Bay of Bengal (Singh and Ramesh, 2015). Eddies also
2162 seem to have a potential for transferring a high fraction of fixed carbon to the deep. A couple of recent studies have
2163 highlighted the role of mesoscale eddies in changing the elemental proportions of carbon:nitrogen:phosphorus in the
2164 organic and nutrient pools in the euphotic layer of the Bay (Sahoo et al., 2020, 2021).

2165

2166 **8. Summary and open questions**

2167 This paper summarises a suite of new studies in the Indian Ocean that have been made possible through national, bilateral,
2168 and international programmes, including the IIOE-2. An increase in high quality observations (both increased spatial
2169 resolution and the acquisition of longer time series) has led to a substantial increase in our understanding of processes and
2170 interactions. These in-situ observations, in combination with remote sensing, detailed syntheses and modeling have
2171 increased our knowledge of the surface circulation and its complex implications for biological production, along with an
2172 increased understanding of air-sea interaction in the Indian ocean.

2173 There are, however, a number of outstanding questions that require prioritised efforts. Compared to the Atlantic and
2174 Pacific, where the important boundary currents are now being monitored with a suite of gliders with repeated and sustained
2175 sections (Todd et al. 2019), the boundary currents and their variability in the Indian Ocean remain poorly constrained.
2176 Given the anomalous warming of the Indian Ocean, the frequency of heatwaves, and the population supported by the
2177 Indian Ocean and Monsoons, the air-sea fluxes and the coupled atmosphere-ocean exchange in this ocean remain poorly
2178 understood at many scales. Understanding of the intermediate, deep and abyssal layer circulation and the vertical
2179 overturning cells that connect these layers in the Indian Ocean is lacking.

2180 There are still many gaps in current understanding of Indian Ocean biogeochemical cycles, which we have presented here
2181 in the context of the physical processes that affect them. Although the characterization of the temporal and spatial
2182 variability in chlorophyll concentration and primary production has greatly improved as a result of recent in situ
2183 measurements and satellite remote sensing, there are still many areas where there is little or no information about how this
2184 relates to changes in planktonic food web structure and particulate organic matter export to the deep ocean. Although
2185 nutrient limitation patterns were not discussed in this review, it should be pointed out that the importance of nitrogen
2186 versus iron and silica limitation in the Arabian Sea and elsewhere in the Indian Ocean is still a subject of debate - more
2187 nutrient and trace metal measurements are needed along with nutrient limitation bioassays throughout the Indian Ocean.

2188 The number of nitrogen fixation rate measurements in the Indian Ocean has increased significantly over the last decade,
2189 but the importance of this process as a source of new nitrogen to the surface ocean has been quantified in only a few
2190 regions (e.g., off northwest Australia) and its contribution to bloom formation (e.g., the Madagascar Bloom) is still
2191 uncertain. From a spatial standpoint, the quantification of biogeochemical variability in the northern Indian Ocean
2192 (Arabian Sea and Bay of Bengal) has benefited, in particular, from numerous shipboard measurements, moorings and
2193 biogeochemical Argo float deployments in the last decade. Many questions still remain, for example, related to the
2194 influence of freshwater inputs on biogeochemical cycles in the Bay of Bengal. Remarkably, the biogeochemical and
2195 ecological impacts of the Indonesian Throughflow have been examined in only a handful of studies. Similarly, there are
2196 very few studies that focus on the biogeochemical and ecological impacts of the Seychelles-Chagos Thermocline Ridge
2197 (SCTR). The ITF and the SCTR are unique features of the Indian Ocean, yet the understanding of their biogeochemical
2198 and ecological impacts is rudimentary at best. Finally, the quantification of biogeochemical variability in the Leeuwin
2199 and Agulhas Currents and adjacent waters has also benefited from recent measurements, though it is important to point
2200 out that the biogeochemical impacts of boundary currents in the Indian Ocean are still poorly understood compared to the
2201 Atlantic and Pacific.

2202 There are still large uncertainties in air-sea fluxes. Even in the regional basin of the Bay of Bengal where there have been
2203 focused international efforts, the river discharge and rain need to be better represented in models, as do the processes that
2204 set the shallow salinity stratification. These have important feedbacks on the SST which impacts atmospheric convection
2205 with a global reach. At longer time scales, the salinity feedbacks to climate at interannual to decadal timescales need to be
2206 investigated in further detail. The decadal variability of the Indian Ocean Dipole and its link to the Pacific decadal
2207 variability also needs to be better understood, particularly given events like the record breaking 2019 positive IOD that
2208 developed independently from ENSO conditions. Marine heatwaves are an increasing threat to marine ecosystems fuelled
2209 by increasing mean temperatures in the ocean and atmosphere. There are still large gaps in our understanding of the Indian
2210 Ocean dynamics that lead to these extremes, and consequently in our ability to predict the onset, intensity and frequency
2211 of extreme weather such as rainfall, flooding and heatwaves, associated with anomalously strong climatic mode events
2212 that have major socioeconomic impacts.

2213 Modeling and observational efforts have both pointed to the increased role of air-sea coupling at higher frequencies to
2214 improve the predictions of sub-seasonal Monsoon forecasts. Observations and models indicate that MISOs may be slowing
2215 down because of the warming in the Indian Ocean (e.g. Sabeerali et al. 2013), which needs to be understood better for
2216 providing reliable monsoon predictions and projections in this climate vulnerable region.

2217 On the influence of small-scale mixing, increased measurements of ocean mixing both along the equator and new long-
2218 term measurements in the Bay of Bengal, have shown intensively enhanced mixing during the passage of eddies and during
2219 cyclones. However, there are still significant uncertainties in subsurface ocean mixing in setting the large-scale balance in
2220 the Indian ocean.

2221 It has been proposed that the hiatus in warming of the surface atmosphere may have ceased as the Pacific Ocean enters an
2222 El Nino like state (Cha et al. 2018). However, the secular trends in the Pacific Ocean trade winds are expected to continue
2223 to affect the Indo-Pacific Ocean heat content through the Indonesian Throughflow (Maher et al. 2018). The Indian Ocean
2224 thus remains a critical component of the Earth's global response to the continued anthropogenic forcing and the ocean's
2225 role as a clearing house for distributing heat to modulate global warming.

2226 **Code Availability**

2227 No original data analyses were undertaken as part of this review paper.

2228 **Data Availability**

2229 No original data analyses were undertaken as part of this review paper. All data presented in this manuscript have been
2230 previously published and are available from sources identified in the original manuscripts.

2231 **Author Contributions**

2232 HEP and AT designed the review, wrote the introductory and concluding parts and sections in their areas of expertise. HP
2233 and AT reviewed the contributions of the authors and made editorial adjustments. RH wrote the sections on
2234 biogeochemical variability in Section 4. All co-authors contributed to the writing of sections relevant to their areas of
2235 expertise and response to reviewer questions. All authors contributed to refining the manuscript for submission. RF, CU,
2236 JB, BW, AS-F, JH and RM contributed editorial advice.

2237 **Competing interests**

2238 The authors declare that they have no conflict of interest.

2239 **Acknowledgements**

2240 The authors acknowledge the sustained efforts of researchers and funding agencies in observing and modelling the oceanic
2241 and atmospheric processes that control climate variability in the Indian Ocean region. These contributions during the
2242 International Indian Ocean Expeditions (I and II) and in the intervening years through national and international programs,
2243 such as CLIVAR and GOOS, are fundamental to improving our knowledge of these systems and increasing our skill at
2244 forecasting variability and extreme events. We thank the IIOE-2 leadership team (<https://iioe-2.incois.gov.in/>) for their
2245 unwavering efforts to share new discoveries and promote understanding of the importance of the Indian Ocean to the
2246 climate system and Earth's inhabitants. We are very grateful to Michael McPhaden, Lisa Beal and an anonymous reviewer
2247 for their encouraging and constructive comments that have led to a more comprehensive and balanced synthesis of recent
2248 advances. HEP acknowledges support from the Earth Systems and Climate Change Hub and Climate Systems Science
2249 Hub of the Australian Government's National Environmental Science Programme and the ARC Centre of Excellence for
2250 Climate Extremes. AT acknowledges the US Office of Naval Research.

2251 **References**

- 2252 Abram, N. J., Gagan, M. K., Cole, J. E., Hantoro, W. S., and Mudelsee, M.: Recent intensification of tropical climate
2253 variability in the Indian Ocean. *Nature Geoscience*, 1, 849–853, <https://doi.org/10.1038/ngeo357>, 2008.
- 2254 Abram, N. J., Hargreaves, J. A., Wright, N. M., Thirumalai, K., Ummenhofer, C. C., and England, M. H.: Palaeoclimate
2255 perspectives on the Indian Ocean Dipole. *Quat. Sci. Rev.*, 237, 106302,
2256 <https://doi.org/10.1016/j.quascirev.2020.106302>, 2020a.
- 2257 Abram, N. J., Wright, N. M., Ellis, B., Dixon, B. C., Wurtzel, J. B., England, M. H., Ummenhofer, C. C., Philibosian, B.,
2258 Cahyarini, S. Y., Yu, T.-L., Shen, C.-C., Cheng, H., Edwards, R. L., and Heslop, D.: Coupling of Indo-Pacific climate
2259 variability over the last millennium, *Nature*, 579, 385–392, <https://doi.org/10.1038/s41586-020-2084-4>, 2020b.
- 2260 Akhil, V. P., Durand, F., Lengaigne, M., Vialard, J., Keerthi, M. G., Gopalakrishna, V. V., Deltel, C., Papa, F. and De
2261 Boyer Montégut, C.: A modeling study of the processes of surface salinity seasonal cycle in the Bay of Bengal, *J.*
2262 *Geophys. Res. Ocean.*, doi:10.1002/2013JC009632, 2014.
- 2263 Amol, P., Shankar, D., Fernando, V., Mukherjee, A., Aparna, S. G., Fernandes, R., Michael, G. S., Khalap, S. T.,
2264 Satelkar, N. P., Agarvadekar, Y., Gaonkar, M. G., Tari, A. P., Kankonkar, A. and Vernekar, S. P.: Observed
2265 intraseasonal and seasonal variability of the West India Coastal Current on the continental slope; *J. Earth Syst. Sci.*
2266 123 1045–1074, <https://doi.org/10.1007/s12040-014-0449-5>, 2014.
- 2267 Alory, G., Wijffels, S., and Meyers, G.: Observed temperature trends in the Indian Ocean over 1960–1999 and
2268 associated mechanisms. *Geophys. Res. Lett.*, 34, L02606, <https://doi.org/10.1029/2006GL028044>, 2007.
- 2269 Anderson, D. L. T., and Gill, A. E.: Spin-up of a stratified ocean, with applications to upwelling, *Deep Sea Res.*, 22(9),
2270 583–596, [https://doi.org/10.1016/0011-7471\(75\)90046-7](https://doi.org/10.1016/0011-7471(75)90046-7), 1975.

2271 Andrews, J.C.: Eddy structure and the West Australian current, *Deep Sea Research*, 24(12), 1133–1148,
2272 [https://doi.org/10.1016/0146-6291\(77\)90517-3](https://doi.org/10.1016/0146-6291(77)90517-3), 1977.

2273 Annamalai, H., Potemra, J., Murtugudde, R., and McCreary, J. P.: Effect of preconditioning on the extreme climate
2274 events in the tropical Indian Ocean, *J. Climate*, 18, 3450–3469, <https://doi.org/10.1175/JCLI3494.1>, 2005.

2275 Anutaliya, A., Send, U., Mcclean, J., Sprintall, J., Rainville, L., M. Lee, C., Jinadasa, S., Wallcraft, A. J., Metzger, E.:
2276 An undercurrent off the east coast of Sri Lanka. *Ocean Sci. Discuss.* 13, 1–15, 2017.

2277 Arzeno, I. B., S. N. Giddings, G. Pawlak, and R. Pinkel: Generation of Quasi Biweekly Yanai Waves in the Equatorial
2278 Indian Ocean. *Geophys Res Lett*, 47, e2020GL088915. <https://doi.org/10.1029/2020GL088915>, 2020.

2279 Ash, K. D., and Matyas, C. J.: The influences of ENSO and the Subtropical Indian Ocean Dipole on tropical cyclone
2280 trajectories in the South Indian Ocean, *Int. J. Climatol.*, 32, 41–56, <https://doi.org/10.1002/joc.2249>, 2012.

2281 Ayers, J. M., Strutton, P. G., Coles, V. J., Hood, R. R. and Matear, R. J.: Indonesian throughflow nutrient fluxes and
2282 their potential impact on Indian Ocean productivity, *Geophys. Res. Lett.*, doi:10.1002/2014GL060593, 2014.

2283 Bahmanpour, M. H., Pattiaratchi, C., Wijeratne, E. M. S., Steinberg, C., and D'Adamo, N.: Multi-year observation of
2284 Holloway Current along the shelf edge of North Western Australia, *J. Coast. Res.*, 517–521,
2285 <https://doi.org/10.2112/SI75-104.1>, 2016.

2286 Banse, K. and English, D. C.: Geographical differences in seasonality of CZCS-derived phytoplankton pigment in the
2287 Arabian Sea for 1978-1986, *Deep. Res. Part II Top. Stud. Oceanogr.*, doi:10.1016/S0967-0645(99)00157-5, 2000.

2288 Banse, K. and McClain, C.: Winter blooms of phytoplankton in the Arabian Sea as observed by the Coastal Zone Color
2289 Scanner, *Mar. Ecol. Prog. Ser.*, doi:10.3354/meps034201, 1986.

2290 Baranowski, D. B., M. K. Flatau, P. J. Flatau, and A. J. Matthews (2016), Impact of atmospheric convectively coupled
2291 equatorial kelvin waves on upper ocean variability, *Journal of Geophysical Research-Atmospheres*, 121(5), 2045–
2292 2059, doi:10.1002/2015jd024150.

2293 Barlow, R., Lamont, T., Kyewalyanga, M., Sessions, H. and Morris, T.: Phytoplankton production and physiological
2294 adaptation on the southeastern shelf of the Agulhas ecosystem, *Cont. Shelf Res.*, doi:10.1016/j.csr.2010.05.007, 2010.

2295 Barlow, R., Lamont, T., Morris, T., Sessions, H. and van den Berg, M.: Adaptation of phytoplankton communities to
2296 mesoscale eddies in the Mozambique Channel, *Deep. Res. Part II Top. Stud. Oceanogr.*,
2297 doi:10.1016/j.dsr2.2013.10.020, 2014.

2298 Beal, L. M. and Bryden, H. L.: The velocity and vorticity structure of the Agulhas Current at 32°S, *J. Geophys. Res.*
2299 *Ocean.*, doi:10.1029/1998jc900056, 1999.

2300 Beal, L. M., De Ruijter, W. P. M., Biastoch, A., Zahn, R., Cronin, M., Hermes, J., Lutjeharms, J., Quartly, G., Tozuka,
2301 T., Baker-Yeboah, S., Bornman, T., Cipollini, P., Dijkstra, H., Hall, I., Park, W., Peeters, F., Penven, P., Ridderinkhof,
2302 H. and Zinke, J.: On the role of the Agulhas system in ocean circulation and climate, *Nature*, doi:10.1038/nature09983,
2303 2011.

2304 Beal, L. M. and Donohue, K. A.: The Great Whirl: Observations of its seasonal development and interannual variability,
2305 *J. Geophys. Res. Ocean.*, doi:10.1029/2012JC008198, 2013.

2306 Beal, L. M., Hormann, V., Lumpkin, R., & Foltz, G. R.: The Response of the Surface Circulation of the Arabian Sea to
2307 Monsoonal Forcing, *Journal of Physical Oceanography*, 43(9), 2008-2022.
2308 <https://journals.ametsoc.org/view/journals/phoc/43/9/jpo-d-13-033.1.xml>, 2013.

2309 Beal, L. M., Elipot, S., Houk, A., and Leber, G. M.: Capturing the Transport Variability of a Western Boundary Jet:
2310 Results from the Agulhas Current Time-Series Experiment (ACT)*, *Journal of Physical Oceanography*, 45, 1302–
2311 1324, <https://doi.org/10.1175/jpo-d-14-0119.1>, 2015.

2312 Beal, L. and Elipot, S.: Broadening not strengthening of the Agulhas Current since the early 1990s. *Nature*, 540, 570–
2313 573, <https://doi.org/10.1038/nature19853>, 2016.

2314 Beal, L. M., Vialard, J., Roxy, M. K. and lead authors: IndOOS-2: A roadmap to sustained observations of the Indian
2315 Ocean for 2020-2030. CLIVAR-4/2019, GOOS-237, 204 pp. doi: <https://doi.org/10.36071/clivar.rp.4.2019> , 2019.

2316 Beal, L. M., Vialard, J., Roxy, M. K., Li, J., Andres, M., Annamalai, H., Feng, M., Han, W., Hood, R., Lee, T.,
2317 Lengaigne, M., Lumpkin, R., Masumoto, Y., McPhaden, M. J., Ravichandran, M., Shinoda, T., Sloyan, B. M.,

2318 Strutton, P. G., Subramanian, A. C., Tozuka, T., Ummenhofer, C. C., Unnikrishnan, A. S., Wiggert, J., Yu, L., Cheng,
2319 L., Desbruyères, D. G., & Parvathi, V.: A Road Map to IndOOS-2: Better Observations of the Rapidly Warming
2320 Indian Ocean, *Bulletin of the American Meteorological Society*, 101(11), E1891-E1913,
2321 <https://journals.ametsoc.org/view/journals/bams/101/11/bamsD190209.xml>, 2020.

2322 Behera, S.K., and Yamagata, T.: Subtropical SST dipole events in the southern Indian Ocean, *Geophys. Res. Lett.*, 28,
2323 327–330, <https://doi.org/2000GL011451>, 2001.

2324 Bellon, G., Sobel, A. H., and Vialard, J.: Ocean-atmosphere coupling in the monsoon intraseasonal oscillation: A simple
2325 model study, *J. Clim.*, 21(20), 5254–5270, <http://doi.org/10.1175/2008JCLI2305.1>, 2008.

2326 Benthuisen, J., Feng, M., and Zhong, L.: Spatial patterns of warming off Western Australia during the 2011 Ningaloo
2327 Niño: quantifying impacts of remote and local forcing, *Continental Shelf Res.*, 91, 232–246,
2328 <https://doi.org/10.1016/j.csr.2014.09.014>, 2014a.

2329 Benthuisen, J., Furue, R., McCreary, J. P., Bindoff, N. L., and Phillips, H. E.: Dynamics of the Leeuwin Current: Part 2.
2330 Impacts of mixing, friction, and advection on a buoyancy-driven eastern boundary current over a shelf, *Dyn. Atmos.*
2331 *Oceans*, 65, 39–63, <https://doi.org/10.1016/j.dynatmoce.2013.10.004>, 2014b.

2332 Benthuisen, J. A., Oliver, E.C.J., Feng, M., and Marshall, A. G.: Extreme marine warming across tropical Australia
2333 during austral summer 2015–2016, *J. Geophys. Res.: Oceans*, 123, 1301-1326, <https://doi.org/10.1002/2017JC013326>,
2334 2018.

2335 Bergman, J. W., Hendon, H. H., and Weickmann, K. M.: Intraseasonal air-sea interactions at the onset of El Niño, *J.*
2336 *Climate*, 14, 1702–1719, 2001.

2337 Beron-Vera, F. J., Wang, Y., Olascoaga, M. J., Goni, G. J. and Haller, G.: Objective detection of oceanic eddies and the
2338 agulhas leakage, *J. Phys. Oceanogr.*, doi:10.1175/JPO-D-12-0171.1, 2013.

2339 Biaostoch, A., Böning, C. W. and Lutjeharms, J. R. E.: Agulhas leakage dynamics affects decadal variability in Atlantic
2340 overturning circulation, *Nature*, doi:10.1038/nature07426, 2008.

2341 Biaostoch, A., Böning, C. W., Schwarzkopf, F. U. and Lutjeharms, J. R. E.: Increase in Agulhas leakage due to poleward
2342 shift of Southern Hemisphere westerlies, *Nature*, doi:10.1038/nature08519, 2009.

2343 Biaostoch, A. and Böning, C. W.: Anthropogenic impact on Agulhas leakage, *Geophys. Res. Lett.*, doi:10.1002/grl.50243,
2344 2013.

2345 Biaostoch, A., Durgadoo, J. V., Morrison, A. K., Van Sebille, E., Weijer, W. and Griffies, S. M.: Atlantic multi-decadal
2346 oscillation covaries with Agulhas leakage, *Nat. Commun.*, doi:10.1038/ncomms10082, 2015.

2347 Boyd, A. J. and Shillington, F. A.: Physical forcing and circulation patterns on the Agulhas Bank, *S. Afr. J. Sci.*, 90(3)
2348 114-122, 1994.

2349 Brock, J. C. and McClain, C. R.: Interannual variability in phytoplankton blooms observed in the northwestern Arabian
2350 Sea during the southwest monsoon, *J. Geophys. Res.*, doi:10.1029/91JC02225, 1992.

2351 Brown, S. L., Landry, M. R., Barber, R. T., Campbell, L., Garrison, D. L. and Gowing, M. M.: Picophytoplankton
2352 dynamics and production in the Arabian Sea during the 1995 Southwest Monsoon, *Deep. Res. Part II Top. Stud.*
2353 *Oceanogr.*, doi:10.1016/S0967-0645(99)00042-9, 1999.

2354 Bryden, H. and Beal, L.: Role of the Agulhas Current in Indian Ocean circulation and associated heat and freshwater
2355 fluxes. *Deep-Sea Research I*, 48(8), 1821-1845, 2001.

2356 Burchall, J. : An evaluation of primary productivity studies in the continental shelf region of the Agulhas Current near
2357 Durban (1961-1966), *Investigational Report*, Oceanographic Research Institute, 20: 16 pp, 1968.

2358 Cai, W., Sullivan, A., and Cowan, T.: Shoaling of the off-equatorial south Indian Ocean thermocline: Is it driven by
2359 anthropogenic forcing? *Geophys. Res. Lett.*, 35, <https://doi.org/10.1029/2008GL034174>, 2008.

2360 Cai, W., Cowan, T., and Sullivan, A.: Recent unprecedented skewness towards positive Indian Ocean Dipole
2361 occurrences and their impact on Australian rainfall. *Geophys. Res. Lett.*, 36, <https://doi.org/10.1029/2009GL037604>,
2362 2009a.

2363 Cai, W., Pan, A., Roemmich, D., Cowan, T., and Guo, X.: Argo profiles a rare occurrence of three consecutive positive
2364 Indian Ocean Dipole events, 2006–2008, *Geophys. Res. Lett.*, 36, <https://doi.org/10.1029/2008GL037038>, 2009b.

2365 Cai, W., Sullivan, A., and Cowan, T.: Climate change contributes to more frequent consecutive positive Indian Ocean
2366 Dipole events. *Geophys. Res. Lett.*, 36 (L23704), <https://doi.org/10.1029/2009GL040163>, 2009c.

2367 Cai, W., Sullivan, A., and Cowan, T.: How rare are the 2006–2008 positive Indian Ocean Dipole events? An IPCC AR4
2368 climate model perspective, *Geophys. Res. Lett.*, 36 (L08702), <https://doi.org/10.1029/2009GL037982>, 2009d.

2369 Cai, W., Zheng, X.-T. , Weller, E., Collins, M., Cowan, T., Lengaigne, M., Yu, W., and Yamagata, T.: Projected
2370 response of the Indian Ocean Dipole to greenhouse warming, *Nat. Geosci.*, 6, 999-1007,
2371 <https://doi.org/10.1038/ngeo2009>, 2013.

2372 Cai, W., Santoso, A., Wang, G., Weller, E., Wu, L., Ashok, K., Masumoto, Y., and Yamagata, T.: Increased frequency
2373 of extreme Indian Ocean Dipole events due to greenhouse warming, *Nature*, 510, 254-258,
2374 <https://doi.org/10.1038/nature13327>, 2014a.

2375 Cai, W. , Borlace, S., Lengaigne, M., van Rensch, P., Collins, M., Vecchi, G., Timmermann, A., Santoso, A., McPhaden,
2376 M. J., Wu, L., and England, M. H.: Increasing frequency of extreme El Niño events due to greenhouse warming, *Nat.*
2377 *Clim. Change*, 4, 2, 111–116, <https://doi.org/10.1038/nclimate2100>, 2014b.

2378 Cai, W. Wang, G., Santoso, A., McPhaden, M. J., Wu, L., Jin, F. F., Timmermann, A., Collins, M., Vecchi, G.,
2379 Lengaigne, M., and England, M. H.: Increased frequency of extreme La Niña events under greenhouse warming, *Nat.*
2380 *Clim. Change*, 5, 2, 132–137, <https://doi.org/10.1038/nclimate2492>, 2015.

2381 Cai, W. et al.: Pantropical climate interactions. *Science*, 363, doi:10.1126/science.aav4236, 2019.

2382 Caley, T., Giraudeau, J., Malaizé, B., Rossignol, L. and Pierre, C.: Agulhas leakage as a key process in the modes of
2383 Quaternary climate changes, *Proc. Natl. Acad. Sci. U. S. A.*, doi:10.1073/pnas.1115545109, 2012.

2384 Caputi, N., de Lestang, S., Feng, M., and Pearce, A. F.: Seasonal variation in the long-term warming trend in water
2385 temperature off the Western Australian coast. *Mar. Freshw. Res.*, 60, 129-139, 2009.

2386 Carter, R. A. and Schleyer, M. H.: Plankton distributions in Natal coastal waters., E. H. Schumann (ed.), *Coastal Ocean*
2387 *Studies off Natal, South Africa* (Springer-Verlag: New York), 2012.

2388 Castellanos, P., Campos, E. J. D., Piera, J., Sato, O. T. and Silva Dias, M. A. F.: Impacts of Agulhas leakage on the
2389 tropical Atlantic western boundary systems, *J. Clim.*, doi:10.1175/JCLI-D-15-0878.1, 2017.

2390 Cessi, P.: The Global Overturning Circulation, *Annual Review of Marine Science*, 11(1), 249-270,
2391 <https://doi.org/10.1146/annurev-marine-010318-095241>, 2019.

2392 Cha, S.-C., Moon, J.-H., and Song, Y. T.: A recent shift toward an El Niño-like ocean state in the tropical Pacific and
2393 the resumption of ocean warming. *Geophysical Research Letters*, 45, 11,885– 11,894.
2394 <https://doi.org/10.1029/2018GL080651>, 2018.

2395 Chatterjee, A., Shankar, D., Shenoi, S. S. C., Reddy, G. V., Michael, G. S., Ravichandran, M., Gopalkrishna, V. V., Rao,
2396 E. P. R., Bhaskar, T. V. S. U. and Sanjeevan, V. N.: A new atlas of temperature and salinity for the North Indian
2397 Ocean, *J. Earth Syst. Sci.*, 121(3), 559–593, doi:10.1007/s12040-012-0191-9, 2012.

2398 Chatterjee, A., Shankar, D., McCreary, J. P. and Vinayachandran, P. N.: Yanai waves in the western equatorial Indian
2399 Ocean, *J. Geophys. Res. Oceans*, 118, 1556–1570, doi:10.1002/jgrc.20121, 2013.

2400 Chatterjee, A., Shankar, D., McCreary, J. P., Vinayachandran, P. N. and Mukherjee, A.: Dynamics of Andaman Sea
2401 circulation and its role in connecting the equatorial Indian Ocean to the Bay of Bengal, *J. Geophys. Res. Ocean.*,
2402 doi:10.1002/2016JC012300, 2017.

2403 Chatterjee, A., Kumar, B. P., Prakash, S., and Singh, P.: Annihilation of the Somali upwelling system during summer
2404 monsoon, *Scientific reports*, 9(1), 7598. <https://doi.org/10.1038/s41598-019-44099-1>, 2019.

2405 Chaudhuri, D., Sengupta, D., D’Asaro, E., Venkatesan, R. and Ravichandran, M.: Response of the salinity-stratified bay
2406 of Bengal to Cyclone Phailin, *J. Phys. Oceanogr.*, doi:10.1175/JPO-D-18-0051.1, 2019.

2407 Chaudhuri, A., Shankar, D., Aparna, S. G., Amol, P., Fernando, V., Kankonkar, A., Micheal, G. S., Satelkar, N. P.,
2408 Khalap, S. T., tari, A. P., Gaonkar, M. G., Ghatkar, S., Khedekar, R. R.: Observed variability of the West India Coastal
2409 Current on the continental slope from 2009–2018, *J. Earth Syst. Sci.*, 129, <https://doi.org/10.1007/s12040-019-1322-3>,
2410 2020.

2411 Chen, G., Han, W., Li, Y., Wang, D. and McPhaden, M. J.: Seasonal-to-interannual time-scale dynamics of the
2412 equatorial undercurrent in the Indian Ocean, *J. Phys. Oceanogr.*, doi:10.1175/JPO-D-14-0225.1, 2015.

2413 Chen, G., Han, W., Shu, Y., Li, Y., Wang, D. and Xie Q.: The role of Equatorial Undercurrent in sustaining the Eastern
2414 Indian Ocean upwelling, *Geophys. Res. Lett.*, 43, 6444–6451, doi:10.1002/2016GL069433, 2016.

2415 Chen, G., Han, W., Li, Y., Yao, J. and Wang, D.: Intraseasonal Variability of the Equatorial Undercurrent in the Indian
2416 Ocean, *Journal of Physical Oceanography*, 49(1), 85-101, 2019.

2417 Cheng, Y., Putrasahan, D., Beal, L. and Kirtman, B.: Quantifying Agulhas leakage in a high-resolution climate model, *J.*
2418 *Clim.*, doi:10.1175/JCLI-D-15-0568.1, 2016.

2419 Cheng, Y., Beal, L.M., Kirtman, B.P., and Putrasahan, D.: Interannual Agulhas Leakage Variability and Its Regional
2420 Climate Imprints, *J. Climate*, 31(24), 10105–10121, 2018.

2421 Cheng, X., McCreary, J. P., Qiu, B., Qi, Y., Du, Y. and Chen, X.: Dynamics of Eddy Generation in the Central Bay of
2422 Bengal, *J. Geophys. Res. Ocean.*, doi:10.1029/2018JC014100, 2018.

2423 Chi, N.-H., Lien, R.-C., D’Asaro, E. A., and Ma, B. B.: The surface mixed layer heat budget from mooring observations
2424 in the central Indian Ocean during Madden-Julian Oscillation events, *J. Geophys. Res. Ocean.*, 119(7), 4638–4652,
2425 <https://doi.org/10.1002/2014JC010192>, 2014.

2426 Chowdary, J. S., Xie, S., Tokinaga, H., Okumura, Y. M., Kubota, H., Johnson, N., and Zheng, X.: Interdecadal
2427 variations in ENSO teleconnection to the Indo–Western Pacific for 1870–2007, *Journal of Climate*, 25(5), 1722-1744,
2428 2012.

2429 Chowdary, J. S., Bandgar, A. B., Gnanaseelan, C., and Luo, J. J.: Role of tropical Indian Ocean air-sea interactions in
2430 modulating Indian summer monsoon in a coupled model, *Atmos. Sci. Lett.*, 16(2), 170–176, doi:10.1002/asl2.561,
2431 2015.

2432 Church, J.A., Cresswell, G.R., and Godfrey J.S.: The Leeuwin Current, in: Poleward Flows Along Eastern Ocean
2433 Boundaries, Coastal and Estuarine Studies (formerly Lecture Notes on Coastal and Estuarine Studies), vol 34, edited
2434 by: Neshyba, S.J., Mooers, C.N.K., Smith, R.L., and Barber, R.T., Springer, New York, 230–254,
2435 https://doi.org/10.1007/978-1-4613-8963-7_16, 1989.

2436 Cirano, M. and Middleton, J.F.: Aspects of the mean wintertime circulation along Australia's southern shelves:
2437 Numerical studies. *J. Phys. Oceanogr.*, 34, 668–684, <https://doi.org/10.1175/2509.1>, 2004.

2438 Coles, V. J., Wilson, C. and Hood, R. R.: Remote sensing of new production fuelled by nitrogen fixation, *Geophys. Res.*
2439 *Lett.*, doi:10.1029/2003gl019018, 2004.

2440 Cullen, K. E. and Shroyer, E. L.: Seasonality and interannual variability of the Sri Lanka dome, *Deep. Res. Part II Top.*
2441 *Stud. Oceanogr.*, doi:10.1016/j.dsr2.2019.104642, 2019.

2442 Currie, J. C., Lengaigne, M., Vialard, J., Kaplan, D. M., Aumont, O., Naqvi, S. W. A., and Maury, O.: Indian Ocean
2443 Dipole and El Niño/Southern Oscillation impacts on regional chlorophyll anomalies in the Indian Ocean.
2444 *Biogeosciences*, 10, 6677-6698, 2013.

2445 Cuypers, Y., X. Le Vaillant, P. Bouruet-Aubertot, J. Vialard and M. J. McPhaden, 2013: Tropical storm-induced near-
2446 inertial internal waves during the Cirene experiment: energy fluxes and impact on vertical mixing. *J. Geophys. Res.*,
2447 118, 358-380, doi: 10.1029/2012JC007881.

2448 Cyriac, A., M. McPhaden, H. Phillips, N. Bindoff, M. Feng: Surface layer heat balance in the subtropical Indian Ocean.
2449 *J. Geophys. Res. Oceans*. 124, 6459–6477. <https://doi.org/10.1029/2018JC014559>, 2019.

2450 Cyriac, A., Phillips, H. E., Bindoff, N. L., Mao, H. & Feng, M.: Observational estimates of turbulent mixing in the
2451 southeast Indian Ocean. *J Phys Oceanogr*, doi:10.1175/jpo-d-20-0036.1, 2021.

2452 D'Adamo, N., Fandry, C., Buchan, S., Domingues, C.: Northern sources of the Leeuwin Current and the "Holloway
2453 Current" on the North West Shelf, *J. Roy. Soc. Western Australia*, 92(2), 53–66,
2454 <http://nora.nerc.ac.uk/id/eprint/526029>, 2009.

2455 Daher, H., Beal, L. M., and Schwarzkopf, F. U.: A new improved estimation of Agulhas Leakage using observations and
2456 simulations of Lagrangian floats and drifters, *Journal of Geophysical Research: Oceans*, 125,
2457 <https://doi.org/10.1029/2019JC015753>, 2020

2458 David, D. T., Kumar, S. P., Byju, P., Sarma, M. S. S., Suryanarayana, A., and Murty, V. S. N.: Observational evidence
2459 of lower-frequency Yanai waves in the central equatorial Indian Ocean, *Journal of Geophysical Research*, 116
2460 (C06009), doi:10.1029/2010JC006603, 2011..

2461 De Boer, A. M., Graham, R. M., Thomas, M. D., and Kohfeld, K. E.: The control of the Southern Hemisphere
2462 Westerlies on the position of the Subtropical Front, *J. Geophys. Res. Oceans*, 118, 5669– 5675,
2463 doi:10.1002/jgrc.20407, 2013.

2464 de Vos, A., Pattiaratchi, C. B. and Wijeratne, E. M. S.: Surface circulation and upwelling patterns around Sri Lanka,
2465 *Biogeosciences*, doi:10.5194/bg-11-5909-2014, 2014.

2466 Demarcq, H., Barlow, R. G. and Shillington, F. A.: Climatology and variability of sea surface temperature and surface
2467 chlorophyll in the benguela and agulhas ecosystems as observed by satellite imagery, *African J. Mar. Sci.*,
2468 doi:10.2989/18142320309504022, 2003.

2469 DeMott, C. A., Klingaman, N. P., and Woolnough, S. J.: Atmosphere-ocean coupled processes in the Madden-Julian
2470 oscillation, *Rev. Geophys.*, 53, 1099–1154, <http://doi.org/10.1002/2014RG000478>, 2015.

2471 Desbruyères, D. G., McDonagh, E. L., King, B. A., and Thierry, V.: Global and Full-Depth Ocean Temperature Trends
2472 during the Early Twenty-First Century from Argo and Repeat Hydrography, *J. Climate*, [https://doi.org/10.1175/JCLI-](https://doi.org/10.1175/JCLI-D-16-0396.1)
2473 [D-16-0396.1](https://doi.org/10.1175/JCLI-D-16-0396.1), 2017.

2474 Deshpande, A., Gnanaseelan, C., Chowdary, J., and Rahul, S.: Interannual spring Wyrтки jet variability and its regional
2475 impacts, *Dyn. Atmos. Oceans*, 78, 26–37, 2017.

2476 Dhage, L., and Strub, P. T.: Intra-seasonal sea level variability along the west coast of India, *J. Geophys. Res. Oceans*,
2477 121, 8172–8188, doi:10.1002/2016JC011904, 2016.

2478 Dileepkumar, M.: Biogeochemistry of the North Indian Ocean; IGBP-WCRP-SCOPE Rep. Ser. 1, Indian Nat. Sci.
2479 Acad., New Delhi, India, 2006.

2480 Dilmahamod, Ahmad Fehmi: Links between the Seychelles-Chagos thermocline ridge and large scale climate modes and
2481 primary productivity and the annual cycle of chlorophyll-a, PhD thesis, University of Cape Town, 2014.

2482 Dilmahamod, A. F., Aguiar-González, B., Penven, P., Reason, C. J. C., De Ruijter, W. P. M., Malan, N., & Hermes, J.
2483 C.: SIDDIES corridor: A major east-west pathway of long-lived surface and subsurface eddies crossing the subtropical
2484 south indian ocean. *Journal of Geophysical Research: Oceans*, 123, 5406– 5425.
2485 <https://doi.org/10.1029/2018JC013828>, 2018.

2486 Dilmahamod, A. F., Penven, P., Aguiar-González, B., Reason, C. J. C., & Hermes, J. C.: A new definition of the South-
2487 East Madagascar Bloom and analysis of its variability. *Journal of Geophysical Research: Oceans*, 124, 1717–1735.
2488 <https://doi.org/10.1029/2018JC014582>, 2019.

2489 Divakaran, P., and Brassington, G.B.: Arterial ocean circulation of the southeast Indian Ocean, *Geophys. Res. Lett.*, 38,
2490 L01802, <https://doi.org/10.1029/2010GL045574>, 2011.

2491 Doi, T., Behera, S. K., and Yamagata, T.: Wintertime impacts of the 2019 super IOD on East Asia, *Geophys. Res. Lett.*,
2492 doi:10.1029/2020GL089456, 2020.

2493 Domingues, C. M., Wijffels, S. E., Maltrud, M. E., Church, J. A. and Tomczak, M.: Role of eddies in cooling the
2494 Leeuwin Current, *Geophys. Res. Lett.*, doi:10.1029/2005GL025216, 2006.

2495 Domingues, C. M., Maltrud, M. E., Wijffels, S. E., Church, J. A., Tomczak, M.: Simulated Lagrangian pathways
2496 between the Leeuwin Current System and the upper-ocean circulation of the southeast Indian Ocean, *Deep Sea Res. II*,
2497 54, 797–817, <http://doi.org/10.1016/j.dsr2.2006.10.003>, 2007.

2498 Dong, L. and M.J. McPhaden: Interhemispheric SST gradient trends in the Indian Ocean prior to and during the recent
2499 global warming hiatus. *J. Climate*, 29, 9077-9095, 2016.

2500 Dong, L., Zhou, T., Dai, A., Song, F., Wu, B., and Chen, X.: The footprint of the inter-decadal Pacific oscillation in
2501 Indian Ocean sea surface temperatures, *Sci. Rep.*, 6, 21251, <https://doi.org/10.1038/srep21251>, 2016.

2502 Donohue, K. A. and Toole, J. M.: A near-synoptic survey of the Southwest Indian Ocean, *Deep. Res. Part II Top. Stud.*
2503 *Oceanogr.*, doi:10.1016/S0967-0645(03)00039-0, 2003.

2504 Drushka, K., Sprintall, J., Gille, S. T. and Brodjonegoro, I.: Vertical structure of Kelvin waves in the Indonesian
2505 throughflow exit passages, *J. Phys. Oceanogr.*, doi:10.1175/2010JPO4380.1, 2010.

2506 Drushka, K., Sprintall, J., Gille, S. T. and Wijffels, S.: In situ observations of Madden-Julian oscillation mixed layer
2507 dynamics in the Indian and western Pacific Oceans, *J. Clim.*, 25(7), 2306–2328, doi:10.1175/JCLI-D-11-00203.1,
2508 2012.

2509 Du, Y., Xie, S.-P., Huang, G., and Hu, K.: Role of air–sea interaction in the long persistence of El Niño–induced north
2510 Indian Ocean warming, *J. Clim.*, 22, 2023-2038, <https://doi.org/10.1175/2008JCLI2590.1>, 2009.

2511 Du, Y., Cai, W., and Wu, Y.: A new type of the Indian Ocean dipole since the mid-1970s, *J. Climate*, 26, 959-972,
2512 <https://doi.org/10.1175/JCLI-D-12-00047.1>, 2013.

2513 Du, Y., Y. Zhang, M. Feng, T. Wang, N. Zhang, and S. Wijffels, S.: Decadal trends of the upper ocean salinity in the
2514 tropical Indo-Pacific since mid-1990s, *Scientific Reports*, 5, 16050, 2015.

2515 Du, Y., Zhang, Y., Zhang, L.-Y., Tozuka, T., Ng, B., & Cai, W.: Thermocline warming induced extreme Indian
2516 Ocean dipole in 2019. *Geophysical Research Letters*, 47, e2020GL090079. <https://doi.org/10.1029/2020GL090079>,
2517 2020.

2518 Dufois, F., Hardman-Mountford, N. J., Greenwood, J., Richardson, A. J., Feng, M., Herbette, S. and Matear, R.: Impact
2519 of eddies on surface chlorophyll in the South Indian Ocean, *J. Geophys. Res. Ocean.*, 119, 8061-77,
2520 doi:10.1002/2014JC010164, 2014.

2521 Duncan, B. and Han, W.: Influence of atmospheric intraseasonal oscillations on seasonal and interannual variability in
2522 the upper Indian Ocean, *J. Geophys. Res. Ocean.*, 117, 1-24 doi:10.1029/2012JC008190, 2012.

2523 Duran, E. R.: An investigation of the Leeuwin Undercurrent source waters and pathways. Honours thesis, University of
2524 Tasmania, 2015.

2525 Duran, E.R., Phillips, H.E., Furue, R., Spence, P., and Bindoff, N.L.: Southern Australia Current System based on a
2526 gridded hydrography and a high-resolution model, *Prog. Oceanogr.*, 181, 102254,
2527 <https://doi.org/10.1016/j.pocan.2019.102254>, 2020.

2528 Durgadoo, J. V., Loveday, B. R., Reason, C. J. C., Penven, P. and Biastoch, A.: Agulhas leakage predominantly
2529 responds to the southern hemisphere westerlies, *J. Phys. Oceanogr.*, 43, 2113-2131, doi:10.1175/JPO-D-13-047.1,
2530 2013.

2531 Durgadoo, J. V., Rühls, S., Biastoch, A. and Böning, C. W. B.: Indian Ocean sources of Agulhas leakage, *J. Geophys.*
2532 *Res. Ocean.*, doi:10.1002/2016JC012676, 2017.

2533 Elipot, S., & Beal, L. M.: Characteristics, energetics, and origins of Agulhas current meanders and their limited
2534 influence on ring shedding. *Journal of Physical Oceanography*, 45(9), 2294-2314. <https://doi.org/10.1175/JPO-D-14-0254.1>, 2015.

2536 Elipot, S. and Beal, L. M.: Observed Agulhas Current Sensitivity to Interannual and Long-Term Trend Atmospheric
2537 Forcings. *Journal of Climate*. 31 (8) p3077–3098. <https://doi.org/10.1175/JCLI-D-17-0597.1>, 2018

2538 Endo, S., and Tozuka, T.: Two flavors of the Indian Ocean dipole, *Climate Dyn.*, 46, 3371-3385, <https://doi.org/10.1007/s00382-015-2773-0>, 2016.

2540 England, M. H., and Huang, F.: On the interannual variability on the Indonesian Throughflow and its linkage with
2541 ENSO, *J. Climate*, 18(9), 1435-1444, <https://doi.org/10.1175/JCLI3322.1>, 2005.

2542 England, M. H., Ummenhofer, C. C. and Santoso, A.: Interannual rainfall extremes over southwest Western Australia
2543 linked to Indian Ocean climate variability, *J. Clim.*, doi:10.1175/JCLI3700.1, 2006.

2544 England, M., McGregor, S., Spence, P., Meehl, G., Timmerman, A., Cai, W., Sen Gupta, A., McPhaden, M., Purich, A.
2545 and Santoso, A.: Recent intensification of wind-driven circulation in the Pacific and the ongoing warming hiatus.
2546 *Nature Clim Change* 4, 222–227, <https://doi.org/10.1038/nclimate2106>, 2014.

2547 Fan, L., Liu, Q., Wang, C., and Guo, F.: Indian Ocean dipole modes associated with different types of ENSO
2548 development, *J. Climate*, 30, 2233–2249, <https://doi.org/10.1175/JCLI-D-16-0426.1>, 2017.

2549 Fang, F., and Morrow, R.: Evolution, movement and decay of warm-core Leeuwin Current eddies, *Deep Sea Res. II*,
2550 50(12–13), 2245–2261, [https://doi.org/10.1016/S0967-0645\(03\)00055-9](https://doi.org/10.1016/S0967-0645(03)00055-9), 2003.

2551 Fang, G., Susanto, R. D., Wirasantosa, S., Qiao, F., Supangat, A., Fan, B., Wei, Z., Sulistiyo, B. and Li, S.: Volume,
2552 heat, and freshwater transports from the South China Sea to Indonesian seas in the boreal winter of 2007-2008, *J.*
2553 *Geophys. Res. Ocean.*, doi:10.1029/2010JC006225, 2010.

2554 Feng, M., and Wijffels, S.: Intraseasonal variability in the South Equatorial Current of the East Indian Ocean. *Journal of*
2555 *Physical Oceanography*, 32, 265-277, 2002.

2556 Feng, M., Meyers, G., Pearce, A., and Wijffels, S.: Annual and interannual variations of the Leeuwin Current at 32°S, *J.*
2557 *Geophys. Res.*, 108(C11), 3355, <https://doi.org/10.1029/2002JC001763>, 2003.

2558 Feng, M., Wijffels, S., Godfrey, S., and Meyers, G.: Do eddies play a role in the momentum balance of the Leeuwin
2559 Current? *J. Phys. Oceanogr.*, 35, 964–975, <https://doi.org/10.1175/JPO2730.1>, 2005.

2560 Feng, M., Majewski, L.J., Fandry, C.B., Waite, A.M., Characteristics of two counter-rotating eddies in the Leeuwin
2561 Current system off the Western Australian coast, *Deep Sea Research II*, 54(8–10), 961–980,
2562 <https://doi.org/10.1016/j.dsr2.2006.11.022>, 2007.

2563 Feng, M., Biastoch, A., Böning, C., Caputi, N., and Meyers, G.: Seasonal and interannual variations of upper ocean heat
2564 balance off the west coast of Australia, *J. Geophys. Res.*, 113, C12025, <http://doi.org/10.1029/2008JC004908>, 2008.

2565 Feng, M., Böning, C.W., Biastoch, A., Behrens, E., Weller, E., Masumoto, Y.: The reversal of the multi-decadal trends
2566 of the equatorial Pacific easterly winds, and the Indonesian Throughflow and Leeuwin Current transports. *Geophys.*
2567 *Res.Lett.* 38, L11604, 2011.

2568 Feng, M., McPhaden, M.J., Xie, S.P., and Hafner, J.: La Niña forces unprecedented Leeuwin Current warming in 2011,
2569 *Sci. Rep.*, 3, 1277, <https://doi.org/10.1038/srep01277>, 2013.

2570 Feng, M., Benthuisen, J., Zhang, N., and Slawinski, D.: Freshening anomalies in the Indonesian throughflow and
2571 impacts on the Leeuwin Current during 2010–2011, *Geophys. Res. Lett.*, 42, 8555–8562,
2572 <https://doi.org/10.1002/2015GL065848>, 2015a.

2573 Feng, M., Hendon, H. H., Xie, S.-P., Marshall, A. G., Schiller, A., Kosaka, Y., Caputi, N., and Pearce, A.: Decadal
2574 increase in Ningaloo Niño since the late 1990s, *Geophys. Res. Lett.*, 42, 1, 104-112,
2575 <https://doi.org/10.1002/2014GL062509>, 2015b.

2576 Feng, M., Zhang, X., Oke, P., Monselesan, D., Chamberlain, M., Matear, R., and Schiller, A.: Invigorating ocean
2577 boundary current systems around Australia during 1979–2014: As simulated in a near-global eddy-resolving ocean
2578 model. *J. Geophys. Res. Oceans*, 121(5), 3395–3408, <https://doi.org/10.1002/2016JC011842>, 2016.

2579 Feng, M., Zhang, N., Liu, Q. and Wijffels, S.: The Indonesian throughflow, its variability and centennial change, *Geosci.*
2580 *Lett.*, doi:10.1186/s40562-018-0102-2, 2018.

2581 Feng, X., and Shinoda, T.: Air-sea heat flux variability in the southeast Indian Ocean and its relation with Ningaloo
2582 Niño. *Front. Mar. Sci.*, 6, 266, <https://doi.org/10.3389/fmars.2019.00266>, 2019.

2583 Fioux, M., Schott, F. and Swallow, J. C.: Deep boundary currents in the western Indian Ocean revisited, *Deep Sea Res.*
2584 Part A, *Oceanogr. Res. Pap.*, doi:10.1016/0198-0149(86)90124-X, 1986.

2585 Fine, R. A., Smethie W. M., Bullister, J. L., Rhein M., Min, D. H., Warner, M. J., Poisson, A., Weiss, R. F.: Decadal
2586 ventilation and mixing of Indian Ocean waters. *Deep-Sea Res I*, 55, 20–37, <https://doi.org/10.1016/j.dsr.2007.10.002>,
2587 2008.

2588 Foltz, G. R., Vialard, J., Kumar, B. P. and Mcphaden, M. J.: Seasonal mixed layer heat balance of the southwestern
2589 tropical Indian Ocean, *J. Clim.*, doi:10.1175/2009JCLI3268.1, 2010.

2590 Fox-Kemper, B., Hewitt, H. T., Xiao, C., Aðalgeirsdóttir, G., Drijfhout, S. S., Edwards, T. L., Golledge, N. R., Hemer,
2591 M., Kopp, R. E., Krinner, G., A. Mix, A., Notz, D., Nowicki, S. Nurhati, I. S., Ruiz, L., Sallée, J-B., Slangen, A. B. A.,
2592 Yu, Y.: Ocean, Cryosphere and Sea Level Change. In: Climate Change 2021: The Physical Science Basis.
2593 Contribution of Working Group I to the Sixth Assessment Report of the Intergovernmental Panel on Climate Change
2594 [Masson-Delmotte, V., P. Zhai, A. Pirani, S. L. Connors, C. Péan, S. Berger, N. Caud, Y. Chen, L. Goldfarb, M. I.
2595 Gomis, M. Huang, K. Leitzell, E. Lonnoy, J.B.R. Matthews, T. K. Maycock, T. Waterfield, O. Yelekçi, R. Yu and B.
2596 Zhou (eds.)]. Cambridge University Press. In press.

2597 Francis, P.A., Jithin, A. K., Effy, J. B., Chatterjee, A., Chakraborty, K. et al.: High-resolution operational ocean
2598 forecast and reanalysis system for the Indian Ocean. *Bulletin of the American Met. Soc.*, 101(8), E1340-E1356,
2599 <https://journals.ametsoc.org/view/journals/bams/101/8/bamsD190083.xml>, 2020.

2600 Furnas, M.: Intra-seasonal and inter-annual variations in phytoplankton biomass, primary production and bacterial
2601 production at North West Cape, Western Australia: Links to the 1997-1998 El Niño event, *Cont. Shelf Res.*,
2602 doi:10.1016/j.csr.2007.01.002, 2007.

2603 Furue, R., McCreary, J. P., Benthuyesen, J., Phillips, H. E., and Bindoff, N. L.: Dynamics of the Leeuwin Current: Part 1.
2604 Coastal flows in an inviscid, variable-density, layer model, *Dyn. Atmos. Oceans*, 63, 24–59,
2605 <https://doi.org/10.1016/j.dynatmoce.2013.03.003>, 2013.

2606 Furue, R., Guerreiro, K., Phillips, H. E., McCreary, J. P., and Bindoff, N. L.: On the Leeuwin Current System and its
2607 linkage to zonal flows in the South Indian Ocean as inferred from a gridded hydrography, *J. Phys. Oceanogr.*, 47, 583–
2608 602, <https://doi.org/10.1175/JPO-D-16-0170.1>, 2017.

2609 Furue, R.: The three-dimensional structure of the Leeuwin Current System in density coordinates in an eddy-resolving
2610 OGCM, *Ocean Modelling*, 138, 36–50, <https://doi.org/10.1016/j.ocemod.2019.03.001>, 2019.

2611 Ganachaud, A., Wunsch, C., Marotzke, J. and Toole, J.: Meridional overturning and large-scale circulation of the Indian
2612 Ocean, *J. Geophys. Res. Ocean.*, doi:10.1029/2000jc900122, 2000.

2613 Gandhi, N., Singh, A., Prakash, S., Ramesh, R., Raman, M., Sheshshayee, M. and Shetye, S.: First direct measurements
2614 of N₂ fixation during a *Trichodesmium* bloom in the eastern Arabian Sea, *Global Biogeochemical Cycles*, 25(4), 2011.

2615 Garrison, D. L., Gowing, M. M., Hughes, M. P., Campbell, L., Caron, D. A., Dennett, M. R., Shalapyonok, A., Olson, R.
2616 J., Landry, M. R., Brown, S. L., Liu, H. Bin, Azam, F., Steward, G. F., Ducklow, H. W. and Smith, D. C.: Microbial
2617 food web structure in the Arabian Sea: A US JGOFS study, *Deep. Res. Part II Top. Stud. Oceanogr.*,
2618 doi:10.1016/S0967-0645(99)00148-4, 2000.

2619 Gaube, P., Chelton, D. B., Strutton, P. G. and Behrenfeld, M. J.: Satellite observations of chlorophyll, phytoplankton
2620 biomass, and Ekman pumping in nonlinear mesoscale eddies, *J. Geophys. Res. Ocean.*, doi:10.1002/2013JC009027,
2621 2013.

2622 George, J. V., Nuncio, M., Chacko, R., Anilkumar, N., Noronha, S. B., Patil, S. M., Pavithran, S., Alappattu, D. P.,
2623 Krishnan, K. P. and Achuthankutty, C. T.: Role of physical processes in chlorophyll distribution in the western tropical
2624 Indian Ocean, *J. Mar. Syst.*, doi:10.1016/j.jmarsys.2012.12.001, 2013.

2625 George, J. V., Vinayachandran, P. N., Vijith, V., Thusaraa, V., Nayaka, A. A, Pargaonkara, S. K., Amol, P.,
2626 Vijaykumar, K., and Matthews, A. J.: Mechanisms of barrier layer formation and erosion from in situ observations in
2627 the Bay of Bengal, *J. Phys. Oceanogr.*, 49, 1183–1200, <https://doi.org/10.1175/JPO-D-18-0204.1>, 2019.

2628 Giddings, Jack, Karen J. Heywood, Adrian J. Matthews, Manoj M. Joshi, Benjamin GM Webber, Alejandra Sanchez-
2629 Franks, Brian A. King, and Puthenveetil N. Vinayachandran. "Spatial and temporal variability of solar penetration
2630 depths in the Bay of Bengal and its impact on SST during the summer monsoon." *Ocean Science Discussions* (2021):
2631 1-33.

2632 Gilmour, J. P., Cook, K. L., Ryan, N. M., Puotinen, M. L., Green, R. H., Shedrawi, G., Hobbs, J.-P. A., Thomson, D.P.,
2633 Babcock, R.C., Buckee, J., Foster, T., Richards, Z. T., Wilson, S. K., Barnes, P. B., Coutts, T. B., Radford, B. T.,
2634 Piggott, C. H., Depczynski, M., Evans, S. N., Schoepf, V., Evans, R. D., Halford, A. H., Nutt, C. D., Bancroft, K. P.,
2635 Heyward, A. J., Oades, D.: The state of Western Australia's coral reefs, *Coral Reefs*, 38, 4, 651-667,
2636 <https://doi.org/10.1007/s00338-019-01795-8>, 2019.

2637 Girishkumar, M. S., M. Ravichandran and M. J. McPhaden: Temperature inversions and their influence on the mixed
2638 layer heat budget during the winters of 2006-07 and 2007-08 in the Bay of Bengal. *J. Geophys. Res.*, 118,
2639 doi:10.1002/jgrc.20192, 2013.

2640 Girishkumar, M. S., Joseph, J., Thangaprakash, V. P., Pottapinjara, V. and McPhaden, M. J.: Mixed Layer Temperature
2641 Budget for the Northward Propagating Summer Monsoon Intraseasonal Oscillation (MISO) in the Central Bay of
2642 Bengal, *J. Geophys. Res. Ocean.*, 122(11), 8841–8854, doi:10.1002/2017JC013073, 2017.

2643 Girishkumar, M.S., K. Ashin, M.J. McPhaden, B. Balaji, and B. Praveenkumar: Estimation of vertical heat diffusivity at
2644 the base of the mixed layer in the Bay of Bengal. *J. Geophys. Res.*, 125, e2019JC015402. doi:10.1029/2019JC015402,
2645 2020.

2646 Gnanaseelan, C., Deshpande, A. and McPhaden, M. J.: Impact of Indian Ocean Dipole and El Nio/Southern Oscillation
2647 wind-forcing on the Wyrтки jets, *J. Geophys. Res. Ocean.*, doi:10.1029/2012JC007918, 2012.

2648 Godfrey, J. S., and Ridgway, K. R.: The large-scale environment of the poleward-flowing Leeuwin Current, Western
2649 Australia: longshore steric height gradients, wind stresses and geostrophic flow, *J. Phys. Oceanogr.*, 15(5), 481–495,
2650 [https://doi.org/10.1175/1520-0485\(1985\)015<0481:TLSEOT>2.0.CO;2](https://doi.org/10.1175/1520-0485(1985)015<0481:TLSEOT>2.0.CO;2), 1985.

2651 Godfrey, J. S., and Weaver, A.: Why are there such strong steric height gradients off Western Australia? In: Proceedings
2652 of the Western Pacific International Meeting and Workshop on TOGA COARE, May 24–30, 1989, Noumea, New
2653 Caledonia, 215–222, <http://hdl.handle.net/102.100.100/262338>, 1989.

2654 Godfrey, J.S., and Weaver, A.J.: Is the Leeuwin Current driven by Pacific heating and winds? *Prog. Oceanogr.*, 27(3–4),
2655 225–272, [https://doi.org/10.1016/0079-6611\(91\)90026-I](https://doi.org/10.1016/0079-6611(91)90026-I), 1991.

2656 Godfrey, J. S.: The effect of the Indonesian throughflow on ocean circulation and heat exchange with the atmosphere: A
2657 review, *J. Geophys. Res.*, 101(C5), 12,217–12,237, 1996.

2658 Goericke, R., Olson, R. J. and Shalapyonok, A.: A novel niche for *Prochlorococcus* sp. in low-light suboxic
2659 environments in the Arabian Sea and the Eastern Tropical North Pacific, *Deep. Res. Part I Oceanogr. Res. Pap.*,
2660 doi:10.1016/S0967-0637(99)00108-9, 2000.

2661 Goes, J. I., Tian, H., Gomes, H. do R., Anderson, O. R., Al-Hashmi, K., deRada, S., Luo, H., Al-Kharusi, L., Al-Azri, A.
2662 and Martinson, D. G.: Ecosystem state change in the Arabian Sea fuelled by the recent loss of snow over the
2663 Himalayan-Tibetan Plateau region, *Sci. Rep.*, doi:10.1038/s41598-020-64360-2, 2020.

2664 Gomes, H. D., Goes, J. I., Matondkar, S. G. P., Buskey, E. J., Basu, S., Parab, S. and Thoppil, P.: Massive outbreaks of
2665 *Noctiluca scintillans* blooms in the Arabian Sea due to spread of hypoxia, *Nat. Commun.*, doi:10.1038/ncomms5862,
2666 2014.

2667 Gordon, A. L., Susanto, R. D. and Vranes, K.: Cool Indonesian throughflow as a consequence of restricted surface layer
2668 flow, *Nature*, doi:10.1038/nature02038, 2003.

2669 Gordon, A. L., Susanto, R. D., Ffield, A., Huber, B. A., Pranowo, W. and Wirasantosa, S.: Makassar Strait throughflow,
2670 2004 to 2006, *Geophys. Res. Lett.*, doi:10.1029/2008GL036372, 2008.

2671 Gordon, A. L., Sprintall, J., Van Aken, H. M., Susanto, R. D., Wijffels, S., Molcard, R., Ffield, A., Pranowo, W. and
2672 Wirasantosa, S.: The Indonesian throughflow during 2004-2006 as observed by the INSTANT program, *Dyn. Atmos.*
2673 *Ocean.*, doi:10.1016/j.dynatmoce.2009.12.002, 2010.

2674 Gordon, A. L., Huber, B. A., Metzger, E. J., Susanto, R. D., Hurlburt, H. E. and Adi, T. R.: South China Sea
2675 throughflow impact on the Indonesian throughflow, *Geophys. Res. Lett.*, doi:10.1029/2012GL052021, 2012.

2676 Gordon, A. L., Shroyer, E. L., Mahadevan, A., Sengupta, D. and Freilich, M.: Bay of Bengal: 2013 Northeast monsoon
2677 upper-ocean circulation, *Oceanography*, doi:10.5670/oceanog.2016.41, 2016.

2678 Gordon, A., Shroyer, E. & Murty, V.: An Intrathermocline Eddy and a tropical cyclone in the Bay of Bengal. *Sci Rep* 7,
2679 46218, <https://doi.org/10.1038/srep46218>, 2017.

2680 Goschen, W. S., Schumann, E. H., Bernard, K. S., Bailey, S. E. and Deyzel, S. H. P.: Upwelling and ocean structures off
2681 Algoa Bay and the south-east coast of South Africa, *African J. Mar. Sci.*, doi:10.2989/1814232X.2012.749810, 2012.

2682 Goswami, B. B., Mukhopadhyay, P., Khairoutdinov, M. and Goswami, B. N.: Simulation of Indian summer monsoon
2683 intraseasonal oscillations in a superparameterized coupled climate model: Need to improve the embedded cloud
2684 resolving model, *Clim. Dyn.*, 41(5–6), 1497–1507, <https://doi.org/10.1007/s00382-012-1563-1>, 2013.

2685 Goswami, B.N., S.A. Rao, D. Sengupta, and S. Chakravorty: Monsoons to mixing in the Bay of Bengal: Multiscale air-
2686 sea interactions and monsoon predictability. *Oceanography* 29(2):18–27, <http://dx.doi.org/10.5670/oceanog.2016.35>,
2687 2016.

2688 Gudka, M., Obura, D., Mwaura, J., Porter, S. Yahya, S., and Mabwa, R.: Impact of the 3rd Global Coral Bleaching
2689 Event on the Western Indian Ocean in 2016, Global Coral Reef Monitoring Network (GCRMN)/Indian Ocean
2690 Commission, pp. 67, <http://hdl.handle.net/20.500.11822/25700>, 2018.

2691 Guemas, V., Corti, S., Garcia-Serrano, J., Doblas-Reyes, F. J., Balmaseda, M., and Magnusson, L.: The Indian Ocean:
2692 The region of highest skill worldwide in decadal climate prediction. *J. Climate*, 26, 726–739, 2013.

2693 Gundersen, J. S., Gardner, W. D., Richardson, M. J. and Walsh, I. D.: Effects of monsoons on the seasonal and spatial
2694 distributions of POC and chlorophyll in the Arabian Sea, *Deep. Res. Part II Top. Stud. Oceanogr.*, doi:10.1016/S0967-
2695 0645(98)00065-4, 1998.

2696 Guo, F., Liu, Q., Sun, S., and Yang, J.: Three types of Indian Ocean dipoles. *J. Climate*, 28, 3073-3092, 2015.

2697 Haarsma, R. J., Campos, E. J. D., Drijfhout, S., Hazeleger, W. and Severijns, C.: Impacts of interruption of the Agulhas
2698 leakage on the tropical Atlantic in coupled ocean-atmosphere simulations, *Clim. Dyn.*, doi:10.1007/s00382-009-0692-
2699 7, 2011.

2700 Haine, T. W. N., Watson, A. J., Liddicoat, M. I. and Dickson, R. R.: The flow of Antarctic bottom water to the
2701 southwest Indian Ocean estimated using CFCs, *J. Geophys. Res. Ocean.*, doi:10.1029/98JC02476, 1998.

2702 Halkides, D. J., Waliser, D. E., Lee, T., Menemenlis, D. and Guan, B.: Quantifying the processes controlling
2703 intraseasonal mixed-layer temperature variability in the tropical Indian Ocean, *J. Geophys. Res. Ocean.*, 120(2), 692–
2704 715, doi:10.1002/2014JC010139, 2015.

2705 Han, W., McCreary, J. P., Anderson, D. L. T. and Mariano, A. J.: Dynamics of the eastern surface jets in the equatorial
2706 Indian Ocean, *J. Phys. Oceanogr.*, doi:10.1175/1520-0485(1999)029<2191:DOTESJ>2.0.CO;2, 1999.

2707 Han, W., Webster, P., Lukas, R., Hacker, P. and Hu, A.: Impact of atmospheric intraseasonal variability in the Indian
2708 Ocean: Low-frequency rectification in equatorial surface current and transport, *J. Phys. Oceanogr.*, doi:10.1175/1520-
2709 0485(2004)034<1350:IOAIVI>2.0.CO;2, 2004.

2710 Han, W., Yuan, D., Liu, W. T. and Halkides, D. J.: Intraseasonal variability of Indian Ocean sea surface temperature
2711 during boreal winter: Madden-Julian Oscillation versus submonthly forcing and processes, *J. Geophys. Res. Ocean.*,
2712 112(4), 1–20, doi:10.1029/2006JC003791, 2007.

2713 Han, W., Vialard, J., McPhaden, M. J., Lee, T., Masumoto, Y., Feng, M. and De Ruijter, W. P. M.: Indian ocean decadal
2714 variability: A review, *Bull. Am. Meteorol. Soc.*, doi:10.1175/BAMS-D-13-00028.1, 2014.

2715 Hanson, C. E., Waite, A. M., Thompson, P. A. and Pattiaratchi, C. B.: Phytoplankton community structure and nitrogen
2716 nutrition in Leeuwin Current and coastal waters off the Gascoyne region of Western Australia, *Deep. Res. Part II Top.*
2717 *Stud. Oceanogr.*, doi:10.1016/j.dsr2.2006.10.002, 2007.

2718 Hazra, A., Chaudhari, H. S., Saha, S. K., Pokhrel, S. and Goswami, B. N.: Progress Towards Achieving the Challenge of
2719 Indian Summer Monsoon Climate Simulation in a Coupled Ocean-Atmosphere Model, *J. Adv. Model. Earth Syst.*,
2720 doi:10.1002/2017MS000966, 2017.

2721 Hermes, J. C. and Reason, C. J. C.: Ocean model diagnosis of interannual coevolving SST variability in the South Indian
2722 and South Atlantic Oceans, *J. Clim.*, doi:10.1175/JCLI3422.1, 2005.

2723 Hermes, J. C., and Reason, C. J. C.: Annual cycle of the South Indian Ocean (Seychelles-Chagos) thermocline ridge in a
2724 regional ocean model, *Journal of Geophysical Research*, 113: C04035, doi:10.1029/2007JC004363, 2008.

2725 Hermes J. C., Masumoto Y., Beal L. M., Roxy M. K., Vialard J., Andres M., Annamalai H., Behera S., D’Adamo N.,
2726 Doi T., Feng M., Han W., Hardman-Mountford N., Hendon H., Hood R., Kido S., Lee C., Lee T., Lengaigne M., Li J.,
2727 Lumpkin R., Navaneeth K. N., Milligan B., McPhaden M. J., Ravichandran M., Shinoda T., Singh A., Sloyan B.,

2728 Strutton P. G., Subramanian A. C., Thurston S., Tozuka T., Ummenhofer C. C., Unnikrishnan A. S., Venkatesan R.,
2729 Wang D., Wiggert J., Yu L., Yu W.: A Sustained Ocean Observing System in the Indian Ocean for Climate Related
2730 Scientific Knowledge and Societal Needs. *Frontiers in Marine Science*, 6, 355, 1-21, doi/10.3389/fmars.2019.00355,
2731 2019.

2732 Hernández-Guerra, A. & Talley, L. D.: Meridional overturning transports at 30°S in the Indian and Pacific Oceans in
2733 2002–2003 and 2009. *Prog Oceanogr* 146, 89–120, 2016.

2734 Hitchcock, G. L., L. Key, E. and Masters, J.: The fate of upwelled waters in the Great Whirl, August 1995, *Deep. Res.*
2735 Part II Top. Stud. Oceanogr., doi:10.1016/S0967-0645(99)00156-3, 2000.

2736 Ho, C. R., Zheng, Q. and Kuo, N. J.: SeaWiFs observations of upwelling south of Madagascar: Long-term variability
2737 and interaction with East Madagascar Current, *Deep. Res. Part II Top. Stud. Oceanogr.*,
2738 doi:10.1016/j.dsr2.2003.05.001, 2004.

2739 Holbrook, N. J., Scannell, H.A., Sen Gupta, A., Benthuyesen, J.A., Feng, M., Oliver, E.C.J., Alexander, L.V., Burrow,
2740 M.T., Donat, M.G., Hobday, A.J., Moore, P.J., Perkins-Kirkpatrick, S.E., Smale, D.A., Straub, S. C., and Wernberg,
2741 T.: A global assessment of marine heatwaves and their drivers, *Nature Commun.*, 10, 2624,
2742 <https://doi.org/10.1038/s41467-019-10206-z>, 2019.

2743 Holloway, P. E.: Leeuwin current observations on the Australian North West Shelf, May-June 1993, *Deep. Res. Part I*,
2744 doi:10.1016/0967-0637(95)00004-P, 1995.

2745 Holloway, P. E. and Nye, H. C.: Leeuwin current and wind distributions on the southern part of the Australian north west
2746 shelf between January 1982 and July 1983, *Mar. Freshw. Res.*, doi:10.1071/MF9850123, 1985.

2747 Holton, L., J. Deshayes, B. C. Backeberg, B. R. Loveday, J. C. Hermes, and C. J. C. Reason, Spatio-temporal
2748 characteristics of Agulhas leakage: a model inter-comparison study, *Climate Dynamics*, 48(7), 2107-2121, 2017.

2749 Hood, R. R., Coles, V. J. and Capone, D. G.: Modeling the distribution of Trichodesmium and nitrogen fixation in the
2750 Atlantic Ocean, *J. Geophys. Res. C Ocean.*, doi:10.1029/2002JC001753, 2004.

2751 Hood, R. R., Beckley, L. E., and Wiggert, J. D.: Biogeochemical and ecological impacts of boundary currents in the
2752 Indian Ocean, *Prog. Oceanogr.*, 156, pp. 290–325, 2017.

2753 Hood, R.R., H.W. Bange, L. Beal, L.E. Beckley, P. Burkill, G.L. Cowie, N. D'Adamo, G. Ganssen, H. Hendon, J.
2754 Hermes, M. Honda, M. McPhaden, M. Roberts, S. Singh, E. Urban, and W. Yu. : Science Plan of the Second
2755 International Indian Ocean Expedition (IIOE-2): A Basin-Wide Research Program. Scientific Committee on Oceanic
2756 Research, Newark, Delaware, USA, 2015

2757 Hood, R. R., V. J. Coles, J. Huggett, M. Landry, M. Levy, J. W. Moffett, and J. Wiggert. in preparation. 'Indian Ocean
2758 Biogeochemistry: Nutrients, Phytoplankton and Zooplankton Variability and Limitations.' in C. C. Ummenhofer and
2759 R. R. Hood (eds.), *The Indian Ocean and its Role in the Global Climate System* (Elsevier).

2760 Horii, T., K. Mizuno, M. Nagura, T. Miyama, and K. Ando: Seasonal and interannual variation in the cross-equatorial
2761 meridional currents observed in the eastern Indian Ocean, *J. Geophys. Res.*, 118, 6658–6671,
2762 doi:10.1002/2013JC009291, 2013.

2763 Hormann, V., Centurioni, L. R., Gordon, A. L.: Freshwater export pathways from the Bay of Bengal, *Deep Sea Research*
2764 Part II: Topical Studies in Oceanography, 168, 104645, 0967-0645, <https://doi.org/10.1016/j.dsr2.2019.104645>, 2019.

2765 Howden, S. D., and Murtugudde, R.: Effects of river inputs into the Bay of Bengal, *J. Geophys. Res. Ocean.*, 106(C9),
2766 19825–19843, <https://doi.org/10.1029/2000jc000656>, 2001.

2767 Hu, D., Wu, L., Cai, W., Sen Gupta, A., Ganachaud, A., Qiu, B., Gordon, A. L., Lin, X., Chen, Z., Hu, S., Wang, G.,
2768 Wang, Q., Sprintall, J., Qu, T., Kashino, Y., Wang, F. and Kessler, W. S.: Pacific western boundary currents and their
2769 roles in climate, *Nature*, doi:10.1038/nature14504, 2015.

2770 Hu, S. and Sprintall, J.: Interannual variability of the Indonesian Throughflow: The salinity effect, *J. Geophys. Res.*
2771 *Ocean.*, doi:10.1002/2015JC011495, 2016.

2772 Hu, S., and Sprintall, J.: Observed strengthening of interbasin exchange via the Indonesian Seas due to rainfall
2773 Intensification, *Geophysical Research Letters*, 44(3), 1448-1456, 2017a.

2774 Hu, S., and Sprintall, J.: A stronger Indonesian Throughflow related to enhanced regional rainfall, *CLIVAR Exchanges*,
2775 71, 21-25, 2017b.

2776 Hu, K., Huang, G., Xie, S.-P., Long, S. M.: Effect of the mean flow on the anomalous anticyclone over the Indo-
2777 northwest Pacific in post-El Niño summers. *Clim. Dyn.*, 53, 5725–5741, 2019.

2778 Huhn, F., von Kameke, A., Pérez-Muñuzuri, V., Olascoaga, M. J., and Beron-Vera, F. J.: The impact of advective
2779 transport by the South Indian Ocean countercurrent on the Madagascar bloom, *Geophys. Res. Lett.*, 39, L06602,
2780 <https://doi.org/10.1029/2012GL051246>, 2012.

2781 Hutchinson, K., Beal, L. M., Penven, P., Ansorge, I., & Hermes, J. :Seasonal phasing of Agulhas Current transport tied
2782 to a baroclinic adjustment of near-field winds. *Journal of Geophysical Research: Oceans*, 123.
2783 <https://doi.org/10.1029/2018JC014319>, 2018

2784 Huussen, T. N., Naveira-Garabato, A. C., Bryden, H. L. and McDonagh, E. L.: Is the deep Indian Ocean MOC sustained
2785 by breaking internal waves?, *J. Geophys. Res. Ocean.*, doi:10.1029/2012JC008236, 2012.

2786 Ibrahim, N., Mohamed, M., Basheer, A., Ismail, H., Nistharan, F., Schmidt, A., Naeem, R., Abdulla, A., and Grimsditch,
2787 G.: Status of Coral Bleaching in the Maldives in 2016, Marine Research Centre, Malé, Maldives, 47 pp.,
2788 <https://portals.iucn.org/library/node/46803>, 2017.

2789 Iskandar, I., Masumoto, Y. and Mizuno, K.: Subsurface equatorial zonal current in the eastern Indian Ocean, *J. Geophys.*
2790 *Res. Ocean.*, doi:10.1029/2008JC005188, 2009.

2791 Iskandar, I., Sasaki, H., Sasai, Y., Masumoto, Y., and Mizuno, K.: A numerical investigation of eddy-induced
2792 chlorophyll bloom in the southeastern tropical Indian Ocean during Indian Ocean Dipole—2006. *Ocean Dyn.*, 60, 731-
2793 742, 2010.

2794 Iskandar, I. and McPhaden, M. J.: Dynamics of wind-forced intraseasonal zonal current variations in the equatorial
2795 Indian Ocean, *J. Geophys. Res. Ocean.*, 116(6), 1–16, doi:10.1029/2010JC006864, 2011.

2796 Izumo, T., C. de Boyer Montegut, J.J. Luo, S.K. Behera, S. Masson, and T. Yamagata: The role of the western Arabian
2797 Sea upwelling in Indian monsoon rainfall variability. *J. Clim.*, 21, 5603–5623, doi:10.1175/2008JCLI2158.1, 2008.

2798 Izumo, T., Vialard, J., Lengaigne, M., de Boyer Montegut, C., Behera, S. K., Luo, J.-J., Cravatte, S., Masson, S. and
2799 Yamagata, T.: Influence of the state of the Indian Ocean Dipole on the following year’s El Niño, *Nat. Geosci.*, 3(3),
2800 168–172, doi:10.1038/ngeo760, 2010.

2801 Jackson, J. M., Rainville, L., Roberts, M. J., McQuaid, C. D. and Lutjeharms, J. R. E.: Mesoscale bio-physical
2802 interactions between the Agulhas Current and the Agulhas Bank, South Africa, *Cont. Shelf Res.*,
2803 doi:10.1016/j.csr.2012.09.005, 2012.

2804 Jain, V., Shankar, D., Vinayachandran, P. N., Kankonkar, A., Chatterjee, A., Amol, P., Almeida, A. M., Michael, G. S.,
2805 Mukherjee, A., Chatterjee, M., Fernandes, R., Luis, R., Kamble, A., Hegde, A. K., Chatterjee, S., Das, U. and Neema,
2806 C. P.: Evidence for the existence of Persian Gulf Water and Red Sea Water in the Bay of Bengal, *Clim. Dyn.*,
2807 doi:10.1007/s00382-016-3259-4, 2017.

2808 Jayakumar, A., Vialard, J., Lengaigne, M., Gnanaseelan, C., McCreary, J. P. and Kumar, B. P.: Processes controlling the
2809 surface temperature signature of the Madden-Julian Oscillation in the thermocline ridge of the Indian Ocean, *Clim.*
2810 *Dyn.*, 37(11–12), 2217–2234, doi:10.1007/s00382-010-0953-5, 2011.

2811 Jayakumar, A., Turner, A. G., Johnson, S. J., Rajagopal, E. N., Mohandas, S. and Mitra, A. K.: Boreal summer sub-
2812 seasonal variability of the South Asian monsoon in the Met Office GloSea5 initialized coupled model, *Clim. Dyn.*,
2813 49(5–6), 2035–2059, doi:10.1007/s00382-016-3423-x, 2017.

2814 Jensen, T. G.: Arabian Sea and Bay of Bengal exchange of salt and tracers in an ocean model, *Geophys. Res. Lett.*,
2815 28(20), 3967–3970, doi:10.1029/2001GL013422, 2001.

2816 Jensen, T. G., Wijesekera, H. W., Nyadjro, E. S., Thoppil, P. G., Shriver, J., Sandeep, K. K. and Pant, V.: Modeling
2817 Salinity Exchanges Between the Equatorial Indian Ocean and the Bay of Bengal, *Oceanography*, 29(2), 92–101,
2818 doi:10.5670/oceanog.2016.42, 2016.

2819 Jia, F., Wu, L., and Qiu, B.: Seasonal modulation of eddy kinetic energy and its formation mechanism in the southeast
2820 Indian Ocean, *J. Phys. Oceanogr.*, 41(4), 657– 665, <https://doi.org/10.1175/2010JPO4436.1>, 2011a.

2821 Jia, F., Wu, L., and Qiu, B.: Interannual modulation of eddy kinetic energy in the southeast Indian ocean by Southern
2822 Annular Mode, *J. Geophys. Res.*, 116, C02029, <https://doi.org/10.1029/2010JC006699>, 2011b.

2823 Jin, D., Waliser, D. E., Jones, C. and Murtugudde, R.: Modulation of tropical ocean surface chlorophyll by the Madden-
2824 Julian Oscillation, *Clim. Dyn.*, 40(1–2), 39–58, doi:10.1007/s00382-012-1321-4, 2013a.

2825 Jin, D., Murtugudde, R. G. and Waliser, D. E.: Intraseasonal atmospheric forcing effects on the mean state of ocean
2826 surface chlorophyll, *J. Geophys. Res. Ocean.*, 118(1), 184–196, doi:10.1029/2012JC008256, 2013b.

2827 Jin, X., Kwon, Y.-O., Ummenhofer, C. C., Seo, H., Schwarzkopf, F. U., Biastoch, A., Böning, C. W. and Wright, J. S.:
2828 Influences of Pacific climate variability on decadal subsurface ocean heat content variations in the Indian Ocean. *J.*
2829 *Climate*, 31, 4157–4174, 2018a.

2830 Jin, X., Kwon, Y.-O., Ummenhofer, C. C., Seo, H., Kosaka, Y., and Wright, J. S.: Distinct mechanisms of decadal
2831 subsurface heat content variations in the eastern and western Indian Ocean modulated by tropical Pacific SST. *J.*
2832 *Climate*, 31, 7751-7769, 2018b.

2833 Jinadasa, S. U. P., Lozovatsky, I., Planella-Morató, J., Nash, J. D., MacKinnon, J. A., Lucas, A. J., Wijesekera, H. W.
2834 and Fernando, H. J. S.: Ocean turbulence and mixing around Sri Lanka and in adjacent waters of the northern Bay of
2835 Bengal, *Oceanography*, doi:10.5670/oceanog.2016.49, 2016.

2836 Johnson, G. C., Musgrave, D. L., Warren, B. A., Ffield, A. and Olson, D. B.: Flow of bottom and deep water in the
2837 Amirante Passage and Mascarene Basin, *J. Geophys. Res.*, 103, 30973-30984. doi:10.1029/1998JC90002, 1998.

2838 Johnson, G. C., Purkey, S. G, Bullister, J. L.: Warming and freshening in the abyssal southeastern Indian Ocean. *J. Clim.*
2839 21, 5351-5363. doi: 10.1175/2008JCLI2384.1, 2008a.

2840 Johnson, G. C., Purkey, S. G, Toole, J. M.: Reduced Antarctic meridional overturning circulation reaches the North
2841 Atlantic Ocean, *Geophys. Res. Lett.*, 35, L22601. doi:10.1029/2008GL035619, 2008b.

2842 José, Y. S., Aumont, O., Machu, E., Penven, P., Moloney, C. L. and Maury, O.: Influence of mesoscale eddies on
2843 biological production in the Mozambique Channel: Several contrasted examples from a coupled ocean-
2844 biogeochemistry model, *Deep. Res. Part II Top. Stud. Oceanogr.*, doi:10.1016/j.dsr2.2013.10.018, 2014.

2845 Joseph, S., Wallcraft, A. J., Jensen, T. G., Ravichandran, M., Shenoi, S. S. C. and Nayak, S.: Weakening of spring
2846 Wyrki jets in the Indian Ocean during 2006–2011, *J. Geophys. Res. Ocean.*, doi:10.1029/2011JC007581, 2012.

2847 Jyothibabu, R., Madhu, N. V., Maheswaran, P. A., Jayalakshmy, K. V., Nair, K. K. C. and Achuthankutty, C. T.:
2848 Seasonal variation of microzooplankton (20–200 μm) and its possible implications on the vertical carbon flux in the
2849 western Bay of Bengal, *Cont. Shelf Res.*, doi:10.1016/j.csr.2007.12.011, 2008.

2850 Jyoti, J., Swapna, P., Krishnan, R. and Naidu, C. V.: Pacific modulation of accelerated south Indian Ocean sea level rise
2851 during the early 21st Century, *Clim. Dyn.*, doi:10.1007/s00382-019-04795-0, 2019.

2852 Kataoka, T., Tozuka, T., Masumoto, Y., and Yamagata, T.: The Indian Ocean subtropical dipole mode simulated in the
2853 CMIP3 models, *Climate Dyn.*, 39, 1385–1399, <https://doi.org/10.1007/s00382-011-1271-2>, 2012.

2854 Kataoka, T., Tozuka, T., Behera, S., and Yamagata, T.: On the Ningaloo Niño/Niña, *Climate Dyn.*, 43, 1463–1482,
2855 <https://doi.org/10.1007/s00382-013-1961-z>, 2014.

2856 Kato, S., Loeb, N. G., Rose, F. G., Doelling, D. R., Rutan, D. A., Caldwell, T. E., Yu, L. and Weller, R. A.: Surface
2857 irradiances consistent with CERES-derived top-of-atmosphere shortwave and longwave irradiances, *J. Clim.*, 26(9),
2858 2719–2740, doi:10.1175/JCLI-D-12-00436.1, 2013.

2859 Keen, T. R., Kindle, J. C. and Young, D. K.: The interaction of southwest monsoon upwelling, advection and primary
2860 production in the northwest Arabian Sea, *J. Mar. Syst.*, doi:10.1016/S0924-7963(97)00003-1, 1997.

2861 Keerthi, M. G., Lengaigne, M., Drushka, K., Vialard, J., Montegut, C. D. B., Pous, S., Levy, M. and Muraleedharan, P.
2862 M.: Intraseasonal variability of mixed layer depth in the tropical Indian Ocean, *Clim. Dyn.*, 46(7–8), 2633–2655,
2863 doi:10.1007/s00382-015-2721-z, 2016.

2864 Kessler, W.S., M.J. McPhaden, and K.M. Weickmann: Forcing of intraseasonal Kelvin Waves in the equatorial Pacific.
2865 J. Geophys. Res., 100, 10,613–10,631, 1995.

2866 Kido, S., and Tozuka, T.: Salinity Variability Associated with the Positive Indian Ocean Dipole and Its Impact on the
2867 Upper Ocean Temperature. Journal of Climate, 30(19), 7885-7907, 2017.

2868 Kim, H. S., Flagg, C. N. and Howden, S. D.: Northern Arabian Sea variability from TOPEX/Poseidon altimetry data: An
2869 extension of the US JGOFS/ONR shipboard ADCP study, Deep. Res. Part II Top. Stud. Oceanogr.,
2870 doi:10.1016/S0967-0645(00)00131-4, 2001.

2871 Kobashi, F., and Kubokawa, A.: Review on North Pacific Subtropical Countercurrents and Subtropical Fronts: role of
2872 mode waters in ocean circulation and climate, J. Oceanogr., 68, 21–43, <https://doi.org/10.1007/s10872-011-0083-7>,
2873 2012.

2874 Kosaka, Y. and Xie, SP: Recent global-warming hiatus tied to equatorial Pacific surface cooling. Nature 501, 403–407,
2875 <https://doi.org/10.1038/nature12534>, 2013.

2876 Kosaka, Y., Takaya, Y., Kamae, Y.: The Indo-western Pacific Ocean capacitor effect. In: Tropical and Extratropical Air-
2877 Sea Interactions, 141-169, 2021.

2878 Koslow, J. A., Pesant, S., Feng, M., Pearce, A., Fearn, P., Moore, T., Matear, R. and Waite, A.: The effect of the
2879 Leeuwin Current on phytoplankton biomass and production off Southwestern Australia, J. Geophys. Res. Ocean.,
2880 doi:10.1029/2007JC004102, 2008.

2881 Krishnamohan, K. S., Vialard, J., Lengaigne, M., Masson, S., Samson, G., Pous, S., Neetu, S., Durand, F., Shenoi, S. S.
2882 C. and Madec, G.: Is there an effect of Bay of Bengal salinity on the northern Indian Ocean climatological rainfall?,
2883 Deep Sea Res. Part II Top. Stud. Oceanogr., doi:10.1016/j.dsr.2019.04.003, 2019.

2884 Krishnamurthy, L., and Krishnamurthy, V.: Decadal and interannual variability of the Indian Ocean SST. Climate Dyn.,
2885 46, 57–70, 2016.

2886 Krug, M., & Tournadre, J. : Satellite observations of an annual cycle in the Agulhas Current. Geophysical Research
2887 Letters, 39, L15607. <https://doi.org/10.1029/2012GL052335>, 2012

2888 Kubokawa, A.: Ventilated thermocline strongly affected by a deep mixed layer: A theory for subtropical countercurrent.
2889 J. Phys. Oceanogr., 29, 1314–1333, [https://doi.org/10.1175/1520-0485\(1999\)029<1314:VTSABA>2.0.CO;2](https://doi.org/10.1175/1520-0485(1999)029<1314:VTSABA>2.0.CO;2), 1999.

2890 Kubokawa, A. and Inui, T.: Subtropical countercurrent in an idealized ocean GCM. J. Phys. Oceanogr., 29, 1303–1313,
2891 [https://doi.org/10.1175/1520-0485\(1999\)029<1303:SCIAIO>2.0.CO;2](https://doi.org/10.1175/1520-0485(1999)029<1303:SCIAIO>2.0.CO;2), 1999.

2892 Kumar, S.P., Madhupratap, M., Dileep Kumar, M., Gauns, M., Muraleedharan, P. M., Sarma, V. V. S. S. and De Souza,
2893 S. N.: Physical control of primary productivity on a seasonal scale in central and eastern Arabian Sea, Proc. Indian
2894 Acad. Sci. Earth Planet. Sci., doi:10.1007/bf02708331, 2000.

2895 Kumar, S.P., Muraleedharan, P. M., Prasad, T. G., Gauns, M., Ramaiah, N., De Souza, S. N., Sardesai, S. and
2896 Madhupratap, M.: Why is the Bay of Bengal less productive during summer monsoon compared to the Arabian Sea?,
2897 Geophys. Res. Lett., doi:10.1029/2002GL016013, 2002.

2898 Kumar, S. P., Nuncio, M., Narvekar, J., Kumar, A., Sardesai, S., De Souza, S. N., Gauns, M., Ramaiah, N. and
2899 Madhupratap, M.: Are eddies nature’s trigger to enhance biological productivity in the Bay of Bengal?, Geophys. Res.
2900 Lett., doi:10.1029/2003GL019274, 2004.

2901 Kumar, S.P., Nuncio, M., Ramaiah, N., Sardesai, S., Narvekar, J., Fernandes, V. and Paul, J. T.: Eddy-mediated
2902 biological productivity in the Bay of Bengal during fall and spring intermonsoons, Deep. Res. Part I Oceanogr. Res.
2903 Pap., doi:10.1016/j.dsr.2007.06.002, 2007.

2904 Kumar, P., Singh, A., Ramesh, R. and Nallathambi, T.: N₂ Fixation in the Eastern Arabian Sea: Probable Role of
2905 Heterotrophic Diazotrophs, Frontiers: Marine Science, 4, 80, 2017.

2906 Kundu, P. K. and McCreary, J. P.: On the dynamics of the throughflow from the Pacific into the Indian Ocean, J. Phys.
2907 Oceanogr., 16,2191–162198, [https://doi.org/10.1175/1520-0485\(1986\)016<2191:OTDOTT>2.0.CO;2](https://doi.org/10.1175/1520-0485(1986)016<2191:OTDOTT>2.0.CO;2), 1986.

2908 Lakshmi, R. S., Chatterjee, A., Prakash, S., and Mathew, T.: Biophysical interactions in driving the summer monsoon
2909 chlorophyll bloom off the Somalia coast. Journal of Geophysical Research: Oceans, 125,
2910 <https://doi.org/10.1029/2019JC015549>, 2020.

2911 Lambert, E., Le Bars, W., and de Ruijter, W. P. M.: The connection of the Indonesian Throughflow, South Indian Ocean
2912 Countercurrent and the Leeuwin Current, *Ocean Science*, 12(3), 771–780, <https://doi.org/10.5194/os-12-771-2016>,
2913 2016.

2914 Lamont, T., Barlow, R. G., Morris, T. and van den Berg, M. A.: Characterisation of mesoscale features and
2915 phytoplankton variability in the Mozambique Channel, *Deep. Res. Part II Top. Stud. Oceanogr.*,
2916 doi:10.1016/j.dsr2.2013.10.019, 2014.

2917 Lamont, T. and Barlow, R. G.: Environmental influence on phytoplankton production during summer on the KwaZulu-
2918 Natal shelf of the Agulhas ecosystem, *African J. Mar. Sci.*, doi:10.2989/1814232X.2015.1108228, 2015.

2919 Latasa, M. and Bidigare, R. R.: A comparison of phytoplankton populations of the Arabian Sea during the Spring
2920 Intermonsoon and Southwest Monsoon of 1995 as described by HPLC-analyzed pigments, *Deep. Res. Part II Top.*
2921 *Stud. Oceanogr.*, doi:10.1016/S0967-0645(98)00066-6, 1998.

2922 Laurindo, L. C., Mariano, A. J. and Lumpkin, R.: An improved near-surface velocity climatology for the global ocean
2923 from drifter observations, *Deep. Res. Part I Oceanogr. Res. Pap.*, doi:10.1016/j.dsr.2017.04.009, 2017.

2924 Le Bars, D., Dijkstra, H. A. and De Ruijter, W. P. M.: Impact of the Indonesian Throughflow on Agulhas leakage,
2925 *Ocean Sci.*, doi:10.5194/os-9-773-2013, 2013.

2926 Le Bars, D., Durgadoo, J. V., Dijkstra, H. A., Biastoch, A. and De Ruijter, W. P. M.: An observed 20-year time series of
2927 Agulhas leakage, *Ocean Sci.*, doi:10.5194/os-10-601-2014, 2014.

2928 Lee, C. M., Jones, B. H., Brink, K. H. and Fischer, A. S.: The upper-ocean response to monsoonal forcing in the Arabian
2929 Sea: Seasonal and spatial variability, *Deep. Res. Part II Top. Stud. Oceanogr.*, doi:10.1016/S0967-0645(99)00141-1,
2930 2000.

2931 Lee, C. M., Jinadasa, S. U. P., Anutaliya, A., Centurioni, L. R., Fernando, H. J. S., Hormann, V., Lankhorst, M.,
2932 Rainville, L., Send, U. and Wijesekera, H. W.: Collaborative observations of boundary currents, water mass
2933 variability, and monsoon response in the southern Bay of Bengal, *Oceanography*, doi:10.5670/oceanog.2016.43, 2016.

2934 Lee, J. Y., Wang, B., Wheeler, M. C., Fu, X., Waliser, D. E. and Kang, I. S.: Real-time multivariate indices for the
2935 boreal summer intraseasonal oscillation over the Asian summer monsoon region, *Clim. Dyn.*, 40(1–2), 493–509,
2936 doi:10.1007/s00382-012-1544-4, 2013.

2937 Lee, S. K., Park, W., Baringer, M. O., Gordon, A. L., Huber, B. and Liu, Y.: Pacific origin of the abrupt increase in
2938 Indian Ocean heat content during the warming hiatus, *Nat. Geosci.*, doi:10.1038/NGEO2438, 2015.

2939 Lee, T.: Decadal weakening of the shallow overturning circulation in the South Indian Ocean, *Geophys. Res. Lett.*,
2940 doi:10.1029/2004GL020884, 2004.

2941 Lee, T., Fournier, S., Gordon, A. L. and Sprintall, J.: Maritime Continent water cycle regulates low-latitude chokepoint
2942 of global ocean circulation, *Nat. Commun.*, doi:10.1038/s41467-019-10109-z, 2019.

2943 Legeckis, R., and Cresswell, G.: Satellite observations of sea-surface temperature fronts off the coast of western and
2944 southern Australia, *Deep Sea Res. I*, 28, 297–306, [https://doi.org/10.1016/0198-0149\(81\)90069-8](https://doi.org/10.1016/0198-0149(81)90069-8), 1981.

2945 Lewandowsky, S., Cowtan, K., Risbey, S., Mann, M., Steinman, B., Oreskes, N. and Rahmstorf, S.: The ‘pause’ in
2946 global warming in historical context: (II). Comparing models to observations. *Environmental Research Letters*, 13
2947 (12): 123007 DOI: 10.1088/1748-9326/aaf372, 2018.

2948 L’Heureux, M. L., Lee, S. Lyon, B.: Recent multidecadal strengthening of the Walker circulation across the tropical
2949 Pacific. *Nat. Clim. Cha.*, 3, 571–576, 2013.

2950 Li, G., Xie, S., Du, Y. A robust but spurious pattern of climate change in model projections over the tropical Indian
2951 Ocean, *J. Clim.*, 29, 5589–5608, 2016.

2952 Li, Y., Han, W., Ravichandran, M., Wang, W., Shinoda, T. and Lee, T.: Bay of Bengal salinity stratification and Indian
2953 summer monsoon intraseasonal oscillation: 1. Intraseasonal variability and causes, *J. Geophys. Res. Ocean.*,
2954 doi:10.1002/2017JC012691, 2017a.

2955 Li, Y., Han, W., Wang, W., Ravichandran, M., Lee, T. and Shinoda, T.: Bay of Bengal salinity stratification and Indian
2956 summer monsoon intraseasonal oscillation: 2. Impact on SST and convection, *J. Geophys. Res. Ocean.*, 122(5), 4312–
2957 4328, doi:10.1002/2017JC012692, 2017b.

2958 Li, Y., Han, W., Wang, W., Zhang, L. and Ravichandran, M.: The Indian summer monsoon intraseasonal oscillations in
2959 CFSv2 forecasts: Biases and importance of improving air-sea interaction processes, *J. Clim.*, 31(14), 5351–5370,
2960 doi:10.1175/JCLI-D-17-0623.1, 2018a.

2961 Li, Y., Han, W., Hu, A., Meehl, G. A. and Wang, F.: Multidecadal changes of the upper Indian ocean heat content
2962 during 1965-2016, *J. Clim.*, doi:10.1175/JCLI-D-18-0116.1, 2018b.

2963 Liu, Q.-Y., Feng, M., Wang, D., and Wijffels, S.: Interannual variability of the Indonesian Throughflow transport: A
2964 revisit based on 30 year expendable bathythermograph data, *J. Geophys. Res.: Oceans*, 120(12), 8270-8282,
2965 <https://doi.org/10.1002/2015JC011351>, 2015.

2966 Llovel, W. and Lee, T.: Importance and origin of halosteric contribution to sea level change in the southeast Indian
2967 Ocean during 2005-2013, *Geophys. Res. Lett.*, doi:10.1002/2014GL062611, 2015.

2968 Longhurst, A.: A major seasonal phytoplankton bloom in the Madagascar Basin, *Deep. Res. Part I Oceanogr. Res. Pap.*,
2969 doi:10.1016/S0967-0637(01)00024-3, 2001.

2970 Lotliker, A. A., Omand, M. M., Lucas, A. J., Laney, S. R., Mahadevan, A. and Ravichandran, M.: Penetrative radiative
2971 flux in the Bay of Bengal, *Oceanography*, doi:10.5670/oceanog.2016.53, 2016.

2972 Lourey, M. J., Dunn, J. R. and Waring, J.: A mixed-layer nutrient climatology of Leeuwin Current and Western
2973 Australian shelf waters: Seasonal nutrient dynamics and biomass, *J. Mar. Syst.*, doi:10.1016/j.jmarsys.2005.10.001,
2974 2006.

2975 Lourey, M. J., Thompson, P. A., McLaughlin, M. J., Bonham, P. and Feng, M.: Primary production and phytoplankton
2976 community structure during a winter shelf-scale phytoplankton bloom off Western Australia, *Mar. Biol.*,
2977 doi:10.1007/s00227-012-2093-4, 2013.

2978 Loveday, B. R., Durgadoo, J. V., Reason, C. J. C., Biastoch, A. and Penven, P.: Decoupling of the Agulhas leakage from
2979 the Agulhas Current, *J. Phys. Oceanogr.*, doi:10.1175/JPO-D-13-093.1, 2014.

2980 Lu, B., and Ren, H. L.: What caused the extreme Indian Ocean Dipole event in 2019? *Geophys. Res. Lett.*,
2981 doi:10.1029/2020GL087768, 2020.

2982 Lübbecke, J. F., Durgadoo, J. V. and Biastoch, A.: Contribution of increased agulhas leakage to tropical Atlantic
2983 warming, *J. Clim.*, doi:10.1175/JCLI-D-15-0258.1, 2015.

2984 Lucas, A., Nash, J., Pinkel, R., MacKinnon, J., Tandon, A., Mahadevan, A., Omand, M., Freilich, M., Sengupta, D.,
2985 Ravichandran, M. and Le Boyer, A.: Adrift Upon a Salinity-Stratified Sea: A view of upper-ocean processes in the
2986 Bay of Bengal during the Southwest Monsoon, *Oceanography*, doi:10.5670/oceanog.2016.46, 2016.

2987 Luis, A. J. and Kawamura, H.: Air-sea interaction, coastal circulation and primary production in the eastern Arabian Sea:
2988 A review, *J. Oceanogr.*, 60, 205-18, doi:10.1023/B:JOCE.0000038327.33559.34, 2004.

2989 Lumpkin, R., and Speer, K.: Global ocean meridional overturning. *J. Phys. Oceanogr.*, 37, 2550–2562,
2990 doi:10.1175/JPO3130.1, 2007.

2991 Lutjeharms, J. R. E.: *The Agulhas Current*, Springer: Berlin, Heidelberg, New York, 2006.

2992 Lutjeharms, J. R. E., Meyer, A. A., Anson, I. J., Eagle, G. A. and Orren, M. J.: The nutrient characteristics of the
2993 Agulhas bank, *South African J. Mar. Sci.*, doi:10.2989/025776196784158464, 1996.

2994 Lutjeharms, J. R. E. and Machu, E.: An upwelling cell inshore of the East Madagascar Current, *Deep. Res. Part I*
2995 *Oceanogr. Res. Pap.*, doi:10.1016/S0967-0637(00)00026-1, 2000.

2996 Ma, J., Feng, M., Sloyan, B. M. and Lan, J.: Pacific influences on the meridional temperature transport of the Indian
2997 Ocean, *J. Clim.*, doi:10.1175/JCLI-D-18-0349.1, 2019.

2998 Macdonald, A. M., Mecking, S., Robbins, P. E., Toole, J. M., Johnson, G. C., Talley, L. D., Cook, M., Wijffels, S., E.:
2999 The WOCE-era 3-D Pacific Ocean Circulation and Heat Budget. *Progress in Oceanography*, 48, 281-325, 2009.

3000 Machu, E. and Garçon, V.: Phytoplankton seasonal distribution from sea WiFS data in the Agulhas current system, *J.*
3001 *Mar. Res.*, doi:10.1357/002224001762674944, 2001.

3002 MacKinnon, J. A., Johnston, T. M. S. and Pinkel, R.: Strong transport and mixing of deep water through the Southwest
3003 Indian Ridge, *Nat. Geosci.*, doi:10.1038/ngeo340, 2008.

3004 Madden, R. A. and Julian, P. R.: Description of Global-Scale Circulation Cells in the Tropics with a 40–50 Day Period,
3005 *J. Atmos. Sci.*, doi:10.1175/1520-0469(1972)029<1109:dogsc>2.0.co;2, 1972.

3006 Madden, R. A. and Julian, P. R.: Detection of a 40–50 Day Oscillation in the Zonal Wind in the Tropical Pacific, *J.*
3007 *Atmos. Sci.*, 28(5), 702–708, doi:10.1175/1520-0469(1971)028<0702:DOADOI>2.0.CO;2, 1971.

3008 Madhupratap, M., Gauns, M., Ramaiah, N., Prasanna Kumar, S., Muraleedharan, P. M., De Sousa, S. N., Sardessai, S.
3009 and Muraleedharan, U.: Biogeochemistry of the Bay of Bengal: Physical, chemical and primary productivity
3010 characteristics of the central and western Bay of Bengal during summer monsoon 2001, *Deep. Res. Part II Top. Stud.*
3011 *Oceanogr.*, doi:10.1016/S0967-0645(02)00611-2, 2003.

3012 Maes, C., Grima, N., Blanke, B., Martinez, E., Paviet-Salomon, T. and Huck, T.: A Surface “Superconvergence”
3013 Pathway Connecting the South Indian Ocean to the Subtropical South Pacific Gyre, *Geophys. Res. Lett.*,
3014 doi:10.1002/2017GL076366, 2018.

3015 Mahadevan, A.: Eddy effects on biogeochemistry, *Nature*, doi:10.1038/nature13048, 2014.

3016 Mahadevan, A., D’Asaro, E., Lee, C. and Perry, M. J.: Eddy-driven stratification initiates North Atlantic spring
3017 phytoplankton blooms, *Science (80-.)*, doi:10.1126/science.1218740, 2012.

3018 Mahadevan, A., Paluszkievicz, T., Ravichandran, M., Sengupta, D. and Tandon, A.: Introduction to the Special Issue on
3019 the Bay of Bengal: From Monsoons to Mixing, *Oceanography*, doi:10.5670/oceanog.2016.34, 2016a.

3020 Mahadevan, A., Spiro Jaeger, G., Freilich, M., Omand, M., Shroyer, E. and Sengupta, D.: Freshwater in the Bay of
3021 Bengal: Its Fate and Role in Air-Sea Heat Exchange, *Oceanography*, 29(2), 72–81, doi:10.5670/oceanog.2016.40,
3022 2016b.

3023 Maher, N., England, M.H., Gupta, A.S. et al.: Role of Pacific trade winds in driving ocean temperatures during the
3024 recent slowdown and projections under a wind trend reversal. *Clim Dyn* 51, 321–336, [https://doi.org/10.1007/s00382-](https://doi.org/10.1007/s00382-017-3923-3)
3025 [017-3923-3](https://doi.org/10.1007/s00382-017-3923-3), 2018.

3026 Manatsa, D. and Behera, S. K.: On the epochal strengthening in the relationship between rainfall of East Africa and IOD,
3027 *J. Clim.*, 26, 5655-5673, doi:10.1175/JCLI-D-12-00568.1, 2013.

3028 Manghnani, V., Morrison, J. M., Hopkins, T. S. and Böhm, E.: Advection of upwelled waters in the form of plumes off
3029 Oman during the Southwest Monsoon, *Deep. Res. Part II Top. Stud. Oceanogr.*, doi:10.1016/S0967-0645(98)00062-9,
3030 1998.

3031 Mantyla, A. W. and Reid, J. L.: On the origins of deep and bottom waters of the Indian Ocean, *J. Geophys. Res.*,
3032 doi:10.1029/94JC02564, 1995.

3033 Marra, J., Dickey, T. D., Ho, C., Kinkade, C. S., Sigurdson, D. E., Weller, R. A. and Barber, R. T.: Variability in
3034 primary production as observed from moored sensors in the central Arabian Sea in 1995, *Deep. Res. Part II Top. Stud.*
3035 *Oceanogr.*, doi:10.1016/S0967-0645(98)00070-8, 1998.

3036 Marsac, F. and Blanc, J.: Oceanographic changes during the 1997-1998 El Niño in the Indian Ocean and their impact on
3037 the purse seine fishery, *IOTC Proc. no. 2*, 1999.

3038 Marin, M., and Feng, M.: Intra-annual variability of the North West Shelf of Australia and its impact on the Holloway
3039 Current: Excitement and propagation of coastally trapped waves, *Cont. Shelf Res.*,
3040 <https://doi.org/10.1016/j.csr.2019.08.001>, 2019.

3041 Marin, M., Feng, M., Phillips, H. E., and Bindoff, N. L.: A global, multiproduct analysis of coastal marine heatwaves:
3042 distribution, characteristics, and long-term trends. *J. Geophys. Res. Oceans*, 126,
3043 <http://dx.doi.org/10.1029/2020JC016708>, 2021.

3044 Marshall, A.G. and Hendon, H. H.: Impacts of the MJO in the Indian Ocean and on the Western Australian coast.
3045 *Climate Dyn.*, 42(3–4), 579–595, <https://doi.org/10.1007/s00382-012-1643-2>, 2014.

3046 Marshall, A. G., Hendon, H. H., Feng, M., and Schiller, A.: Initiation and amplification of the Ningaloo Niño, *Climate*
3047 *Dyn.*, 45, 2367–2385, <https://doi.org/10.1007/s00382-015-2477-5>, 2015.

3048 Martin, A. P. and Richards, K. J.: Mechanisms for vertical nutrient transport within a North Atlantic mesoscale eddy,
3049 *Deep. Res. Part II Top. Stud. Oceanogr.*, doi:10.1016/S0967-0645(00)00096-5, 2001.

3050 Masumoto, Y. and Meyers, G.: Forced Rossby waves in the southern tropical Indian Ocean, *J. Geophys. Res. Ocean.*,
3051 doi:10.1029/98JC02546, 1998.

3052 Masumoto, Y., Hase, H., Kuroda, Y., Matsuura, H. and Takeuchi, K.: Intraseasonal variability in the upper layer
3053 currents observed in the eastern equatorial Indian Ocean, *Geophys. Res. Lett.*, doi:10.1029/2004GL021896, 2005.

3054 Matthews, A. J., Singhruck, P. and Heywood, K. J.: Deep ocean impact of a Madden-Julian oscillation observed by Argo
3055 floats, *Science*, 318(5857), 1765–1769, doi: 10.1126/science.1147312, 2007.

3056 Maximenko, N., Niiler, P., Centurioni, L., Rio, M.-H., Melnichenko, O., Chambers, D., Zlotnicki, V., Galperin, B.:
3057 Mean dynamic topography of the ocean derived from satellite and drifting buoy data using three different techniques,
3058 *J. Atmos. Oceanic Technol.* 26 (9), 1910–1919, <https://doi.org/10.1175/2009JTECHO672.1>, 2009.

3059 Mayer, M., Alonso Balmaseda, M. and Haimberger, L.: Unprecedented 2015/2016 Indo-Pacific Heat Transfer Speeds
3060 Up Tropical Pacific Heat Recharge, *Geophys. Res. Lett.*, doi:10.1002/2018GL077106, 2018.

3061 Mccave, I. N., Kiefer, T., Thornalley, D. J. R. and Elderfield, H.: Deep flow in the Madagascar-Mascarene Basin over
3062 the last 150 000 years, *Philos. Trans. R. Soc. A: Math. Phys. Eng. Sci.*, doi:10.1098/rsta.2004.1480, 2005.

3063 McCreary, J.P.: Equatorial beams. *J. Mar. Res.*, 42(2), 395–430, <https://doi.org/10.1357/002224084788502792>, 1984.

3064 McCreary, J. P., Fukamachi, Y., and Lu, P.: A nonlinear mechanism for maintaining coastally trapped eastern boundary
3065 currents, *J. Geophys. Res.*, 97 (C4), 5677–5692, <https://doi.org/10.1029/92JC00035>, 1992.

3066 McCreary, J.P., Kundu, P. K. and Molinari, R. L.: A numerical investigation of dynamics, thermodynamics, and mixed
3067 layer processes in the Indian Ocean, *Prog. Oceanogr.*, 31, 181-224, 1993.

3068 McCreary, J. P., Han, W., Shankar, D. and Shetye, S. R.: Dynamics of the East India Coastal Current 2. Numerical
3069 solutions; *J. Geophys. Res.*, 101, 13993–14010, 1996.

3070 McCreary, J. P., Shetye, S. R., and Kundu, P. K.: Thermohaline forcing of eastern boundary currents: With application
3071 to the circulation off the west coast of Australia, *J. Mar. Res.*, 44, 71–92,
3072 <https://doi.org/10.1357/002224086788460184>, 1986.

3073 McCreary, J. P., Kohler, K. E., Hood, R. R., Smith, S., Kindle, J., Fischer, A. S. and Weller, R. A.: Influences of diurnal
3074 and intraseasonal forcing on mixed-layer and biological variability in the central Arabian Sea, *J. Geophys. Res.*
3075 *Ocean.*, doi:10.1029/2000jc900156, 2001.

3076 McCreary, J.P., Murtugudde, R., Vialard, J., Vinayachandran, P.N., Wiggert, J.D., Hood, R.R., Shankar, D. and Shetye,
3077 S.: Biophysical Processes in the Indian Ocean. In *Indian Ocean Biogeochemical Processes and Ecological Variability*
3078 (eds J.D. Wiggert, R.R. Hood, S.A. Naqvi, K.H. Brink and S.L. Smith). <https://doi.org/10.1029/2008GM000768>,
3079 2009.

3080 McCreary, J. P., Yu, Z., Hood, R. R., Vinayachandran P. N., Furue, R., Ishida, A., Richards, K. J.: Dynamics of the
3081 Indian-Ocean oxygen minimum zones, *Prog. Oceanogr*, 112, 15–37, 2013.

3082 McDonagh, E. L., Bryden, H. L., King, B. A. & Sanders, R. J. The circulation of the Indian Ocean at 32°S. *Prog*
3083 *Oceanogr* 79, 20–36, 2008.

3084 McGillicuddy, D. J., Anderson, L. A., Bates, N. R., Bibby, T., Buesseler, K. O., Carlson, C. A., Davis, C. S., Ewart, C.,
3085 Falkowski, P. G., Goldthwait, S. A., Hansell, D. A., Jenkins, W. J., Johnson, R., Kosnyrev, V. K., Ledwell, J. R., Li,
3086 Q. P., Siegel, D. A. and Steinberg, D. K.: Eddy/Wind interactions stimulate extraordinary mid-ocean plankton blooms,
3087 *Science* (80-), doi:10.1126/science.1136256, 2007.

3088 McPhaden, M.J.: Genesis and evolution of the 1997-98 El Niño. *Science*, 283, 950-954, 1999.

3089 McPhaden, M. J., Meyers, G., Ando, K., Masumoto, Y., Murty, V. S. N., Ravichandran, M., Syamsudin, F., Vialard, J.,
3090 Yu, L., & Yu, W. : RAMA: The Research Moored Array for African–Asian–Australian Monsoon Analysis and

3091 Prediction, *Bulletin of the American Meteorological Society*, 90(4), 459–480.
3092 https://journals.ametsoc.org/view/journals/bams/90/4/2008bams2608_1.xml, 2009.

3093 McPhaden, M. J. and Foltz, G. R.: Intraseasonal variations in the surface layer heat balance of the central equatorial
3094 Indian Ocean: The importance of zonal advection and vertical mixing, *Geophys. Res. Lett.*, 40(11), 2737–2741,
3095 <https://doi.org/10.1002/grl.50536>, 2013.

3096 McPhaden, M. J. and M. Nagura: Indian Ocean Dipole interpreted in terms of Recharge Oscillator theory. *Clim. Dyn.*,
3097 42, 1569–1586. doi 10.1007/s00382-013-1765-1, 2014.

3098 McPhaden, M. J., Wang, Y. and Ravichandran, M.: Volume transports of the Wyrтки jets and their relationship to the
3099 Indian Ocean dipole, *J. Geophys. Res. Oceans*, 120(8), 5302–5317, 2015.

3100 Menezes, V. V., Phillips, H.E., Schiller, A., Domingues, C.M., and Bindoff, N.L.: Salinity dominance on the Indian
3101 Ocean Eastern Gyral current, *Geophys. Res. Lett.*, 40, 5716–5721, <https://doi.org/10.1002/2013GL057887>, 2013.

3102 Menezes, V. V., Phillips, H. E., Schiller, A., Bindoff, N. L., Domingues, C. M., and Vianna, M. L.: South Indian
3103 Countercurrent and associated fronts, *J. Geophys. Res. Oceans*, 119, 6763–6791,
3104 <https://doi.org/10.1002/2014JC010076>, 2014.

3105 Menezes, V. V.: The structure and dynamics of the eastward flows of the South Indian Ocean, PhD Thesis, University of
3106 Tasmania, 244pp, <http://eprints.utas.edu.au/23392/>, 2015.

3107 Menezes, V. V., Phillips, H. E., Vianna, M. L., and Bindoff, N. L.: Interannual variability of the South Indian
3108 Countercurrent, *J. Geophys. Res. Oceans*, 121, 3465–3487, <https://doi.org/10.1002/2015JC011417>, 2016.

3109 Merle, J., Rotschi, H., and Voituriez, B.: Zonal circulation in the tropical western South Pacific at 170°E. *Bull. Japan*
3110 *Soc. Fish. Oceanogr.*, Special Issue (Prof. Uda’s Commemorative Papers), 91–98, 1969.

3111 Meuleners, M.J., Pattiaratchi, C.B., and Ivey, G.N.: Numerical modelling of the mean flow characteristics of the
3112 Leeuwin Current System, *Deep Sea Res. II*, 54(8–10), 837–858, <https://doi.org/10.1016/j.dsr2.2007.02.003>, 2007.

3113 Meuleners, M.J., Ivey, G.N., and Pattiaratchi, C.B.: A numerical study of the eddying characteristics of the Leeuwin
3114 Current System, *Deep Sea Res. I*, 55(3), 261–276, <https://doi.org/10.1016/j.dsr.2007.12.004>, 2008.

3115 Meyers, G., R. J. Bailey, , and A. P. Worby, 1995: Geostrophic transport of Indonesian Throughflow. *Deep-Sea Res. I*,
3116 42, 1163–1174.

3117 Meyers, G.: Variation of Indonesian throughflow and the El Niño Southern Oscillation, *J. Geophys. Res.*, 101, C5,
3118 12255–12263, <https://doi.org/10.1029/95JC03729>, 1996.

3119 Miyama, T., McCreary, J.P., Jensen, T.G., Loschnigg, J.L., Godfrey, S., and Ishida, A.: Structure and dynamics of the
3120 Indian-Ocean cross-equatorial cell, *Deep Sea Res. II*, 50, 2023–2047, [https://doi.org/10.1016/S0967-0645\(03\)00044-4](https://doi.org/10.1016/S0967-0645(03)00044-4),
3121 2003.

3122 Miyama, T., McCreary, J.P. Sengupta, D., and Senan, R.: Dynamics of biweekly oscillations in the equatorial Indian
3123 Ocean, *J. Phys. Oceanogr.*, 36, 827–846, <https://doi.org/10.1175/JPO2897.1>, 2006.

3124 Moore, T. S., Matear, R. J., Marra, J. and Clementson, L.: Phytoplankton variability off the Western Australian Coast:
3125 Mesoscale eddies and their role in cross-shelf exchange, *Deep. Res. Part II Top. Stud. Oceanogr.*,
3126 doi:10.1016/j.dsr2.2007.02.006, 2007.

3127 Morel, A. and Antoine, D.: Heating Rate within the Upper Ocean in Relation to its Bio–optical State, *J. Phys. Oceanogr.*,
3128 24(7), 1652–1665, doi:10.1175/1520-0485(1994)024<1652:HRWTUO>2.0.CO;2, 1994.

3129 Morioka, Y., Tozuka, T. and Yamagata, T.: Climate variability in the southern Indian Ocean as revealed by self-
3130 organizing maps, *Clim. Dyn.*, doi:10.1007/s00382-010-0843-x, 2010.

3131 Morioka, Y., Tozuka, T., Masson, S., Terray, P., Luo, J. J. and Yamagata, T.: Subtropical dipole modes simulated in a
3132 coupled general circulation model, *J. Clim.*, doi:10.1175/JCLI-D-11-00396.1, 2012.

3133 Moum, J. N. and Nash, J. D.: Mixing Measurements on an Equatorial Ocean Mooring, *J. Atmos. Ocean. Technol.*,
3134 doi:10.1175/2008jtecho617.1, 2009.

3135 Moum, J. N., de Szoek, S. P., Smyth, W. D., Edson, J. B., DeWitt, H. L., Moulin, A. J., Thompson, E. J., Zappa, C. J.,
3136 Rutledge, S. A., Johnson, R. H. and Fairall, C. W.: Air–Sea Interactions from Westerly Wind Bursts During the
3137 November 2011 MJO in the Indian Ocean, *Bull. Am. Meteorol. Soc.*, 95(8), 1185–1199, doi:10.1175/BAMS-D-12-
3138 00225.1, 2014.

3139 Moum, J. N., Pujiana, K., Lien, R. C. and Smyth, W. D.: Ocean feedback to pulses of the Madden-Julian Oscillation in
3140 the equatorial Indian Ocean, *Nat. Commun.*, 7(May), 1–7, doi:10.1038/ncomms13203, 2016.

3141 Mukherjee, A., Shankar, D., Fernando, V. *et al.* Observed seasonal and intraseasonal variability of the East India Coastal
3142 Current on the continental slope. *J Earth Syst Sci* 123, 1197–1232 , <https://doi.org/10.1007/s12040-014-0471-7>, 2014.

3143 Mukherjee, A., Shankar, D., Chatterjee, A. and Vinayachandran, P. N.: Numerical simulation of the observed near
3144 surface East India Coastal Current on the continental slope, *Clim. Dyn.*, 50, 3949–3980,
3145 <https://doi.org/10.1007/s00382-017-3856-x>, 2018.

3146 Mukhopadhyay, S. Shankar, D., Aparna, S.G., Mukherjee, A., Fernando, V., Kankonkar, A., Khalap, S. T., Satelkar,
3147 N.P., Gaonkar, M.G., Tari, A.P., Khedekar, R.R., Ghatkar, S.: Observed variability of the East India Coastal Current
3148 on the continental slope during 2009–2018. *J. Earth Syst. Sci.*, 129, p. 77, 10.1007/s12040-020-1346-8, 2020.

3149 Mulholland, M. R., Bernhardt, P. W., Ozmon, I., Procise, L. A., Garrett, M., O’Neil, J. M., Heil, C. A. and Bronk, D. A.:
3150 Contribution of diazotrophy to nitrogen inputs supporting *Karenia brevis* blooms in the Gulf of Mexico, *Harmful*
3151 *Algae*, doi:10.1016/j.hal.2014.04.004, 2014.

3152 Muralledharan, K. R., Jasmine, P., Achuthankutty, C. T., Revichandran, C., Dinesh Kumar, P. K., Anand, P. and
3153 Rejomon, G.: Influence of basin-scale and mesoscale physical processes on biological productivity in the Bay of
3154 Bengal during the summer monsoon, *Prog. Oceanogr.*, doi:10.1016/j.pocean.2006.09.012, 2007.

3155 Murtugudde, R. and Busalacchi, A. J.: Interannual variability of the dynamics and thermodynamics of the tropical Indian
3156 Ocean, *J. Clim.*, doi:10.1175/1520-0442(1999)012<2300:ivotda>2.0.co;2, 1999.

3157 Murtugudde, R., McCreary, J. P. and Busalacchi, A. J.: Oceanic processes associated with anomalous events in the
3158 Indian Ocean with relevance to 1997-1998, *J. Geophys. Res. Ocean.*, 105(C2), 3295–3306,
3159 doi:10.1029/1999JC900294, 2000.

3160 Murtugudde, R., Beauchamp, J., McClain, C. R., Lewis, M. and Busalacchi, A. J.: Effects of penetrative radiation of the
3161 upper tropical ocean circulation, *J. Clim.*, 15(5), 470–486, doi:10.1175/1520-
3162 0442(2002)015<0470:EOPROT>2.0.CO;2, 2002.

3163 Murty, V. S. N., Gupta, G. V. M., Sarma, V. V., Rao, B. P., Jyothi, D., Shastri, P. N. M. and Supraveena, Y.: Effect of
3164 vertical stability and circulation on the depth of the chlorophyll maximum in the Bay of Bengal during May-June,
3165 1996, *Deep. Res. Part I Oceanogr. Res. Pap.*, doi:10.1016/S0967-0637(99)00071-0, 2000.

3166 Nagura, M. and McPhaden, M. J.: Wyrтки jet dynamics: Seasonal variability, *J. Geophys. Res. Oceans*, 115(C7), 1–17,
3167 2010a.

3168 Nagura, M. and McPhaden, M. J.: Dynamics of zonal current variations associated with the Indian Ocean dipole, *J.*
3169 *Geophys. Res. Oceans*, 115 (C11), 1–12, 2010b.

3170 Nagura, M. and McPhaden, M. J.: The dynamics of wind-driven intraseasonal variability in the equatorial Indian Ocean,
3171 *J. Geophys. Res. Oceans*, 117(2), 1–16, doi: 10.1029/2011JC007405, 2012.

3172 Nagura, M. and M. J. McPhaden: Zonal momentum budget along the equator in the Indian Ocean from a high resolution
3173 ocean general circulation model. *J. Geophys. Res.*, 119, 4444-4461, doi:10.1002/2014JC009895, 2014.

3174 Nagura, M. and McPhaden, M. J.: Zonal Propagation of Near-Surface Zonal Currents in Relation to Surface Wind
3175 Forcing in the Equatorial Indian Ocean, *J. Phys. Ocean.*, 46, 3623–3638, doi: 10.1175/JPO-D-16-0157.1, 2016.

3176 Nagura, M. & McPhaden, M. J. The Shallow Overturning Circulation in the Indian Ocean. *J. Phys. Oceanogr.* 48, 413–
3177 434, 2018.

3178 Nagura, M., & McPhaden, M. J.: Interannual variability in sea surface height at Southern midlatitudes of the Indian
3179 Ocean, *J. Phys. Oceanog.*, 51, 1595-1609, 2021.

3180 Naqvi, S. W. A., Jayakumar, D. A., Narvekar, P. V., Naik, H., Sarma, V. V. S. S., D'Souza, W., Joseph, S. and George,
3181 M. D.: Increased marine production of N₂O due to intensifying anoxia on the Indian continental shelf, *Nature*,
3182 doi:10.1038/35042551, 2000.

3183 Naqvi, S. W., Narvekar, P. V. and Desa, E.: Coastal biogeochemical processes in the North Indian Ocean (14, S-W), *The*
3184 *Sea*, 14, 723–780, 2006.

3185 Narayanasetti, S., Swapna, P., Ashok, K., Jadhav, J., and Krishnan, R.: Changes in biological productivity associated
3186 with Ningaloo Niño/Niña events in the southern subtropical Indian Ocean in recent decades, *Scientific Reports*, 6,
3187 27467, <https://doi.org/10.1038/srep27467>, 2016.

3188 Nethery, D., and Shankar, D.: Vertical propagation of baroclinic Kelvin waves along the west coast of India, *J. Earth.*
3189 *Syst. Sci.*, 116, 331–339, <https://doi.org/10.1007/s12040-007-0030-6>, 2007.

3190 Nicholson, S. E.: Long-term variability of the East African “short rains” and its links to large-scale factors. *Internat. J.*
3191 *Climatol.*, doi:10.1002/joc.4259, 2015.

3192 Nieves, V., Willis, J. K. and Patzert, W. C.: Recent hiatus caused by decadal shift in Indo-Pacific heating, *Science*,
3193 <https://doi.org/10.1126/science.aaa4521>, 2015.

3194 Niiler, P. P., Maximenko, N. A., and McWilliams, J. C.: Dynamically balanced absolute sea level of the global ocean
3195 derived from near-surface velocity observations, *Geophys. Res. Lett.*, 30, 2164,
3196 <https://doi.org/10.1029/2003GL018628>, 2003.

3197 Nof, D. and Olson, D. B.: How do western abyssal currents cross the equator?, *Deep. Res. Part I*, doi:10.1016/0967-
3198 0637(93)90002-K, 1993.

3199 Nyadjro, E. and M. J. McPhaden: Variability of zonal currents in the eastern equatorial Indian Ocean on seasonal to
3200 interannual time scales. *J. Geophys. Res.*, 119, 7969–7986, doi:10.1002/2014JC010380, 2014.

3201 O'Donoghue, S. H., Drapeau, L., Dudley, S. F. J. and Peddemors, V. M.: The KwaZulu-Natal sardine run: Shoal
3202 distribution in relation to nearshore environmental conditions, 1997–2007, *African J. Mar. Sci.*,
3203 doi:10.2989/1814232x.2010.501587, 2010.

3204 Ogata, T., and Masumoto, Y.: Interannual modulation and its dynamics of the mesoscale eddy variability in the
3205 southeastern tropical Indian Ocean, *J. Geophys. Res.*, 116, C05005, doi:10.1029/2010JC006490, 2011.

3206 Ogata, T., and Xie, S.-P.: Semiannual cycle in zonal wind over the equatorial Indian Ocean. *J. Climate*, 24, 6471–6485,
3207 doi:10.1175/2011JCLI4243.1, 2011.

3208 Oke, P. R., Griffin, D. A., Rykova, T., and de Oliveira, H. B.: Ocean circulation in the Great Australian Bight in an
3209 eddy-resolving ocean reanalysis: The eddy field, seasonal and interannual variability, *Deep Sea Res. II*, 157–158, 11–
3210 26, <https://doi.org/10.1016/j.dsr2.2018.09.012>, 2018.

3211 Oliver, E. C. J., and Thompson, K. R.: Madden-Julian oscillation and sea level: Local and remote forcing, *J. Geophys.*
3212 *Res. Ocean.*, 115(1), 1–15, <https://doi.org/10.1029/2009JC005337>, 2010.

3213 Oliver, E.C.J., Herzfeld, M., and Holbrook, N.J.: Modelling the shelf circulation off eastern Tasmania. *Continent. Shelf*
3214 *Res.*, 130, 14–33, 2016.

3215 Oliver, E. C., Donat, M. G., Burrows, M. T., Moore, P. J., Smale, D. A., Alexander, L. V., Benthuyssen, J. A., Feng, M.,
3216 Sen Gupta, A., Hobday, A. J., Holbrook, N. J., Perkins-Kirkpatrick, S. E., Scannell, H. A., Straub, S. C., and
3217 Wernberg, T.: Longer and more frequent marine heatwaves over the past century, *Nature Commun.*, 9, 1324,
3218 <https://doi.org/10.1038/s41467-018-03732-9>, 2018.

3219 Palastanga, V., van Leeuwen, P. J., Schouten, M. W., and de Ruijter, W. P. M.: Flow structure and variability in the
3220 subtropical Indian Ocean: instability of the South Indian Ocean Countercurrent, *J. Geophys. Res.*, 112, C01001,
3221 <https://doi.org/10.1029/2005JC003395>, 2007.

3222 Parab, S. G., Prabhu Matondkar, S. G., Gomes, H. do R. and Goes, J. I.: Monsoon driven changes in phytoplankton
3223 populations in the eastern Arabian Sea as revealed by microscopy and HPLC pigment analysis, *Cont. Shelf Res.*, 26
3224 (20), doi:10.1016/j.csr.2006.08.004, 2006.

3225 Paris, M. L., Subrahmanyam, B., Trott, C. B. and Murty, V. S. N.: Influence of ENSO Events on the Agulhas Leakage
3226 Region, *Remote Sens. Earth Syst. Sci.*, doi:10.1007/s41976-018-0007-z, 2018.

3227 Paterson, H. L., Feng, M., Waite, A. M., Gomis, D., Beckley, L. E., Holliday, D. and Thompson, P. A.: Physical and
3228 chemical signatures of a developing anticyclonic eddy in the Leeuwin Current, eastern Indian Ocean, *J. Geophys. Res.*
3229 *Ocean.*, doi:10.1029/2007JC004707, 2008.

3230 Paterson, J. S., Nayar, S., Mitchell, J. G. and Seuront, L.: Population-specific shifts in viral and microbial abundance
3231 within a cryptic upwelling, *J. Mar. Syst.*, doi:10.1016/j.jmarsys.2012.12.009, 2013.

3232 Pearce, A. F., and Griffiths, R.W.: The mesoscale structure of the Leeuwin Current: A comparison of laboratory model
3233 and satellite images, *J. Geophys. Res.*, 96, 16730–16757, <https://doi.org/10.1029/91JC01712>, 1991.

3234 Pearce, A. and Feng, M.: Observations of warming on the Western Australian continental shelf. *Marine Freshw. Res.*,
3235 58, 914–920, 2007.

3236 Pearce, A., Lenanton, R., Jackson, G., Moore, J., Feng, M., and Gaughan, D.: The “marine heat wave” off Western
3237 Australia during the summer of 2010/11, Fisheries Research Report No. 222, Department of Fisheries, Western
3238 Australia, 40pp, http://fish.wa.gov.au/Documents/research_reports/fr222.pdf, 2011.

3239 Peatman, S. C. and Klingaman, N. P.: The Indian summer monsoon in MetUM-GOML2.0: Effects of air-sea coupling
3240 and resolution, *Geosci. Model Dev.*, 11(11), 4693–4709, doi:10.5194/gmd-11-4693-2018, 2018.

3241 Philander, S. G. H., and Yoon, J.-H.: Eastern boundary currents and coastal upwelling, *J. Phys. Oceanogr.*, 12(8), 862–
3242 879, [https://doi.org/10.1175/1520-0485\(1982\)012<0862:EBCACU>2.0.CO;2](https://doi.org/10.1175/1520-0485(1982)012<0862:EBCACU>2.0.CO;2), 1982.

3243 Phillips, H.E., Wijffels, S.E. and Feng, M.: Interannual variability in the freshwater content of the Indonesian-Australian
3244 Basin. *Geophysical Research Letters*. Vol. 32, L03603, doi:10.1029/2004GL021755, 2005.

3245 Pirro, A., Fernando, H. J. S., Wijesekera, H. W., Jensen, T. G., Centurioni, L. R. and Jinadasa, S. U. P.: Eddies and
3246 currents in the Bay of Bengal during summer monsoons, *Deep. Res. Part II Top. Stud. Oceanogr.*,
3247 doi:10.1016/j.dsr2.2019.104728, 2020a.

3248 Pirro, A., Wijesekera, H. W., Jarosz, E. and Fernando, H. J. S.: Dynamics of intraseasonal oscillations in the Bay of
3249 Bengal during summer monsoons captured by mooring observations, *Deep. Res. Part II Top. Stud. Oceanogr.*,
3250 doi:10.1016/j.dsr2.2019.104718, 2020b.

3251 Poulton, A. J., Stinchcombe, M. C. and Quartly, G. D.: High numbers of Trichodesmium and diazotrophic diatoms in the
3252 southwest Indian Ocean, *Geophys. Res. Lett.*, doi:10.1029/2009GL039719, 2009.

3253 Prerna, S., Chatterjee, A., Mukherjee, A., Ravichandran, M. and Shenoi, S. S. C.: Wyrтки Jets: Role of intraseasonal
3254 forcing, *J. Earth Syst. Sci.*, doi:10.1007/s12040-018-1042-0, 2019.

3255 Probyn, T., Mitchellinnes, B., Brown, P., Hutchings, L. and Carter, R.: A review of primary production and related
3256 processes on the Agulhas Bank, *S. Afr. J. Sci.*, 1994.

3257 Pujiana, K., Gordon, A. L. and Sprintall, J.: Intraseasonal Kelvin wave in Makassar strait, *J. Geophys. Res. Ocean.*,
3258 doi:10.1002/jgrc.20069, 2013.

3259 Pujiana, K. and M.J. McPhaden: Ocean's response to the convectively coupled Kelvin waves in the eastern equatorial
3260 Indian Ocean. *J. Geophys. Res.*, 123, 5727- 5741. <https://doi.org/10.1029/2018JC013858>, 2018.

3261 Pujiana, K. and McPhaden, M. J.: Intraseasonal Kelvin Waves in the Equatorial Indian Ocean and Their Propagation
3262 into the Indonesian Seas, *J. Geophys. Res. Oceans*, 125(5), 1–18, doi: 10.1029/2019JC015839, 2020.

3263 Pujiana, K. and M. J. McPhaden: Biweekly mixed Rossby-Gravity waves in the equatorial Indian Ocean. *J. Geophys.*
3264 *Res.*, <https://doi.org/10.1029/2020JC016840>, 2021.

3265 Pujiana, K., M.J. McPhaden, A.L. Gordon, and A.M. Napitu, 2019: Unprecedented response of Indonesian throughflow
3266 to anomalous Indo-Pacific climatic forcing in 2016. *J. Geophys. Res.*, 124, 3737-3754.
3267 <https://doi.org/10.1029/2018JC014574>.

3268 Purkey, S. G., Johnson, G. C.: Warming of global abyssal and deep Southern Ocean waters between the 1990s and
3269 2000s: Contributions to global heat and sea level rise budgets. *J. Clim.* 23, 6336-6351. doi: 10.1175/2010JCLI3682.1,
3270 2010.

3271 Purkey, S. G. and Johnson, G. C.: Global contraction of Antarctic Bottom Water between the 1980s and 2000s, *J. Clim.*,
3272 doi:10.1175/JCLI-D-11-00612.1, 2012.

3273 Qiu, B., and Chen, S.: Seasonal modulations in the eddy field of the South Pacific Ocean, *J. Phys. Oceanogr.*, 34(7),
3274 1515–1527, [https://doi.org/10.1175/1520-0485\(2004\)034<1515:SMITEF>2.0.CO;2](https://doi.org/10.1175/1520-0485(2004)034<1515:SMITEF>2.0.CO;2), 2004.

3275 Qiu, Y., Li, L., and Yu, W.: Behavior of the Wyrтки jet observed with surface drifting buoys and satellite altimeter.
3276 *Geophys. Res. Lett.*, 36, L18607, <https://doi.org/10.1029/2009GL039120>, 2009.

3277 Qiu, Y., Han, W., Lin, X., West, J., Li, Y., Xing, W., Zhang, X., Arulananthan, K. and Guo, X.: Upper-ocean response
3278 to the super tropical cyclone Phailin (2013) over the freshwater region of the Bay of Bengal, *J. Phys. Oceanogr.*,
3279 doi:10.1175/JPO-D-18-0228.1, 2019.

3280 Qu, T., Fukumori, I. and Fine, R. A.: Spin-Up of the Southern Hemisphere Super Gyre, *J. Geophys. Res. Ocean.*,
3281 doi:10.1029/2018JC014391, 2019.

3282 Quadfasel, D. and Cresswell, G. R.: A note on the seasonal variability of the South Java Current. *Journal of Geophysical*
3283 *Research*, 97(C3), 3685– 3688. <https://doi.org/10.1029/91JC03056>, 1992.

3284 Quartly, G. D. and Srokosz, M. A.: Eddies in the southern Mozambique Channel, *Deep. Res. Part II Top. Stud.*
3285 *Oceanogr.*, doi:10.1016/j.dsr2.2003.03.001, 2004.

3286 Rahaman, H., Bharath Raj, G.N. & Ravichandran, M. Coupled Ocean–Atmosphere Summer Intraseasonal Oscillation
3287 over the Bay of Bengal. *Pure Appl. Geophys.* 176, 5415–5429, <https://doi.org/10.1007/s00024-019-02275-4>, 2019.

3288 Raj, R. P., Peter, B. N. and Pushpadas, D.: Oceanic and atmospheric influences on the variability of phytoplankton
3289 bloom in the Southwestern Indian Ocean, *J. Mar. Syst.*, doi:10.1016/j.jmarsys.2010.05.009, 2010.

3290 Ramanantsoa, J. D., Penven, P., Krug, M., Gula, J., & Rouault, M.: Uncovering a new current: The Southwest
3291 MAdagascar Coastal Current. *Geophysical Research Letters*, 45, 1930–1938. <https://doi.org/10.1002/2017GL075900>,
3292 2018.

3293 Rao, R. R., Molinari, R. L. and Festa, J. F.: Evolution of the climatological near-surface thermal structure of the tropical
3294 Indian Ocean. 1. Description of mean monthly mixed layer depth, and sea surface temperature, surface current, and
3295 surface meteorological fields, *J. Geophys. Res.*, doi:10.1029/jc094ic08p10801, 1989.

3296 Rao, R. R., and Sivakumar, R.: Seasonal variability of sea surface salinity and salt budget of the mixed layer of the
3297 north Indian Ocean, *J. Geophys. Res.*, 108(C1), 3009, doi:10.1029/2001JC000907, 2003.

3298 Rathore, S., Bindoff, N. L., Phillips, H. E. and Feng, M.: Recent hemispheric asymmetry in global ocean warming
3299 induced by climate change and internal variability, *Nat. Commun.*, doi:10.1038/s41467-020-15754-3, 2020.

3300 Ratna, S. B., Cherchi, A., Osborn, T. J., Joshi, M. and Uppara, U.: The extreme positive Indian Ocean Dipole of 2019
3301 and associated Indian summer monsoon rainfall response. *Geophysical Research Letters*, 48, e2020GL091497,
3302 doi:10.1029/2020GL091497, 2021.

3303 Ravichandran, M., Girishkumar, M. S. and Riser, S.: Observed variability of chlorophyll-a using Argo profiling floats in
3304 the southeastern Arabian Sea, *Deep. Res. Part I Oceanogr. Res. Pap.*, doi:10.1016/j.dsr.2012.03.003, 2012.

3305 Reason, C. J. C.: Subtropical Indian Ocean SST dipole events and southern African rainfall, *Geophys. Res. Lett.*,
3306 doi:10.1029/2000GL012735, 2001.

3307 Reason, C.J.C.: Sensitivity of the southern African circulation to dipole sea-surface-temperature patterns in the south
3308 Indian Ocean. *Int. J. Climatol.* 22, 377–393. <https://doi.org/10.1002/joc.744>, 2002.

3309 Reppin, J., Schott, F. A., Fischer, J. and Quadfasel, D.: Equatorial currents and transports in the upper central Indian
3310 Ocean: Annual cycle and interannual variability, *J. Geophys. Res. Ocean.*, doi:10.1029/1999jc900093, 1999.

3311 Resplandy, L., Vialard, J., Lévy, M., Aumont, O. and Dandonneau, Y.: Seasonal and intraseasonal biogeochemical
3312 variability in the thermocline ridge of the southern tropical Indian Ocean, *J. Geophys. Res. Ocean.*,
3313 doi:10.1029/2008JC005246, 2009.

3314 Ridgway, K. R., and Condie, S. A.: The 5500-km-long boundary flow off western and southern Australia, *J. Geophys.*
3315 *Res.*, 109, C04017, <https://doi.org/10.1029/2003JC001921>, 2004.

3316 Ridgway, K. R., Godfrey, J.: The source of the Leeuwin Current seasonality, *J. Geophys. Res.*, 120(10), 6843–6864,
3317 <https://doi.org/10.1002/2015JC011049>, 2015.

3318 Rixen, T., Cowie, G., Gaye, B., Goes, J., do Rosário Gomes, H., Hood, R. R., Lachkar, Z., Schmidt, H., Segsneider, J.,
3319 and Singh, A.: Reviews and syntheses: Present, past, and future of the oxygen minimum zone in the northern Indian
3320 Ocean, *Biogeosciences*, 17, 6051–6080, <https://doi.org/10.5194/bg-17-6051-2020>, 2020.

3321 Robbins, P. E. and Toole, J. M.: The dissolved silica budget as a constraint on the meridional overturning circulation of
3322 the Indian Ocean, *Deep. Res. Part I Oceanogr. Res. Pap.*, doi:10.1016/S0967-0637(96)00126-4, 1997.

3323 Roberts, M. J.: Chokka squid (*Loligo vulgaris reynaudii*) abundance linked to changes in South Africa’s Agulhas Bank
3324 ecosystem during spawning and the early life cycle, *ICES J. Mar. Sci.*, doi:10.1016/j.icesjms.2004.10.002, 2005.

3325 Roberts, M. J., Ternon, J. F. and Morris, T.: Interaction of dipole eddies with the western continental slope of the
3326 Mozambique Channel, *Deep. Res. Part II Top. Stud. Oceanogr.*, doi:10.1016/j.dsr2.2013.10.016, 2014.

3327 Robinson, J., Guillotreau, P., Jiménez-Toribio, R., Lantz, F., Nadzon, L., Dorizo, J., Gerry, C. and Marsac, F.: Impacts
3328 of climate variability on the tuna economy of Seychelles, *Clim. Res.*, doi:10.3354/cr00890, 2010.

3329 Rochford, D. J.: Seasonal interchange of high and low salinity surface waters off south-west Australia, Technical Paper,
3330 Division of Fisheries and Oceanography, CSIRO, Australia, <http://hdl.handle.net/102.100.100/321788?index=1>, 1969.

3331 Roemmich, D., W. J. Gould and J Gilson: 135 years of global ocean warming between the Challenger expedition and the
3332 Argo Programme. *Nature Climate Change* volume 2, 425–428, 2012.

3333 Roman-Stork, H. L., Subrahmanyam, B., & Trott, C. B.: Monitoring
3334 intraseasonal oscillations in the Indian Ocean using satellite observations. *Journal of Geophysical Research: Oceans*,
3335 125, e2019JC015891. <https://doi.org/10.1029/2019JC015891>, 2020.

3336 Rosell-Fieschi, M., Rintoul, S. R., Gourrion, J., and Pelegrí, J. L.: Tasman Leakage of intermediate waters as inferred
3337 from Argo floats, *Geophys. Res. Lett.*, 40, 5456– 5460, <https://doi.org/10.1002/2013GL057797>, 2013.

3338 Roxy, M., Tanimoto, Y., Preethi, B., Terray, P. and Krishnan, R.: Intraseasonal SST-precipitation relationship and its
3339 spatial variability over the tropical summer monsoon region, *Clim. Dyn.*, 41(1), 45–61, doi:10.1007/s00382-012-1547-
3340 1, 2013.

3341 Roxy, M. K., Ritika, K., Terray, P. and Masson, S.: The curious case of Indian Ocean warming, *J. Clim.*,
3342 doi:10.1175/JCLI-D-14-00471.1, 2014.

3343 Roxy, M. K., Modi, A., Murtugudde, R., Valsala, V., Panickal, S., Prasanna Kumar, S., Ravichandran, M., Vichi, M. and
3344 Lévy, M.: A reduction in marine primary productivity driven by rapid warming over the tropical Indian Ocean,
3345 *Geophys. Res. Lett.*, doi:10.1002/2015GL066979, 2016.

3346 Roxy, M.K., P. Dasgupta, M.J. McPhaden, T. Suematsu, C. Zhang, and D. Kim: Twofold expansion of the Indo-Pacific
3347 warm pool warps the MJO life cycle. *Nature*, 575, 647-651. <https://doi.org/10.1038/s41586-019-1764-4>, 2019.

3348 Rouault, M., Penven, P. and Pohl, B.: Warming in the Agulhas Current system since the 1980’s, *Geophys. Res. Lett.*,
3349 doi:10.1029/2009GL037987, 2009.

3350 Rydbeck, A. V. and Jensen, T. G.: Oceanic impetus for convective onset of the Madden-Julian oscillation in the western
3351 Indian ocean, *J. Clim.*, 30(11), 4299–4316, doi:10.1175/JCLI-D-16-0595.1, 2017.

3352 Rydbeck, A. V., Jensen, T. G. and Nyadjro, E. S.: Intraseasonal sea surface warming in the western Indian Ocean by
3353 oceanic equatorial Rossby waves, *Geophys. Res. Lett.*, 44(9), 4224–4232, doi:10.1002/2017GL073331, 2017.

3354 Sabeerali, C. T., Ramu Dandi, A., Dhakate, A., Salunke, K., Mahapatra, S. and Rao, S. A.: Simulation of boreal summer
3355 intraseasonal oscillations in the latest CMIP5 coupled GCMs, *J. Geophys. Res. Atmos.*, 118(10), 4401–4420,
3356 doi:10.1002/jgrd.50403, 2013.

3357 Sabu, P., M.P. Subeesh, J.V. George et al.: Enhanced subsurface mixing due to near-inertial waves: observation from
3358 Seychelles-Chagos Thermocline Ridge. *Ocean Dynamics* 71, 391–409. <https://doi.org/10.1007/s10236-020-01430-z>,
3359 2021

3360 Sahoo, D., Saxena, H., Tripathi, N., Khan, A., Rahaman, A., Kumar, S., Sudheer, A., and Singh, A.: Non-Redfieldian
3361 C:N:P ratio in the inorganic and organic pools of the Bay of Bengal during the summer monsoon, *Mar. Ecol. Prog.*
3362 *Ser.*, 653, 41–55, <https://doi.org/10.3354/meps13498>, 2020.

3363 Sahoo, D., Saxena, H., Nazirahmed, S., Kumar, S., Sudheer, A., Bhushan, R., Sahay, A., and Singh, A.: Role of eddies
3364 and N₂ fixation in regulating C: N: P proportions in the Bay of Bengal, *Biogeochemistry*, 1–17, 2021.

3365 Saji, N. H., Goswami, B. N., Vinayachandran, P. N. and Yamagata, T.: A dipole mode in the tropical Indian Ocean,
3366 *Nature*, 401(6751), 360–363, doi:10.1038/43854, 1999.

3367 Saji, N. H., Xie, s.-P., and Tam, C.-Y.: Satellite observations of intense intraseasonal cooling events in the tropical south
3368 Indian Ocean, *Geophys. Res. Lett.*, 33, L14704, doi:10.1029/2006GL026525, 2006.

3369 Sanchez-Franks, A., Webber, B. G. M., King, B. A., Vinayachandran, P. N., Matthews, A. J., Sheehan, P. M. F., Behara,
3370 A. and Neema, C. P.: The railroad switch effect of seasonally reversing currents on the Bay of Bengal high salinity
3371 core, *Geophys. Res. Lett.*, doi:10.1029/2019gl082208, 2019.

3372 Sanchez-Franks, A., Kent, E. C., Matthews, A. J., Webber, B. G. M., Peatman, S. C. and Vinayachandran, P. N.:
3373 Intraseasonal variability of air-sea fluxes over the Bay of Bengal during the Southwest Monsoon, *J. Clim.*,
3374 doi:10.1175/JCLI-D-17-0652.1, 2018.

3375 Sarkar, S., H.T. Pham, S. Ramachandran, J.D. Nash, A. Tandon, J. Buckley, A.A. Lotliker, and M.M. Omand: The
3376 interplay between submesoscale instabilities and turbulence in the surface layer of the Bay of Bengal. *Oceanography*
3377 29(2):146–157, <https://doi.org/10.5670/oceanog.2016.47>, 2016.

3378 Sarma, V. V. and Aswanikumar, V.: Subsurface chlorophyll maxima in the north-western Bay of Bengal, *J. Plankton*
3379 *Res.*, <https://doi.org/10.1093/plankt/13.2.339>, 1991.

3380 Sasamal, S. K., Panigrahy, R. C. and Misra, S.: Asterionella blooms in the northwestern Bay of Bengal during 2004, *Int.*
3381 *J. Remote Sens.*, <https://doi.org/10.1080/01431160500185391>, 2005.

3382 Sawant, S. and Madhupratap, M.: Seasonally and composition of phytoplankton in the Arabian Sea, *Curr. Sci.*, 1996.

3383 Schloesser, F.: A dynamical model for the Leeuwin Undercurrent, *J. Phys. Oceanogr.*, 44, 1798-1810,
3384 <https://doi.org/10.1175/JPO-D-13-0226.1>, 2014.

3385 Schmitz, Jr, W.J.: On the interbasin-scale thermohaline circulation, *Reviews of Geophysics*, 33, 151–173,
3386 <https://doi.org/10.1029/95RG00879>, 1995.

3387 Schott, F. A. and McCreary, J. P.: The monsoon circulation of the Indian Ocean, *Progr. Oceanogr.*, 51, 1-123, 2001.

3388 Schott, F., Dengler, M., and Schoenefeldt, R.: The shallow overturning circulation of the Indian Ocean. *Progress in*
3389 *Oceanography*, 53, 57–103, 2002.

3390 Schott, F.A., McCreary, J.P., and Johnson, G.C.: “Shallow Overturning Circulations of the Tropical-Subtropical
3391 Oceans.” In *Earth Climate: The Ocean-Atmosphere Interaction*, edited by C. Wang, S.-P. Xie, and J. A. Carton, 261–
3392 304. *Geophysical Monograph*, American Geophysical Union, Washington, D.C., <https://doi.org/10.1029/147GM15>,
3393 2004.

3394 Schott, F. A., Xie, S.-P. and McCreary, J. P.: Indian Ocean circulation and climate variability, *Rev. Geophys.*, 47,
3395 RG1002, <https://doi.org/10.1029/2007RG000245>, 2009.

3396 Schmitz, W.J.: On the interbasin-scale thermohaline circulation. *Reviews of Geophysics* 33:151–173, [http://dx.doi.org/](http://dx.doi.org/10.1029/95RG00879)
3397 [10.1029/95RG00879](http://dx.doi.org/10.1029/95RG00879), 1995.

3398 Schumann, E. H., Churchill, J. R. S. and Zaayman, H. J.: Oceanic variability in the western sector of Algoa Bay, South
3399 Africa, *African J. Mar. Sci.*, doi:10.2989/18142320509504069, 2005.

3400 Sengupta, D., Senan, R. and Goswami, B. N.: Origin of intraseasonal variability of circulation in the tropical central
3401 Indian Ocean, *Geophys. Res. Lett.*, doi:10.1029/2000GL012251, 2001.

3402 Sengupta, D., Bharath Raj, G. N. and Shenoi, S. S. C.: Surface freshwater from Bay of Bengal runoff and Indonesian
3403 Throughflow in the tropical Indian Ocean, *Geophys. Res. Lett.*, doi:10.1029/2006GL027573, 2006.

3404 Sengupta, D., Goddalahundi, B. R. and Anitha, D. S.: Cyclone-induced mixing does not cool SST in the post-monsoon
3405 north Bay of Bengal, *Atmos. Sci. Lett.*, doi:10.1002/asl.162, 2008.

3406 Sengupta, D., Senan, R., Goswami, B. N. and Vialard, J.: Intraseasonal variability of equatorial Indian Ocean zonal
3407 currents, in *Journal of Climate.*, 2007.

3408 Shalapyonok, A., Olson, R. J. and Shalapyonok, L. S.: Arabian Sea phytoplankton during Southwest and Northeast
3409 Monsoons 1995: Composition, size structure and biomass from individual cell properties measured by flow cytometry,
3410 *Deep. Res. Part II Top. Stud. Oceanogr.*, doi:10.1016/S0967-0645(00)00137-5, 2001.

3411 Shankar, D., McCreary, J. P., Han, W. and Shetye, S. R.: Dynamics of the East India Coastal Current 1. Analytic
3412 solutions forced by interior Ekman pumping and local alongshore winds, *J. Geophys. Res.*, 101 13975–13991, 1996.

3413 Shankar, D. and Shetye, S. R.: On the dynamics of the Lakshadweep high and low in southeastern Arabian Sea; *J.*
3414 *Geophys. Res.* 102 12,551–12,562, 1997.

3415 Shankar, D., Vinayachandran, P. N. and Unnikrishnan, A. S.: The monsoon currents in the north Indian Ocean, *Prog.*
3416 *Oceanogr.*, 52(1), 63–120, doi:10.1016/S0079-6611(02)00024-1, 2002.

3417 Shankar, D., Remya, R., Vinayachandran, P., Chatterjee, A. and Behera, A.: Inhibition of mixed-layer deepening during
3418 winter in the northeastern Arabian Sea by the West India Coastal Current, *Climate Dynamics*, 47(3-4), 1049–1072,
3419 2016.

3420 Sharma, G. S.: Water characteristics and current structure at 65°E during the southwest monsoon, *J. Oceanogr. Soc. Jpn.*,
3421 32, 284–296, <https://doi.org/10.1007/BF02107985>, 1976.

3422 Sharma, G.S., Gouveia, A.D., and Satyendranath, S.: Incursion of the Pacific Ocean Water into the Indian Ocean. *Proc.*
3423 *Indian Acad. Sci., A (E & P Sciences)* 87, 29–45, <https://doi.org/10.1007/BF02839383>, 1978.

3424 Sharmila, S., Pillai, P. A., Joseph, S., Roxy, M., Krishna, R. P. M., Chattopadhyay, R., Abhilash, S., Sahai, A. K. and
3425 Goswami, B. N.: Role of ocean-atmosphere interaction on northward propagation of Indian summer monsoon
3426 intraseasonal oscillations (MISO), *Clim. Dyn.*, 41(5–6), 1651–1669, doi:10.1007/s00382-013-1854-1, 2013.

3427 Sheehan, P. M. F., Webber, B. G. M., Sanchez-Franks, A., Matthews, A. J., Heywood, K. J. and Vinayachandran, P. N.:
3428 Injection of Oxygenated Persian Gulf Water Into the Southern Bay of Bengal, *Geophys. Res. Lett.*,
3429 doi:10.1029/2020GL087773, 2020.

3430 Sheno, S., Shankar, D. and Shetye, S. R.: Differences in heat budgets of the near-surface Arabian Sea and Bay of
3431 Bengal: Implications for the summer monsoon; *J. Geophys. Res.* 107, <https://doi.org/10.1029/2000JC000679>, 2002.

3432 Shetye, S. R. and Sheno, S. S. C.: Seasonal cycle of surface circulation in the coastal North Indian Ocean; *Proc.*
3433 *Indian Acad. Sci. (Earth Planet Sci.)* 97 53–62. 1988.

3434 Shetye, S. R., Gouveia, A. D., Shankar, D., Sheno, S. S. C., Vinayachandran, P. N., Sundar, D., Michael, G. S. and
3435 Nampoothiri, G.: Hydrography and circulation in the western Bay of Bengal during the northeast monsoon, *J.*
3436 *Geophys. Res. C Ocean.*, doi:10.1029/95JC03307, 1996.

3437 Shetye, S. R., Gouveia, A.D., Sheno, S. S. C., Sundar, D., Michael, G. S. and Nampoothiri, G.: The western boundary
3438 current of the seasonal subtropical gyre in the Bay of Bengal, *J. Geophys. Res.*, 98, 945-954, 1993.

3439 Shinoda, T., Hendon, H. H. and Glick, J.: Intraseasonal Variability of Surface Fluxes and Sea Surface Temperature in
3440 the Tropical Western Pacific and Indian Oceans, *J. Clim.*, 11, 1685–1702, 1998.

3441 Shinoda, T., Kiladis, G. N. and Roundy, P. E.: Statistical representation of equatorial waves and tropical instability
3442 waves in the Pacific Ocean, *Atmos. Res.*, 94, 37– 44, doi:10.1016/j.atmosres.2008.06.002, 2009.

3443 Shinoda, T., Han, W., Joseph Metzger, E. and Hurlburt, H. E.: Seasonal variation of the Indonesian throughflow in
3444 Makassar Strait, *J. Phys. Oceanogr.*, doi:10.1175/JPO-D-11-0120.1, 2012.

3445 Shroyer, E., Rudnick, D., Farrar, J. T., Lim, B., Venayagamoorthy, S. K., St. Laurent, L., Garanaik, A. and Moum, J.:
3446 Modification of Upper-Ocean Temperature Structure by Subsurface Mixing in the Presence of Strong Salinity
3447 Stratification, *Oceanography*, 29(2), 62–71, doi:10.5670/oceanog.2016.39, 2016.

3448 Siedler, G., Rouault, M., and Lutjeharms, J.: Structure and origin of the subtropical South Indian Ocean Countercurrent,
3449 *Geophys. Res. Lett.*, 33, L24609, <https://doi.org/10.1029/2006GL027399>, 2006.

3450 Siedler, G., Rouault, M., Biastoch, A., Backeberg, B. C., Reason, C. J. C., and Lutjeharms, J.: Modes of the southern
3451 extension of the East Madagascar Current, *J. Geophys. Res.*, 114, C01005, <https://doi.org/10.1029/2008JC004921>,
3452 2009.

3453 Singh, A., Gandhi, N., Ramesh, R. and Prakash, S.: Role of cyclonic eddy in enhancing primary and new production in
3454 the Bay of Bengal, *J. Sea Res.*, doi:10.1016/j.seares.2014.12.002, 2015a.

3455 Singh, A. and Ramesh, R.: Environmental controls on new and primary production in the northern Indian Ocean, *Prog.*
3456 *Oceanogr.*, doi:10.1016/j.pocean.2014.12.006, 2015b.

3457 Singh, D., Tsiang, M., Rajaratnam, B. and Diffenbaugh, N. S.: Observed changes in extreme wet and dry spells during
3458 the south Asian summer monsoon season, *Nat. Clim. Chang.*, doi:10.1038/nclimate2208, 2014.

3459 Smith, R. L., Huyer, A., Godfrey, J. S., and Church, J. A.: The Leeuwin Current off Western Australia, 1986–1987, *J.*
3460 *Phys. Oceanogr.*, 21, 323–345, [https://doi.org/10.1175/1520-0485\(1991\)021<0323:TLCOWA>2.0.CO;2](https://doi.org/10.1175/1520-0485(1991)021<0323:TLCOWA>2.0.CO;2), 1991.

3461 Smyth, W.D., Durland, T. and Moum, J.N.: Energy and heat fluxes due to vertically-propagating Yanai waves observed
3462 in the equatorial Indian Ocean, *J. Geophys. Res. Oceans*, 120, doi:10.1002/2014JC010152, 2014.

3463 Sorokin, Y., Kopylov, A. and Mamaeva, N.: Abundance and dynamics of microplankton in the central tropical Indian
3464 Ocean, *Mar. Ecol. Prog. Ser.*, doi:10.3354/meps024027, 1985.

3465 Speich, S., Blanke, B. and Cai, W.: Atlantic meridional overturning circulation and the Southern Hemisphere supergyre,
3466 *Geophys. Res. Lett.*, doi:10.1029/2007GL031583, 2007.

3467 Sperber, K. R. and Annamalai, H.: Coupled model simulations of boreal summer intraseasonal (30–50 day) variability,
3468 Part 1: Systematic errors and caution on use of metrics, *Clim. Dyn.*, 31(2–3), 345–372, doi:10.1007/s00382-008-0367-
3469 9, 2008.

3470 Sprintall, J., Chong, J., Syamsudin, F., Morawitz, W., Hautala, S., Bray, N. and Wijffels, S.: Dynamics of the South Java
3471 current in the Indo-Australian Basin, *Geophys. Res. Lett.*, 26, 2493–2496, 1999.

3472 Sprintall, J., Wijffels, S. E., Molcard, R. and Jaya, I.: Direct estimates of the Indonesian Throughflow entering the Indian
3473 Ocean: 2004–2006, *J. Geophys. Res. Ocean.*, doi:10.1029/2008JC005257, 2009.

3474 Sprintall, J., Gordon, A. L., Koch-Larrouy, A., Lee, T., Potemra, J. T., Pujiana, K. and Wijffels, S. E.: The Indonesian
3475 seas and their role in the coupled ocean-climate system, *Nat. Geosci.*, doi:10.1038/ngeo2188, 2014a.

3476 Sprintall, J. and Révelard, A.: The Indonesian Throughflow response to Indo-Pacific climate variability, *J. Geophys.*
3477 *Res. Ocean.*, doi:10.1002/2013JC009533, 2014b.

3478 Sprintall, J., Gordon, A. L., Wijffels, S. E., Feng, M., Hu, S., Koch-Larrouy, A., Phillips, H., Nugroho, D., Napitu, A.,
3479 Pujiana, K., Dwi Susanto, R., Sloyan, B., Yuan, D., Riama, N. F., Siswanto, S., Kuswardani, A., Arifin, Z., Wahyudi,
3480 A. J., Zhou, H., Nagai, T., Ansong, J. K., Bourdalle-Badié, R., Chanut, J., Lyard, F., Arbic, B. K., Ramdhani, A. and
3481 Setiawan, A.: Detecting change in the Indonesian seas, *Front. Mar. Sci.*, doi:10.3389/fmars.2019.00257, 2019.

3482 Sree Lekha, J., Buckley, J. M., Tandon, A. and Sengupta, D.: Subseasonal Dispersal of Freshwater in the Northern Bay
3483 of Bengal in the 2013 Summer Monsoon Season, *J. Geophys. Res. Ocean.*, doi:10.1029/2018JC014181, 2018.

3484 Srinivasan, A., Garraffo, Z. and Iskandarani, M.: Abyssal circulation in the Indian Ocean from a 1 / 12° resolution global
3485 hindcast, *Deep. Res. Part I Oceanogr. Res. Pap.*, doi:10.1016/j.dsr.2009.07.001, 2009.

3486 Srokosz, M. A., Quartly, G. D. and Buck, J. J. H.: A possible plankton wave in the Indian Ocean, *Geophys. Res. Lett.*,
3487 doi:10.1029/2004GL019738, 2004.

3488 Srokosz, M. A. and Quartly, G. D.: The madagascar bloom: A serendipitous study, *J. Geophys. Res. Ocean.*,
3489 doi:10.1029/2012JC008339, 2013.

3490 Srokosz, M. A., Robinson, J., McGrain, H., Popova, E. E., and Yool, A.: Could the Madagascar bloom be fertilized by
3491 Madagascan iron?, *J. Geophys. Res. Oceans*, 120, 5790–5803, <https://doi.org/10.1002/2015JC011075>, 2015.

3492 Stramma, L., Bange, H. W., Czeschel, R., Lorenzo, A. and Frank, M.: On the role of mesoscale eddies for the biological
3493 productivity and biogeochemistry in the eastern tropical Pacific Ocean off Peru, *Biogeosciences*, doi:10.5194/bg-10-
3494 7293-2013, 2013.

3495 Strutton, P. G., Coles, V. J., Hood, R. R., Matear, R. J., McPhaden, M. J. and Phillips, H. E.: Biogeochemical variability
3496 in the central equatorial Indian Ocean during the monsoon transition, *Biogeosciences*, doi:10.5194/bg-12-2367-2015,
3497 2015.

3498 Stuecker, M. F., Timmermann, A., Jin, F. F., Chikamoto, Y., Zhang, W., Wittenberg, A. T., Widiasih, E., and Zhao, S.:
3499 Revisiting ENSO/Indian Ocean Dipole phase relationships, *Geophys. Res. Lett.*, 44, 2481–2492, 2017.

3500 Suhas, E., Neena, J. M. and Goswami, B. N.: An Indian monsoon intraseasonal oscillations (MISO) index for real time
3501 monitoring and forecast verification, *Clim. Dyn.*, 40(11–12), 2605–2616, doi:10.1007/s00382-012-1462-5, 2013.

3502 Sun, S., Lan, J., Fang, Y., Tana, and Gao, X.: A triggering mechanism for the Indian Ocean dipoles independent of
3503 ENSO. *J. Climate*, 28, 5063-5076, <https://doi.org/10.1175/JCLI-D-14-00580.1>, 2015.

3504 Suresh, I., Vialard, J., Lengaigne, M., Han, W., McCreary, J., Durand, F., Muraleedharan, P. M.: Origins of wind-driven
3505 intraseasonal sea level variations in the north Indian Ocean coastal waveguide. *Geophys Res Lett* 40:5740–5744.
3506 doi:10.1002/2013GL058312, 2013.

3507 Suresh, I., Vialard, J., Izumo, T., Lengaigne, M., Han, W., McCreary, J. P. and Muraleedharan, P. M.: Dominant role
3508 of winds near Sri Lanka in driving seasonal sea level variations along the west coast of India, *Geophys. Res. Lett.*,
3509 43,7028–7035, doi:10.1002/2016GL069976, 2016.

3510 Susanto, R.D., Gordon, A.L. and Zheng, Q.N.: Upwelling along the coasts of Java and Sumatra and its relation to
3511 ENSO. *Geophys. Res. Lett.*, 28, 1599–1602, 2001.

3512 Susanto, R. D., Wei, Z., Adi, R. T., Fan, B., Li, S. and Fang, G.: Observations of the Karimata Strait throughflow from
3513 December 2007 to November 2008, *Acta Oceanol. Sin.*, doi:10.1007/s13131-013-0307-3, 2013.

3514 Suzuki, R., Behera, S. K., Iizuka, S. and Yamagata, T.: Indian Ocean subtropical dipole simulated using a coupled
3515 general circulation model, *J. Geophys. Res. C Ocean.*, doi:10.1029/2003JC001974, 2004.

3516 Swallow, J. C. and Pollard, R. T.: Flow of bottom water through the Madagascar Basin, *Deep Sea Res. Part A*,
3517 *Oceanogr. Res. Pap.*, doi:10.1016/0198-0149(88)90095-7, 1988.

3518 Takaya, Y., Ishikawa, I., Kobayashi, C., Endo, H., & Ose, T.: Enhanced Meiyu-Baiu rainfall in early summer 2020:
3519 Aftermath of the 2019 super IOD event. *Geophysical Research Letters*, 47, e2020GL090671.
3520 <https://doi.org/10.1029/2020GL090671>, 2020.

3521 Takeuchi, K.: Numerical study of the Subtropical Front and the Subtropical Countercurrent. *J. Oceanogr. Soc. Japan*, 40,
3522 371–381, <https://doi.org/10.1007/BF02303341>, 1984.

3523 Talley, L. D., and Sprintall, J.: Deep expression of the Indonesian Throughflow: Indonesian Intermediate Water in the
3524 South Equatorial Current, *Journal of Geophysical Research, Oceans*, 110: doi:10.1029/2004JC002826, 2005.

3525 Talley, L. D.: Freshwater transport estimates and the global overturning circulation: Shallow, deep and throughflow
3526 components, *Progress in Oceanography*, 78(4), 257-303. doi: 10.1016/j.pocean.2008.05.001, 2008.

3527 Talley, L. D.: Closure of the global overturning circulation through the Indian, Pacific, and Southern Oceans:
3528 Schematics and transports. *Oceanography* 26 (1), 80-97. doi: 10.5670/oceanog.2013.07, 2013.

3529 Talley, L. D., Pickard, G. L., Emery, W. J. and Swift, J. H.: *Descriptive Physical Oceanography: An Introduction*, 6th
3530 Edition. Academic Press, Elsevier Ltd. 983pp, 2011.

3531 Talley, L. D., Feely, R. A., Sloyan, B. M., Wanninkhof, R., Baringer, M.O., Bullister, J. L., et al.: Changes in ocean
3532 heat, carbon content, and ventilation: A review of the first decade of GO-SHIP global repeat hydrography. *Annu. Rev.*
3533 *Mar. Sci.* 8, 185-215. doi: 10.1146/annurev-marine-052915-100829, 2016.

3534 Talley, L., Johnson, G. C., Purkey, S., Feely, R. A. and Wanninkhof, R.: Global Ocean Ship-based Hydrographic
3535 Investigations Program (GO-SHIP) provides key climate-relevant deep ocean observations, *US CLIVAR Variations*,
3536 15, 8-14, 2017.

3537 Tarran, G. A., Burkill, P. H., Edwards, E. S. and Woodward, E. M. S.: Phytoplankton community structure in the
3538 Arabian Sea during and after the SW monsoon, 1994, *Deep. Res. Part II Top. Stud. Oceanogr.*, doi:10.1016/S0967-
3539 0645(98)00122-2, 1999.

3540 Taylor, B. M., Benkwitt, C. E., Choat, H., Clements, K. D., Graham, N. A., and Meekan, M. G.: Synchronous biological
3541 feedbacks in parrotfishes associated with pantropical coral bleaching, *Global Change Biology*, 26, 3, 1285-1294,
3542 <https://doi.org/10.1111/gcb.14909>, 2019.

3543 Terray, P., Delecluse, P., Labattu, S. and Terray, L.: Sea surface temperature associations with the late Indian summer
3544 monsoon, *Clim. Dyn.*, doi:10.1007/s00382-003-0354-0, 2003.

3545 Thadathil, P., Muraleedharan, P. M., Rao, R. R., Somayajulu, Y. K., Reddy, G. V. and Revichandran, C.: Observed
3546 seasonal variability of barrier layer in the Bay of Bengal, *J. Geophys. Res. Ocean.*, 112(2),
3547 doi:10.1029/2006JC003651, 2007.

3548 Thadathil, P., Suresh, I., Gautham, S., Prasanna Kumar, S., Lengaigne, M., Rao, R. R., Nettu, S. and Hegde, A.: Surface
3549 layer temperature inversion in the Bay of Bengal: Main characteristics and related mechanisms, *J. Geophys. Res.*
3550 *Ocean.*, doi:10.1002/2016JC011674, 2016.

3551 Thangaprakash, V. P., Girishkumar, M. S., Suprit, K., Kumar, N. S., Chaudhuri, D., Dinesh, K., Kumar, A.,
3552 Shivaprasad, S., Ravichandran, M., Farrar, J. T., Sundar, R. and Weller, R.: What Controls Seasonal Evolution of Sea
3553 Surface Temperature in the Bay of Bengal? Mixed Layer Heat Budget Analysis Using Moored Buoy Observations
3554 Along 90°E, *Oceanography*, 29(2), 202–213, doi:10.5670/oceanog.2016.52, 2016.

3555 Thompson, P. A., Pesant, S. and Waite, A. M.: Contrasting the vertical differences in the phytoplankton biology of a
3556 dipole pair of eddies in the south-eastern Indian Ocean, *Deep. Res. Part II Top. Stud. Oceanogr.*,
3557 doi:10.1016/j.dsr2.2006.12.009, 2007.

3558 Thompson, P. A., Wild-Allen, K., Lourey, M., Rousseaux, C., Waite, A. M., Feng, M., and Beckley, L. E.: Nutrients in
3559 an oligotrophic boundary current: evidence of a new role for the Leeuwin Current. *Progress in Oceanography* 91, 345–
3560 359, 2011.

3561 Thompson, R. O. R. Y.: Observations of the Leeuwin Current off Western Australia, *J. Phys. Oceanogr.*, 14, 623–628,
3562 [https://doi.org/10.1175/1520-0485\(1984\)014<0623:OOTLCO>2.0.CO;2](https://doi.org/10.1175/1520-0485(1984)014<0623:OOTLCO>2.0.CO;2), 1984.

3563 Thompson, R. O. R. Y.: Continental-shelf-scale model of the Leeuwin Current, *J. Mar. Res.*, 45(4), 813–827,
3564 <https://doi.org/10.1357/002224087788327190>, 1987.

3565 Todd, R. E., Chavez, F. P., Clayton, S., Cravatte, S., Goes, M., Graco, M., Lin, X., Sprintall, J., Zilberman, N. V.,
3566 Archer, M., Arístegui, J., Balmaseda, M., Bane, J. M., Baringer, M. O., Barth, J. A., Beal, L. M., Brandt, P., Calil, P.
3567 H. R., Campos, E., Centurioni, L. R., Chidichimo, M. P., Cirano, M., Cronin, M. F., Curchitser, E. N., Davis, R. E.,
3568 Dengler, M., deYoung, B., Dong, S., Escribano, R., Fassbender, A. J., Fawcett, S. E., Feng, M., Goni, G. J., Gray, A.
3569 R., Gutiérrez, D., Hebert, D., Hummels, R., Ito, S., Krug, M., Lacan, F., Laurindo, L., Lazar, A., Lee, C. M.,
3570 Lengaigne, M., Levine, N. M., Middleton, J., Montes, I., Muglia, M., Nagai, T., Palevsky, H. I., Palter, J. B., Phillips,
3571 H. E., Piola, A., Plueddemann, A. J., Qiu, B., Rodrigues, R. R., Roughan, M., Rudnick, D. L., Rykaczewski, R. R.,
3572 Saraceno, M., Seim, H., Sen Gupta, A., Shannon, L., Sloyan, B. M., Sutton, A. J., Thompson, L., van der Plas, A. K.,
3573 Volkov, D., Wilkin, J., Zhang, D., and Zhang, L.: Global perspectives on observing ocean boundary current systems.
3574 *OceanObs'19 white paper. Frontiers in Marine Science*. 6:423. doi: 10.3389/fmars.2019.00423, 2019.

3575 Toole, J. M., and Warren, B. A.: A hydrographic section across the subtropical South Indian Ocean, *Deep-Sea Res I*, 40,
3576 1973-2019, [https://doi.org/10.1016/0967-0637\(93\)90042-2](https://doi.org/10.1016/0967-0637(93)90042-2), 1993.

3577 Tozuka, T., Kataoka, T., and Yamagata, T.: Locally and remotely forced atmospheric circulation anomalies of Ningaloo
3578 Niño/Niña, *Clim. Dyn.*, 43, 2197–2205, <https://doi.org/10.1007/s00382-013-2044-x>, 2014.

3579 Trott, C., Bulusu, S. and Washburn, C. E.: Investigating the response of temperature and salinity in the Agulhas Current
3580 region to ENSO events, *Remote Sensing*, 13(9), 1829, doi:10.3390/rs13091829, 2021.

3581 Turner, A. G., Joshi, M., Robertson, E. S., and Woolnough, S. J.: The effect of Arabian Sea optical properties on SST
3582 biases and the South Asian summer monsoon in a coupled GCM, *Clim. Dyn.*, 39(3), 811–826,
3583 <https://doi.org/10.1007/s00382-011-1254-3>, 2012.

3584 Ummenhofer, C. C., Biastoch, A., and Böning, C. W.: Multidecadal Indian Ocean variability linked to the Pacific and
3585 implications for preconditioning Indian Ocean dipole events. *J. Climate*, 30, 1739–1751, 2017.

3586 Uz, B. M.: What causes the sporadic phytoplankton bloom southeast of Madagascar?, *J. Geophys. Res. Ocean.*,
3587 doi:10.1029/2006JC003685, 2007.

3588 Van Sebille, E., Biastoch, A., Van Leeuwen, P. J. and De Ruijter, W. P. M.: A weaker Agulhas current leads to more
3589 Agulhas leakage, *Geophys. Res. Lett.*, doi:10.1029/2008GL036614, 2009.

3590 Van Sebille, E., Van Leeuwen, P. J., Biastoch, A. and De Ruijter, W. P. M.: On the fast decay of Agulhas rings, *J.*
3591 *Geophys. Res. Ocean.*, doi:10.1029/2009JC005585, 2010a.

3592 Van Sebille, E., van Leeuwen, P. J., Biastoch, A. and de Ruijter, W. P. M.: Flux comparison of Eulerian and Lagrangian
3593 estimates of Agulhas leakage: A case study using a numerical model, *Deep. Res. Part I Oceanogr. Res. Pap.*,
3594 doi:10.1016/j.dsr.2009.12.006, 2010b.

3595 Van Sebille, E., Beal, L. M. and Johns, W. E.: Advective Time Scales of Agulhas Leakage to the North Atlantic in
3596 Surface Drifter Observations and the 3D OFES Model, *J. Phys. Oceanogr.*, doi:10.1175/2011jpo4602.1, 2011.

3597 Van Sebille, E., Sprintall, J., Schwarzkopf, F. U., Sen Gupta, A., Santoso, A., England, M. H., Biastoch, A. and Böning,
3598 C. W.: Pacific-to-Indian Ocean connectivity: Tasman leakage, Indonesian Throughflow, and the role of ENSO, *J.*
3599 *Geophys. Res. Ocean.*, doi:10.1002/2013JC009525, 2014.

3600 Varna, M., Singh, A., Sahoo, D., and Sengupta, D.: Strengthening of basin-scale ocean currents in winter drives
3601 decadal salinity decline in the eastern Arabian Sea, *Geophys. Res. Lett.*, 48, e2021GL094516, 2021.

3602 Vecchi, G. A. and Soden, B. J.: Global warming and the weakening of the tropical circulation. *J. Climate*, 20, 4316–
3603 4340, 2007.

3604 Vecchi, G. A. and Harrison, D. E.: Monsoon Breaks and Subseasonal Sea Surface Temperature Variability in the Bay of
3605 Bengal, *J. Clim.*, 15(12), 1485–1493, doi:10.1175/1520-0442(2002)015<1485:MBASSS>2.0.CO;2, 2002.

3606 Venkatesan, R., Vedachalam, N., Arul Muthiah, M., Sundar, R., Kesavakumar, B., Ramasundaram, S. and Jossia Joseph,
3607 K.: Reliability metrics from two decades of Indian ocean moored buoy observation network, *Mar. Technol. Soc. J.*,
3608 doi:10.4031/MTSJ.52.3.14, 2018.

3609 Venrick, E. L.: Mid-ocean ridges and their influence on the large-scale patterns of chlorophyll and production in the
3610 North Pacific, *Deep. Res. Part A*, doi:10.1016/s0198-0149(12)80006-9, 1991.

3611 Vialard, J., Foltz, G. R., McPhaden, M. J., Duvel, J. P. and de Boyer Montégut, C.: Strong Indian Ocean sea surface
3612 temperature signals associated with the Madden-Julian Oscillation in late 2007 and early 2008, *Geophys. Res. Lett.*,
3613 35(19), 1–5, doi:10.1029/2008GL035238, 2008.

3614 Vialard, J., Duvel, J. P., Mcphaden, M. J., Bouruet-Aubertot, P., Ward, B., Key, E., Bourras, D., Weller, R., Minnett, P.,
3615 Weill, A., Cassou, C., Eymard, L., Fristedt, T., Basdevant, C., Dandonneau, Y., Duteil, O., Izumo, T., de Boyer
3616 Montégut, C., Masson, S., Marsac, F., Menkes, C. and Kennan, S.: Cirene: Air-sea interactions in the Seychelles-
3617 Chagos thermocline ridge region, *Bull. Am. Meteorol. Soc.*, doi:10.1175/2008BAMS2499.1, 2009a.

3618 Vialard, J., Shenoi, S. S. C., McCreary, J. P., Shankar, D., Durand, F., Fernando, V. and Shetye, S. R.: Intraseasonal
3619 response of the northern Indian Ocean coastal waveguide to the Madden-Julian Oscillation, *Geophys. Res. Lett.*,
3620 36(14), 1–5, doi:10.1029/2009GL038450, 2009b.

3621 Vialard, J., Jayakumar, A., Gnanaseelan, C., Lengaigne, M., Sengupta, D. and Goswami, B. N.: Processes of 30-90 days
3622 sea surface temperature variability in the northern Indian Ocean during boreal summer, *Clim. Dyn.*, 38(9–10), 1901–
3623 1916, doi:10.1007/s00382-011-1015-3, 2012.

3624 Vic, C., Roullet, G., Xavier, C. and Capet, X.: Mesoscale dynamics in the Arabian Sea and a focus on the Great Whirl
3625 life cycle: A numerical investigation using ROMS, *Journal of Geophysical Research: Oceans*, 119, 6422–6443.
3626 <https://doi.org/10.1002/2014JC009857>, 2014.

3627 Vijith, V., Vinayachandran, P., Thushara, V., Amol, P., Shankar, D., and Anil, A.: Consequences of inhibition of mixed-
3628 layer deepening by the West India Coastal Current for winter phytoplankton bloom in the northeastern Arabian Sea.
3629 *Journal of Geophysical Research: Oceans*, 121, 6583–6603. <https://doi.org/10.1002/2016JC012004>, 2016.

3630 Vinayachandran, P. N., Saji, N. H. and Yamagata T.: Response of the equatorial Indian Ocean to an anomalous wind
3631 event during 1994; *Geophys. Res. Lett.* 26 1613–1615, 1999.

3632 Vinayachandran, P. N., Shetye, S. R., Sengupta, D. and Gadgil, S.: Forcing mechanisms of the Bay of Bengal circulation,
3633 *Curr. Sci.*, 71, 753–763, 1996.

3634 Vinayachandran, P. N., T. Kagimoto, T. Masumoto, Y., Chauhan, P., Nayak, S. R. and Yamagata, T.: Bifurcation of
3635 the East India Coastal Current east of Sri Lanka, *Geophys. Res. Lett.*, 32, L15606, doi:10.1029/2005GL022864, 2005.

3636 Vinayachandran, P. N., Shankar, D., Vernekar, S., Sandeep, K. K., Amol, P., Neema, C. P. and Chatterjee, A.: A
3637 summer monsoon pump to keep the Bay of Bengal salty, *Geophys. Res. Lett.*, 40, 1777–1782, doi:10.1002/grl.50274,
3638 2013.

3639 Vinayachandran, P. N., Matthews, A. J., Vijay KuMar, K., Sanchez-Franks, A., Thushara, V., George, J., Vijith, V.,
3640 Webber, B. G. M., Queste, B. Y., Roy, R., Sarkar, A., Baranowski, D. B., Bhat, G. S., Klingaman, N. P., Peatman, S.
3641 C., Parida, C., Heywood, K. J., Hall, R., King, B., Kent, E. C., Nayak, A. A., Neema, C. P., Amol, P., Lotliker, A.,
3642 Kankonkar, A., Gracias, D. G., Vernekar, S., D'Souza, A. C., Valluvan, G., Pargaonkar, S. M., Dinesh, K., Giddings,
3643 J. and Joshi, M.: BoBBLE: Ocean–Atmosphere interaction and its impact on the South Asian monsoon, *Bull. Am.*
3644 *Meteorol. Soc.*, doi:10.1175/BAMS-D-16-0230.1, 2018.

3645 Vivekanandan, E. and Krishnakumar, P.K.: Spatial and temporal differences in the coastal fisheries along the east
3646 coast of India. *Indian Journal of Marine Science*, 39, 380, 2010.

3647 Volkov, D. L., Lee, S.-K., Gordon, A. L., Rudko, M.: Unprecedented reduction and quick recovery of the South Indian
3648 Ocean heat content and sea level in 2014–2018. *Sci. Adv.*, 6, doi:10.1126/sciadv.abc1151, 2020.

3649 Wacogne, S., and Pacanowski, R.C.: Seasonal heat transport in a primitive equation model of the tropical Indian
3650 Ocean, *J. Phys. Oceanogr.*, 26, 2666–2699, 1996.

3651 Wainwright, C. M., Finney, D. L., Kilavi, M., Black, E., and Marsham, J. H.: Extreme rainfall in East Africa,
3652 October 2019–January 2020 and context under future climate change, *Weather*, 76(1), 26-31,
3653 <https://doi.org/10.1002/wea.3824>, 2021.

3654 Waite, A. M., Pesant, S., Griffin, D. A., Thompson, P. A. and Holl, C. M.: Oceanography, primary production and
3655 dissolved inorganic nitrogen uptake in two Leeuwin Current eddies, *Deep. Res. Part II Top. Stud. Oceanogr.*,
3656 doi:10.1016/j.dsr2.2007.03.001, 2007a.

3657 Waite, A. M., Thompson, P. A., Pesant, S., Feng, M., Beckley, L. E., Domingues, C. M., Gaughan, D., Hanson, C. E.,
3658 Holl, C. M., Koslow, T., Meuleners, M., Montoya, J. P., Moore, T., Muhling, B. A., Paterson, H., Rennie, S.,
3659 Strzelecki, J., and Twomey, L.: The Leeuwin Current and its eddies: An introductory overview, *Deep Sea Res. II*,
3660 54(8–10), 789–796, <https://doi.org/10.1016/j.dsr2.2006.12.008>, 2007b.

3661 Waite, A. M., Beckley, L. E., Guidi, L., Landrum, J. P., Holliday, D., Montoya, J., Paterson, H., Feng, M., Thompson, P.
3662 A. and Raes, E. J.: Cross-shelf transport, oxygen depletion, and nitrate release within a forming mesoscale eddy in the
3663 eastern Indian Ocean, *Limnol. Oceanogr.*, doi:10.1002/lno.10218, 2016.

3664 Waliser, D. E., Murtugudde, R. and Lucas, L. E.: Indo-Pacific Ocean response to atmospheric intraseasonal variability:
3665 1. Austral summer and the Madden-Julian Oscillation, *J. Geophys. Res.*, 108(C5), 3160, doi:10.1029/2002JC001620,
3666 2003.

3667 Wang, H., McClean, J. L., Talley, L. D., and Yeager, S.: Seasonal cycle and annual reversal of the Somali Current in an
3668 eddy-resolving global ocean model. *Journal of Geophysical Research: Oceans*, 123, 6562–6580.
3669 <https://doi.org/10.1029/2018JC013975>, 2018.

3670 Wang, H., Kumar, A., Murtugudde, R., Narapusetty, B., and Selp, K. L.: Covariations between the Indian Ocean dipole
3671 and ENSO: a modeling study. *Clim. Dyn.*, doi:10.1007/s00382-019-04895-x, 2019.

3672 Wang, Y. and McPhaden, M. J.: Seasonal cycle of cross-equatorial flow in the Central Indian Ocean. *J. Geophys. Res.*,
3673 122, doi:10.1002/2016JC012537, 2017.

3674 Wang, G., and Cai, W.: Two-year consecutive concurrences of positive Indian Ocean Dipole and Central Pacific El Niño
3675 preconditioned the 2019/2020 Australian “black summer” bushfires. *Geosci. Lett.* 7, 19
3676 <https://doi.org/10.1186/s40562-020-00168-2>, 2020.

3677 Warner, S. J., Becherer, J., Pujiana, K., Shroyer, E. L., Ravichandran, M., Thangaprakash, V. P. and Moum, J. N.:
3678 Monsoon mixing cycles in the Bay of Bengal: A year-long subsurface mixing record, *Oceanography*,
3679 doi:10.5670/oceanog.2016.48, 2016.

3680 Warren, B. A.: Deep flow in the Madagascar and Mascarene basins, *Deep. Res. Oceanogr. Abstr.*, doi:10.1016/0011-
3681 7471(74)90015-1, 1974.

3682 Warren, B. A.: Bottom water transport through the Southwest Indian Ridge, *Deep. Res.*, doi:10.1016/0146-
3683 6291(78)90596-9, 1978.

3684 Warren, B.A.: Transindian hydrographic section at Lat. 18°S: Property distributions and circulation in the South Indian
3685 Ocean. *Deep-Sea Res A.*, 28, 759-788. doi: 10.1016/S0198-0149(81)80001-5, 1981.

3686 Warren, B.A. : Driving the meridional overturning in the Indian Ocean, *Deep. Res. Part I*, doi:10.1016/0967-
3687 0637(94)90101-5, 1994.

3688 Warren, B. A., Whitworth, T. and LaCasce, J. H.: Forced resonant undulation in the deep Mascarene Basin, *Deep. Res.*
3689 *Part II Top. Stud. Oceanogr.*, doi:10.1016/S0967-0645(01)00151-5, 2002.

3690 Weaver, A. J., and Middleton, J. H.: On the dynamics of the Leeuwin Current, *J. Phys. Oceanogr.*, 19, 626–648,
3691 [https://doi.org/10.1175/1520-0485\(1989\)019<0626:OTDOTL>2.0.CO;2](https://doi.org/10.1175/1520-0485(1989)019<0626:OTDOTL>2.0.CO;2), 1989.

3692 Weaver, A.J., and Middleton, J.H.: An analytic model for the Leeuwin Current off western Australia, *Cont. Shelf Res.*,
3693 10(2), 105–122, [https://doi.org/10.1016/0278-4343\(90\)90025-H](https://doi.org/10.1016/0278-4343(90)90025-H), 1990.

3694 Webber, B. G. M., Matthews, A. J. and Heywood, K. J.: A dynamical ocean feedback mechanism for the Madden-Julian
3695 Oscillation, *Q. J. R. Meteorol. Soc.*, 136(648), 740–754, doi:10.1002/qj.604, 2010.

3696 Webber, B. G. M., Stevens, D. P., Matthews, A. J. and Heywood, K. J.: Dynamical ocean forcing of the Madden-Julian
3697 oscillation at lead times of up to five months, *J. Clim.*, 25(8), 2824–2842, doi:10.1175/JCLI-D-11-00268.1, 2012a.

3698 Webber, B. G. M., Matthews, A. J., Heywood, K. J. and Stevens, D. P.: Ocean Rossby waves as a triggering mechanism
3699 for primary Madden-Julian events, *Q. J. R. Meteorol. Soc.*, 138(663), 514–527, doi:10.1002/qj.936, 2012b.

3700 Webber, B. G. M., Matthews, A. J., Heywood, K. J., Kaiser, J. and Schmidtke, S.: Seaglider observations of equatorial
3701 Indian Ocean Rossby waves associated with the Madden-Julian Oscillation, *J. Geophys. Res. Ocean.*, 119(6), 3714–
3702 3731, doi:10.1002/2013JC009657, 2014.

3703 Webber, B. G. M., Matthews, A. J., Vinayachandran, P. N., Neema, C. P., Sanchez-Franks, A., Vijith, V., Amol, P. and
3704 Baranowski, D. B.: The Dynamics of the Southwest Monsoon Current in 2016 from High-Resolution In Situ
3705 Observations and Models, *J. Phys. Oceanogr.*, 48(10), 2259–2282, doi:10.1175/JPO-D-17-0215.1, 2018.

3706 Webster, P. J., Moore, A., Loschnigg, J. P. and R., L. R.: Coupled oceanic-atmospheric dynamics in the Indian Ocean
3707 during 1997-1998, *Nature*, 401(September), 356–360, 1999.

3708 Weijer, W. and van Sebille, E.: Impact of Agulhas leakage on the Atlantic overturning circulation in the CCSM4, *J.*
3709 *Clim.*, doi:10.1175/JCLI-D-12-00714.1, 2014.

3710 Weller, R. A., Farrar, J. T., Buckley, J., Mathew, S., Venkatesan, R., Lekha, J. S., Chaudhuri, D., Suresh Kumar, N. and
3711 Praveen Kumar, B.: Air-sea interaction in the Bay of Bengal, *Oceanography*, doi:10.5670/oceanog.2016.36, 2016.

3712 Wiggert, J. D., Jones, B. H., Dickey, T. D., Brink, K. H., Weller, R. A., Marra, J. and Codispoti, L. A.: The Northeast
3713 Monsoon’s impact on mixing, phytoplankton biomass and nutrient cycling in the Arabian Sea, *Deep. Res. Part II Top.*
3714 *Stud. Oceanogr.*, doi:10.1016/S0967-0645(99)00147-2, 2000.

3715 Wiggert, J. D., Hood, R. R., Banse, K. and Kindle, J. C.: Monsoon-driven biogeochemical processes in the Arabian Sea,
3716 *Prog. Oceanogr.*, doi:10.1016/j.pocean.2005.03.008, 2005.

3717 Wiggert, J. D., Murtugudde, R. G. and Christian, J. R.: Annual ecosystem variability in the tropical Indian Ocean:
3718 Results of a coupled bio-physical ocean general circulation model, *Deep. Res. Part II Top. Stud. Oceanogr.*, 53(5–7),
3719 644–676, doi:10.1016/j.dsr2.2006.01.027, 2006.

3720 Wiggert, J. D., Vialard, J., and Behrenfeld, M. J.: Basin-wide modification of dynamical and biogeochemical processes
3721 by the positive phase of the Indian Ocean Dipole during the SeaWiFS era. In: *Indian Ocean biogeochemical Processes*

- 3722 and Ecological Variability, Geophysical Monograph Series, 185, 385-407, <https://doi.org/10.1029/2008GM000776>,
3723 2009.
- 3724 Wijesekera, H. W., Jensen, T. G., Jarosz, E., Teague, W. J., Metzger, E. J., Wang, D. W., Jinadasa, S. U. P.,
3725 Arulananthan, K., Centurioni, L. R. and Fernando, H. J. S.: Southern Bay of Bengal currents and salinity intrusions
3726 during the northeast monsoon, *J. Geophys. Res. Ocean.*, doi:10.1002/2015JC010744, 2015.
- 3727 Wijesekera, H. W., Shroyer, E., Tandon, A., Ravichandran, M., Sengupta, D., Jinadasa, S. U. P., Fernando, H. J. S.,
3728 Agrawal, N., Arulananthan, K., Bhat, G. S., Baumgartner, M., Buckley, J., Centurioni, L., Conry, P., Thomas Farrar,
3729 J., Gordon, A. L., Hormann, V., Jarosz, E., Jensen, T. G., Johnston, S., Lankhorst, M., Lee, C. M., Leo, L. S.,
3730 Lozovatsky, I., Lucas, A. J., MacKinnon, J., Mahadevan, A., Nash, J., Omand, M. M., Pham, H., Pinkel, R., Rainville,
3731 L., Ramachandran, S., Rudnick, D. L., Sarkar, S., Send, U., Sharma, R., Simmons, H., Stafford, K. M., Laurent, L. S.,
3732 Venayagamoorthy, K., Venkatesan, R., Teague, W. J., Wang, D. W., Waterhouse, A. F., Weller, R. and Whalen, C. B.:
3733 ASIRI: An ocean-atmosphere initiative for Bay of Bengal, *Bull. Am. Meteorol. Soc.*, doi:10.1175/BAMS-D-14-
3734 00197.1, 2016a.
- 3735 Wijesekera, H., Teague, W., Jarosz, E., Wang, D., Jensen, T., Jinadasa, S. U. P., Fernando, H., Centurioni, L., Hallock,
3736 Z., Shroyer, E. and Moun, J.: Observations of Currents Over the Deep Southern Bay of Bengal—With a Little Luck,
3737 *Oceanography*, 29(2), 112–123, doi:10.5670/oceanog.2016.44, 2016b.
- 3738 Wijesekera, H. W., Teague, W. J., Wang, D. W., Jarosz, E., Jensen, T. G., Jinadasa, S. U. P., Fernando, H. J. S. and
3739 Hallock, Z. R.: Low-frequency currents from deep moorings in the southern bay of Bengal, *J. Phys. Oceanogr.*,
3740 doi:10.1175/JPO-D-16-0113.1, 2016c.
- 3741 Wijffels, S., and G. Meyers: An intersection of oceanic waveguides: Variability in the Indonesian throughflow region, *J.*
3742 *Phys. Oceanogr.*, 34, 1232–1253, 2004.
- 3743 Wijffels, S., Meyers, G. and Godfrey, J. S.: A 20-yr average of the Indonesian throughflow: Regional currents and the
3744 interbasin exchange, *J. Phys. Oceanogr.*, 38, 1965–1978, 2008.
- 3745 Wijffels, S., Roemmich, D., Monselesan, D., Church, J. and Gilson, J.: Ocean temperatures chronicle the ongoing
3746 warming of Earth. *Nature Clim Change* 6, 116–118 <https://doi.org/10.1038/nclimate2924>, 2016.
- 3747 Williams, A. P. and Funk, C.: A westward extension of the warm pool leads to a westward extension of the Walker
3748 circulation, drying eastern Africa. *Clim. Dyn.*, 37, 2417-2435, 2011.
- 3749 Wilson, C. and Qiu, X.: Global distribution of summer chlorophyll blooms in the oligotrophic gyres, *Prog. Oceanogr.*,
3750 doi:10.1016/j.pocean.2008.05.002, 2008.
- 3751 Woo, M., Pattiaratchi, C. and Schroeder, W.: Summer surface circulation along the Gascoyne continental shelf, Western
3752 Australia. *Cont Shelf Res* 26, 132–152, 2006.
- 3753 Woo, L. M., Pattiaratchi, C. B.: Hydrography and water masses off the western Australian coast, *Deep Sea Res. I*, 55(9),
3754 1090–1104, <https://doi.org/10.1016/j.dsr.2008.05.005>, 2008.
- 3755 Wyrski, K.: An equatorial jet in the Indian Ocean, *Science*, 181 (4096), 262-264, doi:10.1126/science.181.4096.262,
3756 1973.
- 3757 Xi, J., L. Zhou, R. Murtugudde, and L. Jiang: Impacts of intraseasonal SST anomalies on precipitation during Indian
3758 summer monsoon. *J. Clim.*, 28, 4561-4575, <http://dx.doi.org/10.1175/JCLI-D-14-00096.1>, 2015.
- 3759 Xie, S.-P., Annamalai, H., Schott, F. A., and McCreary, J. P.: Structure and mechanisms of South Indian Ocean climate
3760 variability, *J. Clim.*, 15, 864–878, 2002.
- 3761 Xie, S.-P., Du, Y., Huang, G., Zheng, X.-T., Tokinaga, H., Hu, K. M., and Liu, Q. Y.: Decadal shift in El Niño
3762 influences on Indo–Western Pacific and East Asian climate in the 1970s. *J. Climate*, 23, 3352–3368, 2010.
- 3763 Xie, S., Hu, K., Hafner, J., Tokinaga, H., Du, Y., Huang, G., and Sampe, T.: Indian Ocean Capacitor Effect on Indo–
3764 Western Pacific Climate during the Summer following El Niño. *Journal of Climate* 22, 3, 730-747,
3765 <https://doi.org/10.1175/2008JCLI2544.1>, 2009.

3766 Xie, S.-P., Kosaka, Y., Du, Y., Hu, K., Chowdary, J. S., & Huang, G.: Indo-western Pacific ocean capacitor and
3767 coherent climate anomalies in post-ENSO summer: A review. *Adv. in Atmos. Sci.*, 33(4, SI), 411–432.
3768 <https://doi.org/10.1007/s00376-015-5192-6>, 2016.

3769 Yamagami, Y. and Tozuka, T.: Interdecadal changes of the Indian Ocean subtropical dipole mode, *Clim. Dyn.*,
3770 doi:10.1007/s00382-014-2202-9, 2015.

3771 Yanai, M. and Maruyama, T.: Stratospheric wave disturbances propagating over the equatorial Pacific, *J. Meteorol.*
3772 *Soc. Jap.*, 44, 291–294, 1966.

3773 Yang, J., Liu, Q., Xie, S.-P., Liu, Z. and Wu, L.: Impact of the Indian Ocean SST basin mode on the Asian summer
3774 monsoon. *Geophys. Res. Lett.*, 34, L02708. doi:10.1029/2006GL028571, 2007.

3775 Yang, L., Murtugudde, R., Zhou, L., & Liang, P.: A potential link between the Southern Ocean warming and the South
3776 Indian Ocean heat balance. *Journal of Geophysical Research: Oceans*, 125, e2020JC016132, 2020.
3777 <https://doi.org/10.1029/2020JC016132>

3778 Yang, Y., Xie, S.-P., Wu, L., Kosaka, Y., Lau, N. C., and Vecchi, G. A.: Seasonality and predictability of the Indian
3779 Ocean dipole mode: ENSO forcing and internal variability, *J. Clim.*, 28, 8021–8036, 2015.

3780 Yit Sen Bull, C., and van Sebille, E.: Sources, fate, and pathways of Leeuwin Current water in the Indian Ocean and
3781 Great Australian Bight: A Lagrangian study in an eddy-resolving ocean model, *J. Geophys. Res. Oceans*, 121, 1626–
3782 1639, <https://doi.org/10.1002/2015JC011486>, 2016.

3783 Yoshida, K., and Kidokoro, T.: A subtropical countercurrent II: A prediction of eastward flows at lower subtropical
3784 latitudes, *J. Oceanogr. Soc. Japan*, 23(5), 231–246, 1967.

3785 Yu, L., Jin, X. and Weller, R. A.: Annual, seasonal, and interannual variability of air-sea heat fluxes in the Indian Ocean,
3786 in *Journal of Climate*, 2007.

3787 Yu, L.: Sea Surface Exchanges of Momentum, Heat, and Fresh Water Determined by Satellite Remote Sensing, in
3788 *Encyclopedia of Ocean Sciences*, 1, pp. 15–23, Elsevier, <https://doi.org/10.1016/B978-0-12-409548-9.11458-7>, 2009.

3789 Yuan, D., Zhou, H. and Zhao, X.: Interannual climate variability over the tropical Pacific Ocean induced by the Indian
3790 Ocean dipole through the Indonesian Throughflow, *J. Clim.*, doi:10.1175/JCLI-D-12-00117.1, 2013.

3791 Zang, N., Sprintall, J., Ienny, R., Wang, F., Seasonality of the Somali Current/Undercurrent System, *Deep-Sea Research*
3792 Part II, <https://doi.org/10.1016/j.dsr2.2021.104953>, 2021.

3793 Zhang, C.: Madden-Julian Oscillation, *Rev. Geophys.*, 43(2), RG2003, <https://doi.org/10.1029/2004RG000158>, 2005.

3794 Zhang, L., Han, W., Li, Y., and Maloney, E. D.: Role of North Indian Ocean air-sea interaction in summer monsoon
3795 intraseasonal oscillation, *J. Clim.*, 31(19), 7885–7908, <https://doi.org/10.1175/JCLI-D-17-0691.1>, 2018.

3796 Zhang, N., Feng, M., Hendon, H.H., Hobday, A.J., and Zinke, J.: Opposite polarities of ENSO drive distinct patterns of
3797 coral bleaching potentials in the southeast Indian Ocean. *Scientific Reports*, 7(1), 1–10,
3798 <https://doi.org/10.1038/s41598-017-02688-y>, 2017.

3799 Zhang, D., McPhaden, M. J., and Lee, T.: Observed Interannual Variability of Zonal Currents in the Equatorial Indian
3800 Ocean Thermocline and Their Relation to Indian Ocean Dipole. *Geophys. Res. Lett.*, 41, 7933–7941, doi:
3801 10.1002/2014GL061449, 2014.

3802 Zhang, W., Wang, Y., Jin, F.-F., Stuecker, M. F., and Turner, A. G.: Impact of different El Niño types on the El
3803 Niño/IOD relationship. *Geophys. Res. Lett.*, 42, 8570–8576, 2015.

3804 Zhang, Y., Feng, M., Du, Y., Phillips, H. E., Bindoff, N. L., McPhaden, M. J.: Strengthened Indonesian Throughflow
3805 drives decadal warming in the Southern Indian Ocean. *Geophys. Res. Lett.*, 45, 6167–6175, 2018.

3806 Zheng, X.-T., Xie, S.-P., Du, Y., Liu, L., Huang, G., and Liu, Q. Y.: Indian Ocean Dipole response to global warming in
3807 the CMIP5 multimodel ensemble. *J. Climate*, 26, 6067–6080, 2013.

3808 Zheng, S., Feng, M., Du, Y., Meng, X., and Yu, W.: Interannual variability of eddy kinetic energy in the subtropical
3809 southeast Indian Ocean associated with the El Niño–Southern Oscillation. *J. Geophys. Res.: Oceans*, 123, 1048–1061,
3810 <https://doi.org/10.1002/2017JC013562>, 2018.

3811 Zhou, X., Alves, O. Marsland, S. J., Bi, D., and Hirst, A.C.: Multi-decadal variations of the south Indian Ocean
3812 subsurface temperature influenced by Pacific Decadal Oscillation. *Tellus*, 69A, 1308055,
3813 <https://doi.org/10.1080/16000870.2017.1308055>, 2017.

3814 Zhou, L., Murtugudde, R., Chen, D. and Tang, Y.: A Central Indian Ocean mode and heavy precipitation during Indian
3815 Summer Monsoon. *J. Clim.*, DOI: 10.1175/JCLI-D-16-0347.1, 2017a.

3816 Zhou, L., Murtugudde R., Chen, D. and Tang, Y.: Seasonal and interannual variabilities of the Central Indian Ocean, *J.*
3817 *Clim.*, doi: 10.1175/JCLI-D-16-0616.1, 2017b.

3818 Zhou, Z.-Q., Zhang, R., Xie, S.-P.: Interannual variability of summer surface air temperature over central India:
3819 Implications for monsoon onset. *J. Clim.*, 32, 1693–1706, 2019.

3820 Zhou, Z.-Q., Xie, S.-P., and Zhang, R.: Historic Yangtze flooding of 2020 tied to extreme Indian Ocean conditions,
3821 *Proceedings of the National Academy of Sciences*, 118(12), e2022255118, doi: 10.1073/pnas.2022255118, 2021.

3822 Zhuang, W., Feng, M., Du, Y., Schiller, A. and Wang, D.: Low-frequency sea level variability in the southern Indian
3823 Ocean and its impacts on the oceanic meridional transports, *J. Geophys. Res. Ocean.*, doi:10.1002/jgrc.20129, 2013.

3824 Zinke, J., Rountrey, A., Feng, M., Xie, S.-P., Dissard, D., Rankenburg, K., Lough, J. M., and McCulloch, M. T.: Corals
3825 record long-term Leeuwin current variability including Ningaloo Niño/Niña since 1795, *Nature Comm.*, 5, 3607,
3826 <https://doi.org/10.1038/ncomms4607>, 2014.